uOttawa

L'Université canadienne
Canada's university

FACULTÉ DES ÉTUDES SUPÉRIEURES ET POSTOCTORALES

uOttawa

L'Université canadienne
Canada's university

FACULTY OF GRADUATE AND POSDOCTORAL STUDIES

Roxanne Landry
AUTEUR DE LA THÈSE / AUTHOR OF THESIS

Ph.D. (Biochemistry)
GRADE / DEGREE

Department of Biochemistry, Microbiology and Immunology
FACULTÉ, ÉCOLE, DÉPARTEMENT / FACULTY, SCHOOL, DEPARTMENT

Structure-Function Studies in Antibodies and Glycosyltransferases

TITRE DE LA THÈSE / TITLE OF THESIS

Steve Evans
DIRECTEUR (DIRECTRICE) DE LA THÈSE / THESIS SUPERVISOR

John Baenziger
CO-DIRECTEUR (CO-DIRECTRICE) DE LA THÈSE / THESIS CO-SUPERVISOR

EXAMINATEURS (EXAMINATRICES) DE LA THÈSE / THESIS EXAMINERS

Ken Dimock

David Rose

Mary Alice Hefford

Martin Young

Gary W. Slater
Le Doyen de la Faculté des études supérieures et postdoctorales / Dean of the Faculty of Graduate and Postdoctoral Studies

# STRUCTURE-FUNCTION STUDIES IN ANTIBODIES AND GLYCOSYLTRANSFERASES

Roxanne C. Landry

Thesis submitted to the Department of Biochemistry, Microbiology and Immunology in partial fulfillment of the requirements for the degree of Doctor of Philosophy

University of Ottawa
Ottawa, Ontario, Canada
August 2007

*Your file Votre référence*
*ISBN: 978-0-494-49372-4*
*Our file Notre référence*
*ISBN: 978-0-494-49372-4*

À mes chers parents, ceci n'aurait pas été possible sans votre support et vos encouragements.

To my darling husband, you never gave up on me, always believed in me, always supported me. I love you so much.

À ma douce Mackenzie… grâce à toi, je veux être meilleure tous les jours.

## ABSTRACT

Protein-protein and protein-carbohydrate recognition are key to understanding many critical life processes. One such critical life process is host defense, and the determination of the crystal and molecular structures of complexes involved in synthesizing and recognizing clinically-relevant antigens can provide key insight into fields as diverse as immunotherapy or chemo-enzymatic synthesis.

In the first part, immunotherapeutic antibody candidates MR1 and BEC2 were studied to gain a structural understanding of their potential in the prevention and treatment of cancer. Antibody MR1 binds specifically and with high-affinity to a mutant of the epidermal growth factor receptor (EGFRvIII) defined by an in-frame deletion that generates a novel glycine residue at the fusion junction. It was our hypothesis that this fusion junction glycine residue would form a key recognition element for antibody MR1. The x-ray crystal structure of MR1 in complex with a peptide antigen of the EGFRvIII shows MR1 to possess a J-shaped groove and the EGFRvIII peptide to adopt a hairpin turn – β strand conformation. Interestingly, the fusion junction glycine, although a central feature of the EGFRvIII peptide, does not interact specifically with MR1 but allows the hairpin turn, which is both unique to EGFRvIII and crucial for MR1 recognition. Antibody BEC2 is an anti-idiotypic antibody mimic of the tumor-associated $GD_3$ ganglioside. It has been raised against anti-$GD_3$ antibody R24 and used successfully to immunize hosts that natively express the antigen against $GD_3$. It was our hypothesis that key polar groups of BEC2 would structurally mimic the $GD_3$ antigen; however, several endeavors including isolation of R24-like antibodies for crystallization, purification of digested fragments of BEC2, and expression of BEC2 and

R24 antibody constructs have all failed to yield sufficient amounts of quality protein for crystallization.

In the second part, the structures of mutants of the ABO(H) blood group glycosyltransferase B were solved to gain a greater understanding of substrate specificity and mechanism of catalysis. The x-ray crystal structures of cysteine-to-serine mutants GTB M2 (C80S, C196S) and GTB M3 (C80S, C196S, C209S) show a more ordered catalytic domain with a novel helix being observed as compared to the heavy-atom derivative of wild-type GTB. The addition of the third C-to-S mutation in GTB M3 brings about ordering of the catalytic loop, a loop that is not observed in any of the GTB structures published to date. The C209S mutation allows two water molecules to position themselves in the active site cleft, with one of these waters bridging S209 to a residue important in donor binding, R188. This bridging interaction locks R188 in one position where R188 can interact with the DXD motif D211 and D302.

## ACKNOWLEDGEMENTS

- I once told a brilliant professor that I was going to be smarter than him when this degree would be done. I was naïve. My supervisor Dr. Stephen V. Evans is one of the most knowledgeable professors I know and I am very grateful for having had the privilege to work in his laboratory. I will never forget your generosity, and amazing sense of humor.
- I would like to thank Dr. John E. Baenziger for his friendship, his constructive criticism, and his belief in my ability to be a good researcher. I owe you so much for all of your help in getting through this degree.
- I would also like to thank Dr. C. Roger Mackenzie for selflessly taking me into his laboratory and allowing me to finish my degree in Ottawa. You always trusted in my hypotheses and let me be an independent worker. I am very grateful.
- To Dr. Carol P. Huber for your support and kindness. An accomplished woman such as you is truly an inspiration.
- To Ginette Dubuc, Thanh-Dung Nguyen, Tomoko Hirama, Diane M. Zahab, Anne Besner-Johnston, Dr. Corrie Dacosta, Dr. Nina O. L. Seto and Svetlana Borisova for invaluable help in learning phage display, cell culture, yeast expression, molecular biology, and crystallization as well as for performing some crucial experiments for my work.
- To Joanne Daniels and Carol Ann Kelly for all the help with graduate school-related hassles.
- To Lise Bramall who made all computer work possible. You were always there to fix my computer problems – I could not have done it without you!
- To Anna Cunningham, Sonia Leclerc, and Michael Masotti for all of the sequencing that I sent to them and that was always returned in record time.
- To the day commissionaires at NRC, Paul and Dean, who always greeted me with a smile and a good joke.
- To Nicole and Lise from the NRC cafeteria – thanks for the coffees and cinnamon toasts. You will always be my Kenya-Chiquitas!
- A special thanks to all the friends that I have made through the years as a graduate student: to Dr. Eleanor Altman who always told it like it is and kept it real; to Dr. Hoa P. Nguyen who is the only man I know that can out-shop me at an outlet store – I will always remember

our fun trips to Brookhaven and our good ol' buddy x-ray Ray, and yes, I still consider you the winner of the cheesiest 80's songs with Mitsou classics; to Dr. Claudia Sheedy, the best partner in crime a girl can have, for all the laughter and adventures; to Thanh-Dung Nguyen, our little Belette, teasing took on a whole new meaning with you; to Emily Stone, a shy one at first but she can pack quite a punch; to Maryse Duquette, a friendship that will stand the test of time; to Dr. Melanie Derry, for making me laugh so hard and reminding me that poutine and sports don't mix; and to all past labmates, who have all taught me something about life.

- And last but not least, I would like to thank my family: my parents Cécile and Richard, my sister Marie-Anik, my father- and mother-in-law Murray and Sally, my brothers-in-law Paul, Dave, and Martin, my sister-at-heart Amanda, and my darling Godson Cooper for their support throughout the years. To my loving husband Steve and my gorgeous daughter Mackenzie who sacrificed precious time to have me accomplish my goals.

**TABLE OF CONTENTS**

## PART II

### CHAPTER 5: MUTANTS OF HUMAN ABO(H) BLOOD GROUP GLYCOSYLTRANSFERASE B

## LIST OF FIGURES

### CHAPTER 1



### CHAPTER 2



### CHAPTER 3

**CHAPTER 4**

**CHAPTER 5**

## LIST OF TABLES

### CHAPTER 3



### CHAPTER 4



### CHAPTER 5

## LIST OF ABBREVIATIONS

| | |
|---|---|
| ADA | *N*-(2-acetamido)iminodiacetic acid |
| ADCC | Antibody-dependent cellular cytotoxicity |
| BCR | B-cell receptor |
| B-factor | thermal motion, temperature factor |
| BSA | Bovine serum albumin |
| CAZy | Carbohydrate active enzyme database |
| CDR | Complementarity-determining region |
| $C_{H1}$ | Heavy chain constant domain 1 |
| $C_{H2}$ | Heavy chain constant domain 2 |
| $C_{H3}$ | Heavy chain constant domain 3 |
| $C_L$ | Light chain constant domain |
| DMPC | Dimyristoylphosphatidylcholine |
| dsFv | Disulfide-stabilized variable fragment |
| DTT | Dithiothreitol |
| *E. coli* | *Escherichia coli* |
| EDTA | Ethylenediaminetetraacetic acid |
| EGFR | Epidermal growth factor receptor |
| EGFRvIII | Epidermal growth factor receptor variant III |
| ELISA | Enzyme-linked immunosorbent assay |
| Fab | Antigen-binding fragment |
| Fc | Fragment crystallizable |
| Fv | Fragment variable |
| GT | Glycosyltransferase |
| GTA | Human glycosyltransferase A |
| GTB | Human glycosyltransferase B |
| HAMA | Human anti-mouse antibody |
| HBSE | Hepes buffer saline with 3 mM EDTA |
| HBS-EP | Hepes buffer saline with 3 mM EDTA and 0.005% P-20 |
| HCAb | Heavy chain antibody |

| | |
|---|---|
| H chain | Heavy chain |
| HPLC | High performance liquid chromatography |
| HRP | Horseradish peroxidase |
| IEF | Isoelectric focusing |
| IPTG | Isopropyl-β-D-thiogalactopyranoside |
| $K_D$ | Dissociation constant |
| L chain | Light chain |
| LPS | Lipopolysaccharide |
| mAb | Monoclonal antibody |
| MHC | Major histocompatibility complex |
| MPBS | Milk phosphate buffer saline |
| MPD | Methyl-2,4-pentanediol |
| NaCl | Sodium chloride |
| NANA | *N*-acetylneuraminic acid |
| PAGE | Polyacrylamide gel electrophoresis |
| PBS | Phosphate buffer saline |
| PBST | Phosphate buffer saline with 0.02% Tween-20 |
| PCR | Polymerase chain reaction |
| PE | Pseudomonas exotoxin |
| PEG | Polyethylene glycol |
| pI | Isoelectric point |
| PMSF | Phenylmethylsulfonyl fluoride |
| *P. pastoris* | *Pichia pastoris* |
| R-factor | Reliability factor |
| RGB | Rosetta-gami B cells |
| RMSD | Residual mean square deviation |
| RT | Room temperature |
| RU | Resonance unit |
| scFv | Single-chain variable fragment |
| sdAb | Single-domain antibody |
| SOE | Splice overlap extension |

| | |
|---|---|
| SPR | Surface plasmon resonance |
| $V_H$ | Heavy chain variable fragment |
| $V_L$ | Light chain variable fragment |
| $V_HH$ | Heavy chain variable fragment of a heavy-chain antibody |

# GENERAL INTRODUCTION

The powerful technique of x-ray crystallography allows for the structure of proteins to be resolved at the molecular level. This structural information provides invaluable insight into both protein dynamics and mechanisms of action leading to a greater understanding of biological function. In addition, this knowledge can be exploited for the engineering and design of novel agents for use in a variety of areas including biotechnology and medicine.

The work presented within this thesis can be divided into two branches: the study of the recognition mechanisms of two antibodies involved in cancer-targeted immunotherapy, MR1 and BEC2, and the study of mutants of the human ABO(H) blood group B glycosyltransferase. Antibody MR1 specifically recognizes a tumor-associated variant of the epidermal growth factor receptor termed EGFRvIII while BEC2 anti-idiotypic antibody mimics $GD_3$, a ganglioside over-expressed on tumor cells. Both these antibodies represent excellent potential reagents for the immunotherapy of cancer. Investigation into the structures of relevant complexes of MR1 and BEC2 will provide a detailed insight into how these antibodies recognize their target and mediate anti-tumor effects. This will in turn allow for the design of better antibody-based reagents for use in cancer therapy. GTB M2 and GTB M3 are mutants of the human ABO(H) blood group B glycosyltransferase in which two or three free sulfhydryl groups have been mutated to serine, respectively. These mutants were designed to resolve crystallizability issues and their structures allow a probe of both the mechanisms of recognition and catalysis of glycosyltransferase B.

The thesis will first introduce general concepts of the technique of x-ray crystallography. This will be followed by two sections: the first section will present self-contained chapters for MR1 and BEC2, preceded by a brief introductory chapter on

antibodies, and the second section will present a self-contained chapter on mutants of the human ABO(H) blood group glycosyltransferase B.

# CHAPTER 1

# X-RAY CRYSTALLOGRAPHY

The powerful technique of x-ray crystallography allows for high-resolution protein structure studies and complements other techniques such as mutagenesis and kinetic studies to yield a better understanding of protein function. In order to understand how protein structural models are obtained, it is necessary to have a general knowledge of the technique as well as an appreciation of the methods that are used to assess the quality of models, and an ability to critically judge of the validity of these models. Although these concepts have been well documented (1-7), this chapter is aimed at providing a brief review of the technique of x-ray crystallography for the benefit of the reader.

*Crystallization*

To obtain high quality crystals, the protein of interest needs to be as pure as possible. Any microheterogeneity can adversely affect the quality of the crystal. Following purification, supersaturating conditions that will favor crystallization of the sample are identified. Unfortunately, this procedure can be more of an art form than a science, and several thousand trials may be required before high quality crystals are generated. Crystallization trials include the variation of parameters that affect solubility of a protein, such as protein concentration, buffer species, buffer pH, ionic strength, precipitating agent, and presence of additives as well as a variation of physical parameters such as crystallization setup and temperature (8). Conditions that favor a rapid and disordered assembly of the protein molecules will lead to precipitation. Conditions that allow for semi-ordered assembly of the protein molecules will lead to aggregation. Finally, ordered assembly of the molecules will favor the generation of crystals. In these crystals, protein molecules will interact through few contact points and a high proportion of the crystal will actually consist of solvent. Many types of crystals can be generated from a protein sample; some crystals will diffract poorly

while some may be of good quality for diffraction. A crystal that is of quality for collection of diffraction data is usually of a good size (0.2-1 mm) and has sharp edges.

Crystals of protein complexes can be obtained by co-crystallizing the molecules or, when the ligand is small in size, soaking protein crystals with the ligand. Crystals of diffraction quality can then be used directly in diffraction experiments or be submitted to 'flash-cooling' using liquid propane or liquid nitrogen. This technique offers such advantages as slowing down decay of the crystal in the x-ray beam as well as limiting atomic movement in the crystal.

*Unit Cell, Symmetry, and Space Groups*

Protein crystals have molecules arranged in a three-dimensional array. This three-dimensional array of molecules can be used to define an imaginary grid system that divides the crystal into a lattice of identical subunits. The three axes that define this lattice are termed *x*, *y*, and *z*, and form a right-handed system. Each intersection between these identical subunits is termed 'lattice point' and the subunits themselves are termed 'unit cells' (Figure 1.1). These unit cells are by definition all the same, their lengths along *x*, *y*, and *z* are termed *a*, *b*, and *c* and the angles formed between *c* and *b*, *a* and *c*, and *a* and *b* are termed $\alpha$, $\beta$, and $\gamma$ respectively. Molecules in the unit cell can be related to each other by symmetry operations. The types of symmetry that are allowed in protein crystals include rotation, translation, and a combination of the two, termed screw axis. The smallest part of the unit cell that can generate the complete unit cell by means of these symmetry operations is termed the 'asymmetric unit'.

Although any unit cell could be theoretically chosen that satisfies the crystal lattice, there exist some conventional restrictions on unit cell lengths and angles. These restrictions

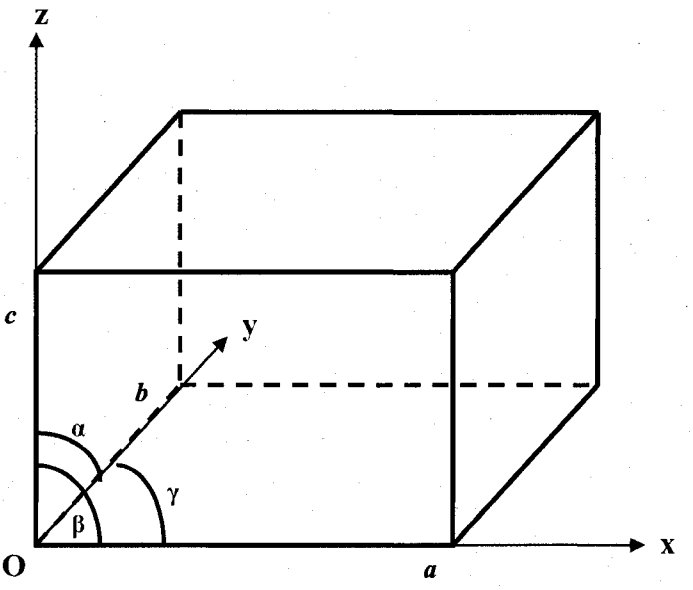


**Figure 1.1. Unit cell.** Schematic representation of a unit cell that is defined by axis lengths *a*, *b*, and *c* and interaxis angles α, β, and γ. The unit cell represents the building block of the crystal.

are defined in seven crystal systems: triclinic, monoclinic, orthorhombic, tetragonal, trigonal, hexagonal, and cubic. All of these crystal systems will allow 'primitive' unit cells, with a lattice point at each corner of the cell while some crystal systems will also allow unit cells that contain additional lattice points, 'non-primitive' unit cells. Although a small unit cell volume is preferred, the bigger volume of the non-primitive cell allows for a higher level of symmetry. There are seven kinds of primitive unit cells and seven kinds of non-primitive unit cells, making up the 14 Bravais lattices. There are also restrictions on the combination of symmetry elements that can occur in a unit cell; only 32 unique combinations exist that generate a closed set. These 32 combinations are referred to as 'point groups' and when combined with the 14 Bravais lattices, give rise to the 230 known 'space groups'. With proteins being chiral molecules, mirror symmetry operations are prohibited and there are only 11 possible point groups and consequently only 65 chiral space groups for protein crystals.

*X-Ray Diffraction*

In an x-ray diffraction experiment, a crystal of sufficient size and quality is mounted and aligned with an x-ray beam (Figure 1.2). Experiments use a monochromatic x-ray beam and entire data sets are collected by systematic rotation of the crystals during data acquisition (oscillation method).

Diffraction, or coherent scattering, occurs when x-rays are scattered by electrons in the protein sample. The diffraction pattern is a physical recording of this coherent scattering. The pattern appears as a collection of spots due to the repetitive nature of the crystal. The spots that are found on the diffraction pattern vary in intensity, which is a direct indication of

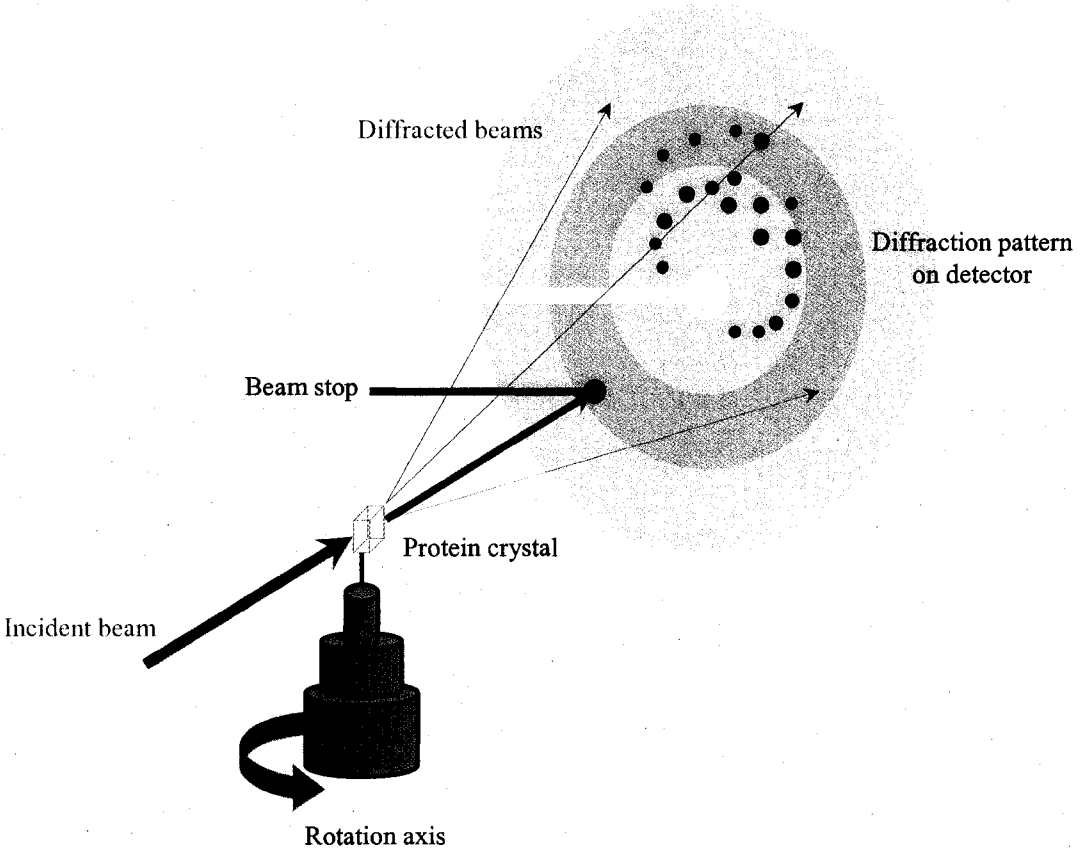


**Figure 1.2. Schematic x-ray diffraction experiment.** The protein crystal is centered in the path of an x-ray beam. Some of the x-rays in the incident beam are diffracted by the electron clouds from the atoms in the protein. The diffracted x-rays that interfere constructively are recorded as spots and form a pattern on a detector. In the oscillation method, the crystal is oscillated through a small arc of 0.5° to 1.0° for each image, then moved by the corresponding amount to collect each subsequent image.

the atomic structure of the protein that comprises the crystal, and are arranged in a way that reflects the unit cell dimensions and the symmetry in the crystal.

The diffraction pattern is the basis for the structural analysis of proteins. As such, it is important to understand what the spots represent, the limits of the data and the quality controls. Spots in a diffraction pattern give information on the structure of the average protein, over time, in the crystal. As such, multiple protein conformations, thermal atomic vibrations as well as general crystal disorder contribute to lower the accuracy and the resolution of the data. Although low-resolution data will provide the gross shape of the molecule, it is high-resolution data that provide the locations and orientations of the amino acid side chains. It is important to collect as many unique spots as possible (completeness), to collect unique spots more than once (redundancy) and to collect symmetry-related spots to ensure accuracy. The final data consists of a list of all the spots collected, their position and measured intensity as well as the associated statistical errors. Measures of quality include the 'reliability factor' or R-factor that indicates the average fractional error. In data collection statistics, the symmetry R-factor or merging R-factor gives an estimate of the disagreement between symmetry-related spots:

$$R_{merge} = \sum_{hkl} \sum_{i} \left| I_i(hkl) - \overline{I(hkl)} \right| \Big/ \sum_{hkl} \sum_{i} I_i(hkl)$$

The merging R-factor is simply the absolute value of the sum of the differences of all measurements from the average value of the measurements divided by the sum of all measurements.

*The hkl Planes*

Diffraction can be visualized as reflection from sets of imaginary planes within the crystals (9). This is why diffraction spots are often termed 'reflections'. These three-dimensional imaginary planes of equal interplanar spacing divide the unit cell in exact fractions (Figure 1.3). Each plane is denoted by an *hkl* index, with the *h* representing the number of times the unit cell's *a* axis is cut by the planes, the *k*, the number of times the *b* axis is cut, and the *l*, the number of times the *c* axis is cut. Diffraction from electron clouds about a set of planes yields one reflection on the diffraction pattern and the intensity of this reflection is directly related to the position of the protein's electron clouds relative to those planes. The bigger the *hkl* indices, the smaller the interplanar distance, or $d_{hkl}$, and thus the finer the sampling of the content of the unit cell, and the better the resolution.

*Bragg's Law*

Using the concepts of the *hkl* planes, Bragg's law can explain where diffraction spots can be observed. Bragg's law states that constructive interference occurs when waves reflected from a set of planes are all in phase, and that this occurs when the distance traveled by the second wave is equal to an integral number of wavelengths:

$$n\lambda = 2d_{hkl}\sin\theta$$

where $\boldsymbol{n}$ is an integer, $\lambda$ is the wavelength, $\boldsymbol{d_{hkl}}$ is the interplanar spacing between a set of planes with index *hkl*, and $\boldsymbol{\theta}$ is the angle between the incident beam and the planes as well as the angle between the reflected x-rays and the same planes (Figure 1.4).

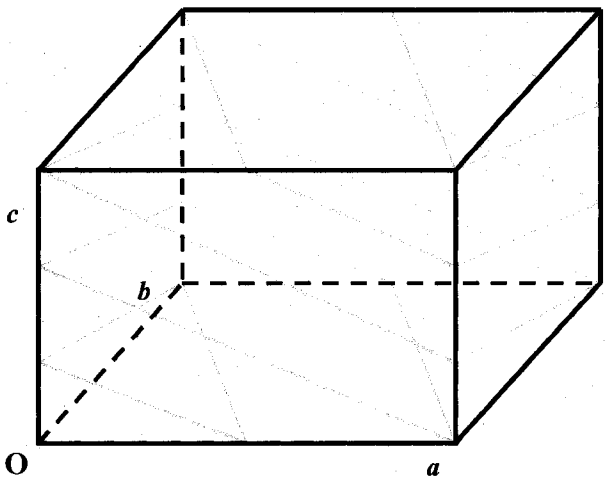


**Figure 1.3. The *hkl* planes.** Diffraction can be seen as the reflection of x-rays from sets of imaginary planes of equal interplanar spacing. These planes are denoted with indices *hkl*, which indicate the number of times the *a*, *b*, and *c* axes are cut by the planes, respectively. Here, the *213* planes cut the *a* axis twice, the *b* axis once, and the *c* axis three times.

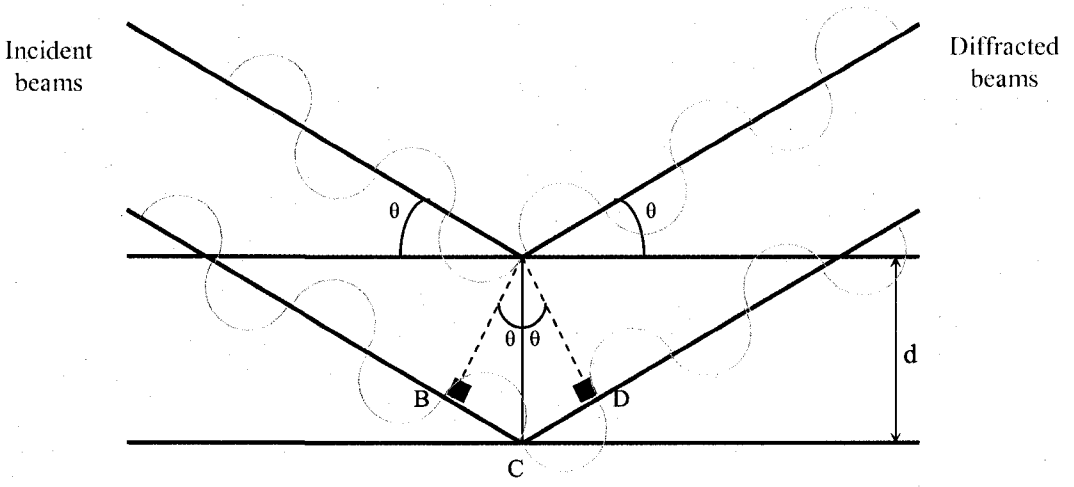


**Figure 1.4. Bragg's law.** According to Bragg's law, diffraction occurs when the interplanar spacing *d* of a set of planes *hkl* is equal to *n* factor of the wavelength: $n\lambda = 2d \sin\theta$. Therefore, for an incident beam striking planes at an angle $\theta$ and being reflected at the same angle, diffraction occurs if the difference between the distances traveled by x-rays reflected from successive planes BC + CD is equivalent to an integral number of wavelength.

*Waves, Fourier Synthesis and Complex Numbers*

To analyze diffraction patterns, x-rays are visualized as waves. These waves are sinusoidal and are characterized by their amplitude, wavelength and phase. Every reflection on a diffraction pattern corresponds to a wave defined by its amplitude, which is proportional to the square root of the spot intensity, and a phase. The electron clouds in crystals, just like reflections, can be thought of as waves that repeat in three-dimension, in every unit cell. To analyze the complicated repetitive wave that is electron density, it is represented as a sum of a series of waves. Each wave in this sum corresponds to one reflection, or diffraction from one set of *hkl* planes, and the sum is termed a Fourier synthesis. The more waves are added, or the more diffraction data are included in the analysis, the more precise the calculated shape of the electron density wave. The Fourier analysis corresponds to the calculation of waves from the electron density. This symmetry of the Fourier provides a mean of having a set of 'observed data' as well as a set of 'calculated data', which comes in handy for electron density analysis as well as quality assessment.

The mathematical equations that describe waves use quantities termed 'structure factors' that represent both the amplitude and the phase of the wave of each reflection. These structure factors can be conveniently described with the use of complex numbers. A complex number can be expressed graphically on a two-dimensional diagram, the Argand diagram, where the $x$ axis represents 'real' components and the $y$ axis, 'imaginary' components. Complex numbers have the general form $\mathbf{a} + \boldsymbol{i}\mathbf{b}$, where $\boldsymbol{i}$ is the square root of $-1$. The structure factor can be thought of as a vector from the origin of the Argand diagram, of length corresponding to the wave amplitude, and making an angle with the $x$ axis corresponding to the wave phase angle (Figure 1.5A). It can also be thought of as a vector

**A**

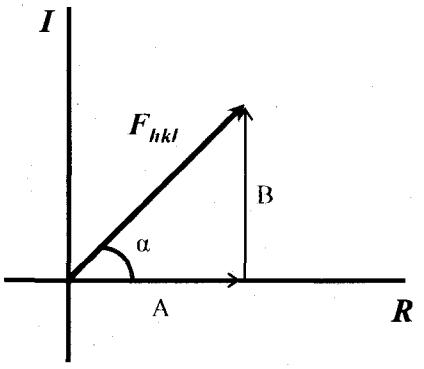


**B**

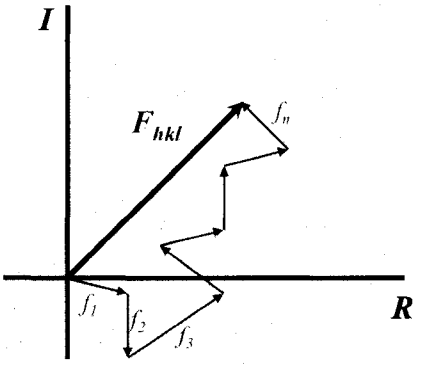


**Figure 1.5. Argand diagram of the structure factor $F_{hkl}$. A.** In the Argand diagram, the structure factor $F_{hkl}$ can be given in terms of its real (A) and imaginary (B) components, where the phase angle corresponds to the angle between the vector $F_{hkl}$ and the $x$ axis. **B.** In the Argand diagram, the structure factor for a Bragg plane $F_{hkl}$ can also be given as a sum of the scattering from individual atoms.

that represents the sum of the scattering contribution of each atom in the unit cell (Figure 1.5B):

$$F_{hkl} = \sum_{j=1}^{n} f_j e^{2\pi i(hx_j + ky_j + lz_j)}$$

where the structure factor $F_{hkl}$ represents the sum over $n$ atoms of the individual atomic scattering factors $f_j$ of atom **j** with coordinates $(x_j, y_j, z_j)$ for a reflection *hkl* whose phase is expressed as the exponent term of $e$. The atomic scattering factor $f_j$ is in turn defined as:

$$f_j = f_o e^{-B(\sin^2\theta)/\lambda^2}$$

where $f_o$ is the scattering factor specific for a given atom, largely dependent on the number of electrons of that atom, and where the exponent term of $e$ corresponds to corrections for thermal motion $B$ as well as scattering angle and wavelength $(\sin^2\theta)/\lambda^2$. The thermal motion $B$ is often referred to as the B-factor or temperature factor and corresponds to:

$$B = 8\pi^2 u^2$$

where $u^2$ is the mean square displacement of an atom.

*The Phase Problem*

To use the Fourier synthesis to define electron density, the structure factors of each wave have to be defined, and this requires both the amplitude and the phase of each reflection to be known. Unfortunately, there is no way to directly measure the phase. This is

a central issue in x-ray crystallography and has been termed 'the phase problem'. Several approaches are available to obtain phase information, but this chapter will focus on the method of molecular replacement.

*Molecular Replacement*

This technique exploits the similarity between two structures, where one of the structures is already known. The known structure can be used to estimate the phases of each reflection from the target's data set, and this provides estimates of the target's structure factors and allows for the electron density of the target structure to be approximated. In order to estimate the phases, the known structure must be positioned in the target's unit cell in such a way that the amplitude of each structure factor of the known structure corresponds to the amplitudes of the target. It is then reasonable to assume that the phases of the structure factors of the known structure are a good estimate of the target's phases.

The repositioning of the known structure relative to the target initially uses rigid body rotation and translation components. These operations are conducted on the known structure and the target's Patterson functions. A Patterson function is a map consisting of peaks that correspond to a molecule's intra- and inter-molecular distances and an origin peak that corresponds to vectors of length zero (or self-vectors). A Patterson function needs no phase information and Patterson peaks ***P(u,v,w)*** are calculated using the intensities $|\mathbf{F}_{hkl}|^2$:

$$P(u,v,w) = \frac{1}{V}\sum_{h}\sum_{k}\sum_{l}\left|F_{hkl}\right|^2 e^{-2\pi i(hu+kv+lw)}$$

The Patterson of the known structure is first rotated over the Patterson of the target, and their agreement is evaluated for every possible rotation using a correlation coefficient. Only Patterson vectors small enough to correspond to intramolecular features are considered in this search. The correlation coefficient is exactly 1 for identical Pattersons and 0 for Pattersons that are totally independent. After applying the rotation, the translation is used to position the correctly oriented known structure relative to the space group elements in the target unit cell. This search utilizes longer Patterson vectors to include clearly intermolecular vectors.

The calculated phases obtained with molecular replacement do not represent an unbiased estimate for the computation of the target's electron density; there will tend to be a bias towards the known structure.

*Electron Density*

Once phases have been estimated, electron density can be computed for the target structure. The Fourier synthesis is calculated as a set of electron density values at every point ***(x,y,z)*** in the unit cell of volume ***V***:

$$\rho(x,y,z) = \frac{1}{V}\sum_{h}\sum_{k}\sum_{l} F_{hkl} e^{-2\pi i(hx+ky+lz)}$$

The electron density is then depicted as contours, where different electron density values correspond to different surfaces. The electron density is the experimental image that is used to build a crystallographic model of the target structure. It is thus clear how the amount of data (resolution) and quality of data are important in the generation of a good electron density map.

Different types of maps are used during model building in order to generate the best possible model. Difference maps correspond to the difference between the observed (Fo) and calculated structure factors (Fc), and are used to indicate the model features that need to be changed. Positive density in a difference Fo-Fc map corresponds to features of the target that are not included in the model whereas negative density corresponds to features of the model that do not fit the real density. Other maps, such as the 2Fo-Fc and 3Fo-2Fc maps, are used to give different relative weight to the Fo and Fo-Fc maps. More thorough elimination of bias can be achieved by using a 'omit map'. The omit map is computed after the removal of ambiguous model atoms and is thought to provide an unbiased estimate of the structure factors for the calculation of the density of these atoms.

*Refinement*

Refinement is the computational procedure that improves the fit of the model to the electron density map. It is undertaken after the model's sequence has been edited to reflect that of the target. Refinement techniques consist of repetitive adjustments of the parameters of each atom within the model to minimize the square of the difference between the observed data and the calculated data while maintaining correct geometry and stereochemistry. Improved agreement between observed and calculated data results in a better estimate of the target's phases and in turn, better electron density maps.

In the first stages, rigid-body refinements use low-resolution data and the parameters of each atom within the model are constrained. This type of refinement treats the model as first one, then several rigid groups, and allows the gross features of the model to settle to the best fit. Further on, energy-minimization procedures are used: more data are added and chemical and stereochemical parameters are allowed to vary within constrained limits. At

each round of energy-minimization, new electron density maps are computed and the model is reviewed for errors. Large changes to the model can be made by manual intervention. In order to avoid the convergence of the refinement to a local minimum, simulated annealing procedures are used. In these procedures, the atomic motions of all atoms in the model are simulated at high temperatures (typically > 2000 K). These high temperatures allow the protein to explore many regions of conformational space, and those that result in an improved agreement with the diffraction pattern tend to be kept as the model 'cools'. Once the model has been determined, other molecules such as water or ligands can be added.

The quality of the model, like that of the collected data statistics, is assessed using the R-factor. Here, the working R-factor is defined as:

$$R_{work} = \sum_{hkl} \left( |Fo| - |Fc| \right) / \sum_{hkl} |Fo|$$

Another value, the cross-validated or free R-factor, is used to monitor the refinement. Its computation uses a small, random subset of data that is not included in the refinement and so is not biased in order to monitor for the possibility of under-determination of the structure.

*Model Quality Assessment*

Other values, beyond the R-factor, are used to evaluate the accuracy of an x-ray crystallography model. The residual mean square deviation (rmsd) of bond lengths and angles indicates the extent to which these depart from theoretical values. Ramachandran plots, which show the distribution of phi and psi angles along the polypeptide chain of a protein, show if any main chain bond angles have refined to values that are energetically disfavoured. Also, B-factors for individual atoms provide a good indication of the

correctness of their position in the electron density. A high temperature factor indicates that electron density placed in that position does not correlate to the observed diffraction pattern, and that the atoms either lie in a disordered region of the protein or have been positioned incorrectly.

# PART I

# CHAPTER 2
# ANTIBODIES

The human immune system has developed several elegant processes that allow it to fight foreign invaders and yet usually not attack self-structures. As a first line of defense, the skin and mucous membranes provide the basic physical and cellular systems that our bodies have developed to kill invading pathogens, systems that are grouped and referred to as 'innate immunity'. The second line of defense, which provides more intricate means of disposing of foreign invaders, is termed 'adaptive immunity'. Lymphocytes, which include T-cells and B-cells, are at the center of this immunity. Both T- and B-lymphocytes are generated in the bone marrow; B-lymphcytes, the cells responsible for antibody production, mature in the bone marrow whereas T-lymphocytes, the cells responsible for cellular immunity, migrate to and mature in the thymus (10).

*Antibody Diversity*

The B-lymphocytes, as a group, have the ability to produce antibodies against almost any antigen they encounter. This high level of diversity in the antibody repertoire cannot however be contained by the genome, and it was apparent early on that antibodies are not encoded by distinct genes but by gene segments (11, 12). These gene segments can combine in a variety of fashions, a process known as 'combinatorial joining', to generate the diversity needed to account for all possible antibodies. There are also other factors that can further increase the diversity during the joining process, such as nucleotide insertions and deletions, and mutations, all of which are referred to as 'junctional diversity' (13). Once antibody gene segments are correctly assembled, the antibodies are expressed and presented at the surface of B-lymphocytes, and are referred to as B-cell receptors (BCRs). Each B-lymphocyte expresses one BCR with definitive specificity. In the bone marrow, a control point exists where all BCRs are tested for reactivity with self-antigens. Any B-lymphocyte

presenting a BCR that reacts strongly with a self-antigen undergoes apoptosis (14). This mechanism is referred to as 'clonal deletion'. B-lymphocytes that pass this checkpoint are released into the body where they can guard against pathogens. One means of recognition of pathogen occurs by binding of a BCR to the foreign body and subsequent engulfment of the pathogen-BCR complex. The proteins of the pathogen are then partially digested and peptide fragments are displayed at the surface in specialized receptors termed major histocompatibility complexes (MHCs) (10, 15). A subset of T-lymphocytes termed 'helper T-cells' has receptors that are able to recognize non-self peptides presented by the MHCs on B-lymphocytes. This 'T-cell dependent' recognition triggers the release of effector molecules by T-cells, which activate proliferation and differentiation of B-cells. In cases where foreign molecules are carbohydrate in nature, the B-lymphocyte cannot present the carbohydrate on MHC receptors and consequently, T-cell help usually cannot be elicited. Responses against carbohydrate antigens are thus referred to as 'T-cell independent'. Both T-cell dependent and T-cell independent mechanisms can activate B-lymphocytes and this activation phenomenon is also termed 'clonal selection'. The activated B-lymphocytes start multiplying at high rates and start producing their BCR as a soluble species: antibodies (16). The soluble antibodies form what has been termed 'humoral immunity' and the B-lymphocytes that produce soluble antibodies are now termed 'antibody forming cells' or 'plasma cells'. In some cases of T-cell independent activation and all cases of T-cell dependent activation, antibody genes undergo changes known as 'somatic mutation' (17) and 'isotype switching'. Somatic mutation refers to the high rate of mutations that the antibody genes undergo during multiplication of the B-lymphocyte. Some B-lymphocyte clones generated will have different antibody affinities: many of the clones will have BCRs

with a lower affinity for the foreign antigen, but a few will be generated that will present BCRs with higher affinity. These higher affinity BCRs will lead to selection of the B-lymphocyte clones for survival and secretion of antibodies (18). Isotype switching refers to the changes that affect the targeting and effector functions of the antibody (isotypes will be presented further below)(19). Some of these newly synthesized antibodies will provide defense in secretions, others will be specialized in targeting specific 'innate immunity' systems to the pathogens in what is referred to as antibody-dependent cellular cytotoxicity (ADCC), but all will have the ability to mediate direct effects such as toxin neutralization and prevention of viral attachment to host cells. Once the infecting agent is disposed of, B-lymphocytes stop proliferating and a subpopulation differentiates into 'memory cells'. These memory B-cells become dormant and keep the specificity to the antigen that they have encountered. They represent one mechanism of acquired immunity and become crucial in the event of a second exposure to the same pathogen, when they are able to provide a timely response.

*Idiotypic Network*

Since some antibodies have the ability to react to different types of molecules, it was proposed early on that antibodies may also have the ability to react with other antibodies (20, 21). These so-called second-generation anti-antibodies, or anti-idiotypic antibodies, are able to recognize part of the first-generation antibody, such as its binding site. Particular anti-idiotypic antibodies that are able to recognize the binding site of antibodies will be complementary to this binding site and appear as the 'internal image' of the original antigen. Antibody-against-antibody reactions could occur over many generations, with third-generation antibodies being able to bind to second-generation antibodies, and so on. The

antibodies involved in such a system are part of what has been termed a 'idiotypic network' (Figure 2.1) (22). The concept of 'idiotypic network' has provided the basis for innovative strategies whereby 'internal image' antibodies can be used to isolate receptor molecules or in the design of vaccines.

*Antibody Structure*

Antibodies are flexible bivalent Y-shaped or T-shaped glycoproteins. They are made up of four chains: two identical heavy chains (H chains) of around 50-77 kDa and two identical light chains (L chains) of around 25 kDa (Figure 2.2A) (23). This pairing of two H and two L chains introduces another means of diversifying the repertoire beyond that of recombination events and mutations, and is referred to as 'combinatorial diversity'. L chains are associated with H chains and the two H chains are associated with each other; the paired chains are linked by non-covalent forces as well as disulfide bridges. Both L and H chains are divided into domains: one variable and one or several constant domains. The variable domains of the L and H chains, $V_L$ and $V_H$ respectively, interact together to form the antigen-binding site, and the first constant domain of the H chains ($C_{H1}$) interacts with the one constant domain of the L chain ($C_L$). These pairing of the two domains of the L chains with domains $V_H$ and $C_{H1}$ of the heavy chain form the antigen-binding fragment (Fab) of the antibody. The two Fabs correspond to the Y- or T-arms and are connected to the base of the antibody, or crystallizable fragment portion (Fc), through a 'hinge region'. The Fc portion of the antibody is made from the second constant domains of both H chains ($C_{H2}$), which cannot interact together due to glycosylation that hinders their packing, and to the third constant domains of both H chains ($C_{H3}$), that can interact with each other (Figure 2.2A).

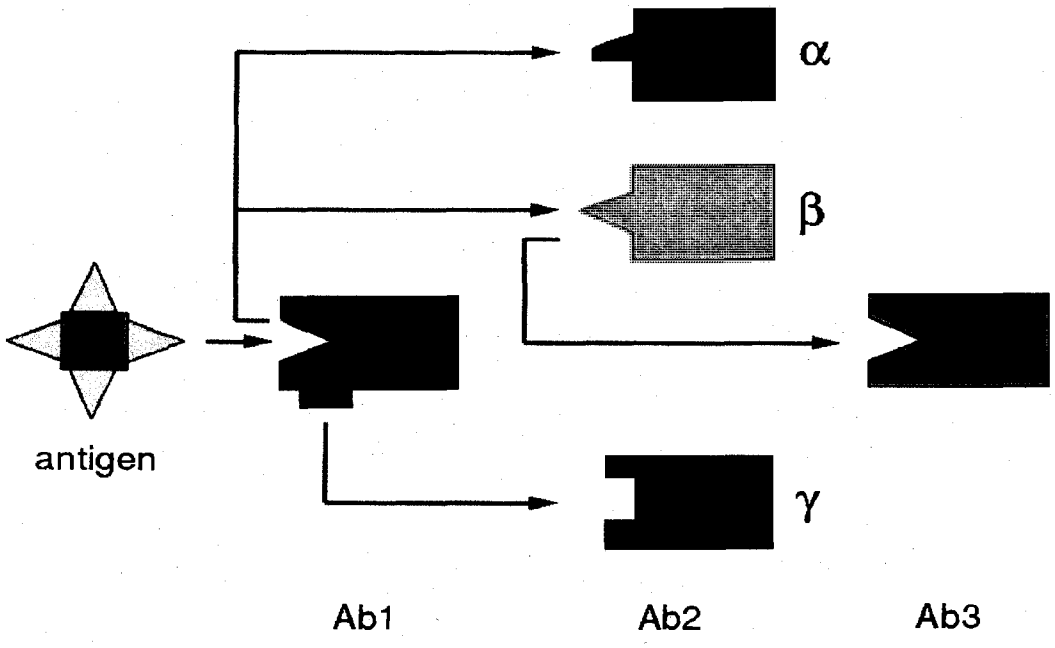


**Figure 2.1. Idiotypic network.** In an idiotypic network, the first generation of antibodies that are raised against an antigen is termed Ab1. Ab1s can be used as immunogen to generate second generation antibodies, Ab2s, which are categorized into α, β, and γ, depending on the epitope they recognize on Ab1. The Ab2β antibodies are considered true mimics of the original antigen, and can be used as immunogen to generate third generation antibodies, Ab3s. Some of these Ab3s will be Ab1-like, and able to mediate binding to the original antigen.

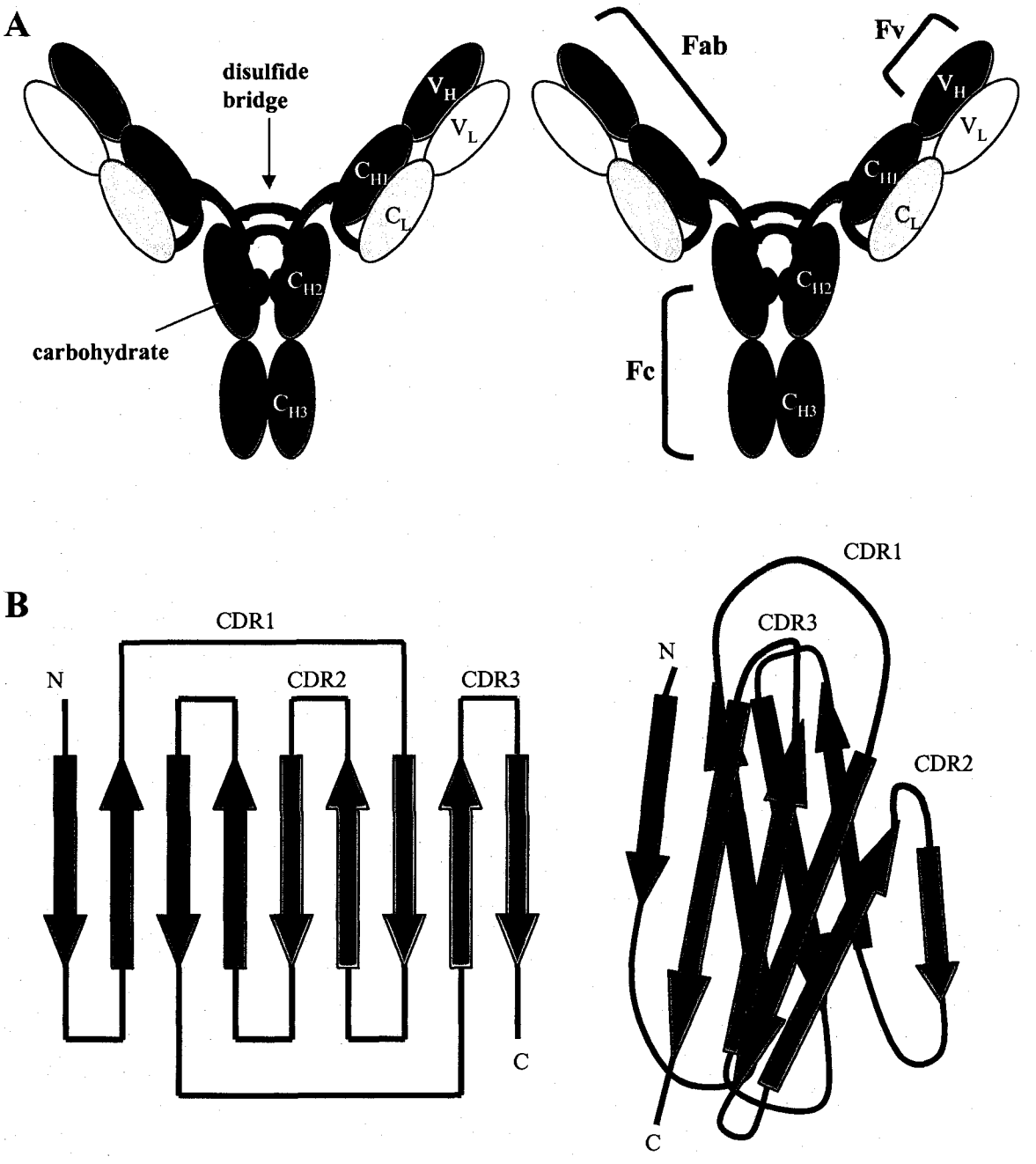


**Figure 2.2. Antibody Structure. A.** Schematic diagrams of a human IgG1 antibody molecule. The heavy chains (shades of blue) and the light chains (shades of yellow) are paired and held together by hydrophobic forces, a few hydrogen bonds and disulfide bridges. Variable and constant domains are indicated, as well as the Fv, Fab, and Fc structures. **B.** Topology diagram and immunoglobulin fold diagram for a variable domain. Two antiparallel β sheets, depicted in different shades of green, are sandwiched to form a barrel. The CDRs are labeled and depicted in red.

The constant domains define the class of the chains. In the human genome, the L chains have two classes, κ and λ, both of which can combine with any of the H chains. The H chains have five classes, α, δ, ε, γ and μ. These different H chain classes can present either 3 or 4 constant domains and are differentially glycosylated (24). It is the H chain domains, regardless of the L chain that they are paired with, that define the isotype of the antibody: IgA, IgD, IgE, IgG, and IgM respectively, and that define the effector functions available to an antibody. Some antibodies, such as the IgG, can take on different subclasses, which differ slightly from each other mostly at the hinge region.

The constant and variable domains have a similar three-dimensional structure. The domains consist of around 110 amino acid residues and form β-barrels composed of two β-pleated antiparallel sheets linked by a disulfide bridge, with strands connected in a greek key pattern (Figure 2.2B) (25). This fold is now commonly referred to as the 'immunoglobulin fold' and has been found in many other proteins. In the variable domains, the loops that are responsible for providing different specificities are termed 'hypervariable loops', to refer to the fact that comparison of the sequences of many antibodies shows a high amount of variation in these regions (26). These loops are also referred to as 'complementarity determining regions' or CDRs (27, 28). The CDRs of the L chain are termed L1, L2, and L3 whereas the CDRs of the H chain are termed H1, H2, and H3. The CDRs vary in size and in sequence between different antibodies, and contain 'hotspots' that represent target positions for mutation. They can possess a limited number of conformations that are termed 'canonical structures' (29-31). However, there is no strict classification for CDR H3; it has high sequence variability (32-34), high variability in length, and its conformation is dependent on local environment. The rest of the variable domain consists of 'framework'

regions which can participate in antigen binding but whose role is mostly to provide support to the CDRs. The layer of framework residues that supports the CDR conformations and dispositions and plays an important role in fine-tuning the fit of an antibody to an antigen is specifically referred to as the 'Vernier' zone (35).

All of the preceding structural features apply to antibodies defined as 'conventional antibodies'. Some species, such as members of the camelids (36) and certain species of sharks (37), have evolved with both conventional antibodies and a second, different kind of antibody. These second antibodies are devoid of L chains and have thus been termed 'heavy chain antibodies' (HCAbs). HCAbs are generated separately from conventional antibodies (38-40) and are found to lack the $C_{H1}$ domain (Figure 2.3) (36, 41-43). The antigen-binding site in HCAbs is thus contained within one variable domain, referred to as the $V_HH$, and the three H chain CDRs replace the Fab of the conventional antibody (44). The $V_HH$ has developed means of stabilizing itself without the help of the usual $V_L$ partner: it possesses more hydrophilic residues on its surface at key residue positions and has developed a longer CDR H3 that can fold over and shield any hydrophobic patches (45). This extra long CDR H3 is also thought to make HCAbs particularly well suited for reacting with crevasses, such as enzyme binding sites (46-49).

*Working With Antibodies*

Antibodies are a useful and common vehicle for studying protein-protein and protein-carbohydrate interactions. When working with antibodies, the antibody class of choice is the IgG since it is the most abundant antibody in plasma. This is the antibody that will be referred to in the following paragraphs as it is the class used in all of the studies described in later chapters. IgGs can be isolated from non-immunized animals, in which

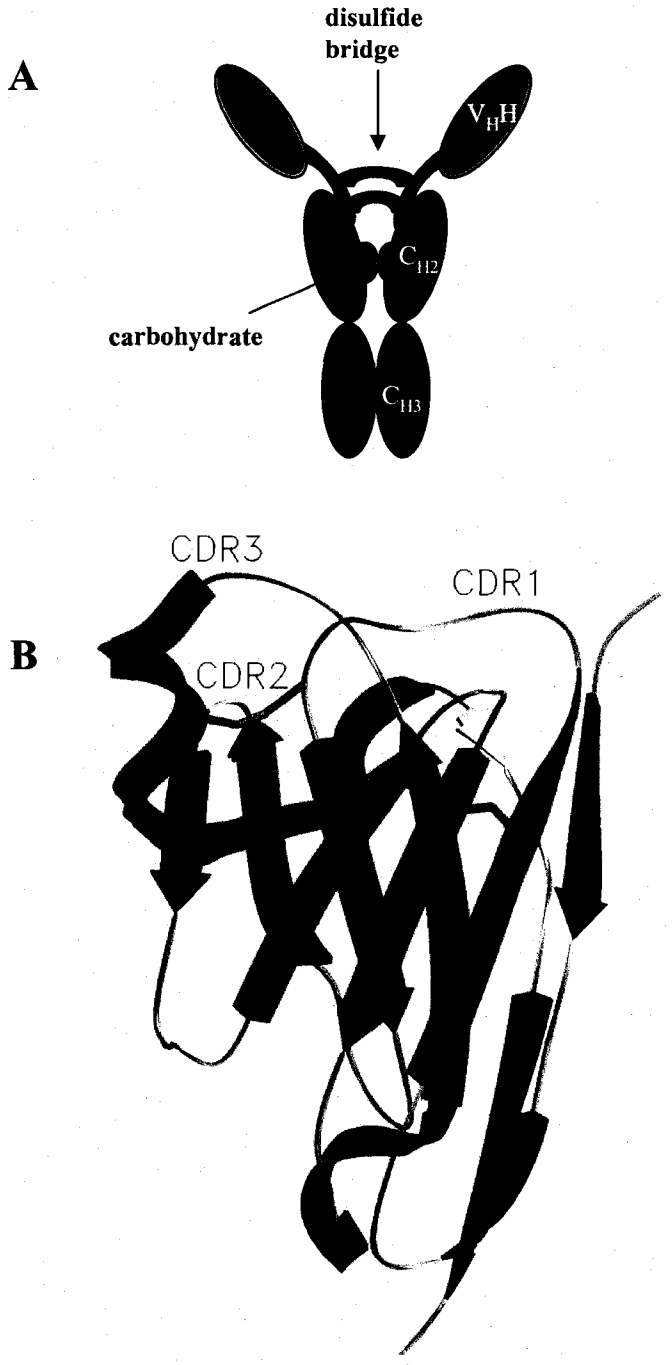


**Figure 2.3. Heavy-chain antibody structure. A.** Schematic diagram of the HCAb. These antibodies have no light chains and are missing the $C_{H1}$ domain. The antigen-binding site is provided by one variable domain, termed the $V_HH$. **B.** Ribbon diagram of a $V_HH$ highlighting the position of the CDRs. Figure prepared with Setor (50).

case they are referred to as 'naïve', or they can be isolated from immunized hosts. Isolation of IgGs used to consist of their purification from plasma. This led to isolation of IgGs with multiple specificities and these were termed 'polyclonal antibodies'. For some applications however, it is necessary to isolate IgGs with one distinct specificity. Such a process became available with the invention of 'hybridoma technology' that allows for eternalisation of B cell clones secreting one type of IgG through their fusion with myeloma cells. The eternalized clones can be kept in culture through several passages and secrete only the antibody of interest, which is termed 'monoclonal antibody' (mAb) (51).

For many applications, monoclonal antibodies have to be purified from contaminating proteins in ascites fluid. This can be easily achieved using affinity matrices such as bacterial protein A and protein G matrices (52-55). These bacterial proteins recognize the Fc portion of antibodies with affinities that vary according to the species and subclass of the IgG (56). Other affinity matrices include the bacterial protein L matrix that can bind the Fab portion of antibodies through interaction with the L chain (57-59). Beyond the use of affinity matrices, IgGs can also be purified using other chromatography techniques such as ion exchange, metal ion affinity, and hydrophobic interaction chromatography.

For certain experiments as well as structural studies, it is desirable to work with smaller fragments of antibodies, as full antibody molecules are known to be quite flexible (60). There are enzymes that can digest full IgGs into specific antibody fragments, enzymes including papain, pepsin, and elastase. Papain is commonly used to digest the H chain of the antibody at the hinge region, and generates the two Fab and the Fc fragments. Pepsin can be used to generate other types of fragments: the F(ab')2 fragment, where the two Fabs are still

linked by disulfide bridges in the hinge region, is generated with short digest times while longer digest times can be used to generate Fv fragments, fragments containing only the $V_H$ and $V_L$ domains. The Fc fragment is sensitive to pepsin digests and is sometimes completely fragmented (Figure 2.4).

*Antibody Engineering - Formats*

With the advances in engineering technology, it has now become possible to generate antibody fragments without the need for purification and digest of full-size antibodies. The gene of the antibody of interest can be designed into many different fragment types and incorporated into different vectors for expression in diverse systems (61-64). Advantages of designing smaller fragments of antibodies are well known, especially, for example, in the design of immunotherapeutic agents where smaller fragments signify better distribution and tumor penetration. Common antibody fragment formats include the single-chain antibody fragment or scFv, in which the genes for the $V_L$ and the $V_H$ are combined into a 'single chain' using a linker. The variable domains can be connected in both the $V_L$-$V_H$ and the $V_H$-$V_L$ orientation, and the linker used can be of various lengths and sequences. The scFv is thus produced from one gene and retains the affinity of the parent antibody (65). The linker of the scFv can be exploited to favor monomers or multimers; it has been shown that longer linkers will favor monomers whereas shorter linkers will force the formation of dimers or trimers (66-69). However, there are some disadvantages associated with the scFv format. Some variable domains possess an intrinsic lack of stability and a difficulty to fold that will affect the production of the scFv (70). The production will also be affected by the highly dissociative nature of the scFv (71), which can be further enhanced depending on the characteristics of the linker (66, 69, 72-75). ScFvs

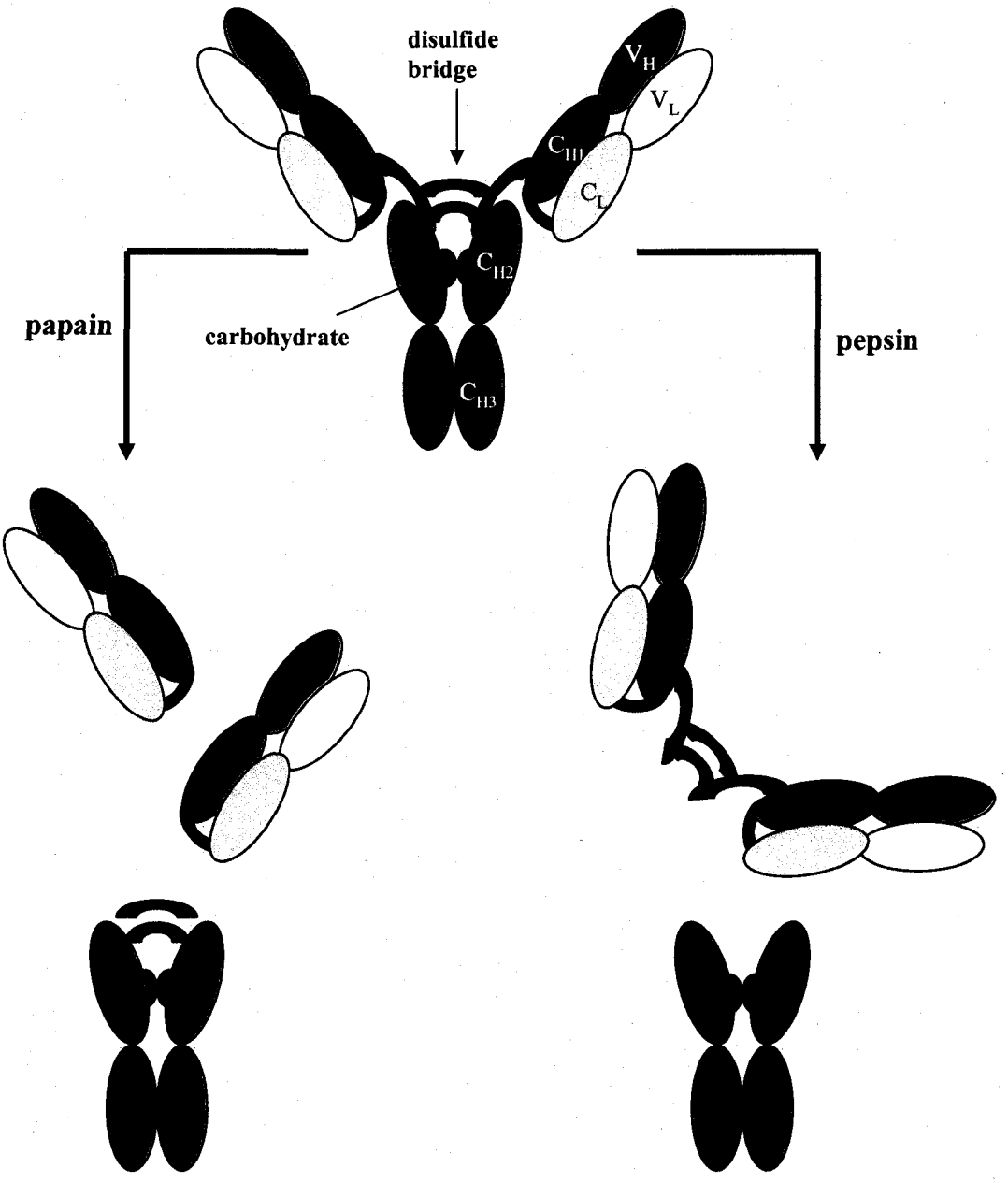


**Figure 2.4. Antibody digest.** The antibody molecule can be digested into smaller fragments using enzymes such as papain and pepsin. With papain, the fragments generated include the Fabs and the Fc fragments, whereas with pepsin, the $F(ab')_2$ and the Fc fragments are generated. Upon longer incubation with pepsin, the $F(ab')_2$ can be further digested into Fv fragments and the Fc can be completely broken down.

that are produced in the soluble fraction require their linkers to be digested after purification to prevent aggregation, a common effect for the scFv at high protein concentrations (66, 67, 76-80). Another popular format is the disulfide-stabilized antibody fragment or dsFv. For the dsFv, the $V_L$ and $V_H$ are produced separately as inclusion bodies, refolded and recombined in a 1:1 ratio. Although there exists an intrinsic difficulty in refolding proteins and pairing accuracy cannot be well controlled, the dsFv remains popular since the engineered disulfide bond not only stabilizes the pairing of the domains (81, 82) but also prevents the formation of multimers. Many other formats of antibody fragments exist: examples include the scFv-Fc, an scFv connected to an Fc fragment, which provides ease of purification using bacterial affinity matrices (83); the scAb, an scFv bearing a $C_L$ domain, that allows formation of stable dimers (84); and the scdsFv, an scFv stabilized by an engineered disulfide bond between the variable domains, which combines the advantages of the scFv and the dsFv all in one protein (85-87).

The $V_HH$ of HCAbs can also be produced as an engineered fragment, and is termed single-domain antibody or sdAb. SdAbs can also be designed from conventional antibody variable domains (88). The sdAbs from conventional antibodies are not very soluble (89), so mutation of the region corresponding to the $V_L$-$V_H$ interface provides a means to increase their solubility. Such mutation processes are referred to as camelization (90), when key mutations found in camel HCAbs are applied to the sequence of the conventional domain, or llamalization (MacKenzie, unpublished results), when those of llama HCAbs are applied. Another, newer, antibody format termed the 'pentabody' exploits the compactness of the sdAb to generate a multivalent fragment with increased avidity. The pentabody is generated by the fusion of sdAbs to the B subunit of the *E. coli* O157:H7 verotoxin 1 in order to

generate a pentamer of sdAbs (91). The process of 'pentamerization' does not alter accessibility to the sdAb binding-site and has been shown to provide an avidity gain of 3-4 fold (91).

*Antibody Engineering - Expression*

Antibody fragments can be expressed in many different hosts, such as mammalian cells (92, 93), insect cells (94), plants (95), in vitro translation systems (96), bacterial cells and yeast cells, with a wide range of expression levels. The most popular systems are bacteria and yeast cells which provide both ease and cost effectiveness.

In bacteria, *Escherichia coli* (*E. coli*) represents by far the most widely used host (62, 97). Many different strains and compatible vectors exist that allow for selection of optimal features for production of any given protein. Strains of *E. coli* have been engineered for maximum expression of foreign proteins such as antibody fragments. In some instances, certain genes have been mutated, such as those of native proteases that could digest the expressed antibody fragments. In other instances, genes have been added to provide additional features that might be beneficial to expression of antibody fragments, genes such as those of chaperones and of rare tRNA codons. *E. coli* expression vectors are also available with a wide variety of features and promoters. Most include tags that serve for purification and/or detection purposes (98), popular tags including the histidine tag (99) and the c-myc tag (100). Others might contain secretion leaders to target expression to a given compartment such as the periplasm (101-103) or fusion proteins to increase solubility of the antibody fragment (104). In addition to the various host strain and vector combinations that are available, expression in *E. coli* can be adjusted using many different strategies, including change of medium, growth temperature (105) and supplementation with various additives.

In the case of antibody fragments, the most important factor is that of secretion to the periplasm, as the reductive environment of the *E. coli* cytoplasm does not allow for formation of the disulfide bridges that are important in the stability of the fragments. But even in the periplasm environment, most antibody fragments are produced as inclusion bodies (65, 70, 72, 106-109). This occurs not only because of the intrinsic instability of the fragments and features of the primary sequence (110, 111), but also due to the limited export process (112) and high protein concentration in the periplasmic lumen (113, 114). These later limiting factors can be reduced by addition of non-metabolizable sugars to the culture medium (113-115). Once an antibody fragment is produced in inclusion bodies, refolding protocols are required to regenerate the native three-dimensional structure. These protocols often result is low yields of functional protein due to the high level of irreversible protein aggregation (116) and to the inherent difficulty of reforming the correct disulfide bridges in antibody fragments (76, 117). Some strategies are being developed to address these expression issues, strategies such as evolutionary mutagenesis and rational mutagenesis. Although some initiatives have showed limited success, most are still in their infancy and not well understood.

A second popular system for the expression of antibody fragments is that of yeast cells, particularly the methylotropic yeast *Pichia pastoris (P. pastoris)*. This host presents many advantages as it possesses the general features of eukaryotic hosts combined with fast and aerobic growth (118, 119), a strong and tightly regulated promoter (120, 121) as well as the ability to reach high cell densities (122) and target the expression of foreign proteins to the cytoplasm or to secretion. Like in bacteria, expression of foreign proteins can be adjusted using simple strategies such as modification of culture medium, expression

temperature, and induction level. The *P. pastoris* system has been used with success in the expression of antibody fragments, with some fragments being expressed at levels reaching upwards of 50 mg per liter of culture (123, 124).

*Antibody Engineering – Display Technologies*

The possibility of isolating and expressing antibody genes also led to the development of display methodologies that allowed for expression of a multitude of antibody fragments with diverse specificities and subsequent selection of antibodies with desired specificities (125-127) or desired stability (128-130). Methodologies such as phage display (131), ribosome display (132), yeast display (133), and bacterial display (134) are now routinely used to isolate antibody fragments of desired specificity. The libraries of antibodies used in these technologies can be designed from naïve (125, 126, 135, 136), immune (137) or even semisynthetic (127, 138) and fully synthetic (139) sets of antibody genes, with naïve and synthetic libraries possessing antibodies with more moderate affinities (125, 140).

One of the more popular display technologies used currently is that of phage display. In phage display technology, antibody genes are fused to viral coat protein genes of bacteriophage in order to allow expression of the antibody fragments on the surface of the phage (Figure 2.5A) (141). The library of phage-displayed antibodies is used in a biopanning process to select for antibody fragments with specific affinities (142). In the biopanning process, selection of antibody fragments able to bind a chosen antigen is undertaken; the chosen antigens may be immobilized in wells, such as protein and carbohydrate antigens, or may be used in suspensions, such as cultured cells (139, 143). Phage displaying antibody fragments that are able to bind the chosen antigen are captured,

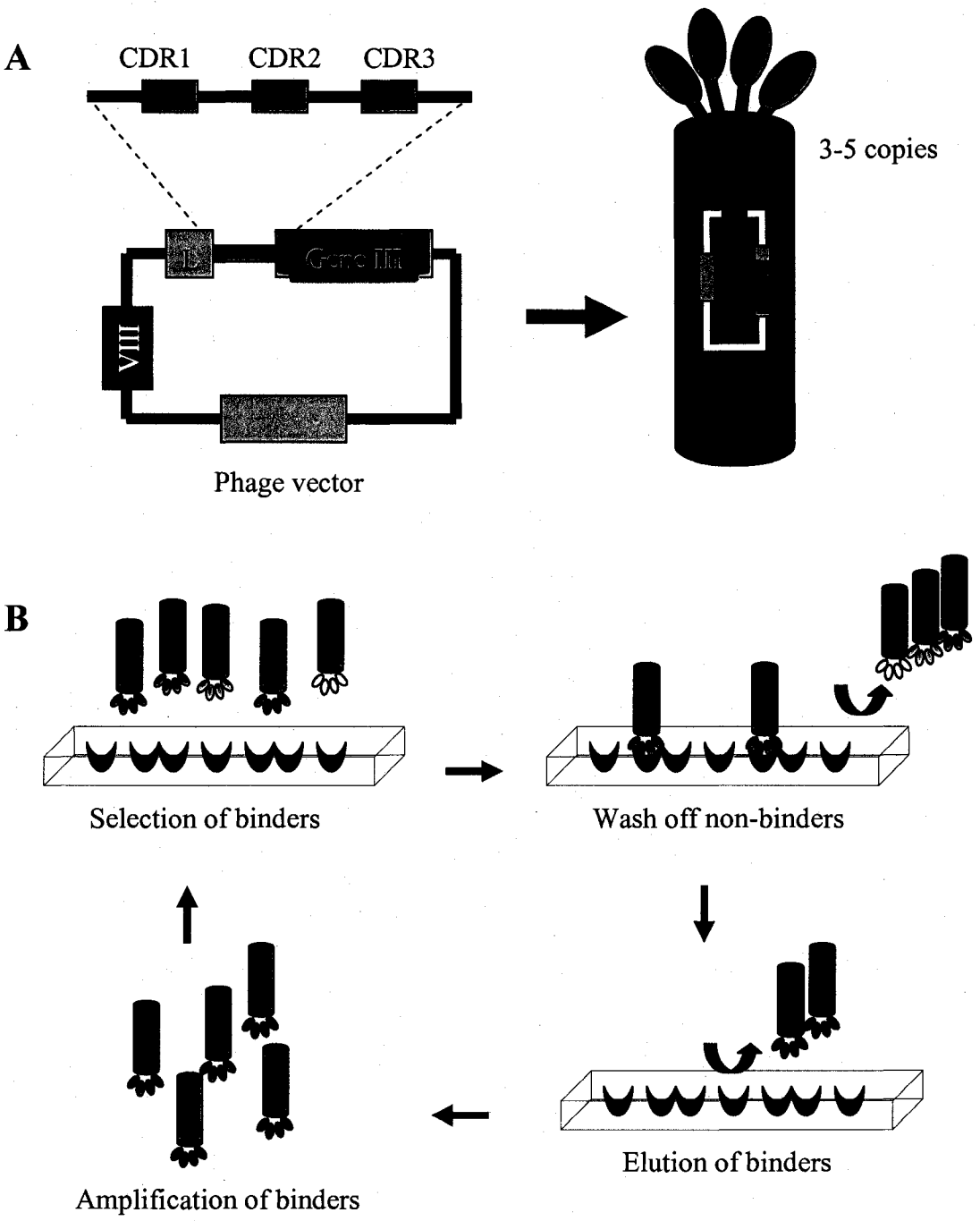


**Figure 2.5. Phage display and biopanning. A.** Antibody fragments are inserted into a phage vector and are linked to gene III for expression of the fragments on the tip of the phage. **B.** Biopanning of a phage library includes incubation of the phage antibody library in a well coated with the antigen of interest followed by a wash to remove the non-specific phage-antibodies, recovery of binders, and amplification of binders for further rounds of panning.

recovered and amplified for further rounds of selection (Figure 2.5B). These steps ensure that binders are enriched with each further round of selection. But, selection results are also dependent on experimental conditions such as library size (144) and stringency of selection conditions (145).

*Antibody-Antigen Interactions*

Study of antibody structure is mostly centered about understanding the mechanism for recognition, specificity and/or cross-reactivity. This allows for a better knowledge of how the immune system works, and how it fails. Antibody binding sites are available in a variety of shapes, with grooves, pockets, and protruberances, and can be referred to as 'paratopes'. They are shaped by the CDRs. Parts of antigens that are recognized and bound by antibodies are also termed 'epitopes'. Epitopes can be linear or continuous, or can be composed of residues from different parts of a chain and be termed 'conformational' (146). An epitope can either fit in an antibody binding site without the requirement for rearrangement of the CDRs, in which case the recognition is classified as a 'lock-and-key' mechanism, or may require movement of the main chain and side chains to obtain a perfect fit, in which case the recognition is classified as an 'induced-fit' mechanism (147). It is thought that primary response antibodies use the 'induced-fit' mechanism whereas high-affinity antibodies that are very specific for their antigen use the 'lock-and-key' mechanism (148). In the binding site, numerous types of interactions stabilize the complex between antibody and antigen: hydrophobic forces, van der Waals contacts, electrostatic interactions and hydrogen bonds (149). In the case of full antibody molecules, which display bivalency, and antibody fragments such as the pentabody that display higher levels of multivalency,

both avidity and affinity come into play. The avidity, or strength of binding, is not dependent only on the affinity of each site and is greater than the sum of the affinities.

The measure of affinity is an important part of antibody characterization. The reaction of an antigen with an antibody in a 1:1 complex can be described with the following equation:

$$Ag + Ab \underset{k_{off}}{\overset{k_{on}}{\rightleftharpoons}} AbAg$$

where the affinity constant ($K_D$) is defined by

$$K_D = [Ab][Ag]/[AbAg]$$

$$K_D = k_{off}/k_{on}$$

Methods commonly used to measure the affinity of an antibody for its antigen include equilibrium dialysis, fluorescence quenching, titration calorimetry, and ELISA. A more precise means of measuring affinity is that of surface plasmon resonance or SPR (150, 151). SPR utilizes the optical phenomenon that arises in thin metal films under conditions of total internal reflection (152). SPR experiments are conducted in real time and are commonly done using BIAcore technology (153). In these BIAcore experiments, either the antigen or the antibody is immobilized on a sensor surface and the corresponding reagent is flowed over the sensor surface (Figure 2.6A). Binding events lead to mass changes on the sensor surface and are measured as changes in the refractive index of the sample over time. These changes of refractive index produce shifts in the resonance signal that are proportional to the

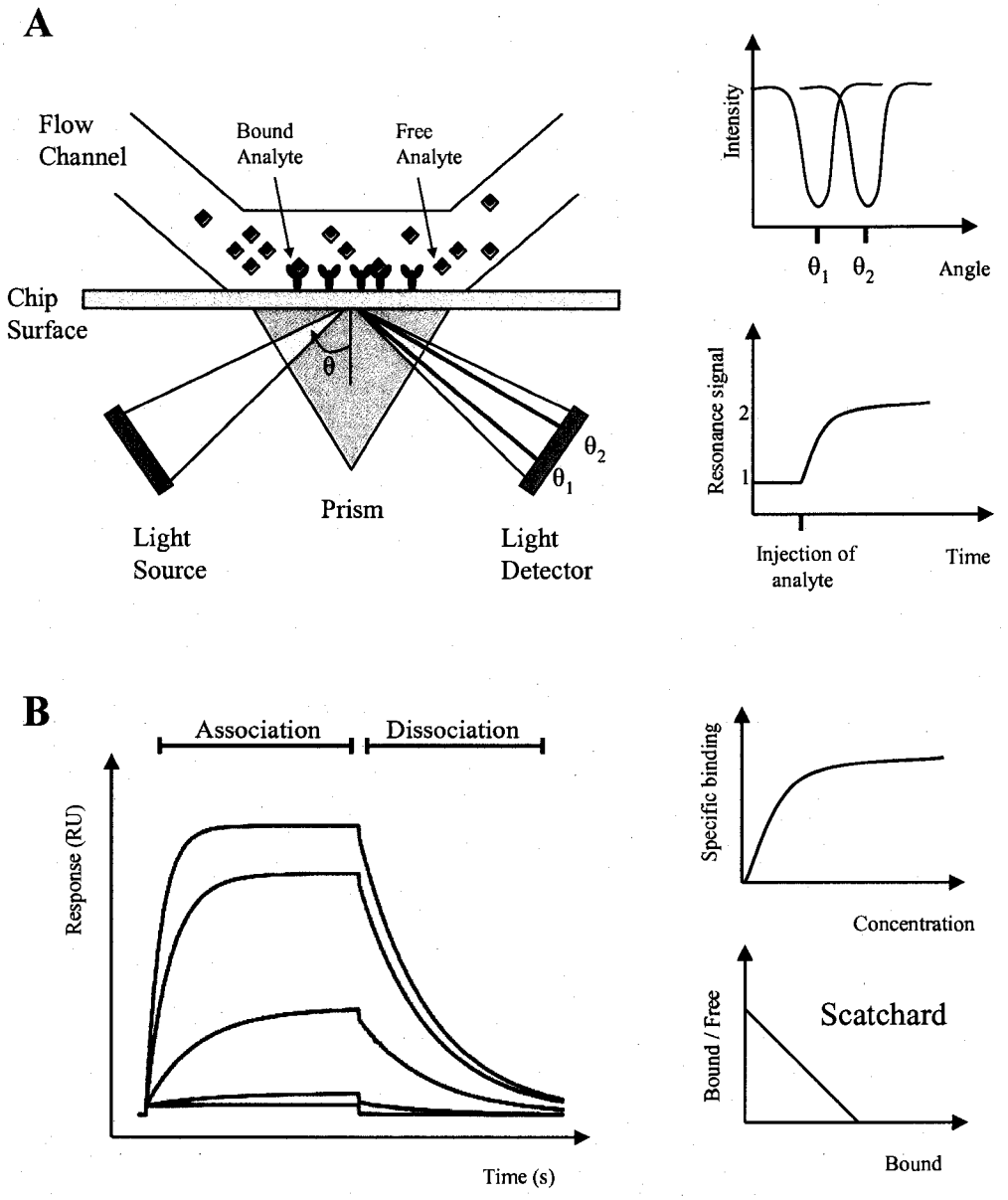


**Figure 2.6. SPR and BIAcore analysis. A.** Schematic diagram of an SPR experiment. Antibodies are immobilized on a sensor surface and analyte is flowed over this surface. Binding events are measured as a change in refraction index, and are monitored over time to yield a sensorgram. **B.** Results obtained during a BIAcore analysis. To the left is an example of overlaid sensorgrams where association and dissociation of analyte to antibodies is monitored over time with different concentrations of analyte. To the right are the steady state affinity plot and Scatchard plot that are generated from the overlaid sensorgram data.

mass that is bound to the sensor surface, where one resonance unit (RU) corresponds to a density of 1 pg/mm$^2$. The continuous change in resonance signal, which represents a record of the progress of association/dissociation of the antibody-antigen complex in real time, is output as a sensorgram. These sensorgrams are recorded over a range of flowed reagent concentrations (Figure 2.6B).

For weak interactions, the sensorgrams show a rapid rise to equilibrium after injection of the flowed reagent and rapid dissociation when the injection is terminated. Sometimes the interaction is so weak that the analyte needs to be present in high concentrations in the flow buffer and this can lead to bulk changes in the RUs recorded. For data generated for weakly interacting pairs, Scatchard analyses can be used to extrapolate the affinity constant (154). In Scatchard analyses, the ratio of concentrations of one analyte free and engaged in complex is plotted against the concentration of this same analyte, and this generates a linear graph where the affinity constant is given by the slope of the graph, with $K_D$ = -1/slope (Figure 2.6B). In the cases where stronger interactions are measured, the on- and off-rates can be extrapolated and the ratio of these two values provides the affinity constant. When the data obtained are of high quality, a simultaneous curve fitting analysis can be performed. This 'global fitting' constrains the kinetic parameters ($k_{on}$ and $k_{off}$) to single values that best fit all sensorgrams to yield the estimate of $K_D$.

# CHAPTER 3

# ANTIBODY RECOGNITION OF A TUMOR ANTIGEN: MR1 dsFv IN COMPLEX WITH EGFRvIII PEPTIDE

## INTRODUCTION

To understand the significance of antibody recognition of EGFRvIII, it is necessary to briefly review the biochemistry of this important receptor.

*Epidermal Growth Factor Receptor*

The human ErbB family of receptor tyrosine kinases consists of four members: HER-1 [epidermal growth factor receptor (EGFR) or erbB-1], HER-2 (Neu or erbB-2), HER-3 (erbB-3), and HER-4 (erbB-4) (155, 156). These receptors play a crucial role in regulating cellular processes such as proliferation, differentiation, motility, and survival. EGFR is expressed on most cell types, particularly those of epithelial origin (e.g. skin, liver, and gastrointestinal tract), but is not found on hemopoietic cells (157). These cells express up to 40,000 to 100,000 EGFRs per cell (156); the EGFRs are randomly distributed at the cell surface (158-160) and undergo rapid lateral (161) and rotational (162) diffusion.

EGFR is a 170 kD trans-membrane protein that has 12 potential N-glycosylation sites (163-165). The oligosaccharides found at these glycosylation sites are thought to be essential for receptor insertion into the membrane as well as for ligand-binding and tyrosine kinase activity (165, 166). The 1186 residues of EGFR are divided into an extracellular domain, a transmembrane domain, and an intracellular domain (Figure 3.1) (164, 167). The extracellular domain has four subdomains: subdomain I is a ligand-binding domain also termed L1 comprising residues 1-165, subdomain II is a cysteine-rich domain also termed CR1 or S1 comprising residues 166-309, subdomain III is a second ligand-binding domain termed L2 comprising residues 310-481, and subdomain IV is a second cysteine-rich domain termed CR2 or S2 comprising residues 482-621 (168). Subdomains I and III are right-

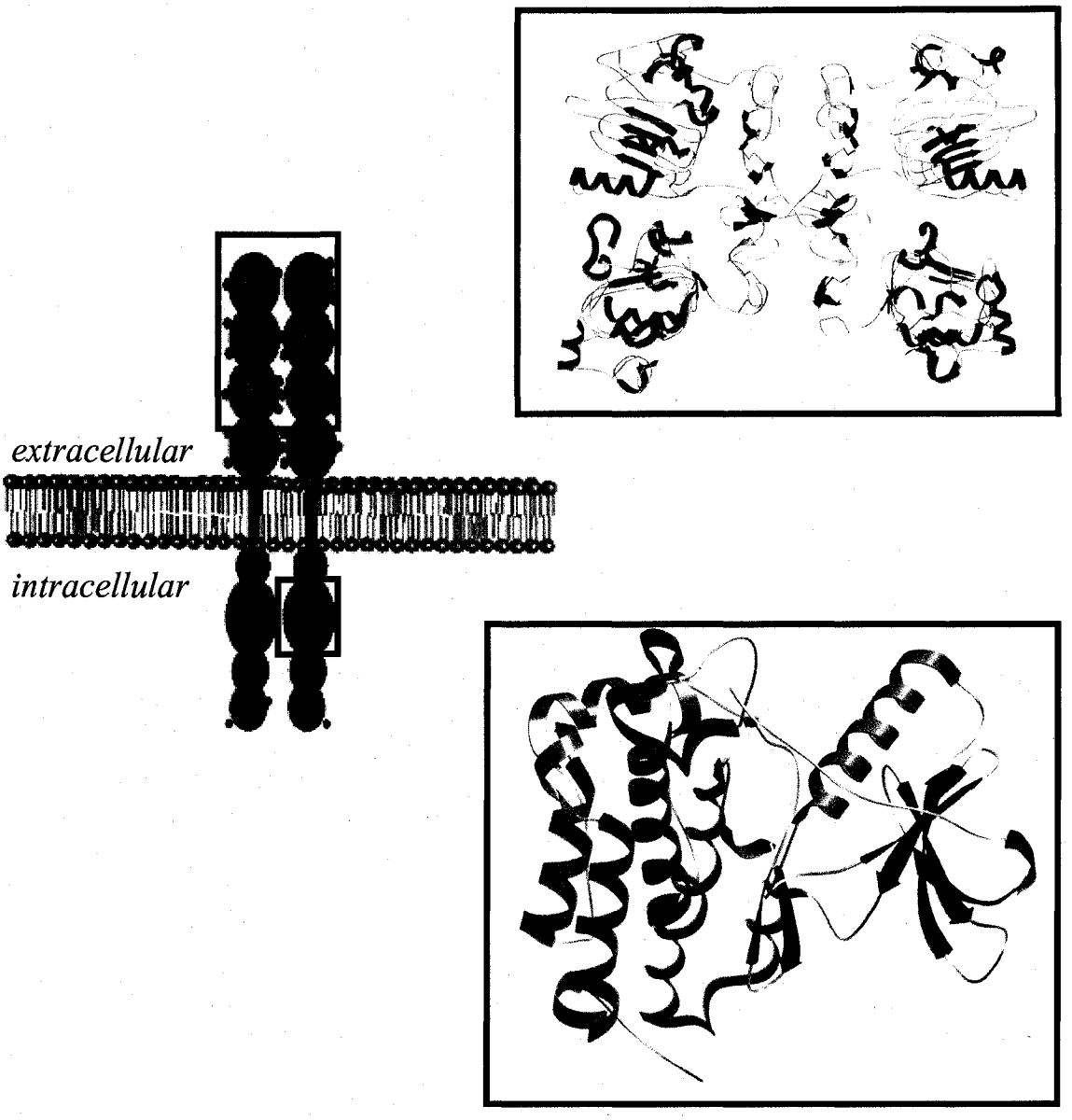


**Figure 3.1. Epidermal growth factor receptor domain organization.** Schematic diagram depicting a dimer of EGFR. Extracellular sub-domains L1, S1, L2, and S2 are colored in shades of green, red spheres represent *N*-glycosylation sites, transmembrane domains are grey cylinders, intracellular sub-domains are colored in shades of brown, and grey spheres represent autophosphorylation sites. Crystal structure of a dimer of sub-domains L1, S1, and L2 (PDB ID 1MOX) is rendered in green in the top window – corresponding sub-domains have been highlighted in the schematic diagram. Crystal structure of the tyrosine kinase sub-domain (PDB ID 1M14) is rendered in orange and red in the bottom window – corresponding sub-domain has been highlighted in the schematic diagram. Crystal structure pictures prepared with Setor (50).

handed β-helices that resemble leucine-rich repeat proteins (169-171) and play minor (subdomain I) and major (subdomain III) roles in ligand binding (172-176). Subdomains II and IV together contain approximately 22 disulfide bonds (177) and are thought to give the extracellular domain a rigid, two-lobal structure (178). Located between the transmembrane and intracellular domains is the juxtamembrane region that plays a regulatory function in receptor sensitization and down-regulation. This region comprises three phosphorylation sites (167), one of which has been shown to be associated with attenuation of tyrosine kinase activity (179, 180).

EGFR can be activated by several ligands such as the epidermal growth factor and transforming growth factor alpha (181). These ligands bind to the receptor in a 1:1 stoichiometry (182). Following ligand binding, the receptor-ligand complexes diffuse in the plane of the membrane and aggregate to form clusters where receptor dimerization occurs (158-162, 183-186). The receptor dimers display a 2:2 receptor:ligand stoichiometry (187-190) and are the primary signaling system for EGFR (191, 192). The crystal structure of the extracellular domain of EGFR in complex with ligand reveals that each ligand interacts with subdomains I and III of only one receptor, which is consistent with biochemical data (173, 174, 176). Receptor dimerization is followed by autophosphorylation of tyrosine residues within the intracellular domain (156, 183, 193-195) resulting in receptor activation and subsequent mobilization of signal transducers and activators of transcription (196, 197).

Following continuous stimulation of EGFR by ligand, the receptor loses its ability to dimerize (198) and the signal is attenuated. Attenuation of the signal can also be achieved by receptor internalization and down-regulation (156). Following internalization, and

possibly several rounds of recycling to the surface (199, 200), the receptors are degraded by lysosomal enzymes (156, 201-204).

*EGFR and Cancer*

EGFR is known for its proto-oncogenic properties (205, 206). Initial studies revealed that some cancer cells possess increased concentrations of EGFRs within their membranes due to overexpression (207). Overexpression of EGFR has been associated with cancers of the breast (208), lung (209), brain (210, 211), prostate (212), neck (213, 214), colon (215), pancreas (216), kidney (217, 218), and ovary (215, 219). The percentage of tumors that overexpress EGFR varies by tumor type and is thought by many to be inversely correlated with disease prognosis (155).

EGFR has been proposed as a target for cancer therapy (155, 211, 220-228). It has been postulated that blocking the binding of ligand to the receptor may prevent EGFR activation and thus inhibit tumor growth (228). EGFR blockers currently in development include immunotoxins, various ligand conjugates, and anti-EGFR mAbs (229, 230). Anti-EGFR mAbs are of particular interest as they have been shown to induce down-regulation of the receptor (231) and inhibit the growth of the cancerous cells (232-235). Unfortunately, most of these mAbs have also been shown to target normal tissues (236).

*Variants of EGFR in Cancer*

The overexpression of EGFR that is observed in some cancer cells has been found to be the result of an increase in the transcription of the EGFR gene. In some cases, this gene amplification is associated with alternate splicing of some mRNA transcripts resulting in the production of variant EGFRs (206, 237-241). There are seven reported classes of variant

EGFRs: class I mutants lack the extracellular domain; class II mutants contain an in-frame deletion of 83 residues in the extracellular domain that does not involve the ligand-binding site; class III mutants contain an in-frame deletion of 267 residues in the extracellular domain that includes the ligand-binding site; class IV and V mutants carry deletions in the cytoplasmic domain; class VI and VII mutants have extracellular domain deletions that coexist with the intracellular domain deletions of class IV and V, respectively. These variant EGFRs display ligand-independent activation and spontaneous oligomerization accompanied by receptor tyrosine autophosphorylation (242, 243).

The most common EGFR variant is the class III mutant. This class III mutant is also referred to as EGFRvIII, de2-7EGFR, and ΔEGFR (244). EGFRvIII not only arises due to alternative splicing of the mRNA (245), but can also result from a genomic deletion during the amplification process (Figure 3.2) (246, 247). EGFRvIII contains an in-frame deletion of 801 nucleotides that spans exons 2 to 7 (246, 248). This deletion results in the loss of 267 residues within the extracellular domain that includes the ligand-binding subdomain I and a portion of subdomain II (249). In addition, the deletion generates a novel glycine residue at the fusion junction site (position 6 between residues 5 and 274) (241, 250, 251). The result is a 145 kD protein that contains a unique junctional peptide at its N-terminus (244), is constitutively activated and unresponsive to ligand (243, 252-254).

As mentioned previously, dimerization of EGFR is required for autophosphorylation and receptor activation. In contrast, some studies suggest that receptor dimerization is not a prerequisite for EGFRvIII activation (243, 245, 255, 256). In addition, studies have shown that the extent of EGFRvIII phosphorylation is less than that of the ligand-activated EGFR (252, 256, 257). This decreased level of phosphorylation is sufficient to trigger signaling,

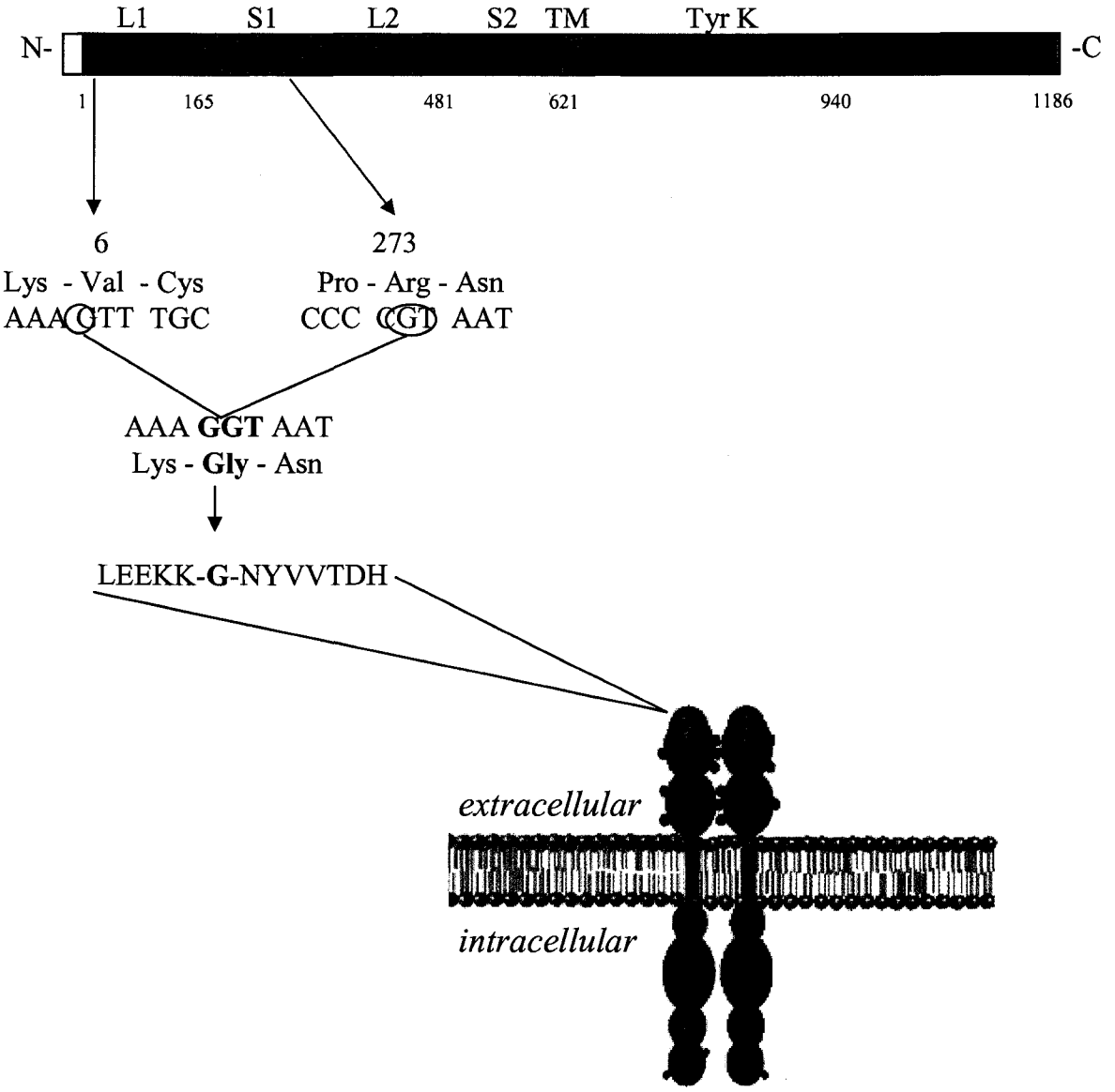


**Figure 3.2. Epidermal growth factor receptor variant III.** Schematic diagram illustrating the mRNA for the native EGFR, with sub-domains color-coded according to the scheme in figure 3.1. The EGFRvIII is generated when residues 6 through 273 of the extracellular domain are deleted at the gene level or due to alternative splicing of the mRNA construct. The deletion occurs with fusion of normally distant protein sequences and yields a novel glycine residue at the junction site. The deletion in the extracellular domain of EGFRvIII leads to a receptor that is unable to be activated by ligand and is constitutively activated.

but is insufficient in inducing receptor down-regulation through endocytosis (243) thus resulting in unregulated cellular growth. Further evidence of the oncogenic properties of EGFRvIII is that many cell lines undergo malignant transformation following transfection with the receptor (243, 252, 258, 259). As an example, transfected cells exhibit tumor characteristics such as poor adherence, enhanced motility, disordered growth pattern, lack of growth inhibition, and decreased apoptosis (252, 254, 260-262). EGFRvIII was first reported in human glioblastomas (263), and has since been shown to be present in other human cancers, including breast (258), ovarian (247), lung (247), brain (241, 263-267), and prostate (268). EGFRvIII has not been detected in normal tissues (244).

*Cancer Treatments Targeting EGFRvIII*

Since EGFRvIII is isolated to cancer cells, it represents a promising target for immunotherapy (244). Some Abs that have been raised against EGFR are capable of recognizing both over-expressed EGFR and EGFRvIII (269). To specifically target EGFRvIII, antibodies are raised against the fusion junction sequence. This fusion junction sequence, which has been termed Pep3 (270), has the sequence LEEKKGNYVVTDHC which is specific to EGFRvIII.

Vaccination of animals with the Pep3 peptide has been shown to successfully generate anti-tumor B-cell lines and reduce tumor initiation (271-273). Polyclonal and monoclonal antibodies have both been isolated from animals vaccinated with Pep3 alone or in combination with tumor cells bearing EGFRvIII, and these antibodies have been shown to be specific for the mutant receptor (250, 257, 265, 270). Some of these antibodies demonstrate the ability to inhibit cellular proliferation, induce cellular-dependent cytotoxicity and ADCC *in vitro* and *in vivo* (274), resulting in antibody-mediated

endocytosis of EGFRvIII transformed cells (251). Immunotoxins generated from these antibodies have been shown to target EGFRvIII-bearing cells and to exhibit selective toxicity against them (275). Other means of targeting EGFRvIII include the use of anti-EGFRvIII antibodies to generate anti-idiotypic antibodies that mimic the mutant receptor. These anti-idiotypic antibodies have previously been used in vaccine preparations and have been shown to generate a response against EGFRvIII (276, 277).

One of the most investigated mAbs against EGFRvIII is MR1. This mAb was isolated from an scFv library constructed from a mouse immunized with both Pep3 and purified EGFRvIII. MR1 is able to bind to both Pep3 and surface EGFRvIII, with $K_D$s of 22 nM and 11 nM, respectively (278). MR1 has been used in the construction of several immunotoxins, with all but one showing specific targeting, excellent tumor retention, rapid clearance from normal tissues and good cytotoxic activity (279-282). Random CDR mutagenesis and phage display library selection have been used to identify MR1 scFvs with higher affinity for EGFRvIII. Randomization of both CDRs H3 and L3, have lead to the isolation of a triple mutant L3 F92W, H3 S98P, H3 T99Y named MR1-1. This mutant has a 15-fold increase in affinity while maintaining specificity for EGFRvIII (283) and has proven to be beneficial for tumor cell surface retention and internalization (284).

## RATIONALE

EGFRvIII represents an excellent target for immunotherapy. EGFRvIII is restricted to cancer cells thus allowing for specific targeting of cancer cells with less danger of cross-reaction and toxicity to normal tissues. MR1 is an antibody that binds specifically to

EGFRvIII with high affinity. MR1, therefore, represents a potential candidate for use in the design of immunotherapeutic agents against tumor cells bearing EGFRvIII and preliminary studies have shown great promise.

The objective of this research is to solve the x-ray crystal structure of MR1 in complex with the EGFRvIII fusion junction peptide in order to understand how MR1 achieves high affinity and specificity for the mutant receptor. This information will allow for the creation of potential designer immunotoxins based on MR1 that provide greater specificity to cancer cells with less toxicity to normal tissues. It is hypothesized that the novel fusion junction glycine present in EGFRvIII confers a higher degree of flexibility and allows for the formation of a novel conformation that is essential for recognition by MR1.

## MATERIALS AND METHODS

### *Epitope Mapping*

Epitope mapping experiments were performed by Dr. Ian A.J. Lorimer's group, Ottawa Regional Cancer Centre (ORCC), Centre for Cancer Therapeutics, Ottawa, ON, Canada. Peptide epitopes, connected to domains II and III of Pseudomonas exotoxin A (PE) by a short linker (278), and each containing a single, different peptide residue mutated to alanine, were made by cassette mutagenesis. A negative control, consisting of the myc epitope, was also generated. *E. coli* TOP10F' (Invitrogen, Carlsbald, CA) was transformed with the different peptide epitope fusion proteins substituted for MR1 scFv in the pMR1scFvPE38KDEL vector (278). Plasmids were purified from individual colonies and peptide epitope sequences were verified by DNA sequencing. Peptide epitope fusion

proteins were expressed in *E. coli* BL21(DE3)pLysS (Novagen, Madison, WI) and periplasmic extracts containing the fusion proteins were purified to >90% homogeneity as assessed by SDS-PAGE (285). Fusion proteins were purified using Q-sepharose, Resource Q, and Superdex 200 (all GE Healthcare, Piscataway, NJ) and purity was assessed by SDS-PAGE (275).

*Expression and Purification of MR1 dsFv*

The design, expression and purification of MR1 dsFv was performed by Dr. Ian A.J. Lorimer's group, ORCC. One vector was designed for expression of MR1 $V_H$ and one was designed for expression of MR1 $V_L$. In the $V_H$, polymerase chain reaction (PCR) was used to mutate residue R H44 to cysteine as well as to add a C-terminal Factor Xa digest site. The two PCR products were gel-purified and spliced together in a second PCR. The final product was cloned into pCR2.1 (Invitrogen, Carlsbald, CA) and subcloned into pMR1scFvPE38KDEL, substituting the gene for MR1 scFv. For $V_L$, PCR was used to mutate residue D L100 to cysteine and to add restriction enzyme digestion sites as well as a stop codon. The final product was cloned into pCR2.1 and subcloned into pMR1scFvPE38KDEL, substituting the gene for MR1 scFv. The two plasmids were transformed into *E. coli* BL21(DE3). Both the $V_H$ and $V_L$ constructs were expressed as inclusion bodies, purified and solubilized as previously described (286). The solubilized proteins were combined in a 1:1 molar ratio and refolded using a buffer of pH 9.0 as previously described (81). The MR1dsFv-PE protein was purified using Q-Sepharose followed by Mono-Q columns (both GE Healthcare, Piscataway, NJ). The buffer was subsequently exchanged to 10 mM Tris-HCl pH 8.0, 100 mM sodium chloride (NaCl) using a PD10 column (GE Healthcare, Piscataway, NJ). To cleave off the PE, 50 ug of FactorXa

(New England Biolabs, Ipswich, MA) was added per 25 mg of protein in the presence of 2 mM calcium chloride and left at room temperature (RT) overnight. The dsFv was purified from the cleaved exotoxin using a NaCl gradient on a Mono-Q column with the dsFv eluting at 70 mM salt and the exotoxin eluting at 200 mM salt. The purified dsFv was stored in aliquots at –80 °C.

*Production of MR1 scFv Phage*

Production of the MR1 scFv phage was performed by Dr. Ian A.J. Lorimer's group, ORCC. 10 mL of *E. coli* TG1 were grown to an $OD_{600}$ of 0.3 in 2YT medium supplemented with 2% glucose. The cells were infected with $10^9$ transducing units of M13 phage expressing MR1 scFv for 1 hour at 37 °C with shaking. $4x10^{10}$ plaque forming units of M13KO7 helper phage and ampicillin to a final concentration of 100 μg/mL were added to the cells and left for an additional hour at 37 °C with shaking. The infected cells were centrifuged in a Sorvall RT6000D for 10 minutes at 2500 rpm. The pellet was resuspended in 10 mL of 2YT medium supplemented with 100 μg/mL ampicillin and 50 μg/mL kanamycin and incubated overnight at 37 °C with shaking. The cells were centrifuged and the supernatant was stored in aliquots at –80 °C for later use in phage enzyme-linked immunosorbent assay (ELISA).

*Phage and MR1 dsFv ELISAs*

The ELISAs were performed by Dr Ian A.J. Lorimer's group, ORCC. Immulon 4 ELISA plates (Dynex, San Francisco, CA) were coated overnight at 4 °C with 200 μL of 10 μg/mL peptide epitope fusion protein in phosphate buffer saline (PBS). The plates were washed three times with PBS - 0.05% Tween-20 (PBST) and blocked with 200 μL of 2%

milk-PBS (MPBS) for 1 hour at RT. The plates were washed and 100 µL of phage in 2YT was added to the well with 100 µL of 4% MPBS and allowed to bind for 1 hour at RT. The plates were washed and a 1:5000 dilution of anti-M13 HR-conjugated antibody (GE Healthcare, Piscataway, NJ) in MPBS was added and left to incubate for 1 hour at RT. The plates were washed and developed with 2,2'-azinobis-[3-ethylbenzthiazoline-6-sulfonic acid] (ATBS) substrate. A readout at 405 nm was acquired after 20-60 minutes of reaction.

The ELISA performed with MR1 dsFv was completed as described above for MR1 scFv. The detection was performed using murine anti-myc mAb 9E10 (provided by Dr. Atkins, Ottawa Hospital, Ottawa, ON, Canada) followed by a goat-antimouse HR-conjugated IgG (BioRad, Hercules, CA).

*Peptide Synthesis for Crystallization*

The peptide of sequence EEKKGNYVVTDH, similar to Pep3 (287), was synthesized and purified by high-performance liquid chromatography (HPLC) by Queen's Peptide Synthesis Laboratory, Queen's University, Kingston, ON, Canada.

*Crystallization of MR1 dsFv – Peptide Complex*

The MR1 dsFv – peptide complex was crystallized using the hanging drop vapour diffusion method by Dr. Svetlana Borisova, University of Ottawa, Ottawa, ON, Canada. The dsFv was washed with 40 mM sodium acetate buffer pH 4.6, 100 mM NaCl and concentrated to 15-25 mg/mL using a Centricon 10K device (Millipore, Billerica, MA). The peptide was dissolved in water to a final concentration of approximately 7 mM. MR1 dsFv and peptide were mixed in a 1:5 ratio with final dsFv concentration of 8-10 mg/mL and the complex was left to form overnight. 10 µL drops containing 4 mg/mL complex in 40 mM

N-(2-acetamido)iminodiacetic acid (ADA) buffer pH 7.0, 25 mM NaCl, 1% (w/v) methyl-2,4-pentanediol (MPD), 6% PEG 10K were suspended over a 1 mL reservoir containing 200 mM ADA buffer pH 7.0, 2-3% MPD and 16% PEG 4K. Crystals grew at 18 °C over a period of 5-10 days.

*Data Collection Low-Temperature Set (LT Set)*

The crystals were washed with cryoprotectant solution consisting of mother liquor with 30% (w/v) glycerol, mounted in cryo-loops (Hampton Research, Aliso Viejo, CA) and flash-frozen in liquid propane. Data were collected at beamline X8C of the National Synchrotron Light Source (NSLS), Brookhaven National Laboratories (BNL) in Upton, New York, USA using an ADSC Quantum 4R detector (Area Detector Systems Corporation, Poway, CA) and an Oxford Cryosystem model 600 (Oxford Cryosystems, Oxford, UK). Data were collected at 100 °Kelvin (K) using a wavelength of 0.9789 Å. The crystal-to-detector distance was set to 150 mm, oscillation range was set to 0.5° and exposures were 10 seconds. The data were reduced and scaled using the DENZO/HKL program suite (288).

*Structure Determination and Analysis (LT Set)*

Phases were estimated with the molecular replacement method using the programs MERLOT (289) and X-PLOR 3.1 (290-292). The search model used was that of YsT9.1 Fv [1PLG] (293), an antibody specific for the capsular polysaccharide of *Brucella abortus*, based on sequence homology with the Fv of MR1. Rotation and translation searches were conducted in a resolution range of 8.0 – 4.5 Å. One dsFv was found in the asymmetric unit and was subjected to rigid body refinement in X-PLOR (294). Three rounds were

performed at resolution 6.0 – 4.0 Å, 6.0 – 3.5 Å, and 6.0 – 2.8 Å with an overall B-factor. The sequence of YsT9.1 was mutated to that of MR1. Further refinement and simulated annealing were carried out with individual B-factors and were combined with manual intervention using the program FRODO (295, 296). Using both 3Fo-2Fc and Fo-Fc maps, no clear electron density could be initially seen for the peptide antigen.

*Data Collection Room-Temperature Set (RT Set)*

The crystals were washed using a solution of 100 mM ADA pH 7.0, 10% PEG 10K, 2% MPD, and 1 mM peptide and mounted in capillaries. Data were collected at Queen's University, Kingston, ON, Canada, using Cu Kα radiation from a Rigaku RUIII rotating anode X-ray source (1.5418 Å) and a MAR300 image plate. Data were collected at RT, the crystal-to-detector distance was set to 200 mm, oscillation range was set to 1° and exposures were 300 seconds. The data were reduced and scaled using the DENZO/HKL program suite (288).

*Structure Determination and Analysis*

The LT-Fv was used as search model for the RT data. Rigid body refinement was carried out as described for the LT set. Upon manual repositioning of the CDR chains at 2.8 Å resolution, clear electron density for the peptide antigen was revealed. The peptide was constructed using the program SETOR (50). The RT set was then subjected to refinement and simulated annealing using X-PLOR and manual refinement using FRODO. Water molecules were added using the PEAK and CLOSEST scripts (Evans, unpublished results) and the RT set was refined to maximum resolution. The RT dsFv-peptide model was then used as a starting model for the LT set. The LT set was later refined in parallel with the RT

set. Quality of the structures was assessed throughout using Ramachandran plots and monitoring the values for the R-factor, Rfree, isotropic B-factors, and bond length and bond angle rmsd values. Data collection and refinement statistics are presented in Table 3.1.

The coordinates for the RT and the LT structures have been deposited in the Protein Data Bank under accession codes 1I8I and 1I8K, respectively.

## RESULTS AND DISCUSSION

*Epitope Mapping Study*

The epitope mapping study of the peptide antigen was conducted in Dr. Ian A. J. Lorimer's laboratory, ORCC, to determine the relative importance to binding of each peptide residue. Epitope peptides were generated as PE fusion proteins where each peptide residue was sequentially mutated to alanine. Fusion proteins using Pep3 and myc were also generated as positive and negative controls, respectively. Fusion proteins were assayed for binding to MR1 scFv and MR1 dsFv (not shown) using ELISA. As expected, the data reveal binding of MR1 scFv to Pep3 but not to the negative control myc epitope (Figure 3.3). The ELISA signal obtained from the binding of MR1 scFv to Pep3 was normalized to 1.0. Regarding the EGFRvIII peptide, the data show that MR1 scFv recognizes the C-terminal half of the peptide, consisting of residues K P5 to D P12[a]. This epitope spans the fusion junction glycine, which is at position 6 in the peptide antigen. The data also show Y P8, V P10, and D P12 to be of greater importance, as mutation of these residues to alanine completely abrogates binding of the peptide to MR1 scFv. Residues K P5, N P7, V P9, and

[a] Residues in the peptide antigen are preceded by the letter P as those of the light chain and heavy chain of the dsFv are preceded by the letters L and H, respectively.

**Table 3.1 Data collection and refinement statistics for the LT and RT data sets of dsFv MR1 in complex with the EGFRvIII peptide antigen**

| | LT | RT |
|---|---|---|
| *Data collection* | | |
| Space group | $C222_1$ | $C222_1$ |
| Cell dimensions (Å) | a = 110.5 | a = 111.6 |
| | b = 44.8 | b = 45.3 |
| | c = 108.6 | c = 110.4 |
| Max. resolution (Å) | 1.8 | 2.4 |
| No. observations | 25,654 | 10,214 |
| Unique reflections | 24,641 | 9684 |
| Completeness (%)[a] | 98.5 (95.7) | 86.6 (58.6) |
| R symm (%)[a] | 5.2 (13.7) | 6.0 (12.1) |
| Overall I/σI | 22.8 | 16.6 |
| *Refinement Statistics* | | |
| Resolution (Å) | 6.0 – 1.8 | 6.0 – 2.4 |
| R cryst (%) | 17.2 | 15.6 |
| R free (%) | 22.5 | 26.2 |
| Rmsd | | |
| bond lengths (Å) | 0.014 | 0.015 |
| bond angles (°) | 2.6 | 3.3 |
| No. solvent atoms | 260 | 84 |
| B-factors (Å$^2$) | | |
| overall protein | 11.0 | 21.8 |
| peptide | 19.5 | 34.9 |

a Values in parentheses are for the highest resolution shell.

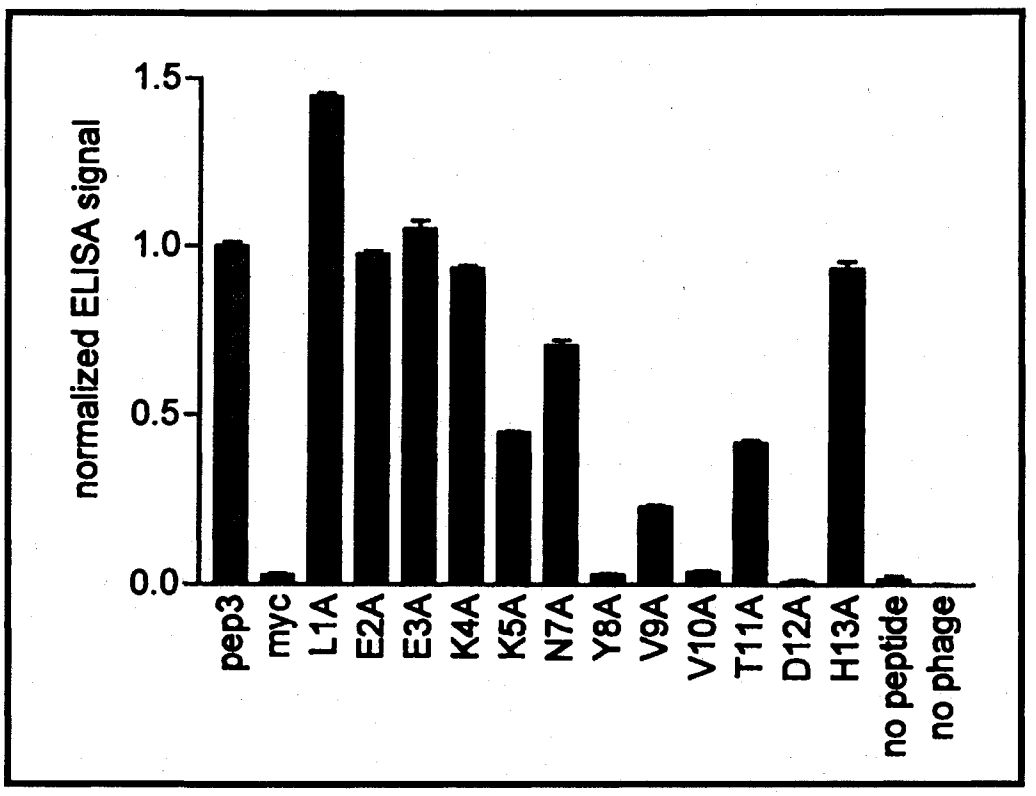


**Figure 3.3. Epitope mapping results.** Diagram showing the ELISA results for control epitopes and alanine mutant peptide epitopes. Binding of the alanine mutant peptide epitopes is normalized to the binding of positive-control Pep3 epitope and error bars show standard deviation. Mutation of peptide residues Y8, V10, and D12 to alanine significantly affects binding of the peptide epitope to MR1, demonstrating the importance of these residues in binding the antibody fragment. These experiments were performed by Dr. Lorimer's group, ORCC.

T P11 show a lesser importance in binding as mutation of these residues to alanine leads only to a decrease in peptide binding to MR1 scFv. Residues L P1, E P2, E P3, K P4, and H P13 are most likely not part of the epitope that binds to MR1 scFv as mutation of those residues to alanine does not change, or even increases, the strength of binding. Together, these results seem to reveal a pattern where every second residue, from N P7 to H P13, shows higher relative importance in binding.

At first glance, it would seem that since the epitope recognized by MR1 scFv overlaps the fusion junction G P6, the mechanism of recognition of MR1 scFv could lie in its ability to recognize residues that are both N-terminal and C-terminal to the fusion junction. These residues, in EGFR, are located at remote positions and this type of recognition by MR1 scFv could not be achieved with the native receptor. Yet, a closer look at the epitope mapping data reveals that most of the epitope lies with residues that are all C-terminal to the fusion glycine. These residues could also play the role of epitope for MR1 scFv in EGFR. The one residue that is important in peptide binding to MR1 scFv and that is N-terminal to the fusion junction glycine is K P5, and this residue has been shown to increase the binding affinity of the peptide by about 7-fold over alanine when assayed by competition ELISA (data not shown). However, given that the glycine, which is the only residue completely different, is not a central feature in recognition by MR1 scFv and that only one residue N-terminal to the glycine seems of importance to binding to MR1 scFv, further studies needed to be undertaken to fully understand the highly specific recognition mechanisms of MR1 scFv.

*Crystallization*

Determination of the X-ray crystal structure of MR1 in complex with the EGFRvIII peptide antigen was undertaken to resolve the issue of MR1 - EGFRvIII specificity that was not fully answered by epitope mapping studies. The dsFv format of MR1 was chosen above that of the scFv since it is produced in higher yields and cannot form multimers in solution as scFvs have been shown to do. Crystals of the dsFv MR1 in complex with the EGFRvIII peptide antigen were obtained in 5-10 days and grew to maximum dimensions of 0.5 x 0.3 x 0.1 mm (Figure 3.4). Data were collected at low temperature using crystals flash-frozen in liquid propane (LT) and at RT using crystals mounted in capillaries. The crystals were found to be orthorhombic, with space group $C222_1$, and the data extend to high resolution for the LT set (see Table 3.1 for data collection and refinement statistics). In both data sets, there is one dsFv-peptide complex per asymmetric unit. As often seen in crystals of antibody fragments, the dsFv-peptide molecules pack in a head-to-head fashion (297-300). Here, the antigen-binding sites of symmetry-related partners face each other around crystallographic 2-fold axes. This allows for numerous inter-molecular contacts (Table 3.2), including the packing of CDR L2 of one dsFv in a depression formed by CDR H1 of a symmetry-related partner (Figure 3.5). Although the binding sites of symmetry-related dsFv are face-to-face, there are no observed interactions between the antigen and the binding site of a neighboring molecule.

*Low Temperature vs Room Temperature*

The LT and RT data sets were refined in parallel. There are no significant deviations that are observed between the backbone or side chain atom positions for the two data set structures. The only differences that are seen between the data sets are: the isotropic B-

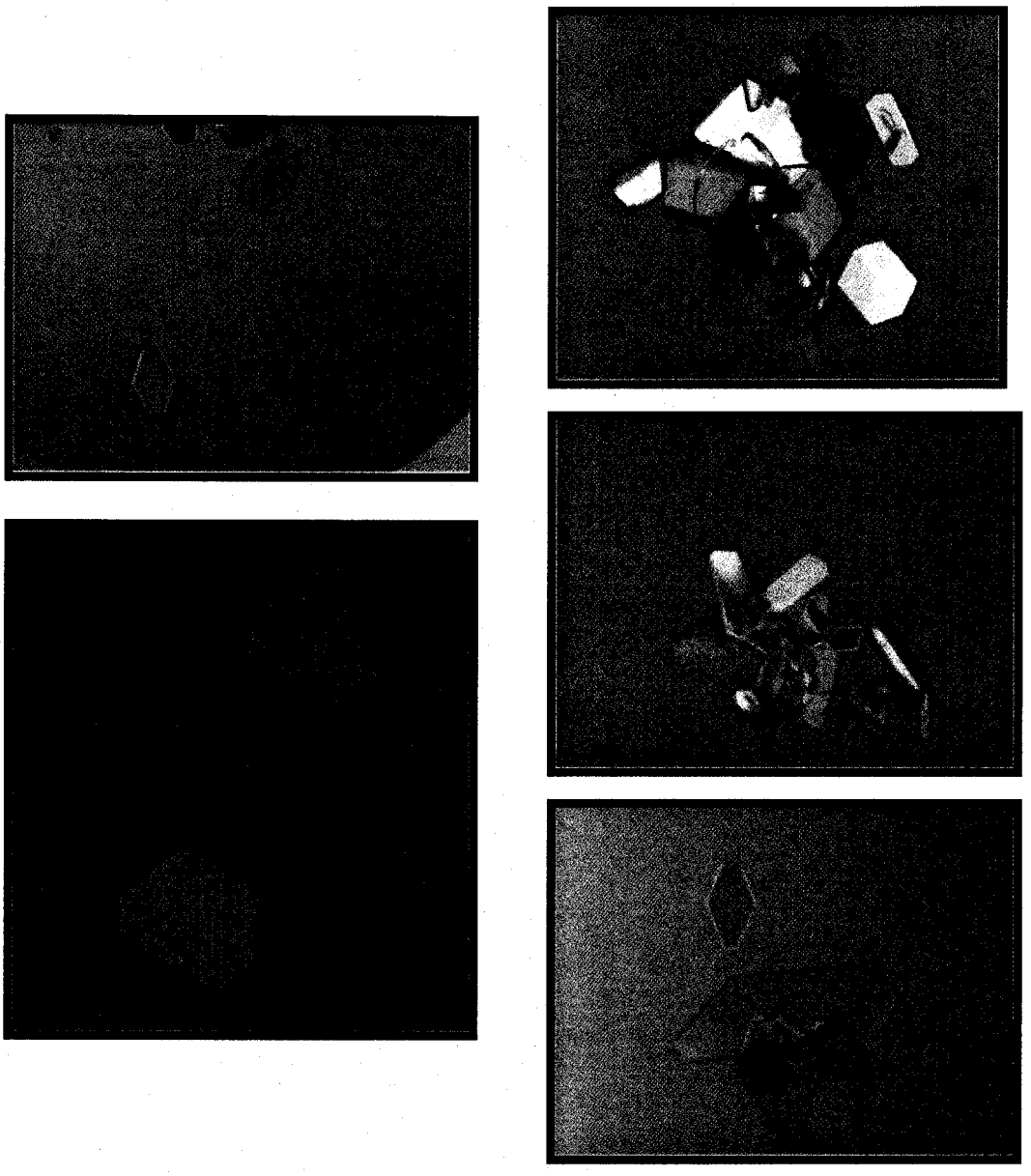

**Figure 3.4. Crystals of dsFv MR1 in complex with EGFRvIII peptide antigen.** Using the hanging drop method, orthorhombic crystals were obtained in 5-10 days, grew to maximum dimensions of 0.5 x 0.3 x 0.1 mm, and diffracted to 1.8 Å at beamline X8C of the National Synchrotron Light Source, Brookhaven National Laboratories, Upton, NY, USA.

**Table 3.2 Molecular interactions observed between dsFv MR1 – EGFRvIII peptide symmetry-related partners**

| | | | Distance (Å) |
|---|---|---|---|
| OG Ser L7 | --- | SD Met L24 | 3.50 |
| NE Arg L22 | --- | OD2 Asp L70 | 2.87 |
| NH1 Arg L22 | --- | OD1 Asp L70 | 2.80 |
| OG Ser L63 | --- | NE2 Gln H1 | 2.95 |
| NE2 Gln H1 | --- | O Phe L62 | 3.04 |
| NZ Lys H3 | --- | OG Ser H82b | 2.62 |
| NE2 Gln H3 | --- | O Gly H65 | 3.22 |
| NE2 Gln H5 | --- | OG Ser H82a | 2.84 |
| N Thr H28 | --- | O Gly L51 | 2.93 |
| NZ Lys H31 | --- | OD2 Asp L32 | 2.77 |
| NZ Lys H31 | --- | O Asp L30 | 2.84 |
| OH Tyr H55 | --- | O Ser H112 | 2.78 |
| OG Ser H82b | --- | OE1 Gln H5 | 2.71 |
| NH2 Arg H94 | --- | OG1 Thr L53 | 2.72 |

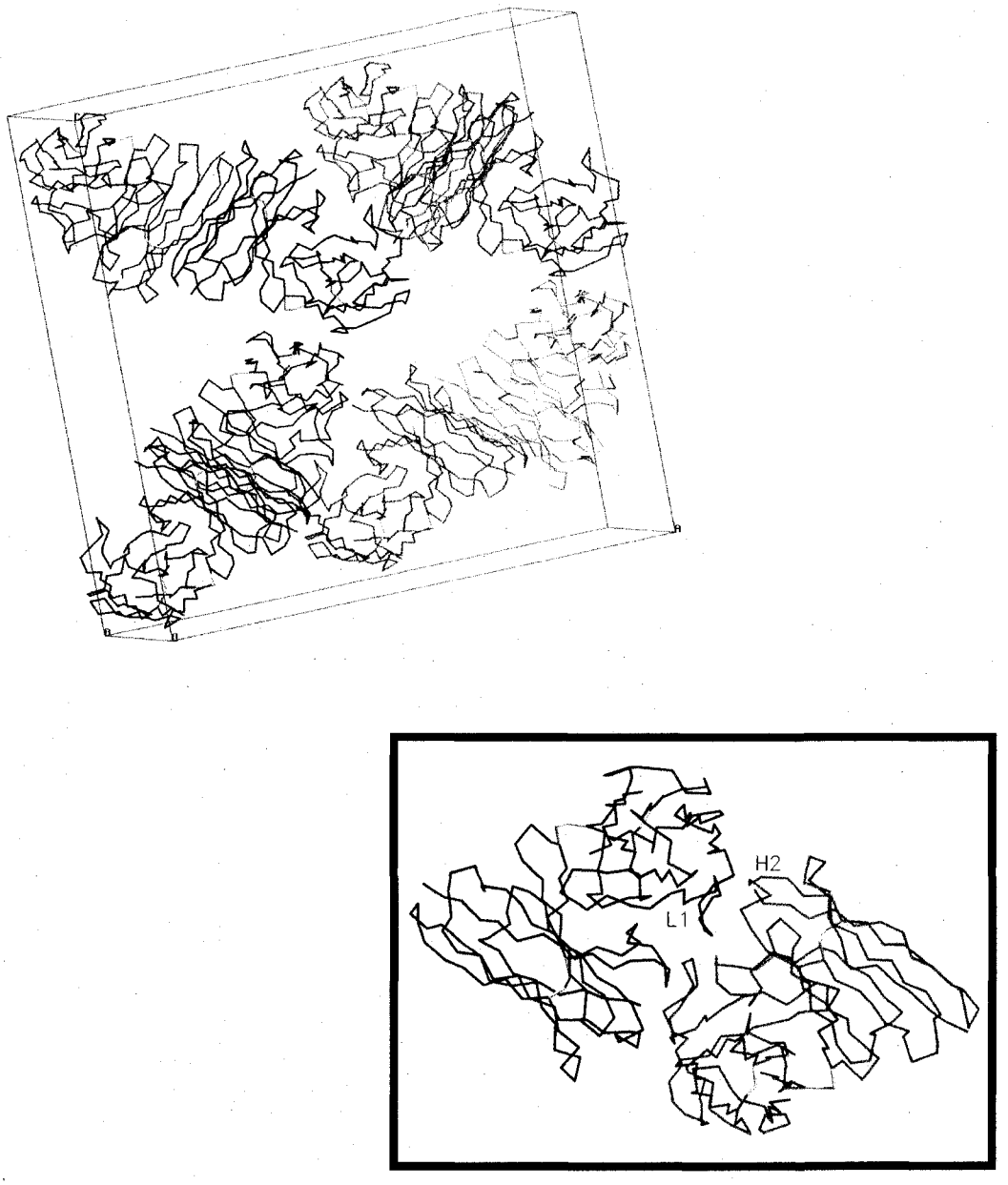


**Figure 3.5. Crystal packing of MR1 dsFv in complex with the EGFRvIII peptide antigen.** The antibody fragment – peptide complex crystallizes in space group $C222_1$. The molecule in the asymmetric unit (black) is shown in the unit cell with its symmetry-related partners. Highlighted in the close-up picture is the head-to-head interaction observed in the crystals, whereby CDR H2 of one dsFv molecule (blue) packs in a depression adjacent to CDR L1 of another dsFv molecule (red). Figures prepared with Setor (50).

factors, which are higher in the RT data set (Table 3.1), the number of observed water molecules, which is higher in the LT data set (Table 3.1), and the electron density for the peptide, which allows for modeling of the K P4 in the LT data set but not in the RT data set. These results parallel those obtained in another study of the refinement of an RT and LT data set of cubic insulin crystals, conducted by Yu and Caspar (301).

*Overall Structure*

Residues of the dsFv are all observed to lie in appropriate electron density and have conformations that fall within allowed regions of Ramachandran plots. The sequence, topology diagram, and secondary structure for the dsFv are shown in Figures 3.6 and 3.7A. The dsFv contains a third (engineered) disulfide bridge between L100 and H44, which is known to stabilize Fvs and the conformation of their binding site (Figure 3.7B) (302). The presence of this engineered bond does not alter the immunoglobulin fold of the MR1 fragment, a finding that is consistent with previous reports (303). Although the residue at position 51 in the L chain of antibodies often adopts an unfavorable conformation as part of a γ-turn (304-307), this is not the case with G L51 in MR1. MR1's CDRs are all seen to adopt canonical structures (Figure 3.7C) (29). For the L chain, L1 presents the structure that is most common for class 2 murine antibody canonical structures, L2 adopts the one class seen for this CDR, and L3 presents the structure that is most common for class 1 murine antibody canonical structures. For the H chain, H1 adopts the one class available for this CDR and H2 presents the class 3 canonical structure, the least expected structure for murine antibodies. H3 has not been classified into canonical structures based on its great structural diversity, but it is found to adopt an extended conformation based on another structural

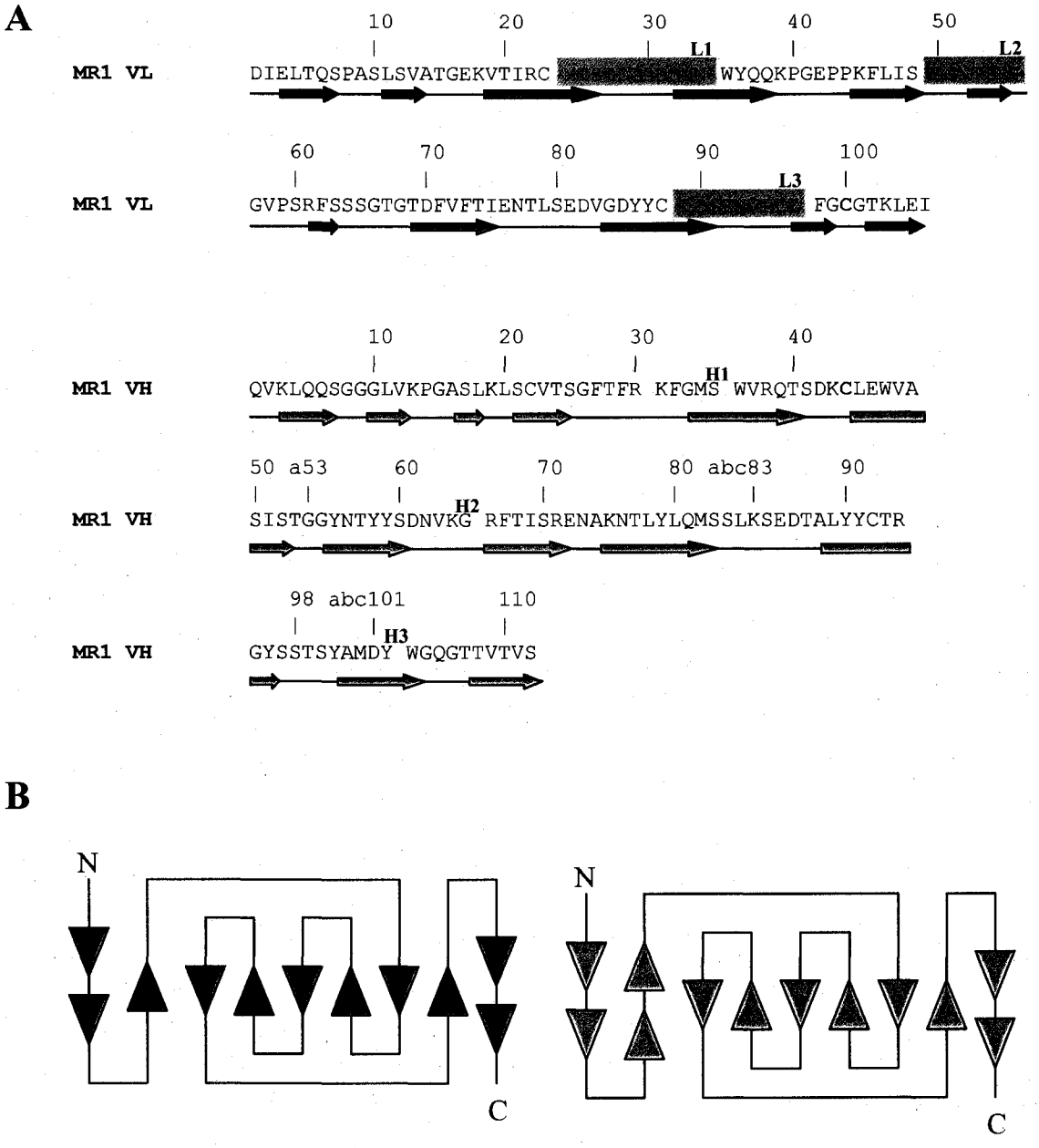


**Figure 3.6. Organization of dsFv MR1. A.** Sequence of the $V_L$ and $V_H$ chains of dsFv MR1 numbered according to Kabat. The cysteine mutations that take part in the engineered third disulfide bond are highlighted in red and the CDRs are indicated. The secondary structure is imposed below the sequence, where β-sheets are depicted in blue arrows for $V_L$ and in orange arrows for $V_H$. **B.** Topology diagram showing the arrangement of the secondary structure elements, with the same color code as in **A**.

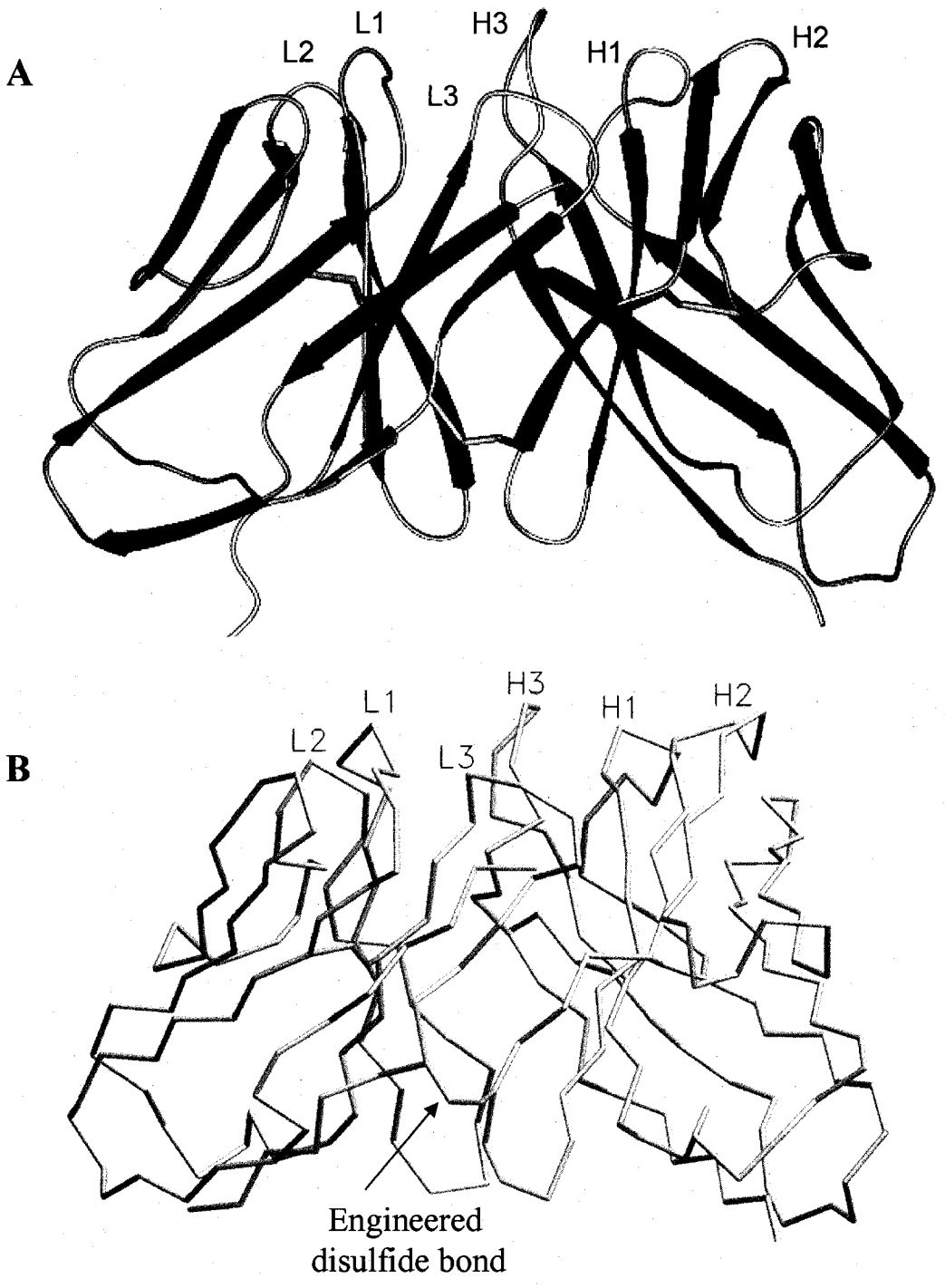


**Figure 3.7. Overall structure of dsFv MR1. A.** Ribbon diagram of MR1 dsFv showing the L chain in red and the H chain in green. The disulfide bridges are colored in yellow. **B.** Backbone structure of MR1 dsFv highlighting the engineered disulfide bond and the position of the L chain and H chain CDRs. (Continued on the next page.)

C

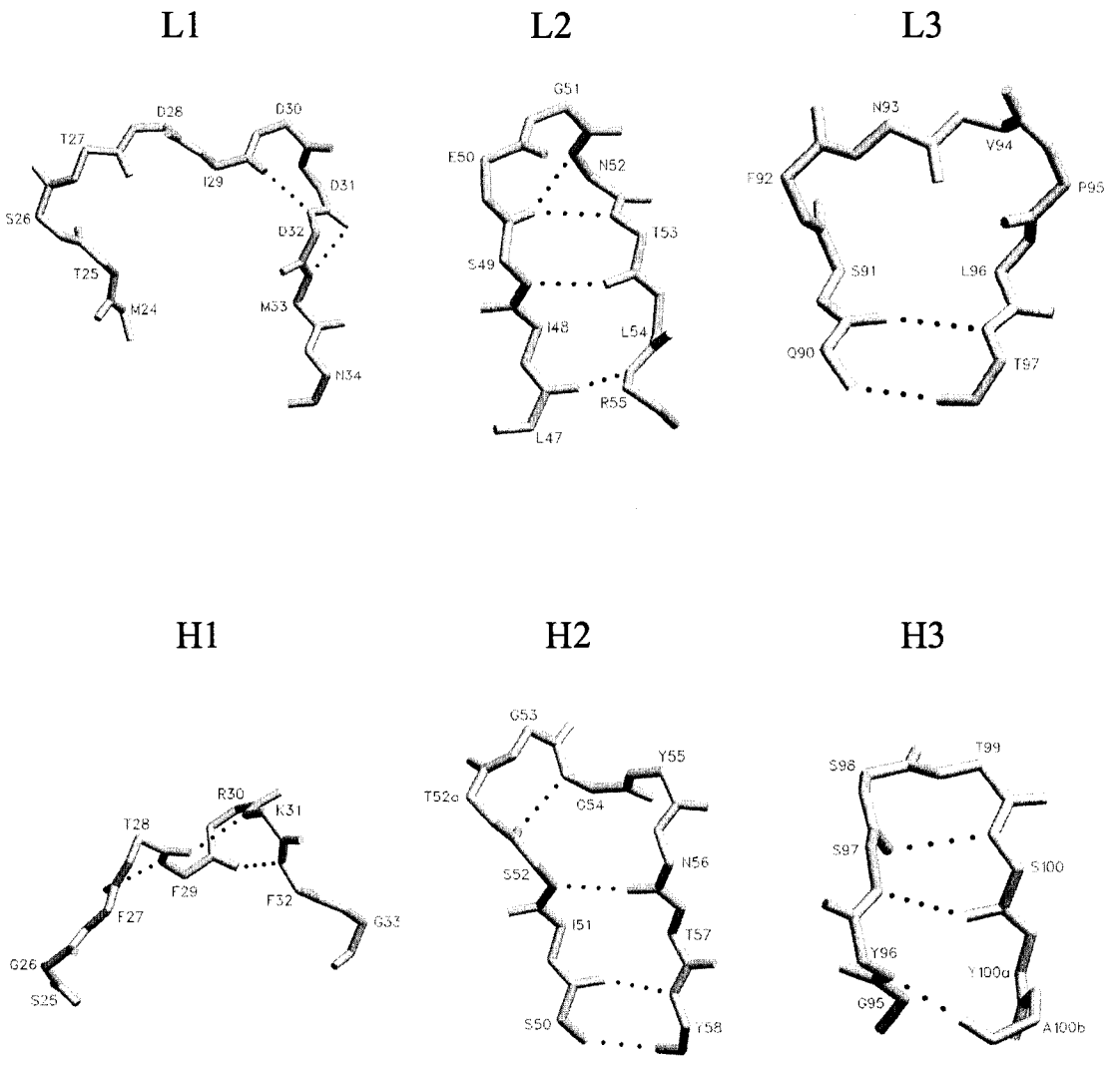


**Figure 3.7. Overall structure of dsFv MR1 (continued). C.** Main chain atoms and intra-chain hydrogen bonds for residues of the light chain and heavy chain CDRs showing the canonical structures adopted in MR1 dsFv. Figures prepared with Setor (50).

classification system (32). The binding site for MR1 is found to adopt a J-shaped groove that is fashioned by CDRs H2, H3, L3, and to a lesser extent, H1 (Figures 3.8A and B).

*Antigen Binding*

The peptide that is crystallized with MR1 dsFv consists of 12 residues. In the LT data set, residues K P4 to D P12 can be seen in the electron density whereas residues K P5 to D P12 can be seen in the RT data set. The residues that are observed in density correlate with the length of the epitope defined by epitope mapping results (Figure 3.9). A total of 537 $Å^2$ and 440 $Å^2$ are buried for the dsFv and peptide, respectively (calculated using CNS). This amount of buried surface area is consistent with other antibody-antigen complex structures (308). The peptide occupies the J-shaped groove by adopting a hairpin turn – β-strand conformation, with residues K P5 to Y P8 giving rise to the turn and residues N P7 to D P12 forming the strand (Figures 3.8A and B).

The residues of the peptide bound to MR1 that are found to adopt the β-strand conformation alternatively face the binding pocket and the solvent, with residues Y P8, V P10, and D P12 facing the binding site. Residues V P9 and T P11 face the solvent and make no contact with the antibody binding interface. This finding is consistent with the epitope mapping results and can be directly attributed to the conformation of that stretch of the peptide. Residue Y P8 lies in the deepest pocket, which is hydrophobic and shaped by CDRs L3, H2, and H3. It is able to form stacking interactions with Y H100a as well as make hydrogen bonds with the main chain atoms of residues S L91 and Y H100a (Figure 3.9). Residue V P10 lies in a hydrophobic pocket formed by H3, where it is able to make a main chain – main chain hydrogen bond with residue T H52a (Figure 3.9). Residue D P12 resides in a neutral pocket formed by H2 where it is able to establish many stabilizing

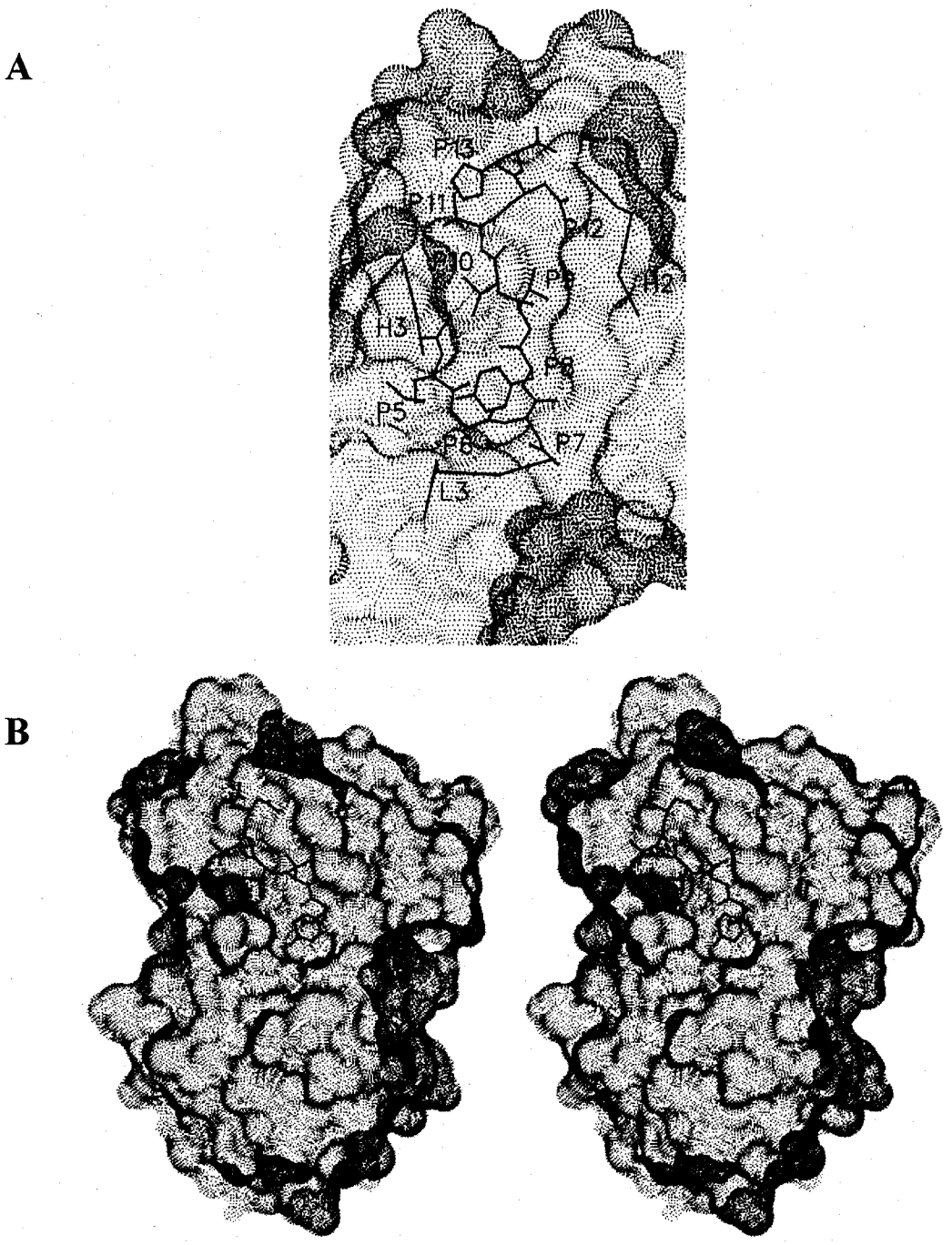


**Figure 3.8. MR1 dsFv solvent accessible surface and EGFRvIII peptide antigen binding site. A.** Binding site of MR1 dsFv showing the solvent accessible surface (SAS), with blue indicating positively-charged surface and red indicating negatively-charged surface. Backbone of CDRs L3, H2, and H3 are drawn as well as the peptide antigen. **B.** Stereoview of the SAS of MR1 dsFv (red) showing the J-shaped groove and the β-strand portion of the EGFRvIII peptide antigen (black trace). Figures prepared with Setor (50).

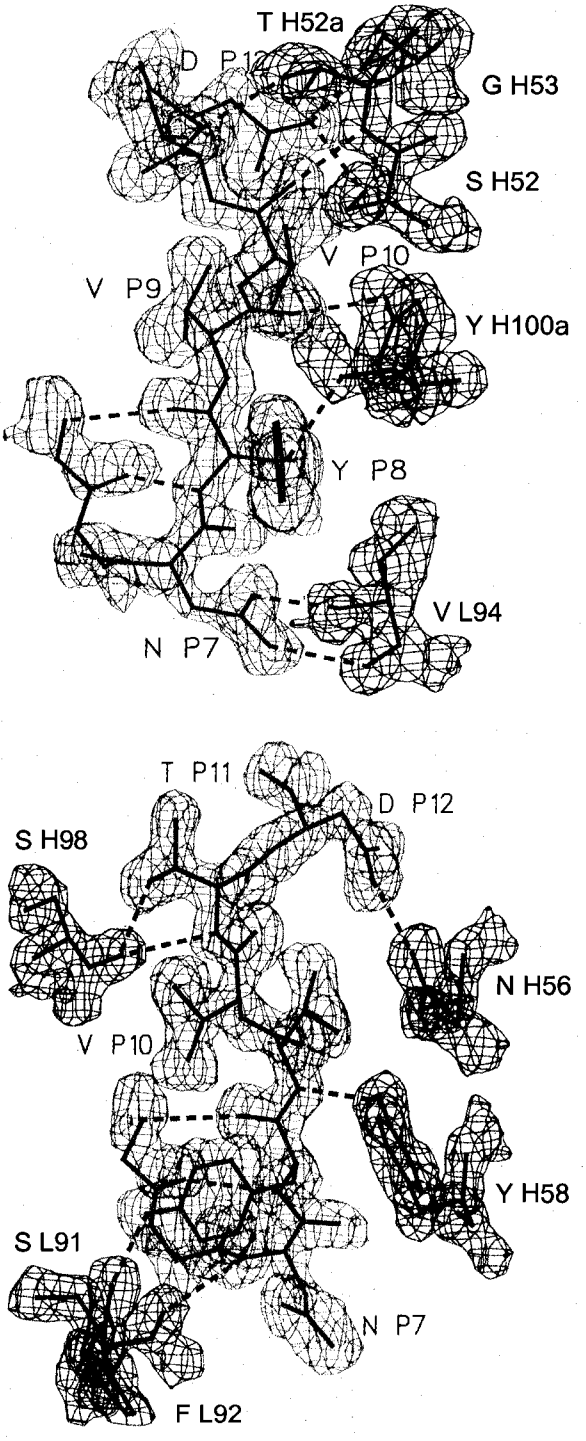


**Figure 3.9. Electron density for the EGFRvIII peptide antigen.** 3Fo-2Fc map electron density is contoured at 1.5σ for the peptide antigen (red) and hypervariable region residue side-chains (blue). Broken lines connect hydrogen bonding groups. Figures prepared with Setor (50).

interactions. The side chain atoms can make hydrogen bonds with residues S H52, T H52a, G H53 and the main chain atoms can make hydrogen bonds with the side chain of residue N H56 (Figure 3.9). Residues of the peptide that are found in the hairpin turn do not make extensive contact with the binding site of MR1 (Table 3.3). Residue K P5 lies on a negative patch of the binding site, which results from the clustering of aspartic and glutamic acid residues between CDRs L3 and H3. Residue N P7 lies in a depression between CDRs L3 and H2, where it is able to make stacking interactions with residue F L92 and N L93, as well as make hydrogen bonds with water molecules. More interesting is the fact that the central feature of the EGFRvIII peptide, residue G P6, has no direct interaction with MR1.

*Conformational Peptide*

The hairpin turn – β-strand conformation that is adopted by the EGFRvIII peptide in complex with MR1 has also been previously reported for a peptide antigen from influenza virus hemagglutinin crystallized in complex with both antibodies 17/9 and 26/9 (308, 309). Other antibody-peptide crystal structures have also revealed peptide antigens that bind in a β-strand manner (310) or in turn conformations (311, 312). Thus, the recognition of the EGFRvIII antigen by MR1 does not rely on the presentation of a novel peptide conformation. And yet, MR1 also does not directly contact residue G P6, the fusion junction glycine that defines the EGFRvIII peptide. The mechanism of recognition of the EGFRvIII peptide by MR1 thus seems to rely on the ability of the fusion junction glycine residue to adopt the hairpin turn conformation. The hairpin turn, which closely resemble a type II' β-turn, is usually but not strictly found to have a glycine residue at position $i$+1 (Table 3.4). The recognition by MR1 of this peptide conformation, rather than the peptide key glycine residue, is also revealed when looking at mutants of the peptide. In epitope

**Table 3.3 Molecular interactions observed between dsFv MR1 and the EGFRvIII peptide antigen**

| | | | | | Distance (Å) |
|---|---|---|---|---|---|
| N | Val L94 | --- | OD | Asn P7 | 2.85 |
| N | Thr H52a | --- | O | Val P10 | 2.86 |
| N | Gly H53 | --- | OD2 | Asp P12 | 2.96 |
| ND2 | Asn H56 | --- | OD2 | Asp P12 | 2.97 |
| N | Tyr H100a | --- | OH | Tyr P8 | 3.01 |
| OH | Tyr H100a | --- | O | Val P9 | 2.83 |
| NE | Lys P4 | --- | O | Tyr P8 | 3.08 |
| ND2 | Asn P7 | --- | O | Val L94 | 3.04 |
| N | Tyr P8 | --- | O | Lys P5 | 3.31 |
| OH | Tyr P8 | --- | O | Ser L91 | 2.74 |
| N | Val P9 | --- | OH | Tyr H58 | 2.85 |
| N | Thr P11 | --- | O | Ser H98 | 2.69 |
| OD | Thr P11 | --- | O | Ser H98 | 2.76 |
| N | Asp P12 | --- | OD | Thr H52a | 2.98 |
| OD1 | Asp P12 | --- | OD | Ser H52 | 2.72 |

**Table 3.4 Observed and literature values, in degrees, for the φ, ψ angles of the type II' β-turn of the EGFRvIII peptide antigen**

| | $\Phi_{i+1}$ | $\psi_{i+1}$ | $\varphi_{i+2}$ | $\psi_{i+2}$ |
|---|---|---|---|---|
| Literature | 60 | -120 | -80 | 0 |
| EGFRvIII peptide | 58.7 | -127.6 | -121.3 | 30.5 |

mapping studies, replacing G P6 with alanine generates a peptide that is still able to bind MR1. This can be justified by the small bulk of the alanine side chain, which would not clash with the binding pocket, as well as by the tolerance of type II' β-turns to alanine at position *i*+1 (308, 313). Furthermore, the peptide containing the native R P6 residue, with a bulky side chain that would most likely clash with packing in the binding pocket, shows no binding to MR1. Thus, MR1 can recognize the mutant receptor EGFRvIII and not cross-react with native EGFR based, not on specific recognition of a novel fusion residue or on the recognition of a novel peptide conformation, but on a conformation adopted by the mutant residue that cannot occur in the native sequence. This ability of peptides to form a stable hairpin turn in solution has been found to be an important factor in the presentation of conformational epitopes by otherwise flexible peptides (314).

## CONCLUSION

In this study, the complex of dsFv MR1 and the EGFRvIII peptide antigen was crystallized and its structure solved by X-ray crystallography. The results reveal that the EGFRvIII peptide antigen binds to a J-shaped groove on MR1 by adopting a hairpin turn – β strand conformation. The peptide residues that take part in the strand alternately face the binding pocket of MR1, and this observation correlates well with epitope mapping results. The residues that adopt the hairpin turn include the fusion junction glycine. Although the glycine residue is a central feature of the EGFRvIII antigen, this residue is not found to interact directly with MR1. Instead, the fusion junction glycine facilitates the formation of

the hairpin turn, a conformation that is both unique to EGFRvIII and crucial for MR1 recognition and binding.

# CHAPTER 4

# ANTIBODY BEC2 MIMICRY OF THE $GD_3$ GANGLIOSIDE EPITOPE

## INTRODUCTION

### *Gangliosides*

Cell-surface carbohydrates are involved in many important biological processes: they play key roles in cell-cell recognition, signal transduction, and have also been implicated in cancer cell metastasis and cell recognition by various toxins and pathogens (315, 316). Cell-surface carbohydrates attached to membrane lipid moieties are termed glycolipids. Many forms of glycolipids exist that are defined by both the nature of the lipid moiety and glycosyl head group. Glycolipids that are composed of a ceramide moiety and a mono- or oligosaccharide head group are termed glycosphingolipids. Some glycosphingolipids are further differentiated by the presence of one or more sialic acid residues within their head group. These glycosphingolipids are referred to as gangliosides (317, 318). Most gangliosides are expressed within cells of the nervous system, although expression is also seen within other tissues and is known to vary by cell type and from one species to another.

Malignant cell transformation has been shown to bring about both quantitative and qualitative changes in ganglioside expression (319, 320). Changes in the ganglioside lipid moiety have been identified in some cancers and have been shown to affect both the presentation (321, 322) and immunogenicity (323) of the ganglioside head group. Up-regulation of gangliosides at the surface of cancer cells has also been shown to provide tumors with enhanced metastatic activity (324) that can be correlated with disease prognosis (325, 326). In addition, tumor-associated gangliosides can be shed into the circulation and are useful markers for both disease diagnosis and prognosis (327). Consequently, gangliosides have become the focus of intense investigation as potential tumor-associated antigens in the development of highly specific cancer therapies.

The exploitation of gangliosides as potential targets for cancer therapies poses significant challenges. Gangliosides are carbohydrates and are thus inherently poor immunogens (328-330). In addition, gangliosides lack the advantage of being solely tumor specific (331). To overcome these obstacles, efforts have focused on enhancing the immunogenicity of gangliosides. Gangliosides have been conjugated to protein carriers, combined with potent adjuvants (332) and chemically modified (333) for use in vaccine preparations, all of which have been shown to render the resultant structures more immunogenic. Chemical modification has also been shown to render the resultant gangliosides less susceptible to enzymatic action (334).

The development of more immunogenic gangliosides has led to the generation of antibodies that are able to react with the original, unmodified gangliosides (335-337). These anti-ganglioside antibodies have the potential to be used in immunotoxins to target cancer cells and can also serve to stimulate immune cells that bear gangliosides. Unfortunately, anti-ganglioside antibodies are also capable of cross-reacting with gangliosides present on normal tissues (338). Such 'auto-antibodies' have been found in patients with peripheral neuropathy (339), Guillain-Barre syndrome (340), Miller Fisher syndrome (341) and other neurological disorders (342-344) and are thought to play in important role in the pathogenesis of these conditions (345, 346).

*Disialoganglioside $GD_3$*

The disialoganglioside $GD_3$ contains a glucose (Glc), a galactose (Gal) and two sialic acid [or *N*-acetylneuraminic acid (NANA)] residues in its glycosyl moiety that are linked as follows: NANA(α2-8)NANA(α2-3)Gal(β1-4)Glc-ceramide (Figure 4.1). Although $GD_3$ is only a minor component of surface gangliosides in those normal tissues in which it is

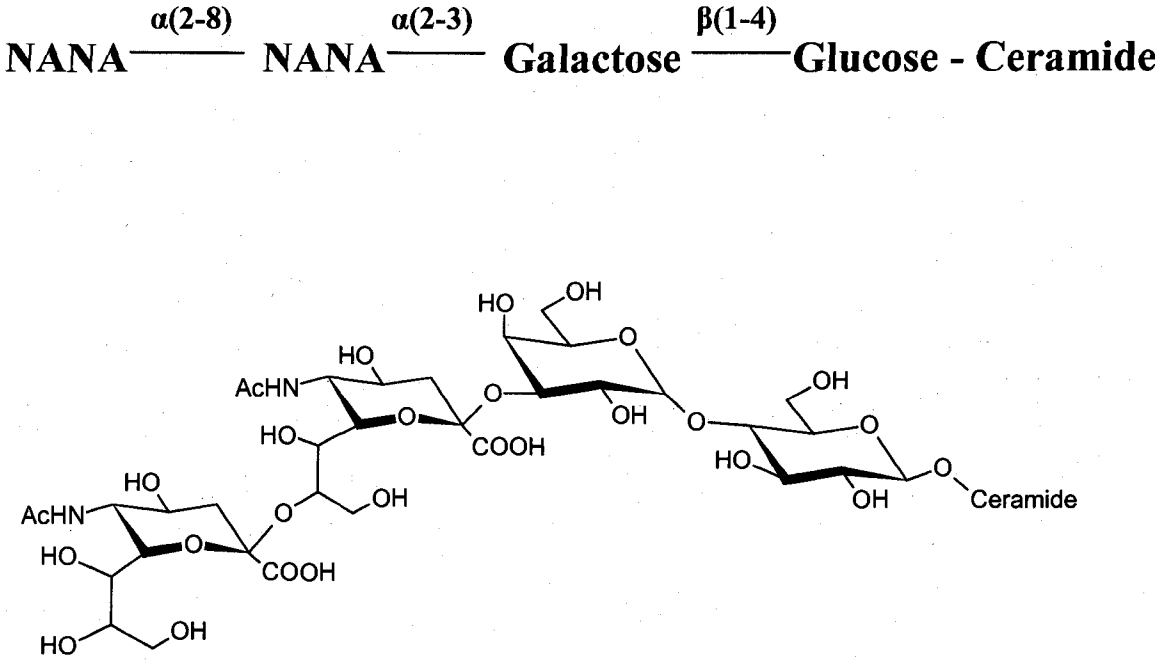


**Figure 4.1. Disialoganglioside $GD_3$ antigen.** Schematic structure of the $GD_3$ ganglioside consisting of a glucose, galactose and two *N*-acetylneuraminic acid (NANA) residues linked as NANA(α2-8)NANA(α2-3)Gal(β1-4)Glc-ceramide.

expressed, the disialoganglioside is widely distributed throughout the body including neuronal tissue, the retina (347) and in small quantities within the connective tissue elements of the breast, prostate, stomach, uterus, and ovary (348, 349) as well as within skin cells, pancreatic islet cells, cells of the adrenal medulla (331, 349-354) and a subset of peripheral blood T-lymphocytes (355).

Like other gangliosides, $GD_3$ undergoes both qualitative and quantitative changes within cells that have undergone malignant transformation. The lipid moiety of $GD_3$ is substituted for longer fatty acid chains (323), which has been shown to affect the presentation of the $GD_3$ epitope at the tumor cell-surface. The expression of $GD_3$ is also up-regulated (326, 356) resulting in a clustering of the $GD_3$ epitope at the tumor cell surface (357). This clustering is considered a key element in the uncontrolled cell growth and increased metastatic potential seen in $GD_3$-bearing tumors (354, 358-360). Accordingly, up-regulation of $GD_3$ is associated with a more aggressive tumor phenotype (324, 361) and correlates with decreased patient survival (359, 362). In addition, tumor-associated $GD_3$ is shed into the circulation. This soluble $GD_3$ not only serves as a marker for disease, but more importantly, suppresses the normal immune response (327, 363-365). The changes in $GD_3$ described above have been documented in human tumors such as melanoma (323, 350, 366, 367), glioma, neuroblastoma (354), small-cell lung cancer (368), acute lymphoblastic leukemia (369, 370), and other acute and chronic leukemias (371, 372).

The changes in tumor-asociated $GD_3$ render $GD_3$ an attractive target for cancer immunotherapy. The novel presentation of the $GD_3$ epitope at the tumor cell surface raises the possibility of generating tumor-associated $GD_3$ antibodies that either lack or display limited cross-reactivity with normal $GD_3$-bearing tissues. However, the fact that $GD_3$ is

both a carbohydrate and found natively within normal tissues (325, 373) limits the inherent immunogenicity of $GD_3$ and presents a significant challenge in the use of tumor-associated $GD_3$ as a potential cancer target.

*Vaccinating With $GD_3$*

In an attempt to produce anti-$GD_3$ antibodies, purified $GD_3$ was introduced into patients with $GD_3$-bearing malignant melanoma in the hopes of inducing an immune response against the ganglioside. Unfortunately, these efforts were unsuccessful (373). To overcome the tolerance of the immune system to the $GD_3$ epitope, the $GD_3$ glycone was conjugated to protein carriers and/or used in conjunction with powerful adjuvants. In the mouse model, these efforts all lead to the generation of low titers of IgM antibodies (323, 374-376). More importantly, some carrier-adjuvant combinations also lead to the generation of IgG antibodies. The success in the mouse model has been attributed to the restricted expression of $GD_3$ on normal mouse tissue (377). Unfortunately, attempts at reproducing these results in humans have proven ineffective (373, 378, 379).

Another means of overcoming the tolerance to $GD_3$ is the use of $GD_3$ derivatives (379). The goal of these derivatives is to increase the immunogenicity of the $GD_3$ epitope to produce antibodies capable of binding both the $GD_3$ derivative and the unmodified $GD_3$. One derivative, the 9-*O*-acetyl-$GD_3$, or CDw60, is found natively within cancers such as melanoma (326, 380), basal cell carcinoma and squamous cell carcinoma (381). CDw60 is more immunogenic than $GD_3$ probably due to its weaker and more restricted expression within normal tissues (382, 383). In both mice and melanoma patients, immunizations with CDw60 lead to the development of IgM antibodies. Unfortunately, these antibodies could not cross-react with unmodified $GD_3$ (375, 384). Similarly, trials with other $GD_3$ derivatives

such as $GD_3$ amine, gangliosidol, lactones I and II, *N*-propionyl, *N*-butyryl, and *N*-benzoyl also failed to generate antibodies capable of reacting with unmodified $GD_3$ (325, 373, 375).

*Passive Immunity: Anti-$GD_3$ Antibodies*

The failure to induce an active immune response against $GD_3$ has shifted efforts towards the use of passive immunity through the injection of anti-$GD_3$ antibodies. Anti-$GD_3$ antibodies have been shown to block the attachment (385), growth and proliferation of cancer cells *in vitro* (386) as well as enhance the immune response against cancer cells by both increasing the proliferation and sensitivity of lymphocytes to growth signals (355, 387). The most investigated anti-$GD_3$ antibody is a murine IgG3 termed R24. MAb R24 was isolated from a mouse immunized with the melanoma cell line SK-MEL-28 (367, 374) and has been shown to be specific for the terminal sialic acid residue of $GD_3$ (388). R24 reacts with $GD_3$-bearing melanomas and astrocytomas (367) and is able to prevent tumor adherence, mediate ADCC and CDC (385, 389), and prevent tumor growth in animal models (385, 390, 391). These promising results have paved the way for the use of mAb R24 in human clinical trials.

In phase I clinical trials, injections of mAb R24 led to partial response and mild toxicity (391). In general, the response has been influenced by both the strength and heterogeneity of $GD_3$ expression on tumor cells (389). Other clinical trials have focused on boosting the immune response by testing combinations of mAb R24 with various cytokines. Unfortunately, the results of these treatments have paralleled those obtained with mAb R24 alone (392-403). Although regression of tumors after mAb R24 treatment has been demonstrated (404) and trials have shown a consistent 10% response rate (390), the potential therapeutic value of mAb R24 is limited due to the development of human anti-mouse

antibodies (HAMA) in all patients (405). Ongoing studies using a humanized version of mAb R24 (chimeric R24 or chR24) may prove valuable to address this issue (406).

Several studies have focused on elucidating the recognition mechanism of mAb R24 for $GD_3$ with the intent of using this information to design a more effective tumor-associated $GD_3$-binding antibody for use in cancer therapy. Many of these studies have investigated the ability of mAb R24 to exhibit what is termed 'homophilic binding'. This type of interaction allows mAb R24 to bind additional mAb R24 molecules and/or anti-$GD_3$ antibodies (376) through an idiotope referred to as $ID_{HOM}$. For this interaction to occur, however, R24 must first bind to membrane-displayed $GD_3$ (407, 408). An investigation into the binding of R24 to cancer cells displaying $GD_3$ revealed that binding saturation of mAb R24 could not be achieved and suggested this to be a consequence of homophilic binding (385). In addition, homophilic binding was proposed as a means to increase the valency of mAb R24 for the membrane-displayed $GD_3$ epitope (Figure 4.2).

Mutants of mAb R24 constructed by substituting the light chain of mAb R24 with other light chains reveal that both homophilic and $GD_3$ binding are predominantly mediated through the H chain of mAb R24 (385). In addition, a single mutation of S H52a to Thr in the CDR H2 of R24 has been shown to be sufficient to abolish homophilic binding without disturbing $GD_3$ binding (376). The crystal structure of an R24 antibody fragment supports the above findings by showing that homophilic binding occurs between the H2 of individual R24 antibodies while the binding of $GD_3$ is proposed to be mediated through the H chain alone (Figure 4.3) (408).

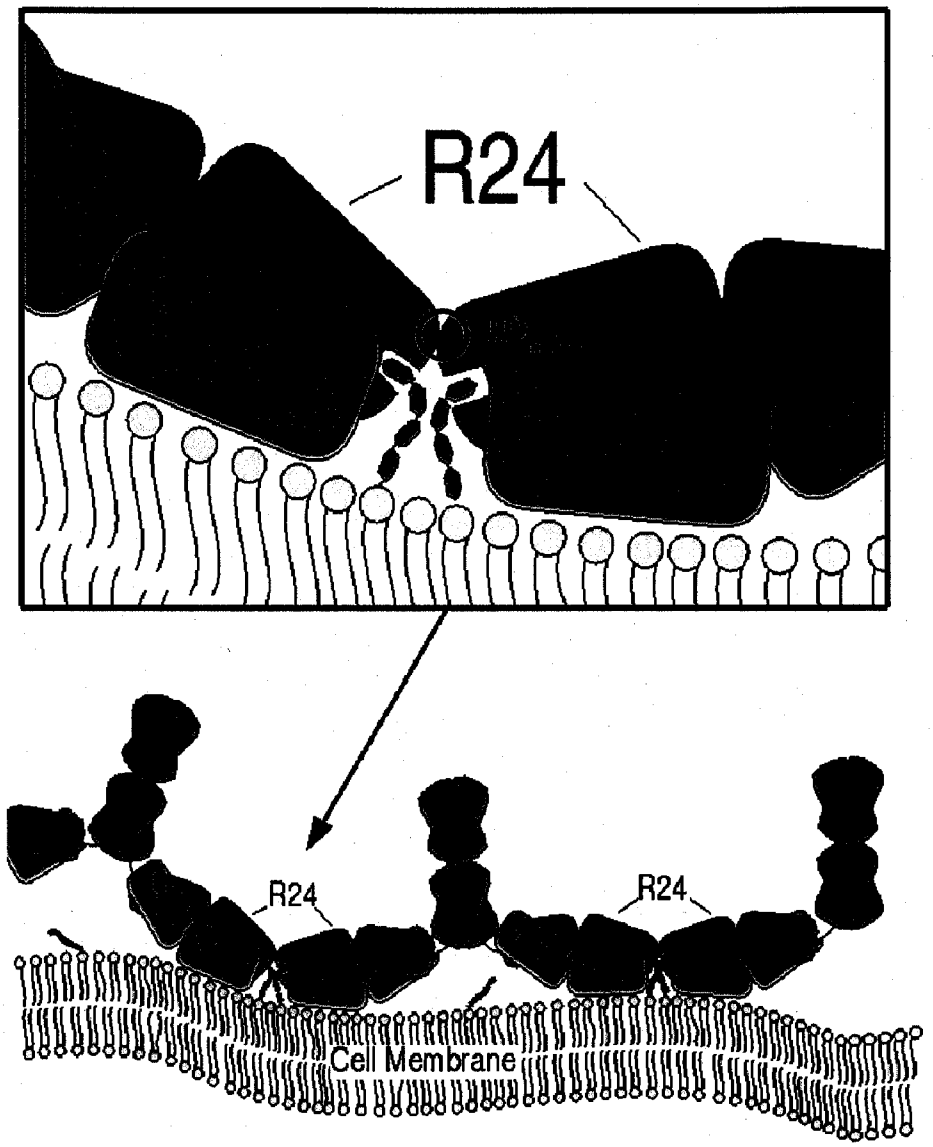


**Figure 4.2. R24 mechanism at the cell surface.** R24 IgG is able to interact with itself and other anti-$GD_3$ antibodies through an epitope termed "$ID_{HOM}$". This mechanism of recognition occurs at cell surfaces and could serve to increase the valence of antibodies for carbohydrate antigens. Figure adapted from Kaminski *et al.* (408).

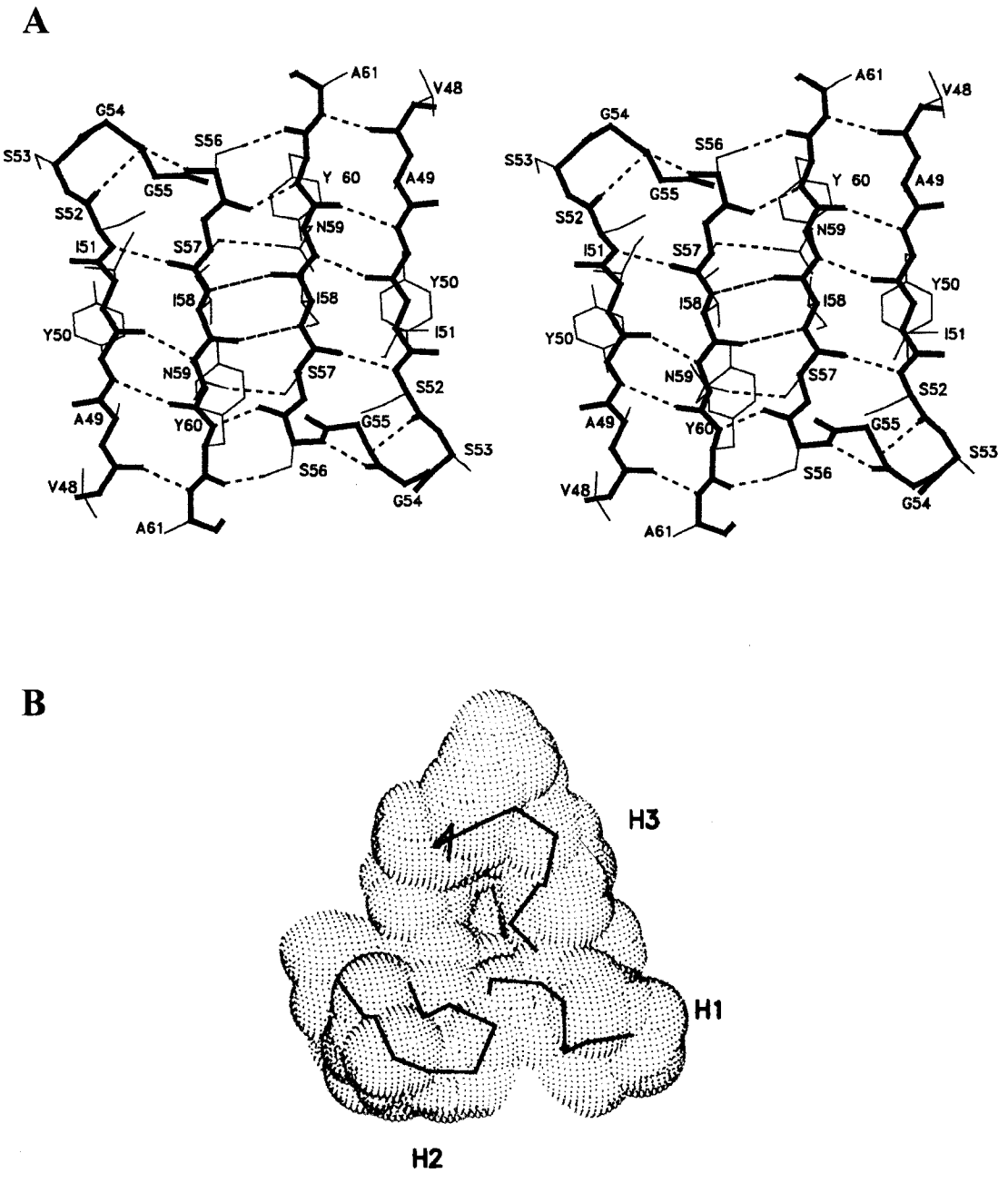


**Figure 4.3. Structural features of R24. A.** The crystal structure of R24 Fab revealed that the homophilic binding site $ID_{HOM}$ is mostly mediated through the CDR H2. In this stereo picture, a network of hydrogen bonds is seen between symmetry-related partners in the crystal. **B.** The binding site for the $GD_3$ ganglioside antigen is proposed to consist of a deep pocket, seen as the red dotted accessible surface area, formed by all three CDRs of the H chain. Figures from Kaminski *et al.*(408).

*Active Immunity: Anti-Anti-$GD_3$ or Anti-Idiotypic Antibodies*

Anti-idiotypic antibodies can bear the internal image of a targeted antigen, and those that do can be used effectively to break tolerance to these antigens (409, 410). To isolate anti-idiotypic antibodies mimicking $GD_3$, mice were immunized with mAb R24. One of the antibodies isolated, an IgG2b termed BEC2, displayed specific binding to mAb R24 as well as to other anti-$GD_3$ antibodies. More importantly, BEC2 was able to immunize New-Zealand White rabbits against $GD_3$ even though they display $GD_3$ on their normal tissues (411). Half of the animals generated anti-$GD_3$ IgG antibodies with no observed cross-reaction with normal tissues indicating great potential for BEC2 in immunizations against $GD_3$-bearing tumors.

Human clinical trials with BEC2 are promising. Whether used alone (412-414), in conjunction with adjuvants (415, 416), or conjugated to highly immunogenic carriers (417), BEC2 has consistently generated a response rate of 20% in patients with melanoma or small cell lung cancer. BEC2 is still under clinical study, under the name Mitumomab, with phase III trials currently underway (418).

## RATIONALE

$GD_3$ represents an excellent target for cancer immunotherapy. The inherent poor immunogenicity of carbohydrates, such as $GD_3$, and the presence of $GD_3$ within normal tissues, however, has presented significant obstacles in the development of high affinity cancer-specific anti-$GD_3$ antibodies. Although attempts at passive immunization using the anti-$GD_3$ mAb R24 have shown some degree of success in the treatment of various cancers,

the development of HAMA responses has limited its application. Consequently, efforts have shifted towards inducing an active immune response in cancer patients through the use of anti-idiotypic antibodies. In this regard, the anti-idiotypic mAb BEC2 has shown great promise. BEC2 is a good $GD_3$ mimic because not only is it specific for both R24 and other anti-$GD_3$ antibodies, but it has also been used successfully to immunize against tumor-associated $GD_3$ in hosts that natively express $GD_3$.

The objective of this research is to gain a greater understanding of the mechanism by which BEC2 mimics $GD_3$ using the technique of x-ray crystallography. This knowledge will aid in directing specific modifications of BEC2 with the ultimate goal of creating a more effective vaccine by designing a novel antibody with greater immunogenicity. To accomplish this objective, the structures of R24 in complex with BEC2 and R24 in complex with $GD_3$ are required. Unfortunately, the inability of R24 to bind $GD_3$ in solution inhibits the production of R24-$GD_3$ complex crystals. To overcome this obstacle, attempts were made at isolating R24-like antibodies capable of binding both BEC2 and $GD_3$, and more importantly, capable of forming a complex with $GD_3$ in solution. It is hypothesized that BEC2 mimics the terminal sialic acid residues of $GD_3$ with its longest L chain CDR and that the recognition mechanisms with mAb R24 and other anti-$GD_3$ antibodies rely on overall shape and charge complementarity.

## MATERIALS AND METHODS

### *First Approach: Isolating a Novel Anti-$GD_3$ Antibody*

#### *Part A: Human R24-like Antibodies*

*Expression and Purification of R24-like Human scFvs*

Constructs for PC30 and PC41, human antibodies isolated from patients immunized with BEC2, were received from Dr. Paul B. Chapman, Memorial Sloan-Kettering Cancer Center (MSKCC), New York, NY, USA. Dr. Nina O.L. Seto, IBS, NRCC, redesigned the scFvs into pUCE8 and pCW vectors adding an ompA secretion leader and a $His_6$ tail, and the constructs were transformed into *E. coli* BL21 cells. Clones were grown in 1L of TBII medium (Bio 101, Vista, CA) supplemented with 100 μg/mL ampicillin, with vigorous aeration at 30 °C overnight. The cells were induced with 1 mM isopropyl-β-D-thiogalacto-pyranoside (IPTG) at mid-log and left to grow for 24 hours. The cultures were centrifuged at 8000 rpm for 10 minutes and the supernatant was discarded. The cell pellets were stored at –20 °C until processing.

For processing, the pellets were put on ice and resuspended in 25 mL of 10 mM sodium phosphate, 500 mM NaCl, 10 mM imidazole. The periplasm was extracted on ice with a sonicator. ScFv was purified with a HiTrap metal chelate affinity column (GE Healthcare, Piscataway, NJ) using a step gradient of increasing imidazole concentration. The eluted peaks were dialyzed against 100 mM Tris pH 8.0, 150 mM NaCl. ScFv was subjected to subtilisin treatment to digest the linker connecting the H and L chains of the antibody construct, with a subtilisin:scFv ratio of 1:20 for 5 hours at 37 °C. The reaction was quenched with a 10-fold excess of phenylmethylsulfonyl fluoride (PMSF).

*Surface Plasmon Resonance Analysis*

Binding kinetics were determined using a BIAcore 3000 biosensor system (Biacore, Piscataway, NJ) by Tomoko Hirama, IBS, NRCC. BEC2 IgG (ImClone Systems, Somerville, NJ) and a negative control protein were immobilized on a research grade CM5 chip by amine coupling according to the manufacturer's instructions. The analysis of scFv binding was carried out in 10 mM Hepes pH 7.4, 150 mM NaCl, 3.4 mM ethylenediaminetetraacetic acid (EDTA), 0.005% P-20 (HBS-EP) at a flow rate of 20 μL/min. Additional testing included immobilization of scFv on a CM5 chip to analyze BEC2 IgG binding. This was carried out in HBS-EP at 10 μL/min.

For analysis of $GD_3$ binding, $GD_3$ liposomes were generated. Liposomes were prepared as follows: 90 μL of 10 mg/mL dimyristoylphosphatidylcholine (DMPC)/chloroform solution was added to a glass vial containing 140 μL of 0.71 mg/mL of $GD_3$/chloroform:MeOH solution. The mixture was purged with nitrogen gas while rotating the vial, in order to generate a thin lipid film. Liposomes were lyophilized overnight. 300 μL of HBS-E and 5 μL of 2 mg/mL Salmonella lipopolysaccharide (LPS) were added to the vial, vortexed and placed in a sonic bath for 20 seconds. Liposomes were extruded with a 50 nm polycarbonate membrane. Control liposomes containing only DMPC were generated similarly. $GD_3$ and control liposomes were immobilized via the LPS on a chip covered with Se155-4 IgG, an anti-Salmonella LPS antibody, at a flow rate of 5 μL/min. ScFv binding was tested at a flow rate of 10 μL/min. Positive control for the integrity of the liposome chip consisted of injections of R24 IgG.

*Part B: Llama R24-like sdAbs*

*Phage Biopanning of Llama sdAbs Naïve Library With BEC2 and $GD_3$*

A naïve phage library (5.4 X $10^8$) was used for the selection (135). For the first round, a well was coated with 150 µL of 100 µg/mL BEC2 IgG in PBS overnight at 4 °C. The BEC2 solution was discarded and the well was blocked with 300 µL of 2% gelatin solution in PBS for 2 hours at 37 °C. $10^{12}$ transducing units of phage were incubated in 150 µL blocking buffer for 2 hours at RT. Non-binding phage were discarded and the well was washed ten times with 0.05% PBST followed by ten PBS washes. Bound phage were eluted with 200 µL of 0.2 M glycine pH 2.3 and neutralized with 100 µL of 1M Tris pH 7.4. For further rounds of biopanning, half of the total volume of eluted phage solution was used to infect 10 mL of mid-log *E. coli* TG1 in 2YT culture, for 30 minutes at 37 °C no shaking. Infected *E. coli* TG1 cells were centrifuged for 10 minutes at 2000 rpm and the supernatant was discarded. The cell pellet was resuspended in 900 µL fresh 2YT medium. Three aliquots of 300 µL concentrated infected *E. coli* TG1 were each added to 3 mL of warm agarose top and plated onto 2YT agar. Plates were incubated overnight at 37 °C. Phage titers were generated as follows: phage solution was sequentially diluted in PBS and 10 µL from each dilution was used to infect 200 µL of mid-log *E. coli* TG1 in 2YT culture, 30 minutes at 37 °C no shaking. Each 200 µL of infected *E. coli* TG1 as well as an aliquot of 200 µL control mid-log *E. coli* TG1 were added to 3 mL warm agarose top and plated onto 2YT agar. Plates were incubated overnight at 37 °C.

Plates with concentrated infected *E. coli* TG1 were each washed with 5 mL PBS for 3 hours at 4 °C with shaking. Washes were pooled and additional quick washes of 5 mL PBS per plate were added to the pool. The pool was centrifuged for 10 minutes at 2000 rpm

to pellet debris. 25 mL of supernatant was collected in a sterile centrifuge tube and phage were precipitated by addition of 5 mL of a solution of 20% PEG 8K / 2.5 M NaCl for 1 hour on ice. Precipitated phage were centrifuged for 30 minutes at 10,000 rpm. The supernatant was discarded and the pellet was resuspended in 3 mL of sterile water, then precipitated a second time by addition of 600 μL of the same PEG/NaCl solution for 1 hour on ice, centrifuged for 30 minutes at 10,000 rpm, the supernatant was discarded, phage resuspended in 500 μL PBS and subjected to a quick spin at 13,000 rpm, and the clean supernatant was transfered to a new tube. Phage titers were generated as previously described.

For the second round, a well was coated with 150 μL of 100 μg/mL $GD_3$ (Advanced ImmunoChemical Inc, Long Beach, California) in 100% methanol overnight at RT to let the methanol evaporate (419). The well was blocked with 300 μL of 2% bovine serum albumin (BSA) in PBS for 2 hours at 37 °C. The blocking solution was discarded and eluted phage were incubated in 150 μL blocking buffer for 2 hours at RT. Further procedures were done as described for the first round of biopanning. The third and last round of biopanning consisted of biopanning against BEC2 IgG, as described for the first round.

*Phage ELISA*

Three microtiter plates (Nunc, Naperville, IL) were used for ELISA: a plate coated with BEC2 IgG, one coated with $GD_3$ and one control plate coated with BSA. Both BEC2 and BSA plates were coated with 150 μL of 10 μg/mL protein in PBS solution per well at 4 °C overnight while the $GD_3$ plate was coated with 150 μL of 10 μg/mL $GD_3$ in 100% methanol per well at RT overnight. The BEC2 and BSA plates were blocked with 300 μL of a 2% gelatin solution in PBS while the $GD_3$ plate was blocked with 300 μL of a 2% BSA solution in PBS, at 37 °C for 2 hours. Phage-infected *E. coli* TG1 grown in 2YT was

centrifuged 15 min at 2000 rpm and the supernatant was transferred to the plates with the respective blocking proteins. The plates were incubated for 2 hours at RT. Unbound phage were discarded and all plates washed ten times with PBST followed by ten washes with PBS. The plates were incubated with horseradish peroxidase (HRP)-conjugated mouse anti-M13 antibody (GE Healthcare, Piscataway, NJ) diluted 1:1,000 in PBS, for 1 hour at RT. The antibody solution was discarded and the plates washed as before. Binders were identified by adding 150 ul of HRP substrate – a 1:1 mixture of TMB peroxidase:$H_2O_2$ (KPL, Gaithersburg, MD) - per well. After 5 minutes, the reaction was quenched with 150 µL of 1 M phosphoric acid per well, and a readout was taken at 405 nm.

*Growth of SK-MEL-28 Malignant Melanoma Cell Line*

Cell line HTB-72 (lot# 2090287) was purchased from ATCC (Manassas, VA). Cells were cultured in DMEM (Gibco, Rockville, MA) supplemented with 10% fetal bovine serum (FBS) - 1x antibiotic/antimycotic (Gibco, Rockville, MA) and maintained at 37 °C in a 5% $CO_2$ atmosphere. The culture medium was renewed every 2-4 days when cells were confluent. When medium was changed, cells were first washed with 10 mL of Hank's Balanced Salt Solution (Gibco, Rockville, MA) followed by 1 mL of trypsin solution (0.25% trypsin, 1 mM EDTA) and incubated at 37 °C for 1-2 minutes. Cells were resuspended with DMEM and redivided.

*Phage Biopanning of Llama sdAbs Naïve Library With BEC2 and SK-MEL-28*

First and third rounds of biopanning were done with BEC2 IgG as described previously. For the second round, a 5 mL culture tube was blocked with a 4% BSA in PBS solution overnight at 4 °C, rotating. Six bottles of confluent SK-MEL-28 cells were used for

biopanning. The cells were washed with 10 mL PBS and detached by using 1 mL of a 5 mM EDTA in PBS solution, per bottle, for 10 minutes at 37 °C. After incubation, cells were released by addition of PBS. A small aliquot of cells was diluted with trypan blue for counting. There were $2x10^5$ cells/mL (or a total of $7x10^6$ cells). The cells were centrifuged for 5 minutes at 500xg (Sorvall Legend RT centrifuge from Mandel). The supernatant was discarded and the cell pellet was washed with 45 mL of PBS. Cells were centrifuged again for 5 minutes at 500xg, the supernatant discarded, the pellet resuspended in 2 mL of 2% BSA in PBS and transfered to the blocked tube. Cells were blocked for 2 hours at 4 °C, rotating. The cells were centrifuged for 5 minutes at 500xg and the supernatant was discarded. The cells were resuspended in 1.9 mL of 2% BSA in PBS and 100 µL of the phage eluted and multiplied from first round was added. The cells were incubated with phage for 2 hours at 4 °C, rotating. The cells were centrifuged for 5 minutes at 500xg and the supernatant was discarded. Cells were washed five times with 2 mL PBS. A $6^{th}$ wash was done using PBS pH 6.1 to increase stringency (420). The bound phage were eluted by adding 200 µL of PBS-76 mM citric acid pH 2.8 for 10 minutes at RT and then neutralized with 200 µL of 1M Tris pH 7.4. 250 µL of the eluted phage was used to infect 10 mL of mid-log *E. coli* TG1 in 2YT medium for 30 minutes, 37 °C no shaking. Infected *E. coli* TG1 were diluted and plated as previously described.

*Phage ELISA 2*

Cells from 6 bottles were detached using a 5 mM EDTA solution. Cells were counted and totaled $2x10^7$ cells (or $7x10^5$ cells per mL for 35 mL). Half of the volume of cells was used to prepare a 96-well microtiter plate with a final concentration of $1x10^5$ cells/well. The microtiter plate was incubated at 37 °C overnight.

One plate was coated with 150 μL of a 10 μg/mL BEC2 IgG in PBS solution per well. A third plate was coated with 150 μL of a 10 μg/mL BSA in PBS solution per well. Both these plates were put at 4 °C overnight to coat. The SK-MEL-28 plate was washed twice with PBS and then the cells were fixed for 20 minutes in 0.25% formaldehyde in PBS. This was followed by another three washes with PBS. All plates were blocked for 2 hours at 37 °C, the SK-MEL-28 plate in a solution of 2% BSA in PBS, and the BEC2 and BSA plates in a solution of 2% gelatin in PBS. The infected *E. coli* TG1 were centrifuged to retrieve phage in the supernatant, 15 minutes at 2000 rpm. The phage was incubated with 2% BSA in PBS in the SK-MEL-28 plate and with 2% gelatin in PBS in the BEC2 and BSA plates, for 2 hours at RT. The BEC2 and BSA plates were washed ten times with PBST followed by ten times with PBS. The SK-MEL-28 plate was washed five times with PBS. Plates were developed as previously described.

*Expression and Purification of SdAbs*

For the BEC2 - $GD_3$ biopanning, ELISA-positive phages were grouped into 7 consensus sequences termed RCL1 through RCL7. For the BEC2 – SK-MEL-28 biopanning, all ELISA-positive phages were grouped into one consensus sequence, termed RCL8. All eight clones, RCL1 through RCL8, were incorporated into the expression vector pSJF2, which added an N-terminal OmpA secretion leader as well as C-terminal myc detection and $His_5$ purification tags (421, 422). Following transformation into *E. coli* TG1 cells, clones expressing sdAbs were selected. Overnight cultures were used to each inoculate 1 L of LB medium supplemented with 100 μg/mL ampicillin and the 1 L cultures were left to grow at 30 °C with vigorous agitation. At mid-log, cultures were induced for expression using 1 mM IPTG for 5 hours. Expression of soluble sdAbs was confirmed by

SDS-PAGE and Western blot. Cultures were centrifuged at 8000 rpm for 10 minutes and supernatant was discarded. Pellets were stored at –20 °C until processing.

Culture pellets were put on ice with 25 mL of 10 mM Hepes pH 7.5, 500 mM NaCl, 10 mM imidazole and a tablet of COMPLETE protease inhibitor (Roche Diagnostics, Laval, Québec). Pellets were resuspended and cells were lysed by EmulsiFlex (Avestin, Ottawa, ON). Lysed cells were incubated with DNAseI for 1 hour on ice and then were spun down at 10,000 rpm for 1 hour. Supernatants were dialyzed against 4 L of 10 mM Hepes pH 7.5, 500 mM NaCl, 50 mM imidazole overnight at 4 °C. Supernatants were filtered with 0.45 um membrane and loaded onto HiTrap metal chelate affinity column (GE Healthcare, Piscataway, NJ). SdAbs were eluted with a linear gradient of 0-500 mM imidazole. Pooled sdAb peaks for each clone were dialyzed against 10 mM Hepes pH 7.4, 150 mM NaCl, 3.4 mM EDTA (HBSE), concentrated using a Centricon YM3 ultrafiltration device (Millipore, Billerica, MA), and loaded onto a Superdex 75 size-exclusion chromatography column (GE Healthcare, Piscataway, NJ) for final purification.

*SPR Analysis of SdAbs*

Binding kinetics were determined using a BIAcore 3000 biosensor system (Biacore, Piscataway, NJ) by Tomoko Hirama, IBS, NRCC. BEC2 IgG and control protein BSA were immobilized on a research grade CM5 chip by amine coupling according to the manufacturer's instructions. Analysis of the sdAbs was carried out in HBS-EP at a flow rate of 40 μL/min. Analysis of sdAbs for $GD_3$ binding was done on liposomes as previously described.

*Expression and Purification of Pentabodies*

To measure multivalent binding to $GD_3$, sdAbs shown to bind BEC2 by SPR were incorporated into the expression vector pVT2, which added an N-terminal OmpA secretion leader, a C-terminal verotoxin B subunit as well as c-myc detection and $His_5$ purification tags (91). Following transformation into *E. coli* TG1 cells, clones expressing pentabodies were selected. Cultures of 20 mL M9 medium supplemented with 100 μg/mL ampicillin were inoculated with a single colony from fresh plated pentabody clones and left to grow overnight at 37 °C, 250 rpm. The overnight cultures were used to each inoculate 900 mL of M9 medium with 100 μg/mL ampicillin and were left to grow 12 hours. Cultures were induced with 100 mL of 10xTB nutrients and 1 mM IPTG, and were left to grow for 3 days at 30 °C. Cells were centrifuged at 8000 rpm for 10 minutes and supernatant was discarded. Pellets were stored at –20 °C until processing. Expression of soluble pentabodies was confirmed by SDS-PAGE and Western blot.

Soluble pentabodies were extracted from cell pellets as described for sdAb extraction. Supernatant containing soluble pentabodies was loaded onto a HiTrap metal chelate affinity column (GE Healthcare, Piscataway, NJ) and the proteins were eluted using a linear gradient of 0-1 M imidazole. Pooled pentabody peaks for each clone were dialyzed against HBSE, concentrated using a Centricon YM10 ultrafiltration device (Millipore, Billerica, MA), and loaded onto a Superdex 200 size-exclusion chromatography column (GE Healthcare, Piscataway, NJ) for final purification.

*SPR Analysis of Pentabodies*

Binding kinetics were determined using a BIAcore 3000 biosensor system (Biacore, Piscataway, NJ) by Tomoko Hirama, IBS, NRCC. $GD_3$ liposomes as well as control DMPC

liposomes were generated as previously described. Liposomes were immobilized at a flow rate of 5 μL/min. Pentabody analysis was carried out in HBS-EP at a flow rate of 10 μL/min. Positive control for the integrity of the liposome chip was injection of R24 IgG.

***Second Approach: Digest of BEC2 and Purification of BEC2 Fab for Crystallization***

*Papain Digest of BEC2 IgG*

BEC2 IgG (ImClone Systems, Somerville, NJ), final concentration 0.8 mg/mL, was digested with papain (Sigma Aldrich) in a ratio of 1:50 in the presence of 15 mM dithiothreitol (DTT), 50 mM Tris pH 8.0 and 2 mM EDTA for 2 hours at 37 °C. The reaction was quenched with a 10-fold excess of iodoacetamide for 30 minutes at RT in the dark.

*Ion Exchange Purification*

The BEC2 digest was dialyzed against 20 mM 2-Bis(2-hydroxyethyl)amino-2-(hydroxymethyl)-1,3-propanediol pH 5.8. Strong anion exchange Shodex QA-825 column (Phenomenex, Torrance, CA) was washed with this same buffer. 1 mL of BEC2 digest was injected and Fab peaks eluted. Bound protein was eluted with a 2-step linear gradient of 0-1.2 M sodium acetate. Fractions were analyzed by SDS-PAGE.

*Chromatofocusing*

Chromatofocusing was assayed using both commercial polybuffers as well as with custom buffers according to Shan and Anderson (423). For the later, the BEC2 digest was dialyzed against 15 mM Bis-Tris Propane, 25 mM Piperazine, pH 7.6 (starting buffer). A 50% slurry of weak anion exchanger PBE 94 matrix (GE Healthcare, Piscataway, NJ) was

packed into a glass column and washed with starting buffer. BEC2 sample was applied and bound protein was eluted with a linear gradient of 25 mM acetic acid, 25 mM lactic acid, 25 mM chloroacetic acid, pH 2.3. Fractions were analyzed by SDS-PAGE. For commercial polybuffers, BEC2 digest was dialyzed against 25 mM imidazole pH 7.4. BEC2 sample was applied to PBE 94 column and elution buffer was applied [62.5 mL Polybuffer 74 (GE Healthcare, Piscataway, NJ) was diluted to 500 mL with water and pH was adjusted to 5.0]. Peaks collected were analyzed by SDS-PAGE.

*Protein A Purification*

The BEC2 digest was dialyzed against 100 mM Hepes pH 7.2, 150 mM NaCl (starting buffer). A HiTrap Protein A 1 mL affinity column (GE Healthcare, Piscataway, NJ) was washed with 5 mL of the starting buffer. The digest was applied to the column and flow through was collected. The column was washed with an additional 5 mL of starting buffer and bound protein was eluted with 100 mM glycine pH 2.5. Fractions of 1 mL were collected, neutralized with 100 µL Tris pH 9.1 and analyzed by SDS-PAGE.

*Protein G Purification*

The BEC2 digest was dialyzed against an equivalent starting buffer as for protein A purification. Equilibration of the HiTrap Protein G 1 mL affinity column (GE Healthcare, Piscataway, NJ), sample application, column washing and elution of bound protein were done as described for protein A purification. Fractions were analyzed by SDS-PAGE.

*Protein L Purification*

The BEC2 digest was dialyzed against equivalent starting buffer as for protein A and G purifications. Equilibration of the Protein L 2 mL column (Pierce, Rockford, IL), sample application, column washing and elution of bound protein were done as described for protein A purification. Fractions were analyzed by SDS-PAGE.

*Metal Ion Affinity Purification*

The BEC2 digest was dialyzed against 10 mM Hepes pH 7.5, 500 mM NaCl (starting buffer). A 1 mL HiTrap column (GE Healthcare, Piscataway, NJ) was loaded with 1 mL of a 1% $CuSO_4$ solution and washed with water. The column was equilibrated with starting buffer and BEC2 sample was applied. Flow through was collected and the column was washed again with starting buffer. Bound protein was eluted with a linear gradient of 10 mM Hepes pH 7.5, 1 M ammonium chloride. Fractions were analyzed by SDS-PAGE.

*Hydrophobic Interaction Purification*

The BEC2 digest was dialyzed against 100 mM Tris pH 7.0. One part BEC2 digest was mixed with one part 4 M ammonium sulfate to generate a BEC2 sample in 50 mM Tris pH 7.0, 2 M ammonium sulfate. A 1 mL HiTrap Phenyl HP hydrophobic interaction column (GE Healthcare, Piscataway, NJ) was equilibrated with 50 mM Tris pH 7.0, 2 M ammonium sulfate. The BEC2 sample was applied to the column and the flow through was collected. Bound protein was eluted with linear gradient of 2 M – 0 M ammonium sulfate in 50 mM Tris pH 7.0. Fractions were analyzed by SDS-PAGE.

***Third Approach: Expression of R24 and BEC2 Constructs for Crystallization***

*Design and Expression of sdAbs of R24 $V_H$*

Llama mutations E6A, S84P, and T93A, as well as camel mutations V37F, G44E, L45R, and W47G, and a combination of both sets of mutations were introduced into R24 $V_H$ to increase its solubility. R24 fragments were amplified using Touchdown PCR on a Perkin-Elmer thermocycler model GeneAmp 9700. Amplified fragments were purified using Qiagen kits (Qiagen, Mississauga, ON) and combined using the splice-overlap extension method (SOE) (424, 425). Constructs were incorporated into the pSJF2 vector as described previously and transformed into *E. coli* TG1 cells. Small-scale expression of R24 sdAbs was subject to a time course study. Briefly, overnight cultures were used to inoculate 20 mL of TB medium with 100 μg/mL ampicillin and left to grow at 30 °C with vigorous agitation. At mid-log, cultures were induced for expression using 1 mM IPTG and the temperature was dropped to 25 °C. Fractions were taken at various timepoints to assess level of expression of the construct. For each timepoint, fractions were treated as follows: to check for insoluble expression, 100 μL of whole culture was mixed with 100 μL water and 50 μL of 5x SDS-PAGE dye; to check for soluble expression, 2 mL of whole culture was centrifuged 2 minutes at 15,000 rpm, the supernatant was discarded and the pellet was lyzed with 100 μL CelLytic B reagent (Sigma-Aldrich, St-Louis, MO). The lysate was centrifuged 5 minutes at 15,000 rpm and 80 μL of supernatant was mixed with 20 μL 5x SDS-PAGE dye. Fractions were then analyzed on SDS-PAGE and Western blot. The llama R24 sdAb construct was also incorporated into the pGEX-4T-3 vector for expression with a GST tag in *E. coli* BL21 and Rosetta-gami B (Novagen, Madison, WI) cells. Expression in these backgrounds was assessed as described for pSJF2/TG1. Finally, the llama R24 sdAb construct was

incorporated into the pPIC9 vector for secreted expression in yeast *P. pastoris* SMD1168 cells (Invitrogen, Carlsbad, CA). The construct was amplified with primers designed to incorporate a C-terminal $His_6$ tail preceded by a Factor Xa cleavage site, as well as an N-terminal αF secretion signal sequence. Transformants were selected for 3 days at 30 °C as described (Invitrogen, Carlsbald, CA). Transformants were screened for MutS or Mut+ growth phenotype. Briefly, 100 colonies per transformant were picked to score minimal media plates containing dextrose. After two days of growth at 30 °C, all colonies were picked again to score minimal media plates containing methanol. After two days of growth at 30 °C, colonies that grew on the methanol plates were deemed Mut+ whereas colonies that did not grow were deemed MutS. MutS colonies were used for expression screens (426). Six MutS colonies were picked per transformant, and used to inoculate 8-9 mL of K-BMGY medium. Cultures were grown at 30 °C with vigorous shaking overnight, then centrifuged for 5 minutes at 2000 rpm and resuspended in 1 mL of CA-BMMY for induction. Timepoints were taken every 24 hours for five days to check for expression of recombinant antibody species. Fractions were centrifuged for 1 minute 15,000 rpm and 80 μL medium was combined with 20 μL of 5x SDS-PAGE dye. Time course expression was analyzed by SDS-PAGE.

*Expression of BEC2 and R24 scFvs*

Constructs for BEC2 and R24 scFvs with $(GGGGS)_3$ linker were designed by Dr. Nina O. L. Seto, IBS, NRCC and incorporated into pUCE8 and pCW vectors in *E. coli* BL21 cells. Constructs were also incorporated into pGEX-4T-3 for expression in *E. coli* BL21 and Rosetta-gami B cells, as well as in pPIC9 for secreted expression in yeast *P.*

*pastoris* SMD1168 cells. Expression was tested by time course experiments as previously described.

*Expression of Chimeric BEC2 $V_L$ - R24 $V_H$ scFvs*

The BEC2 $V_L$ and R24 $V_H$ fragments were amplified using Touchdown PCR. Amplified fragments were purified using Qiagen kits (Qiagen, Mississauga, ON) and combined using SOE. The scFv constructs were designed with the long linker $(GGGGS)_3$ in both the $V_L$-$V_H$ and the $V_H$-$V_L$ orientations. Constructs were incorporated into the pSJF2 vector as described previously and transformed in *E. coli* TG1 cells. Constructs were also incorporated into pGEX-4T-3 for expression in *E. coli* BL21 and Rosetta-gami B cells, as well as in pPIC9 for secreted expression in yeast *P. pastoris* SMD1168 cells. Small-scale expression of all these constructs was done with time course experiments as described previously.

## RESULTS AND DISCUSSION

### *First Approach: Isolating a Novel Anti-$GD_3$ Antibody*

*Part A: Human R24-like Antibodies*

The group of Dr. Paul B. Chapman, MSKCC, isolated antibodies from patients previously immunized with BEC2. Using ELISA, they identified two antibodies that showed binding to both BEC2 and $GD_3$. These antibodies were selected for further analysis and termed PC30 and PC41.

PC30 and PC41 were designed into scFvs and incorporated into vectors pUCE8 and pCW for bacterial expression by Dr. Nina O. L. Seto, IBS, NRCC. These vectors include an ompA leader sequence for targeted expression in the periplasm and correct processing of the disulfide bonds of the scFvs (82). Expression of scFvs PC30 and PC41 was verified using time course experiments. For PC30 scFv, the best expression was observed in pCW whereas it was seen in pUCE8 for PC41 scFv (Figure 4.4). However, only low levels of PC41 scFv expression were achieved. Optimization of PC41 scFv expression was performed using different media, growth temperatures (105, 107), concentrations of IPTG for induction, cell densities at induction, and lengths of induction (115, 427). Unfortunately, these efforts at best resulted in only marginal expression of the scFv. PC30 scFv was expressed in large amounts and purified using a HiTrap metal chelate affinity column and a 150 mM imidazole elution buffer. PC30 scFv was then subjected to subtilisin digest to cleave the linker bridging the $V_L$ and $V_H$ domains to avoid formation of scFv multimers or daisy chains (66, 428).

Pure digested PC30 Fv was analyzed by SPR using BIAcore technology by Tomoko Hirama, NRCC, to verify the results obtained by ELISA and to evaluate in more detail the binding of PC30 Fv to both BEC2 IgG and $GD_3$. To analyze PC30 Fv-BEC2 IgG binding, approximately 3000 RUs of BEC2 IgG and 1950 RUs of control protein BSA were immobilized on a CM5 chip. A flow cell from this same chip containing immobilized Se155-4 anti-Salmonella LPS IgG also served as a negative control surface. The sensorgrams showed no binding of PC30 Fv to immobilized BEC2 IgG (Figure 4.5A). Since PC30 IgG was reported to bind to BEC2 IgG by ELISA, a second approach was taken to analyze the binding by BIAcore. PC30 Fv was immobilized on a CM5 chip at a density

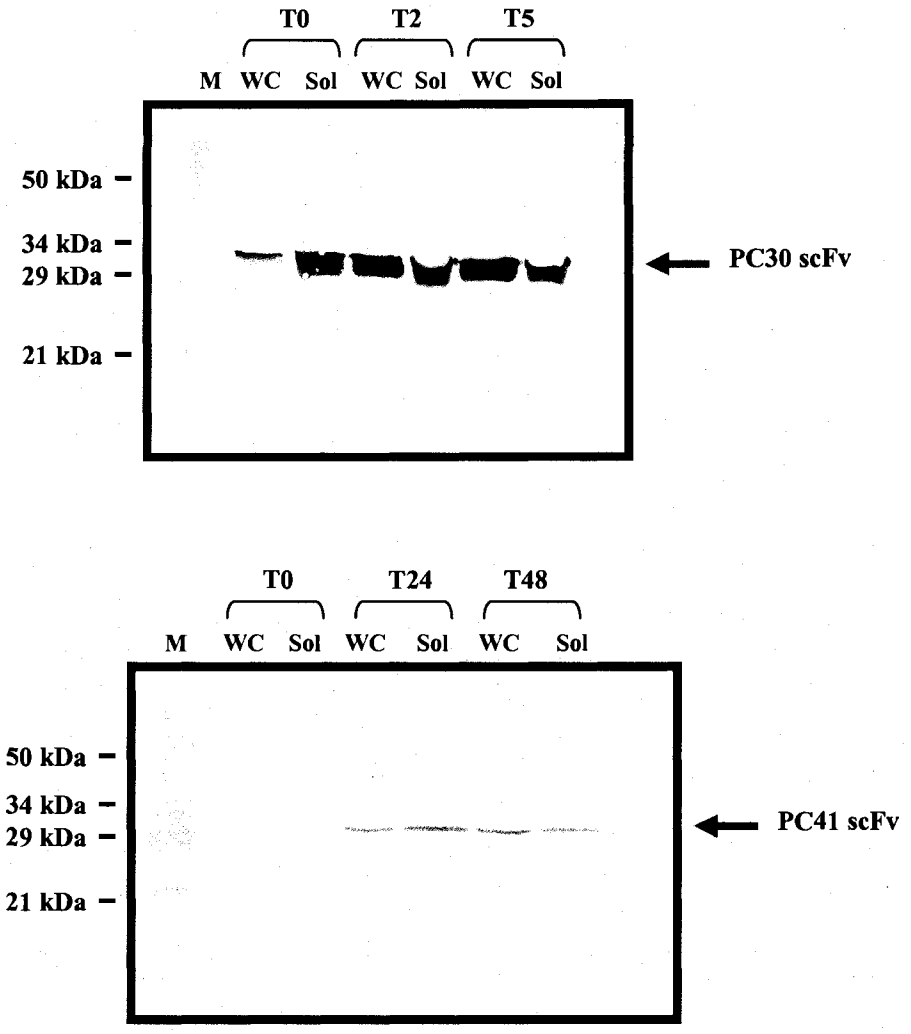


**Figure 4.4. Time course experiments for human scFvs PC30 and PC41.** Whole culture (WC) and soluble (Sol) expression fractions were analyzed at different time points for PC30 and PC41 scFvs. The fractions were run on SDS-PAGE 12.5% and transferred to PVDF membranes. Western blotting was done with an anti-$His_6$ primary antibody and an alkaline phosphatase-conjugated goat anti-mouse secondary antibody. Basal expression is seen at time point T0 for PC30 scFv. Maximum expression of soluble scFv is seen after 5 hours induction for PC30 scFv and after 24 hours induction for PC41 scFv. There was not enough soluble expression of PC41 scFv to warrant further analysis.

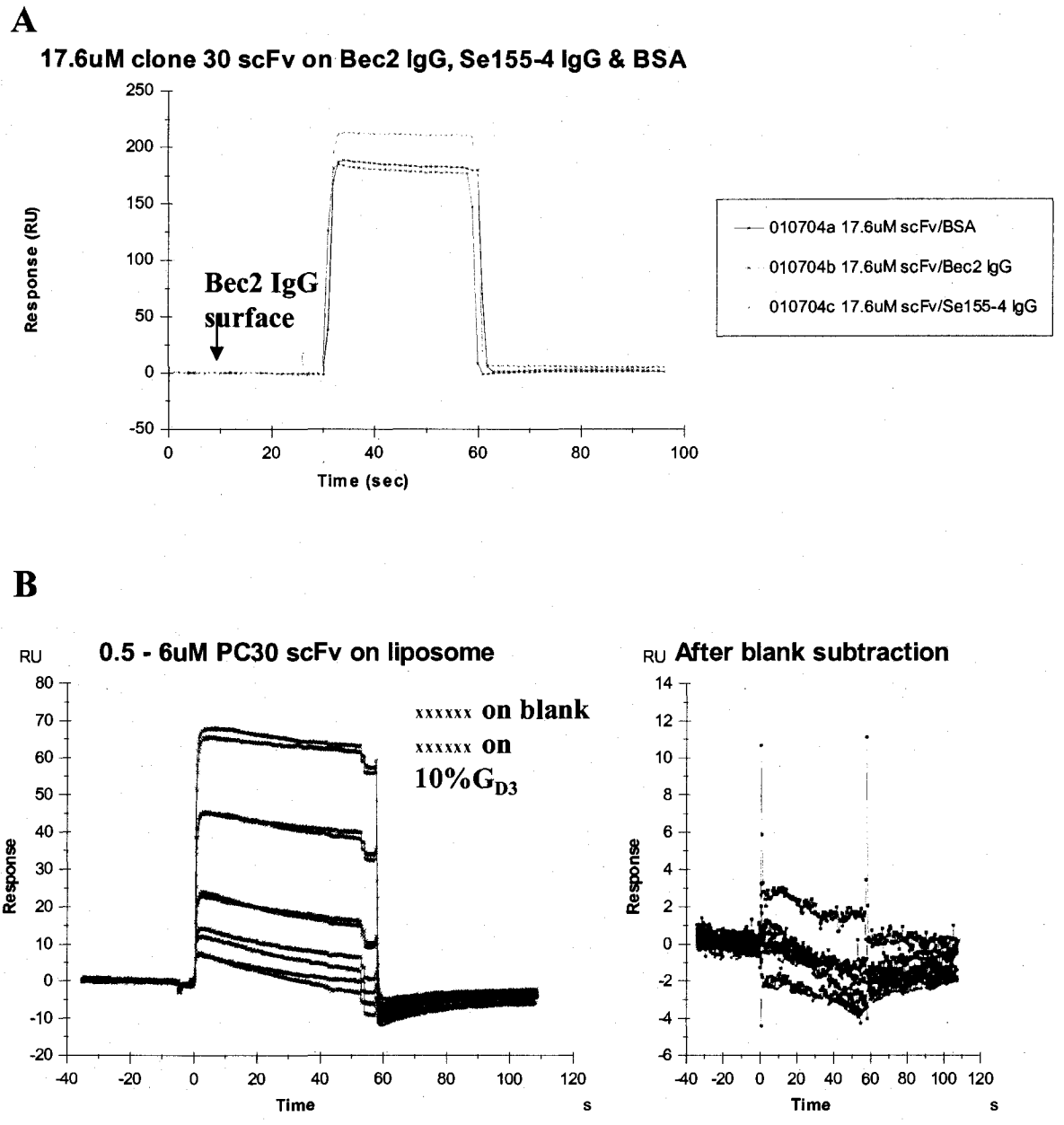


**Figure 4.5. SPR data for PC30 scFv on BEC2 IgG and $GD_3$ liposomes. A.** Overlaid sensorgrams of the interaction of scFv PC30 with BEC2 IgG surface as well as reference surfaces BSA and Se155-4 IgG. BEC2 binding is equivalent to reference surface binding, therefore there was no specific interaction of PC30 scFv with BEC2 IgG. **B.** Overlaid sensorgrams of the interaction of scFv PC30 with liposomes containing 10% GD3 as well as with the reference surface containing blank liposomes. As seen in green, after subtraction of the reference surface, there is essentially no binding observed for PC30 scFv on $GD_3$ liposomes.

of 2990 RUs and BEC2 IgG binding was assessed. Due to the bivalency of the BEC2 IgG, a ten-fold binding increase was expected when compared to the binding response of PC30 Fv to immobilized BEC2 IgG. Unfortunately, the sensorgrams again showed no BEC2 IgG-PC30 Fv binding (data not shown). To analyze PC30 Fv-$GD_3$ binding, approximately 800 RUs of both LPS-containing $GD_3$ liposomes and LPS-containing blank liposomes were each immobilized by Se155-4 IgG that had been previously coupled to a CM5 chip. Although a marginal response was detected with the $GD_3$ liposomes, this response was non-specific as it was independent of the PC30 Fv concentration (Figure 4.5B).

The conflicting results of the ELISA and SPR may be due to a number of factors. It is possible that the binding of PC30 IgG identified by ELISA reflects either non-specific interactions (i.e. PC30 IgG binding to the blocking protein) or 'stickiness' due to the presence of aggregates. Furthermore, multivalency may be required for $GD_3$ binding and this is not addressed in the analysis of PC30 as an Fv. The results from the experiments using PC30 and PC41 indicate that no R24-like human antibodies capable of binding both BEC2 and $GD_3$ were isolated from patients previously immunized with BEC2 IgG.

*Part B: Llama R24-like sdAbs*

Efforts to isolate an R24-like antibody were redirected on the use of a phage display system. A naïve llama sdAb library was generously provided by Dr. Roger C. MacKenzie, IBS, NRCC. The sdAbs were thought to be an interesting alternative to the scFv format as they are known to have excellent physical properties (429) and can be expressed in high amounts (46, 47, 135), features that are both critical in crystallization experiments. The use of a naïve, as opposed to an immune, library has been known to lead to isolation of antibody

fragments of moderate affinity (125, 140). In the following experiments however, these lower affinities could benefit the isolation of antibody fragments with the ability to bind the two distinct antigens BEC2 and $GD_3$. To maximize the probability of isolating sdAbs able to bind both BEC2 IgG protein antigen and $GD_3$ carbohydrate antigen, biopanning experiments were done by alternating between the two antigens in successive rounds. The first round of biopanning was always done with BEC2 IgG, as this would ensure that the sdAbs selected would recognize the $GD_3$ conformation that is displayed by the BEC2 IgG.

*Phage Display Llama sdAbs That Bind BEC2 and $GD_3$*

The biopanning experiment was performed in three rounds: a first round against BEC2 IgG, followed by a round against solubilized $GD_3$, and then a final round against BEC2 IgG. To verify that the amplified phage purified after three rounds could bind both BEC2 and $GD_3$, 226 phage clones were randomly selected for screening by phage ELISA. Of these clones, only 31 showed binding to both BEC2 and $GD_3$ and not to the BSA control. Following sequencing analysis of the 31 phage clones, seven sdAb consensus sequences were identified that showed little similarity. These seven sdAb sequences were termed RCL1, RCL2 and so forth to RCL7 (Figure 4.6). Although RCL1 was by far the most represented sequence, other sdAb sequences were also chosen for analysis as some sdAbs can be maintained through rounds of biopanning for their growth advantages rather than their binding specificity (430).

Most isolated sdAb sequences were found to belong to the $V_HH$ subfamily 1 (431). However, RCL1 belongs to the $V_HH$ subfamily 3 (431). RCL1 possesses a cysteine residue at position 50 in its CDR H2 and a cysteine residue at position 98 in its CDR H3. These two residues are known to form a cystine bridge that is characteristic of $V_HH$ subfamily 3 (432).

```
                      10        20        30          40
                      |         |         |           |
RCL1          DVQLQASGGGLVQPGGSLRLSCAASANTVD IYALG WFRQAPGK
RCL2          DVQLQASGGGLVQAGGSLRLSCKASGRAFS DYYMA WFRQAPGK
RCL3          DVQLQASGGGLVQHGGSLRLSCAASGGTFS SYAMG WFRQAPGK
RCL4          DVQLQASGGGLVQAGGSLRLSCEASGRISR INNMG WYRQAPGK
RCL5          DVQLQASGGGLVQAGGSLRLSCVASGRRVS DYAMG WFRQAPGK
RCL6          DVQLQASGGGLVQAGGSLRLSCAASGRAFS SSSTG WFRQAPGK
RCL7          DVQLQASGGGLVQAGGSLRLSCKGSDYLFT TYGMG WFRQAPGK

RCL8          DVQLQASGGGLVQAGGSLRLSCAASGRTFS GYAMG WFRQGPGK

R24 VH        DVQLVESGGGLVQPGGSRKLSCAASGFTFS NFGMH WVRQAPEK
                                                CDR 1

                     50 a53     60          70         80 abc83
                     |   |      |           |          |      |
RCL1          QREAVA CIKSRDGSVIYADSVKG RFTVSRDNARKSVYLQMNNLKP
RCL2          DREFVT AISWSGRSAHYADSVRG RFLVSRDNDQNTVYLEMNSLKR
RCL3          EREFVA LITWRGRTKYYSDSVKG RFTISRDNGKNAVYLEMNSLKP
RCL4          QREMVA TIT KTGSTDYALSVKG RFTISRDYAQNTVYLQMNSLKP
RCL5          EREIVA AATWSGDMTYYADSVKG RFTASRDNAKNTVHLQMSSLKP
RCL6          EREFVA AISYRGLTLYYTDSVKG RFTISRNNAKNTVYLQMNSLKP
RCL7          VREFVA VVRRHDGNTRYAKSVKG RFTISKDNAKNTLYLQMNSLKP

RCL8          EREFVA AISWNGGRTIYADSLKG RFTISRDNAANTVYLEMNSLKP

R24 VH        GLEWVA YISSGGSSINYADTVKG RFTISRDNPKNTLFLQMTSLRS
                     CDR 2

                   90       98 abcdefghijklmn10l       110
                   |        |                 |        |
RCL1          EDTAVYYCAE APRCSSRSSTWLGETPLPL    WGQGTQVTVSS
RCL2          EDTAVYYCAA INKDLVGLRVSSLPSRPLYYD  WGQGTQVTVSS
RCL3          EDTAIYYCAA TPIYGGSRRDNEYTI        WGQGTQVTVSS
RCL4          EDTAVYYCAV RKMSGYIPTMTSYENGS      WGQGTQVTVSS
RCL5          EDTAVYYCAA DPNYVGQDPGLYNF         WGQGTQVTVSS
RCL6          EDTAIYYCAA TPIYGGSRRDNGNTI        WGQGTQVTVSS
RCL7          EDTAVYYCAA DLGDTGDPDVAGFRS        WGQGTQVTVSS

RCL8          EDTAVYYCAA NPQGTVTSASVYNY         WGRGTQVTVSS

R24 VH        EDTAIYYCTR GGTGTRSLYYFDY          WGQGATLIVSS
                                          CDR 3
```

**Figure 4.6. Sequence alignment of the isolated sdAbs and of R24 $V_H$.** Residues in red are key positions in llama sdAbs whereas residues in blue are key positions in camel sdAbs that differ from conventional antibody $V_H$ in order to adapt to the absence of L chain.

Furthermore, RCL4 belongs to the $V_HH$ subfamily 2. This is due to the presence of a tyrosine residue at position 37 in the framework 2 region and a residue missing at position 52a in CDR H2 (431). Analysis of the CDRs of the sdAb sequences reveals long CDR H3 comprising between 14 (RCL5) and 21 (RCL2) residues. This is expected as CDR H3 is usually longer in sdAbs, with an average length of 15 residues (433). The sdAb sequences were further examined to assess the similarity with the R24 $V_H$ sequence, a process that could reveal residue stretches that are important in binding to both BEC2 and $GD_3$. There were no significant resemblances uncovered, although some CDRs were found to contain a high number of serine residues like the CDR H2 of R24 $V_H$. This finding could highlight the importance of hydrogen bonds in binding both BEC2 and $GD_3$.

To analyze the binding of the isolated sdAb sequences to both BEC2 IgG and $GD_3$ by SPR, the sequences were recovered from positive phage clones, incorporated into the pSJF2 vector, and transformed into *E. coli* TG1 cells. Growth of individual colonies for 24 hours without induction allowed screening for sdAbs with maximal expression in the pSJF2-TG1 system (Figure 4.7). Coomassie-stained SDS-PAGE and Western blots show the sdAbs to migrate with an apparent molecular mass of 20 kDa. For each sdAb, the best expressing colonies were chosen for SPR analysis. All sdAbs except for RCL4 could be produced in high yields as soluble monomeric species. The sdAbs were purified in a two-step procedure: HiTrap metal chelate affinity chromatography, with sdAb eluting with approximately 200 mM imidazole, followed by size-exclusion Superdex 75 chromatography to get rid of contaminating proteins and aggregates (434, 435).

The binding specificities and kinetic parameters of the six purified llama sdAbs were determined by SPR using BIAcore technology by Tomoko Hirama, IBS, NRCC. To analyze

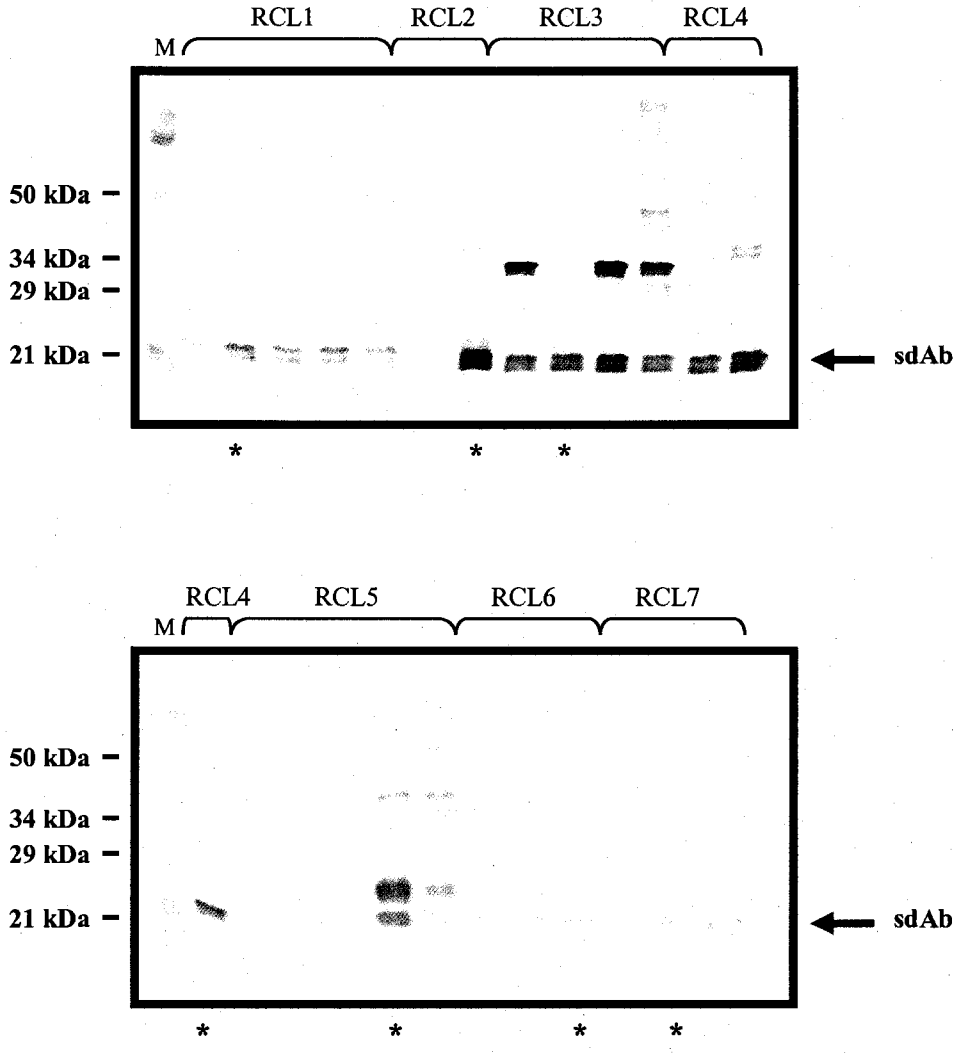


**Figure 4.7. Expression experiments for sdAbs RCL1 to RCL7.** Whole culture fractions for colonies of each sdAb were run on SDS-PAGE 12.5% and transferred to PVDF membranes. Western blotting was done with an anti-myc primary antibody and an alkaline phosphatase-conjugated goat anti-mouse secondary antibody. Colonies expressing good amounts of sdAb (marked with asterisks) were chosen for scale-up cultures.

sdAb-BEC2 IgG binding, a total of 3400 RUs of BEC2 IgG and 8400 RUs of control protein BSA were immobilized on a CM5 chip. Results of these experiments are shown in Figure 4.8. It is seen that only RCL2, RCL3, and RCL7 can bind BEC2 IgG since their steady-state affinity plots reach a reasonable Rmax and their Scatchard plots can be extrapolated (see Table 4.1 for kinetic data). However, the Rmax attained with RCL3 is less than that for RCL2 and RCL7. This indicates that RCL3 does not have the same surface capacity on the immobilized BEC2 IgG as the other two clones, and that RCL3 may recognize a BEC2 epitope that is different from the BEC2 epitope recognized by RCL2 and RCL7. RCL1 and RCL5 showed only little binding to BEC2 IgG and their steady state affinity plots show no plateau, yielding unreasonably high $K_D$s. Furthermore, RCL5 and RCL6 showed biphasic binding, which could indicate the presence of aggregates in the analyte solution, and could not be analyzed in more detail. For the BEC2 binders (RCL2, RCL3, RCL7), the $K_D$s were calculated from association and dissociation rate constants (Table 4.1). The SPR results obtained for RCL7 were of sufficient quality to also calculate a $K_D$ based on a global fit to a 1:1 Langmuir model. All $K_D$ values obtained were in the low micromolar range, as had been observed and was expected with this naïve library (91, 135).

To analyze sdAb-$GD_3$ binding, a total of 24,000 RUs of 10% $GD_3$/DMPC liposomes and 25,500 RUs of control DMPC liposomes were immobilized on an L1 chip. Sensorgrams show no interaction of maximal concentrations of each sdAb with $GD_3$ liposomes (Figure 4.9A). Although the interaction of RCL1 and RCL2 with $GD_3$ liposomes may look positive, the binding was deemed negligible when considering the huge bulk change on both the $GD_3$ and blank DMPC liposome surfaces. Further analysis to verify for $GD_3$ binding was done using the best BEC2-binder, RCL7. Competition experiments were

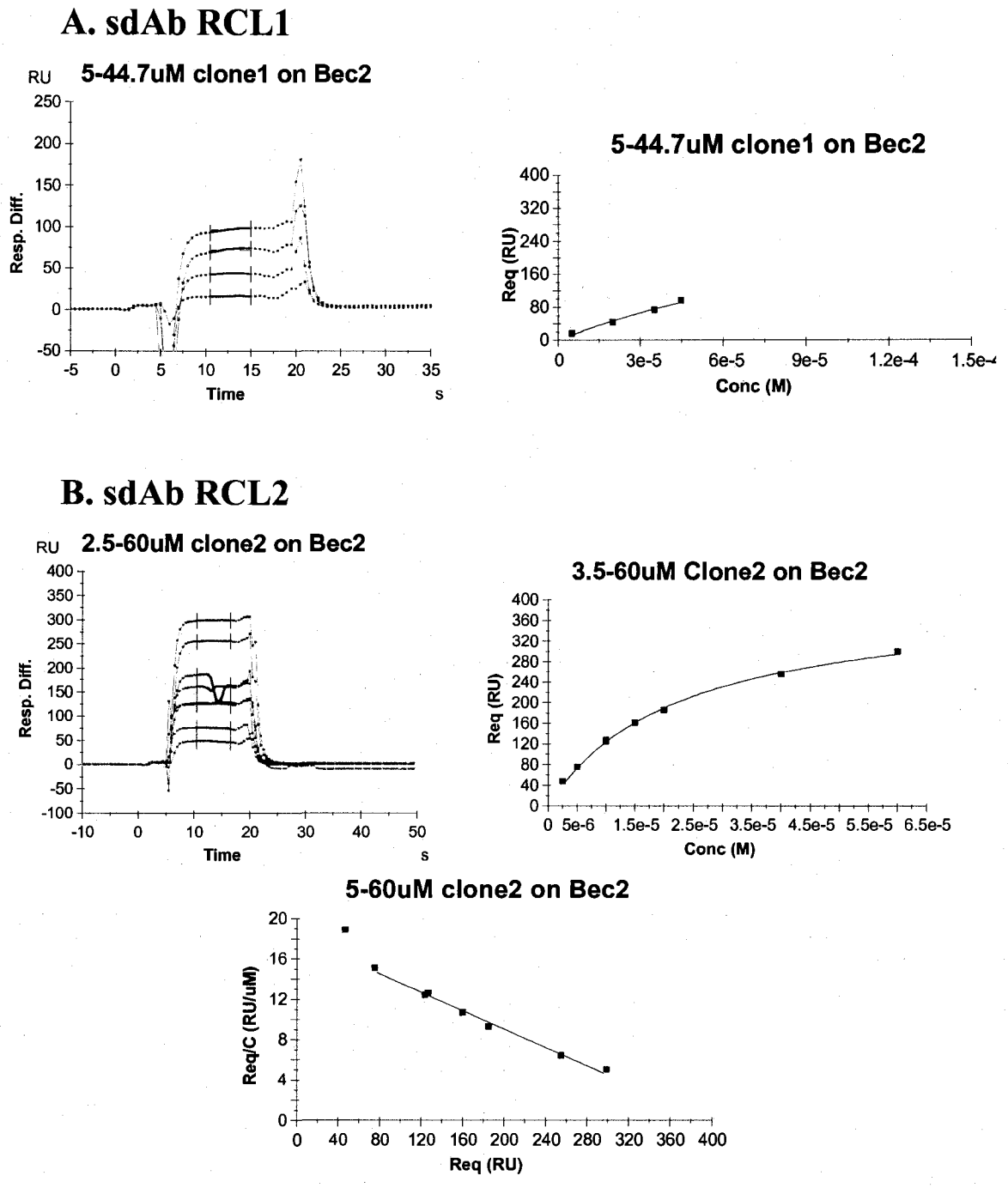


**Figure 4.8. SPR data for sdAbs RCL1 to RCL7 on BEC2 IgG. A.** Overlaid sensorgrams and steady state affinity plot of the interaction of sdAb RCL1 with BEC2 IgG surface after subtraction of BSA reference surface. The linear affinity plot yielded unreasonable Rmax and Kd values **B.** Overlaid sensorgrams, steady affinity plot and Scatchard plot of the interaction of sdAb RCL2 with BEC2 IgG surface after subtraction of BSA reference surface. The Rmax is 400 RUs and the $K_D$ is 22 uM. (Continued on the next page.)

# C. sdAb RCL3

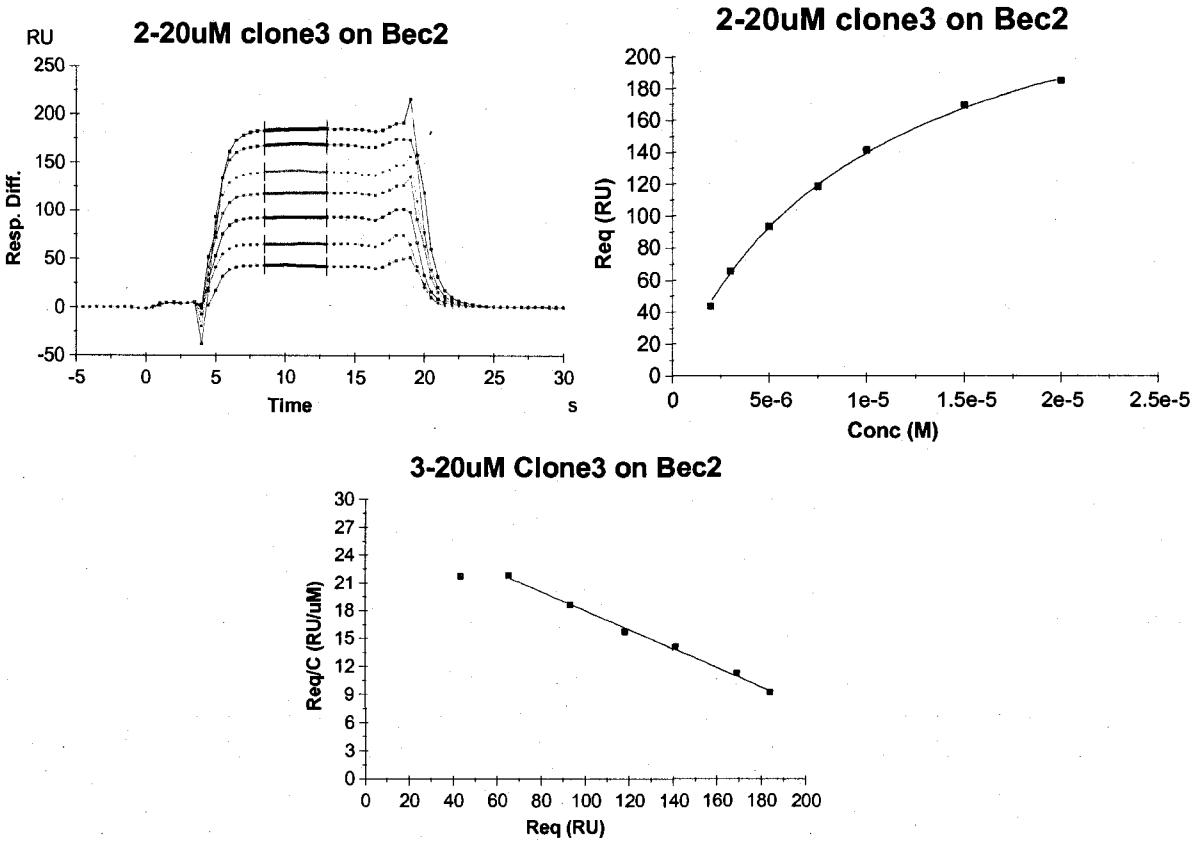


# D. sdAb RCL5

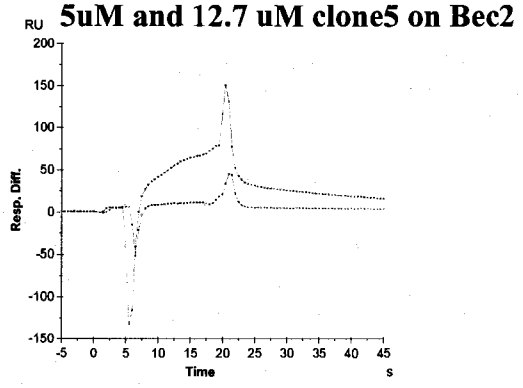


**Figure 4.8. SPR data for sdAbs RCL1 to RCL7 on BEC2 IgG (continued). C.** Overlaid sensorgrams, steady state affinity plot and Scatchard plot of the interaction of sdAb RCL3 with BEC2 IgG surface after subtraction of BSA reference surface. The Rmax is 280 RUs and the $K_D$ is 10 uM. **D.** Overlaid sensorgrams of the interaction of sdAb RCL5 with BEC2 IgG surface after subtraction of BSA reference surface. RCL5 shows little binding to BEC2 IgG and biphasic binding which probably reflects the presence of aggregates. (Continued on the next page.)

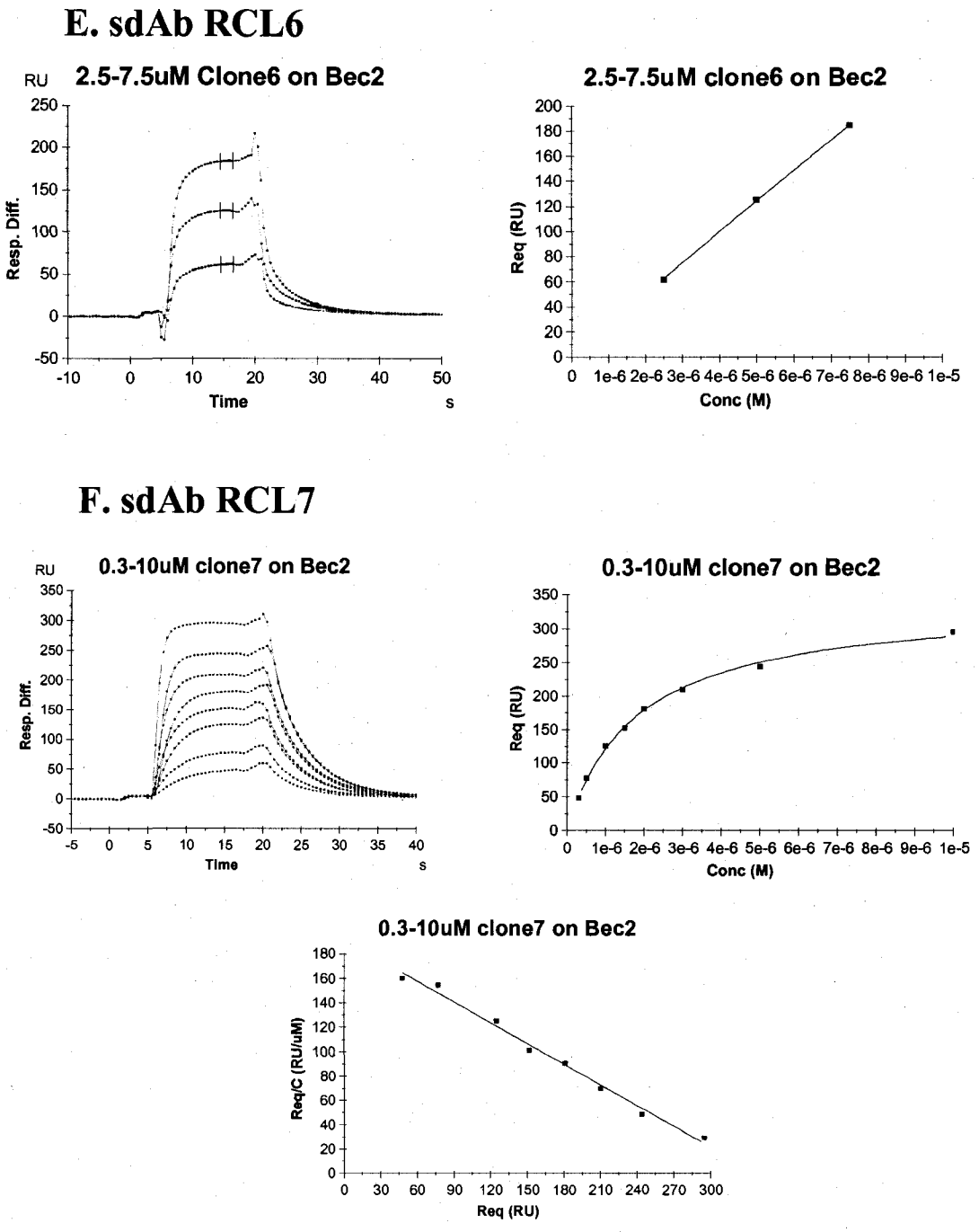


**Figure 4.8. SPR data for sdAbs RCL1 to RCL7 on BEC2 IgG (continued). E.** Overlaid sensorgrams and steady state affinity plot of the interaction of sdAb RCL6 with BEC2 IgG surface after subtraction of BSA reference surface. The linear affinity plot yielded unreasonable Rmax and $K_D$ values. **F.** Overlaid sensorgrams, steady state affinity plot, and Scatchard plot of the interaction of sdAb RCL7 with BEC2 IgG surface after subtraction of BSA reference surface. The Rmax is 340 RUs and the $K_D$ is 1.8 uM.

**Table 4.1 Kinetic values obtained with SPR for interaction of sdAbs with BEC2 IgG**

| | Rmax (RU) | $K_D$ (uM) | $k_a$ (1/Ms) | $k_d$ (1/s) |
|---|---|---|---|---|
| **RCL1** | > | > | - | - |
| **RCL2** | 400 | 23 | - | - |
| **RCL3** | 280 | 10 | - | - |
| **RCL5** | - | - | - | - |
| **RCL6** | > | > | - | - |
| **RCL7** | 340 | 1.8 | - | - |
| **RCL7*** | 400 | 2.3 | $1.0 \times 10^5$ | 0.25 |
| **RCL8** | 320 | 8 | - | - |

* Global fit values; data were fit to a 1:1 Langmuir model to obtain the best kinetic rate constants

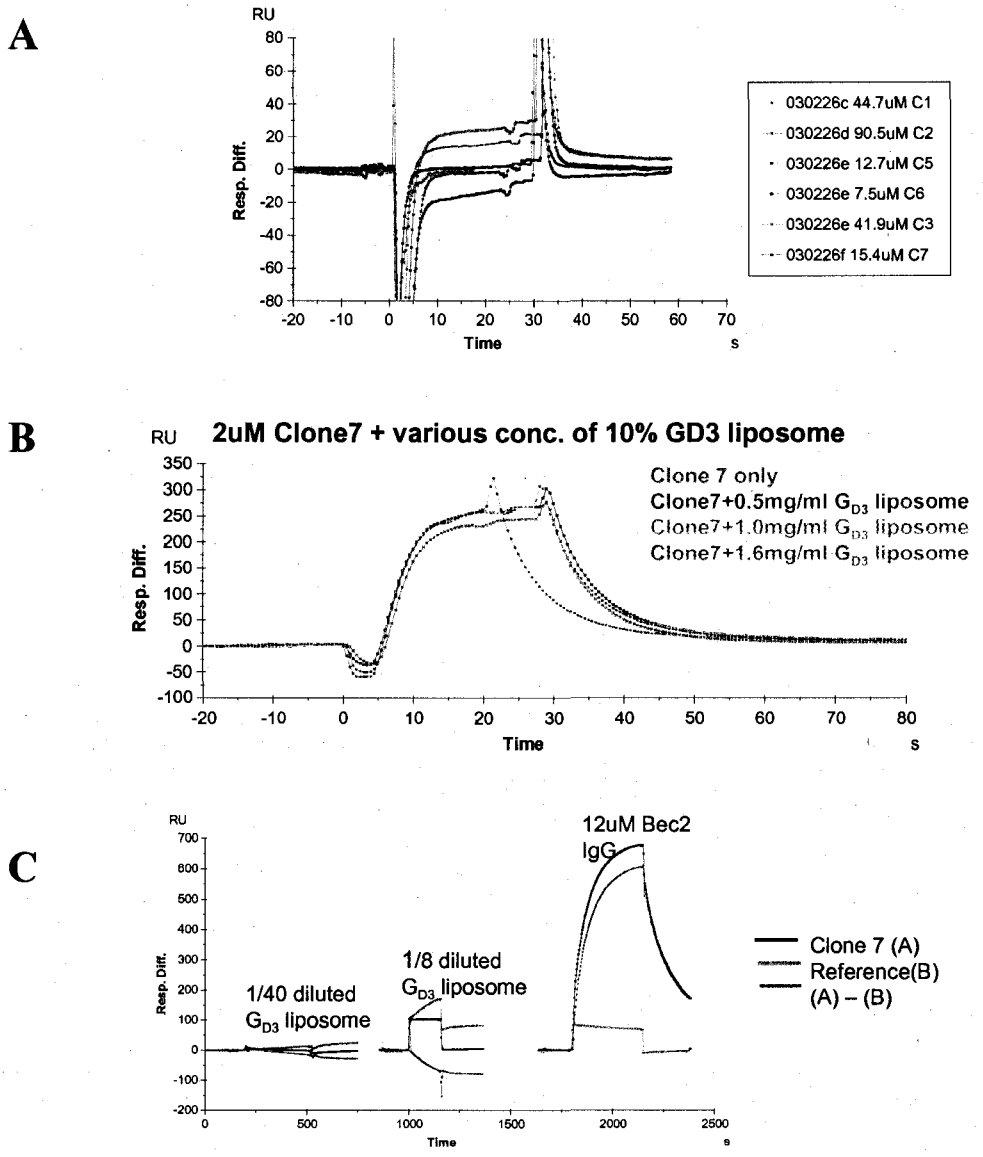


**Figure 4.9. SPR data for sdAbs RCL1 to RCL7 on $GD_3$ liposomes. A.** Overlaid sensorgrams of the interaction of high concentration RCL1 to RCL7 (see legend) to the $GD_3$ liposome surface after subtraction of blank liposome reference surface. The interaction of RCL1 and RCL2 may seem positive, but was deemed negligible when considering the huge bulk change associated with interaction with both the reference and $GD_3$ liposome surfaces. Additional assays were conducted with clone RCL7 to test for $GD_3$ interaction. **B.** Competition assay. Overlaid sensorgrams of interaction of mixtures of clone RCL7 and $GD_3$ liposome with BEC2 IgG surface. No amount of $GD_3$ liposome is able to compete for binding of RCL7 to BEC2 IgG. **C.** Overlaid sensorgrams of interaction of $GD_3$ liposomes and BEC2 IgG with immobilized RCL7. There is strong interaction of BEC2 IgG with immobilized RCL7, but no interaction of the $GD_3$ liposomes.

conducted whereby interaction of RCL7 to immobilized BEC2 IgG was probed in the presence of increasing amounts of $GD_3$ liposomes (Figure 4.9B). The overlaid sensorgrams indicate that the interaction of RCL7 to BEC2 is not inhibited by the presence of $GD_3$ liposomes. These results agree with initial findings and show that RCL7 is not able to interact with $GD_3$. Finally, RCL7 was immobilized on a CM5 chip at a density of 871 RUs to assess both BEC2 IgG and $GD_3$ binding. Sensorgrams showed that BEC2 IgG interacts with immobilized RCL7 whereas $GD_3$ liposomes did not (Figure 4.9C).

Together, the SPR results indicate that only three of the sdAbs isolated by phage display from the naïve llama sdAb library were able to bind to BEC2 IgG, and that none had the ability the bind $GD_3$. As such, no R24-like antibody was isolated with the library and biopanning protocol used. Competition elution using soluble $GD_3$ instead of an acidic buffer to elute phage bound to BEC2 IgG would have provided a better means of selecting for R24-like sdAbs, but this was not possible due to the availability, expense, and solubility of the ganglioside. The phage ELISA results were positive for sdAb binding to both BEC2 IgG and $GD_3$. It is possible that the binding recorded in the ELISA is due to sdAb aggregates or 'stickiness'. Some antibody fragments reported as 'sticky' have sequences that contain stretches of residues that are known to bind plastic, such as WxxY or WxxW (430), although such sequences were not identified in the sdAb studied. With regards to $GD_3$ binding, it is also possible that the positive ELISA signal be due to the multivalent nature of the sdAb as presented by the phage (78, 140) and this would not be addressed in the SPR experiments. Furthermore, the presentation of the $GD_3$ carbohydrate epitope in the phage display experiments may not reflect the true conformation of tumor-associated $GD_3$. As the wells for biopanning experiments were prepared with soluble $GD_3$, and not $GD_3$

presented in the context of a membrane, it is possible that the $GD_3$ epitope displayed by BEC2 was simply not featured by the soluble $GD_3$. This would signify that phage binding the BEC2 epitope mimicking $GD_3$ could not survive the second round of biopanning against soluble $GD_3$. In an attempt to resolve this last issue, a second biopanning protocol was designed using the human melanoma cell line SK-MEL-28 as source of membrane-displayed $GD_3$. This cell line is known to over-express $GD_3$ and to bind strongly to R24 IgG.

*Phage Display Llama sdAbs That Bind BEC2 and Human Melanoma Cell Line SK-MEL-28*

The biopanning was performed in three rounds: a first round against BEC2 IgG, followed by a round against SK-MEL-28, and finally a round against BEC2 IgG. Here, the selection of phage on BEC2 IgG in the first round not only provides a mean of selecting for the $GD_3$ epitope displayed by BEC2 IgG, but also allows for selection against phage that could bind other human cell antigens (436, 437). To verify that individual phage clones could bind to both BEC2 and $GD_3$, 95 phage clones were randomly selected for screening by phage ELISA. Of these clones, 11 showed binding to both BEC2 and SK-MEL-28 and not to the BSA control. Following sequencing of the 11 phage clones, one consensus sdAb sequence was found that differed from the sequences isolated in the previous biopanning experiment and this sdAb was termed RCL8 (Figure 4.6). RCL8 belongs to the $V_HH$ subfamily 1, has a shorter CDR3 of 14 residues and does not show significant homology with the R24 $V_H$ sequence. RCL8 was incorporated into pSJF2, expressed and purified as described previously (Figure 4.10A). To analyze RCL8-BEC2 IgG binding by SPR, a total of 3573 RUs of BEC2 IgG was immobilized on a CM5 chip by Tomoko Hirama, IBS,

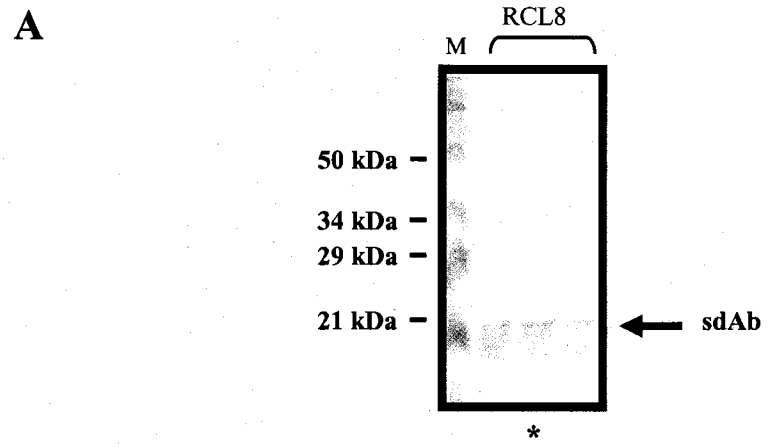


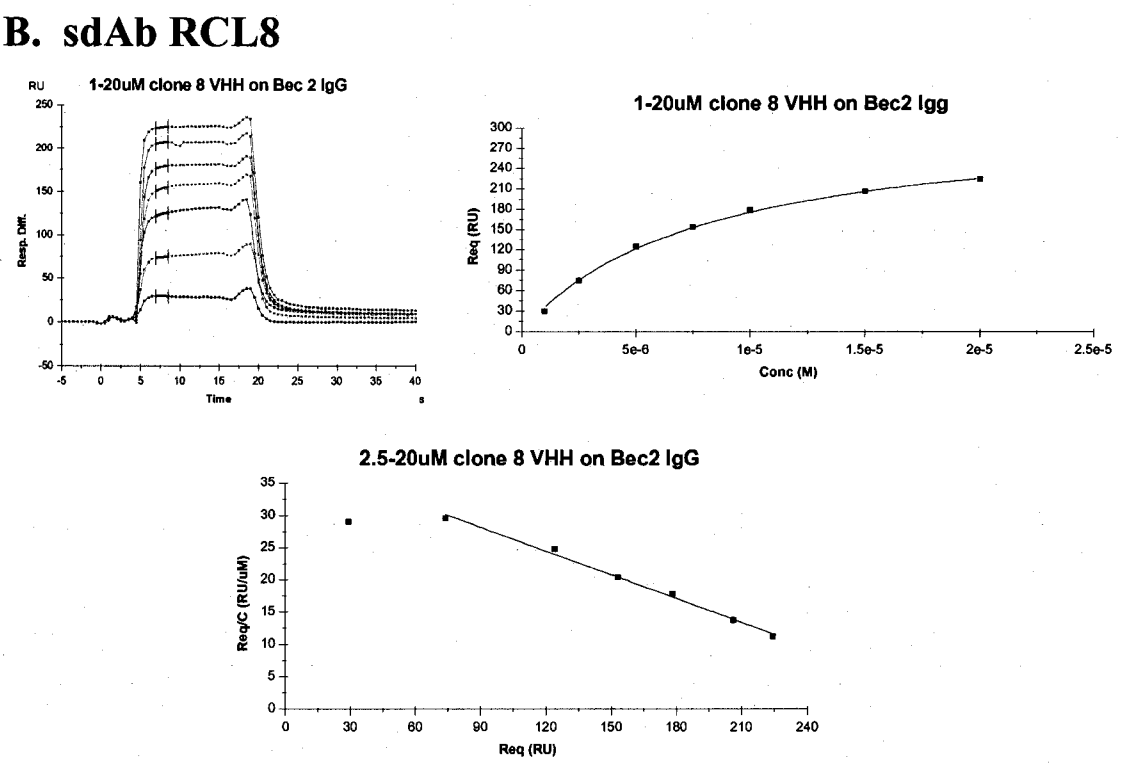


**Figure 4.10. Expression experiment and SPR data for sdAb RCL8 on BEC2 IgG. A.** Whole culture fractions for colonies of RCL8 were run on SDS-PAGE 12.5% and transferred to PVDF membranes. Western blotting was done with an anti-myc primary antibody and an alkaline phosphatase-conjugated goat anti-mouse secondary antibody. The colony expressing good amounts of sdAb (marked with asterisk) was chosen for scale-up cultures. **B.** Overlaid sensorgrams, steady state affinity plot and Scatchard plot of the interaction of sdAb RCL8 with BEC2 IgG surface after subtraction of BSA reference surface. The Rmax is 320 RUs and the $K_D$ is 8 uM.

NRCC. Results indicated that RCL8 binds to BEC2 IgG and that its affinity for the protein antigen is similar to that of RCL3 (Figure 4.10B and Table 4.1).

*Construction of Pentabodies of the BEC2-Binding SdAbs*

To investigate whether multivalency is a factor in the binding of $GD_3$ liposomes by the isolated BEC2-binding sdAbs, pentabodies of the sdAbs were designed. The sequences for RCL2, RCL3, RCL7, and RCL8 were incorporated into the pVT2 vector where they were fused at the N-terminus of a verotoxin B subunit. The corresponding constructs are termed V2NRCL2[b], V2NRCL3, V2NRCL7, and V2NRCL8 and naturally form homopentamers when expressed in bacteria (91). Growth of colonies for a 24-hour induction period allowed for screening of clones with maximal expression (Figure 4.11A). On SDS-PAGE, the pentabody monomers migrate with an apparent molecular mass of 30 kDa and are sometimes seen as a doublet (E. Stone and J. Zhang, personal communication). The best expressing colonies were chosen for SPR analysis. All pentabodies, except V2NRCL3, could be produced in high yields. The pentabodies were purified in a two-step procedure: HiTrap metal chelate affinity chromatography, with pentabodies eluting with approximately 500 mM imidazole, followed by size-exclusion Superdex 200 chromatography to get rid of contaminating proteins and aggregates.

The binding specificities and kinetic parameters of the three purified pentabodies were determined by SPR using BIAcore technology by Tomoko Hirama, IBS, NRCC. A total of 4600 RUs of 10% $GD_3$/DMPC liposomes and 4800 RUs of control DMPC liposomes were immobilized on an L1 chip. The sensorgrams show no binding of the

[b] SdAb is termed RCL2 while the pentabody made with the same sdAb is termed V2NRCL2: the V stands for verotoxin, 2 stands for pVT2 vector which contains the verotoxin mutant D17E/W34A, N stands for the positioning of the sdAb, N-terminal to the verotoxin subunit.

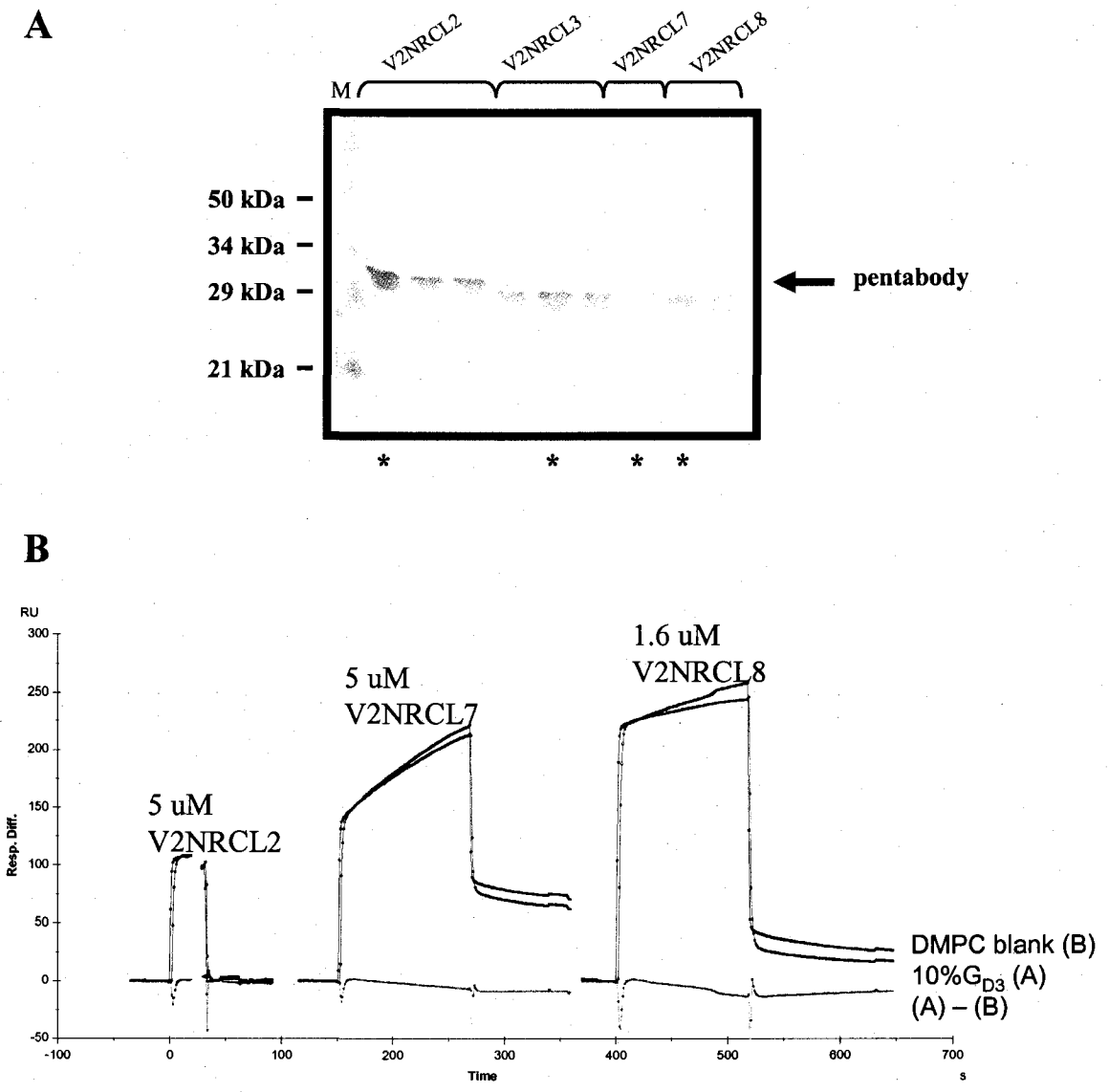


**Figure 4.11. Expression experiment and SPR data for pentabodies on $GD_3$ liposomes. A.** Whole culture fractions for colonies of each pentabody were run on SDS-PAGE 12.5% and transferred to PVDF membranes. Western blotting was done with an anti-myc primary antibody and an alkaline phosphatase-conjugated goat anti-mouse secondary antibody. As seen, pentabodies can display bands of different molecular weight. Colonies expressing good amounts of pentabodies (marked with asterisks) were chosen for scale-up cultures. **B.** Overlaid sensorgrams of the interaction of pentabodies V2NRCL2, V2NRCL7, and V2NRCL8 with liposomes containing 10% $GD_3$. The response seen with the $GD_3$ liposomes is equivalent to that seen for the reference surface, therefore there is no significant amount of interaction of the pentabodies with $GD_3$.

pentabodies to $GD_3$ liposomes at maximal pentabody concentration (Figure 4.11B). The SPR results suggest that not only was sdAb multivalency not a factor in the positive signals obtained in ELISAs but also that the use of membrane-displayed $GD_3$ in the biopanning protocol did not lead to the isolation of an sdAb able to bind both BEC2 and $GD_3$.

Overall, no llama sdAb could be isolated that could mimic R24 in its ability to mediate binding to both BEC2 and $GD_3$. This could be explained by several factors. First, the size of the library is not maximal (438-440) and possible BEC2-$GD_3$ binders may not be featured in the library. Secondly, if llamas display $GD_3$ on their normal tissues, there could be an inherent tolerance to the $GD_3$ antigen that is reflected in the lack of $GD_3$ binders in the naïve repertoire. Thirdly, the library is naïve: the use of an immune library would increase the chances of isolating an antibody able to mediate binding to both BEC2 and $GD_3$. This, of course, assumes that an antibody response could be raised against BEC2 and $GD_3$, and that the response would be of HCAbs. It may be that an immune response to BEC2 and $GD_3$ would consist solely of conventional antibodies, in which case the design of a $V_HH$ library would be meaningless. Fourth, sdAbs are more suited to reacting with crevasses, such as enzyme active sites, because of their long CDR3 (45, 47, 49). However, some $V_HHs$ have been reported to bind to haptens, molecules that are in the same size range as that of sugars. Lastly, the inability to isolate BEC2 and $GD_3$ binders might also be a result of the biopanning conditions selected (145). For example, in the biopanning against the SK-MEL-28 cell line, selection specificity could have been increased by recovering internalized phage (441, 442).

It was not possible to isolate any R24-like antibodies, whether by using antibodies generated in humans against BEC2 vaccines or by using llama sdAbs isolated by phage

display from a naïve library. Although some antibodies did seem like potential candidate by ELISA, the more sensitive method of SPR revealed those to be false positives. All BEC2 and $GD_3$ binders reported to date have only been analyzed with ELISA, and have not been characterized with real-time assays such as SPR. Currently, there are no known examples of purified R24-like Ab3s.

***Second Approach: Digest of BEC2 and Purification of BEC2 Fab for Crystallization***

To study the mechanism of mimicry of BEC2 IgG, it is not only important to isolate an R24-like antibody, but also to have a source of pure BEC2 protein for crystallization of the relevant complexes. BEC2 IgG was generously provided by Dr. Paul B. Chapman, MSKCC. The inherent flexibility of IgGs and the associated difficulty in crystallizing these molecules makes it necessary to digest the IgG molecule into its Fab and Fc fragments. The epitope that mimics $GD_3$ is thought to reside in the variable domain of BEC2 IgG, and therefore would be present in the Fab fragment. Thus, the second approach in this project is to successfully digest and purify the BEC2 Fab.

BEC2 IgG was digested with papain for 2 hours at 37°C at a ratio of 1:50 to yield Fab and Fc fragments. The disappearance of the BEC2 intact heavy chain band on SDS-PAGE attests to the complete digest of the IgG (Figure 4.12). However, isoelectrofocusing gels of papain-digested BEC2 raise two concerns: the BEC2 Fab and Fc have similar acidic isoelectric points (pIs), a property which differs from most antibodies where the Fab is very basic and the Fc is acidic, and the digest contains many Fab and/or Fc pI species (Figure 4.12).

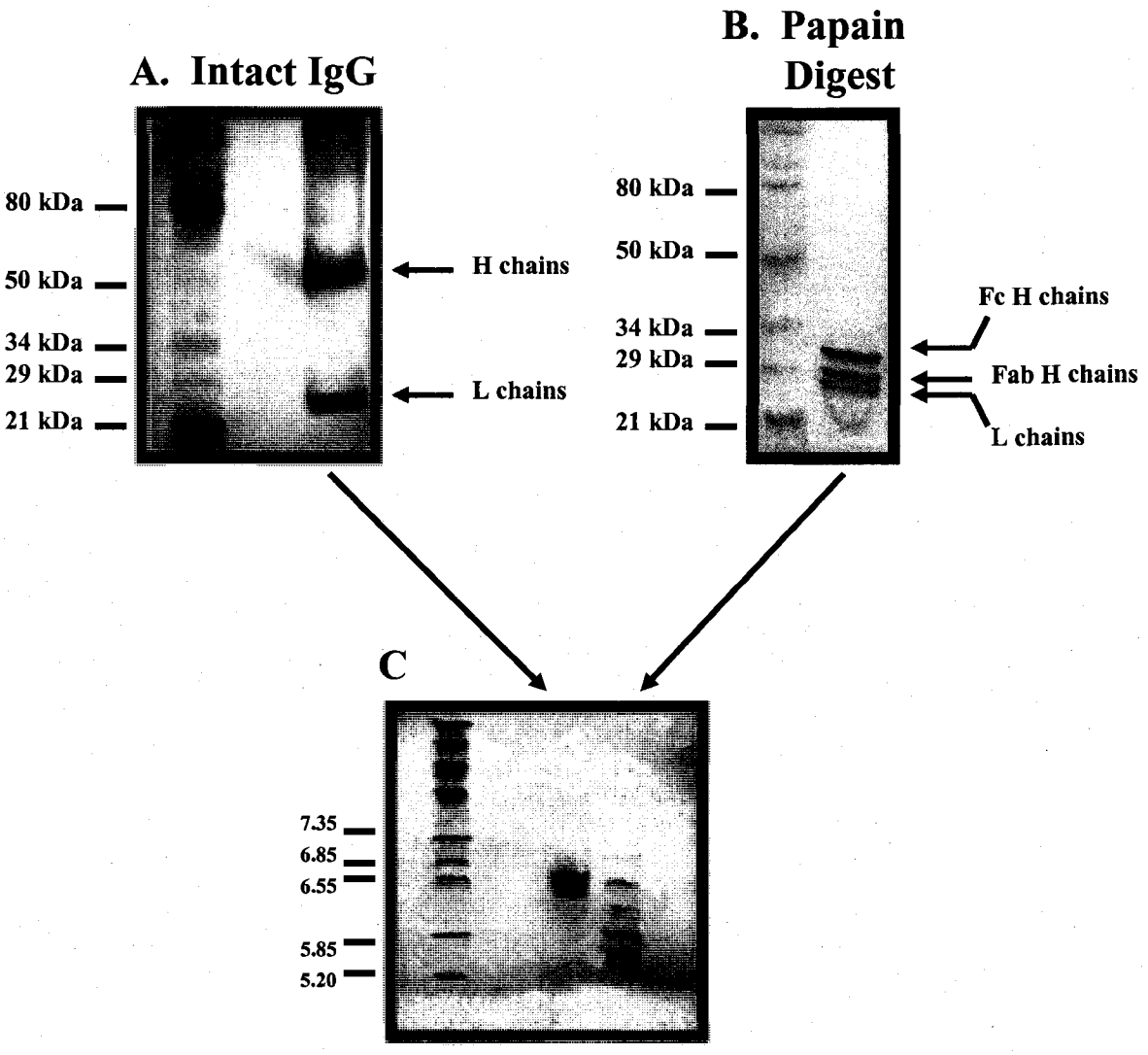


**Figure 4.12. Papain digest of BEC2 IgG. A.** Silver-stained Phast SDS-PAGE homogeneous 12% gel showing the intact H chains and L chains bands for BEC2 IgG. **B.** Silver-stained Phast SDS-PAGE homogeneous 12% gel showing the papain-digested BEC2 IgG at ratio of 1:50 for 2 hours. The H chains are digested into two fragments of slightly different molecular weight. **C.** Coomassie-stained Phast IEF 3-9 gel showing both intact (first lane) and papain-digested (second lane) BEC2 IgG. The digest shows many Fc and Fab peaks of different pIs, all situated in the acidic portion of the gel.

Hybridoma antibodies such as BEC2 are known to show charge heterogeneity (443-446). These charge variants can arise during cell culture, from the enzymatic removal of C-terminal lysine from one or both H chains (447, 448). Additional charge variants can arise from cyclization of N-terminal glutamine of both H and L chains to produce pyroglutamate, a deamidation reaction that serves as a signal for protein degradation (448). Furthermore, papain exhibits a low level of exopeptidase activity. This secondary activity results in the sequential removal of histidine and threonine residues from newly generated C-termini of Fab H chain fragments (448), which can lead to further heterogeneity of the antibody fragments. Since the BEC2 samples are over 8 years old, deamidation at glutamine or asparagine residues could explain the pI shift to the acidic side seen for the Fab (446), and papain digest could further enhance this pI heterogeneity. Other therapeutic antibodies, such as OKT3, have shown structural changes after only 1 year in storage at 5°C (449). These changes were accounted for by deamidation, but also by oxidation of labile amino acids and fragmentation of peptide chains. OKT3 stored for 2 to 5 years in the fridge showed 25-50% deamidation (449). Another possible explanation for the acidic pI of the BEC2 Fab is that this Fab mimics a ganglioside – as $GD_3$ contains two sialic acid residues, the carbohydrate mimicry ability of BEC2 could partly stem from presentation of acidic residues in its paratope. Although there does not seem to be an increased amount of acidic residues in the paratope of BEC2 based on the sequence, the overall local charge of the paratope could be affected by the three-dimensional structure of the BEC2 CDRs.

It is well known that Fab and Fc cannot be separated by size-exclusion chromatography since the fragments both have a molecular weight of approximately 50 kDa. A common method of separating the antibody fragments is through the exploitation of their

difference in charge. However, this method is not optimal in this case as the Fab and Fc fragments of BEC2 have similar pIs. Ion exchange chromatography was still attempted in initial purification trials in order to investigate whether careful selection of buffer, pH and elution salt could provide a means of obtaining pure BEC2 Fab. Using a Shodex QA-825 strong anion exchanger column and a running buffer of pH 5.8, the best separation achieved shows most of the Fab to be excluded from the column and most of the Fc and IgG to be retained by the column (Figure 4.13). The chromatogram displays several peaks, which reflects the numerous pI species, and this correlates well with the isoelectrofocusing gel data. Furthermore, it is seen from SDS-PAGE analysis of the eluted peaks that each peak consists of a mixture of Fab and Fc. Ultimately, there was no perfect condition of buffer and pH that could lead to full separation of the BEC2 Fab and BEC2 Fc.

Some studies suggest that it is possible to separate Fab from Fc even when the pIs differ by no more than 0.5 pH units. The techniques used in these studies include Gradiflow electrophoresis (450) and chromatofocusing. Chromatofocusing uses an ion exchanger matrix and a gradient of pH rather than a salt gradient to elute bound proteins. The buffers used in chromatofocusing consist of a mixture of buffering species to ensure a linear pH gradient. Protein samples are usually eluted at a pH close to their pKa, although some proteins may elute at a different pH because of local charge distribution (451). Here, chromatofocusing experiments used the PBE94 anion exchanger in conjunction with commercial polybuffers as well as with custom buffers, as described in Shan and Anderson (423). With the commercial Polybuffer, none of the BEC2 fragments could be eluted off the column (data not shown). The pH of the eluate fractions were verified and show a linear gradient that covers the range of pI for all the BEC2 fragment species. The PBE94 column

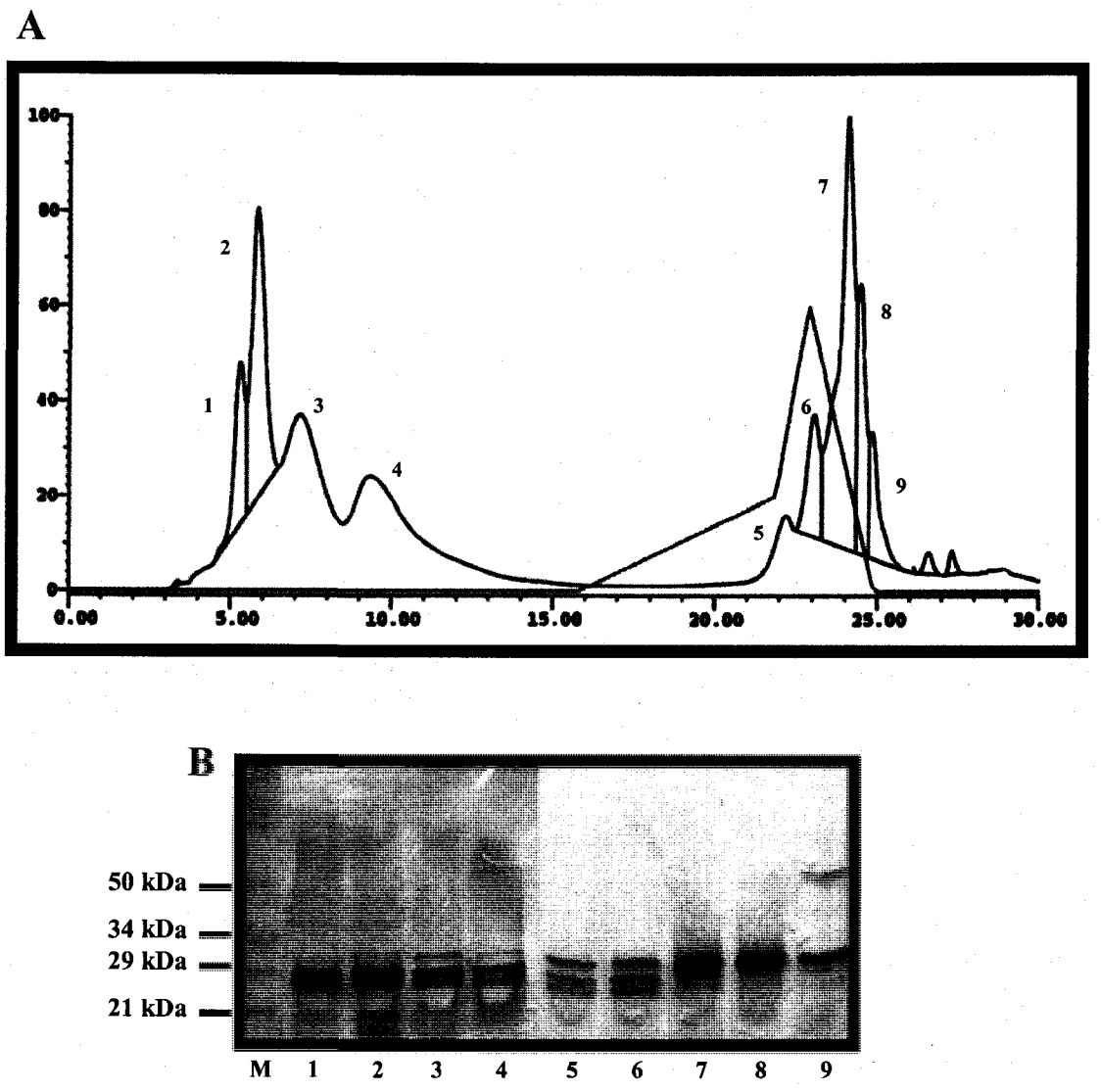


**Figure 4.13. Ion exchange chromatography of BEC2 digest. A.** Chromatogram from Shodex QA-825 elution of BEC2 digest. The salt gradient is in red and the many peaks, representing different pI species, are numbered sequentially. **B.** Silver-stained Phast SDS-PAGE homogeneous 12%of the peaks eluted off of the Shodex QA-825 with fraction numbers corresponding to peak numbers on the chromatogram. As seen from the SDS-PAGE, there is considerable overlap between the Fc and Fab species, making separation impossible with ion exchange chromatography.

was therefore stripped with a concentrated salt solution and a peak was observed indicating that the BEC2 fragments were still on the column. It is known that some proteins can precipitate when reaching a pH near their pI. In chromatofocusing, the risk of precipitation is even greater as the amount of salt used in buffers is very low to avoid salting out effects. Thus, the BEC2 digest could not be eluted with the commercial Polybuffer. The PBE94 anion exchanger was then used in conjunction with low concentration custom buffers and similar results were observed. The custom buffer concentrations were increased to avoid precipitation but this interfered with the ability of the BEC2 fragments to interact with the matrix. It is possible that the BEC2 fragments may not bear enough of a charge to interact with the PBE94 matrix at high buffer concentrations since the gradient of pH that is established in the chromatofocusing experiment is done in a small margin, with the pH always close to the pKa of the proteins (423).

Since there were no ion exchange protocols that could be used to separate BEC2 Fab from BEC2 Fc, other chromatography techniques were tested. Affinity chromatography was tested with the use of Staphylococcal protein A and streptococcal protein G, bacterial proteins that are able to recognize and bind to antibodies. Protein A and protein G affinity chromatography is a standard method for purification of polyclonal and monoclonal antibodies (52-55) and the interaction affinity is known to vary with the antibody species and subclass (56). The binding of the bacterial proteins occurs with the Fc fragment, between the $C_{H2}$ and $C_{H3}$ domains (452); protein A relies on hydrophobic interactions (453) whereas protein G relies on ionic and hydrogen bond interactions (454). Both protein A and protein G affinity columns were tested to purify the BEC2 digest. With both matrices, BEC2 Fc co-eluted with BEC2 Fab (Figure 4.14A and B). The bound Fc was eluted off the

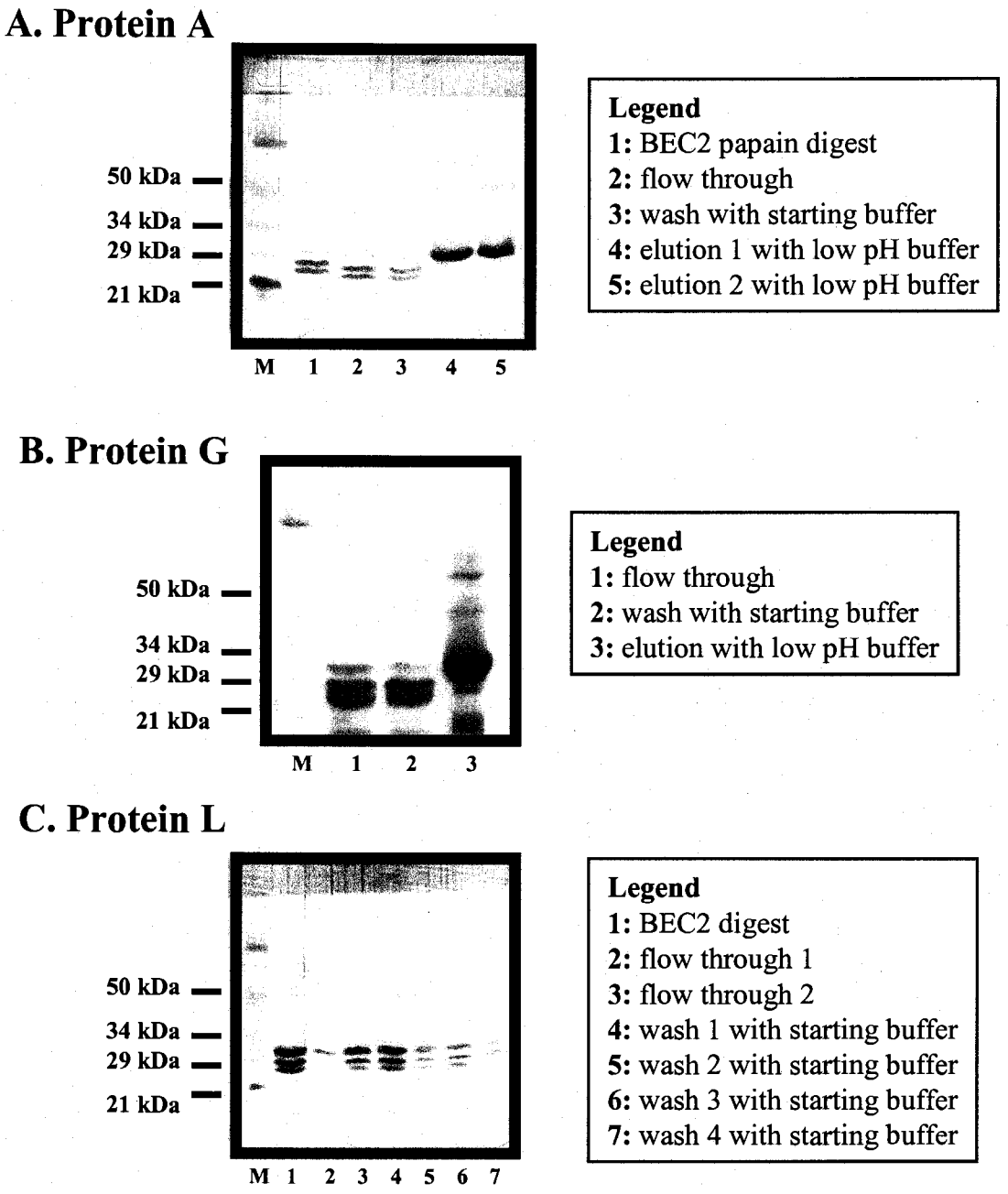


**Figure 4.14. Affinity purifications of BEC2 digest. A.** Silver-stained Phast SDS-PAGE homogeneous 12% gel showing protein A purification of the BEC2 digest. Fc is present in the flow through and wash, and pure Fab could not be obtained. **B.** Silver-stained Phast SDS-PAGE homogeneous 12% gel showing protein G purification of the BEC2 digest. The results obtained mimic those obtained for protein A purification. **C.** Silver-stained Phast SDS-PAGE homogeneous 12% gel showing protein L purification of the BEC2 digest. Both Fab and Fc are washed off the column; there is no interaction of the Fab with the protein L column.

column, the column was regenerated, and the flow through containing both Fab and Fc was reapplied to the column. The results of this second purification did not lead to pure Fab (data not shown). It has been reported that the pH dependency of binding is different from protein A to protein G, and therefore different pH and salt concentrations where also analyzed. None of these experiments allowed for capture of all the BEC2 Fc. Upon further investigation, it was noted that an asparagine residue is important in binding of Fc fragments to protein G; the possible deamidation of this residue in some Fc fragments of the old BEC2 samples could explain the lack of binding of a portion of the BEC2 Fc (454). Ultimately, all changes in the BEC2 protein could possibly lead to a portion of the Fc not being able to bind protein A or protein G.

Another bacterial protein used to purify antibodies is *Streptococcus magnus* protein L (455). Chromatography matrices conjugated with protein L are designed to capture Fab fragments regardless of the subtype of the antibody since the interaction is mediated through the L chain. The high-affinity interaction is known to be highly specific to kappa L chains (456, 457). Even though BEC2 IgG contains kappa L chains, no binding of BEC2 Fab to the matrix was observed (Figure 4.14C). The Fab recognition by Protein L is highly dependent on backbone conformation (59). It was noted that a proline residue located in the BEC2 Fab region recognized by protein L could distort the surrounding Fab segment enough to abolish binding.

Since none of the affinity chromatography techniques yielded pure Fab, focus was redirected at other, less popular methods. It has been reported early on that IgG could be isolated from human serum using immobilized metal chelate affinity chromatography (99, 458). It has also been reported that Fab can be separated from Fc using metal chelate

affinity chromatography (459). The heavy chain $C_{H3}$ domain of antibodies has been reported to contain a site, near the C-terminus, that has affinity for nickel (459). This site is histidine-rich and creates a metal binding site that is not present in the Fab. Based on this finding, Fc fragments can be bound to the charged column and Fab can flow through. In the case of the BEC2 digest, although most of the Fc bound a $Cu^{2+}$ -loaded matrix, some Fc was unable to bind and remained in the flow through with the Fab (Figure 4.15). In an IgG2b like BEC2, there might not be a histidine-rich site in the Fc that ensures a big enough difference of affinity to divalent metal cation, compared to the Fab, to warrant the use of this technique.

Another chromatography technique that has been used successfully to separate Fab from Fc is hydrophobic interaction chromatography. This technique has also been used to separate species of mAb secreted from one hybridoma (460). In the case of the BEC2 digest, the separation shows that BEC2 Fab and Fc have similar hydrophobicity and no pure Fab or Fc fractions could be obtained (data not shown).

Finally, none of the chromatographic techniques described above, by themselves or in combination, could separate BEC2 Fab from BEC2 Fc. This obstacle made it impossible to go forward with crystallization experiments using BEC2 Fab, and future efforts were focused on expression of antibody fragments for the purpose of crystallization.

***Third Approach: Expression of R24 and BEC2 Constructs for Crystallization***

Since no pure BEC2 Fab could be generated by purification of the BEC2 digest, work was directed towards constructing antibody fragments of BEC2 as well as of R24 that

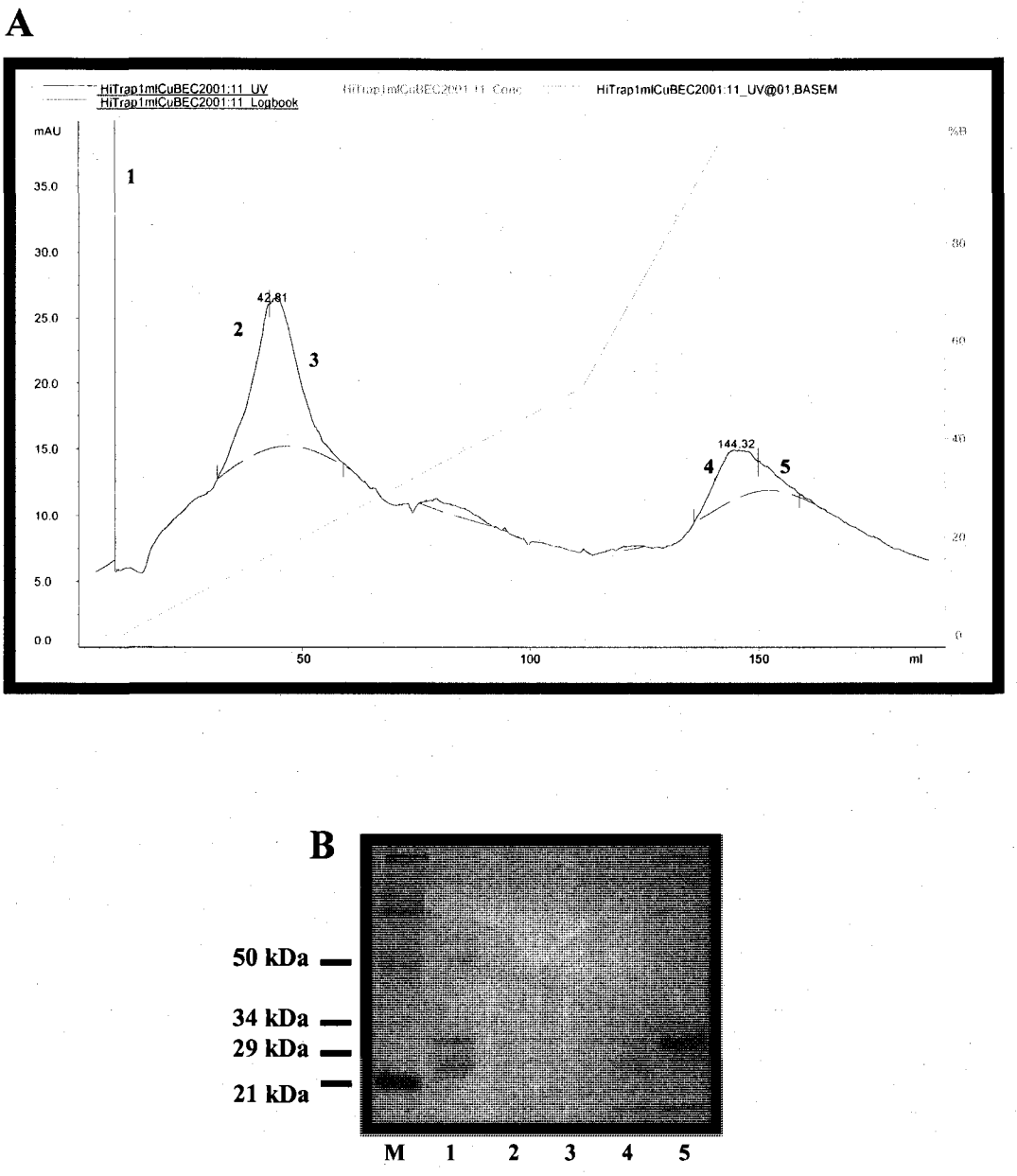


**Figure 4.15. Metal ion affinity chromatography of BEC2 digest. A.** Chromatogram from the $Cu^{2+}$-HiTrap column elution of BEC2 digest showing two distinct elution peaks. **B.** Silver-stained Phast SDS-PAGE homogeneous 12% of the peaks eluted off of the HiTrap column, with fraction numbers corresponding to peak numbers. It is seen that the second peak contains both BEC2 Fc and Fab, and therefore this method was not suitable to generate pure BEC2 Fab.

could be expressed in different systems and used for crystallization of the relevant complexes of the project.

*Design and Expression of sdAbs of R24 $V_H$*

From the crystal structure of R24 Fab as well as from biochemical data, it is postulated that R24 could mediate binding to $GD_3$ and possibly to BEC2 with the heavy chain only (408). The structure of the $V_H$ domain of R24 shows a deep pocket that could accomodate the terminal residues of the disialoganglioside (Figure 4.3B). This importance of the H chain in binding antigen has also been noted with other anti-ganglioside antibodies (461). Furthermore, since it is known that llama and camel sdAbs are soluble, monomeric species that can be produced in large quantities (135, 429), the design of llamalized and/or camelized (90) sdAbs of R24 $V_H$ was undertaken. The sequence for the $V_H$ domain was amplified from an R24 scFv construct and incorporated into the pSJF2 vector to test for expression. Without any mutations, the R24 $V_H$ fragment is expressed in good amounts but all the material is found to be insoluble. The DNA sequence for the R24 $V_H$ was also subjected to mutagenesis to transform the fragment into a llama R24 $V_H$, a camel R24 $V_H$ as well as a llama/camel R24 $V_H$ (see Figure 4.6 for the key residues of llama and camel sdAbs). Expression experiments show all three mutants R24 $V_H$ to produce a fair amount of protein, but only the llama R24 $V_H$ is produced as a soluble species (data not shown). Other studies have also reported aggregation of camelized $V_H$ domains (90, 462-466).

To analyze the binding of llama R24 $V_H$ to BEC2 and $GD_3$, expression of the llama R24 $V_H$ was scaled-up. Unfortunately, even 6 liters of culture did not generate a sufficient amount of pure, soluble protein for analysis with BIAcore. The failure to produce good

quantities of the llama R24 $V_H$ indicates that although the llama R24 $V_H$ is produced in soluble form, the construct is most likely not stable and would require further mutations to enhanced its solubility. Efforts were redirected towards the production of scFv constructs of R24 and BEC2. ScFv fragments are the smallest units that can maintain the binding specificity and affinity of the original antibody (65).

*Expression of R24 and BEC2 scFvs*

R24 scFv was engineered in the $V_L$-$V_H$ and $V_H$-$V_L$ orientations with the long linker $(GGGGS)_3$ whereas BEC2 was only engineered in the $V_H$-$V_L$ orientation, with the same linker, by Dr. Nina O.L. Seto, IBS, NRCC. The 15-residue long $(GGGGS)_3$ linker is used to ensure that the scFvs show monovalence (467, 468). The R24 and BEC2 constructs were incorporated in both pCW and pUCE8 vectors with the ompA secretion leader sequence and a $His_6$ tail, and showed poor expression in *E. coli* BL21 cells (N. O. L. Seto, personal communication). The constructs were transfered to two other vectors: pGEX-4T-3, for expression with a GST tag in *E. coli*, which could augment soluble expression (104), and pPIC9, for expression in the methylotrophic yeast *P. pastoris*. In both of these systems, a Factor Xa digestion site was engineered between the scFv and the $His_6$ tag to cleave off the tag following purification.

Expression of the constructs was tested by time course experiments. Although the yeast *P. pastoris* has been used successfully for high-level expression of various proteins (118, 120, 469, 470) including antibody fragments (123, 426, 471-473), secreted expression of R24 and BEC2 scFvs was too low to detect with either silver staining of SDS-PAGE gels or Western blots (data not shown). Optimization of yeast expression conditions (474) using strategies such as protease inhibitors, different concentrations of MeOH for induction (475),

growth temperature, and media composition, only lead to minor improvements of expression. The amounts of R24 scFv and BEC2 scFv were not considered sufficient to pursue optimization in *P. pastoris* since crystallization experiments require many milligram amounts of protein. It is possible that the little scFv that was secreted by the yeast was digested by the proteases that are secreted by the host (426), although addition of casamino acids to reduce proteolytic digest did not result in significant improvement of expression.

Expression of R24 scFv and BEC2 scFv in pGEX-4T-3 differed with host *E. coli* cells. There was no expression in *E. coli* BL21 cells, but there was strong expression of the $V_H$-$V_L$ scFvs as inclusion bodies in Rosetta-gami B cells (Figure 4.16). Rosetta-gami B cells are of the B834 background and possess many additional features that can enhance expression: they are deficient in the lon and ompT proteases, are lacZY deletion mutants for precise control with IPTG, they harbor an extra plasmid encoding six rare tRNAs, and they are trxB/gor mutants greatly facilitating cytoplasmic disulfide bond formation. Favored expression of scFvs in one particular orientation, whether $V_H$-$V_L$, as is the case for the BEC2 and R24 scFv constructs, or $V_L$-$V_H$, has been observed with other antibody fragments expressed in bacteria (422, 471, 476). In the case of the $V_H$-$V_L$ orientation being favored, it has been proposed to be the result of the distance between the C-terminus of the $V_H$ and the N-terminus of the $V_L$ being shorter and better able to accomodate the linker, than the distance between the C-terminus of the $V_L$ and the N-terminus of the $V_H$ (106).

The fact that the R24 and BEC2 $V_H$-$V_L$ constructs are expressed as inclusion bodies in pGEX-4T-3/Rosetta-gami B is not surprising. Most scFvs are expressed as inclusion bodies in bacteria (65, 70, 106, 108-110). Even when directed to the periplasm, high-level expression of scFvs as been linked to aggregation (477) possibly due to the high protein

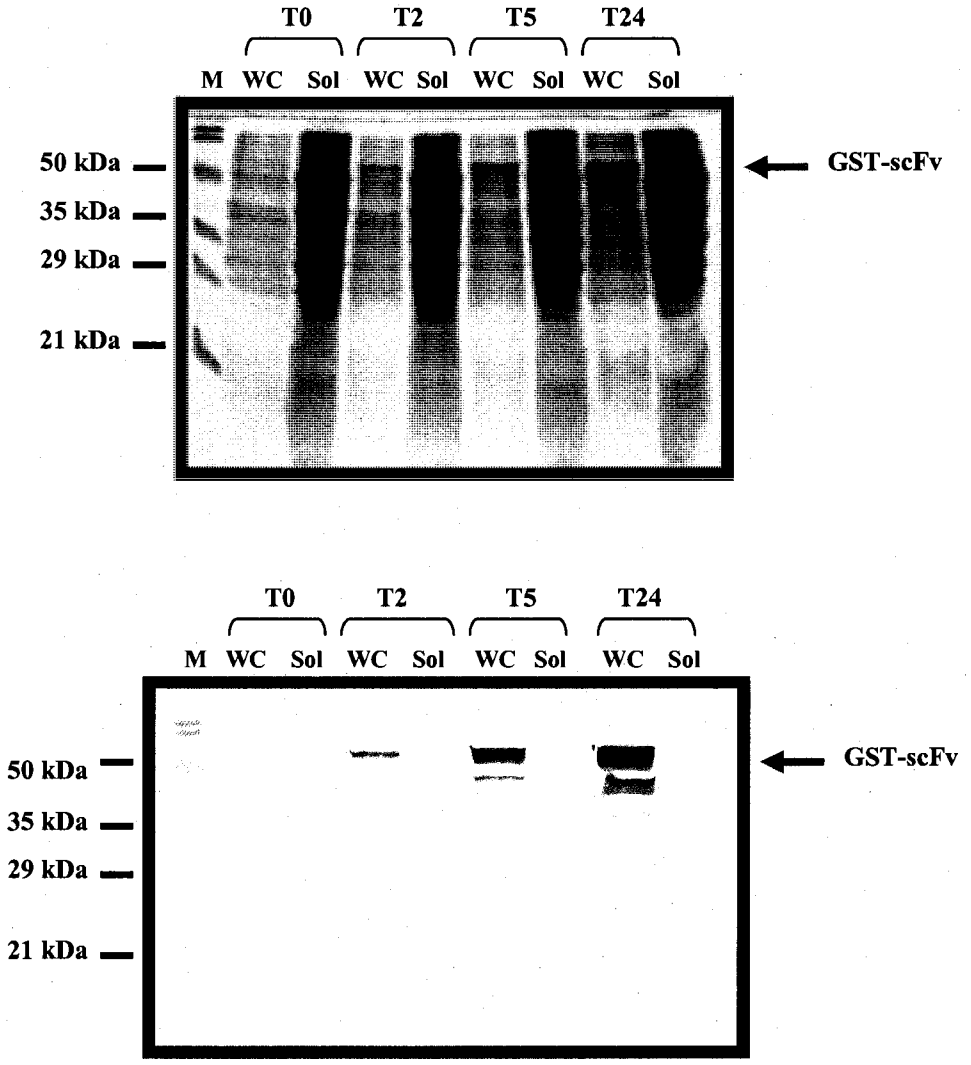


**Figure 4.16. Time course experiments for BEC2 and R24 scFvs, as examplified by R24 $V_H$-$V_L$ scFv.** Whole culture (WC) and soluble (Sol) expression fractions were analyzed at different time points. The fractions were run on SDS-PAGE 12.5% and transferred to PVDF membranes. Western blotting was done with an anti-$His_6$ primary antibody and an alkaline phosphatase-conjugated goat anti-mouse secondary antibody. Maximum expression is seen after a 24-hour induction. There is no soluble expression of the construct.

concentration in the periplasmic space (113, 114). Some sugars such as sucrose have been shown to reduce the aggregation of recombinant proteins in the periplasm when added to growing cells (113-115). Alas, in the case of the R24 and BEC2 scFvs, the addition of sucrose to the cultures did not lead to an increase in production of folded, soluble scFv (data not shown). Other factors that play a decisive role in the folding efficiency of an scFv are the primary sequence (105, 110) and the intrinsic stability of the individual domains (478, 479). Also, it is possible that the fragments are not stable because of the buried surface area and quality of interaction at the $V_H$-$V_L$ interface, which can be related with dissociation of the domains (71). Finally, it is known that the linker in scFvs can influence the stability, refolding kinetics and expression of the fragment (69, 77, 480); although the $V_H$-$(GGGGS)_3$-$V_L$ scFv format has been described not to interfere with the folding of the molecule (481).

Future efforts could look at refolding the scFvs produced in inclusion bodies, although it is well known that this process is inefficient (482, 483). As well, stability constructs could be designed where mutations thought to augment stability of antibody fragments could be incorporated into the gene by protein engineering (110, 484) or directed evolution (128, 485, 486). It is known that even single amino acid mutations can alter folding rates and product yield (110, 112). Stabilization of the $V_H$-$V_L$ interface has also shown to be a successful approach (81). For some scFvs, construction of light-chain shuffling library resulted in the isolation of antibodies that kept the antibody's original specificity and affinity (487).

*Design and Expression of Chimeric BEC2 $V_L$ – R24 $V_H$ scFv*

It has been proposed that the H chain of R24 may contain the full binding site for $GD_3$. Also, based on modeling studies of BEC2, it has been proposed that the BEC2 CDR

that could mimic $GD_3$ is situated in the light chain. Consequently, an antibody fragment consisting of the BEC2 $V_L$ and R24 $V_H$ was designed in the hopes of isolating the domain from R24 that is thought to be responsible for binding BEC2, and the domain from BEC2 that is thought to be responsible for mimicking $GD_3$. Such a chimeric antibody is postulated to be able to bind to itself and reveal the interaction of both R24 to BEC2 and BEC2 to R24. The BEC2-R24 chimeric antibody could also simplify crystallization since the complex of R24 and BEC2 could be revealed by interaction of one chimeric antibody to another. This type of chimeric antibody has been designed by other groups, such as Cupit et al. (426), where antibodies anti-TRAP and anti-LPI were combined into one construct to verify if the low expression of the antibodies was due to the L chain or to the H chain folding properties.

The BEC2-R24 chimeric antibody fragment was designed in both the $V_H$-$V_L$ and $V_L$-$V_H$ orientations, linked by the long linker $(GGGGS)_3$. The constructs were incorporated in the vector pGEX-4T-3 for expression with a GST tag in *E. coli* as well as in the vector pPIC9 for secreted expression in the methylotrophic yeast *P. pastoris*. As reported for the R24 scFv and BEC2 scFv constructs, expression in the yeast system was too low to detect, even after ample optimization procedures. In the bacterial systems, the expression seen mirrors that of the R24 scFv and BEC2 scFv constructs: there is no detectable expression using the BL21 host, but there is a fair amount of expression by the $V_H$-$V_L$ construct in the Rosetta-gami B host. All protein is expressed in inclusion bodies, and similar steps as those suggested earlier, could be taken to remedy this obstacle.

Finally, after much effort was put into design and expression optimization, none of the BEC2 and R24 constructs could be expressed as soluble species and in amounts deemed reasonable to undertake structural studies.

## CONCLUSION

The objective of this study was to elucidate the mechanism by which BEC2 mimics $GD_3$ by solving the structures of both R24 in complex with BEC2 and R24 in complex with $GD_3$. To generate crystals of R24 in complex with BEC2, adequate quantities of purified BEC2 and R24 fragments are required. Unfortunately, sufficient amounts of pure BEC2 and R24 samples could not be produced. Not only was purifying BEC2 Fab from the BEC2 digest unsuccessful, but the expression of BEC2 and R24 antibody fragments in various hosts also failed. Crystals of the R24-$GD_3$ complex cannot be obtained due to the inherent inability of R24 to bind $GD_3$ in solution. This was addressed by trying to isolate an R24-like antibody that could bind both BEC2 and $GD_3$ in solution. Unfortunately, antibodies isolated from patients immunized with BEC2 as well as antibodies isolated from a llama naïve phage library panned against BEC2 and $GD_3$ were found to be unable to mimic R24.

# PART II

# CHAPTER 5

# MUTANTS OF HUMAN ABO(H) BLOOD GROUP GLYCOSYLTRANSFERASE B

## INTRODUCTION

*ABO Blood Group Antigens*

The antigens of the ABO(H) blood groups are present in a wide range of tissue cells such as epithelium, sensory neurons, platelets and vascular endothelium as well as in soluble form in the cytoplasm (488). Only humans and higher anthropoid apes express the antigens on their red blood cells (489-491). The ABO(H) blood group antigens have been shown to play key roles in cell development and differentiation (492-494), but they are mostly recognized for their role in the disastrous effects of unmatched blood transfusions and tissue transplantations.

The ABO blood group antigens were first identified on red blood cells at the beginning of the twentieth century (495). It was thought that two molecules, termed A and B, and later determined to be the antibodies against those molecules anti-A and anti-B, explained the presentation of three blood groups, A, B, or C. Individuals with the blood group A molecules would have anti-B antibodies, individuals with the blood group B molecules would have anti-A antibodies and individuals with blood group C would have neither molecules and both antibodies. Blood group C was later renamed O (496), and only a year later was the fourth and rarest group, AB, described and defined as the presence of both the A and B molecules and the absence of either antibody (497). Later on, it was found that antibodies also existed against blood group O cells (498, 499) and that these antibodies could cross-react with red blood cells of individuals with blood groups A, B, and AB (500-502).

Experiments designed to characterize the blood group antigens revealed that the antigens could be extracted from red blood cells using hot aqueous ethanol and that the

extracted material could be precipitated with rabbit antisera to human A or B cells (503). Further characterization revealed that N-acetylgalactosamine (GalNAc) played a role in A specificity (504) while Gal played a role in B specificity (505), and not much later the complex carbohydrate structure of the antigens was elucidated (506, 507). The A antigen corresponds to the structure GalNAc(α1-3)[Fuc(α1-2)]Gal-β1-R while the B antigen corresponds to the structure Gal(α1-3)[Fuc(α1-2)]Gal-β1-R, with the O antigen corresponding to Fuc(α1-2)Gal-β1-R and where R refers to a glycoprotein or glycolipid (Figure 5.1) (508, 509). The O antigen was renamed H-antigen to highlight the fact that it is common to all cells regardless of the blood group (502) and that it represents the precursor for the synthesis of the A and B antigens (510, 511).

Aside from the well-known importance of blood group antigens in blood transfusions and tissue transplantations, the antigens have also been shown to be associated with oncogenic transformation. Because of their role in cell differentiation (319, 331, 489), it has been found that certain cancers have increased expression of blood group antigens (512, 513), loss of expression of blood group antigens (514) or even *de novo* expression of blood group antigens different than an individual's own blood group (515-518). Furthermore, the blood group antigens have been shown to be associated with an increased susceptibility to certain infections and diseases. Non-group O individuals have been associated with an increased risk for heart and vascular disease (519-521). As well, it is known that group A individuals are more susceptible to *Pseudomonas* infections, group B individuals to *Salmonella typhi* and group O individuals to *Helicobacter pylori*.

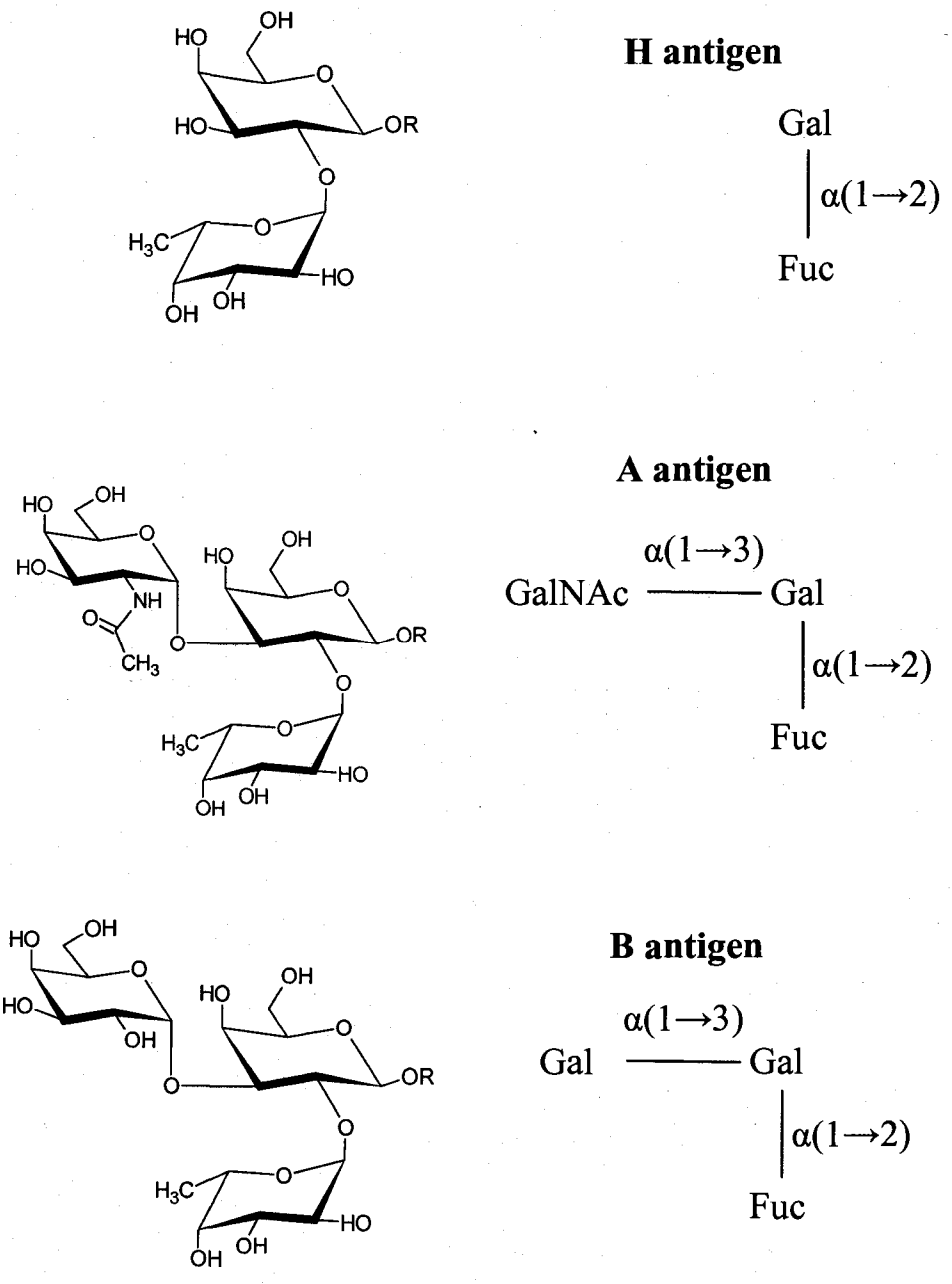


**Figure 5.1. ABO(H) blood group antigens.** Schematic structure of the blood group antigens. The H antigen, Fuc(α1-2)Gal-β1-R, is the precursor for the synthesis of the A antigen, GalNAc (α1-3)[Fuc(α1-2)]Gal-β1-R, and the B antigen, Gal(α1-3)[Fuc(α1-2)]Gal-β1-R. The chemical groups that define, and differentiate between the A and B antigens are highlighted in yellow.

*ABO Genetics*

Extensive family studies established early on that blood groups were inherited (522, 523). Some believed that the antibodies as well as the antigens were under genetic control (524), while others believed the antibodies to be generated by exogenous factors with activities similar to the blood group antigens (525-527). Once the structure of the antigens was elucidated as carbohydrate, it was known that the antigens themselves could not be the inherited factors. It was demonstrated that the blood group phenotypes were associated with inheritance of glycosyltransferases (GTs), enzymes that could act on the H-antigen to synthesize the A and B antigens (528, 529) and that the mechanism of inheritance of these enzymes was the model of multiple alleles at one locus, as proposed by Bernstein (530). With this model, three alleles A, B, and O could explain the four phenotypes, with AA and AO genotypes yielding the A blood group, BB and BO genotypes yielding the B blood group, OO genotype the O blood group and AB genotype the AB blood group. The gene for the H-antigen is independent from the ABO locus and encodes a fucosyltransferase (531, 532).

The ABO locus is mapped to chromosome 9 and the gene contains seven exons spanning about 18-20 kbp (533-535). The isolation and characterization of the ABO genes was reported in 1990 (536, 537), and sequencing of the cDNA showed that the coding regions of the blood group A glycosyltransferase (GTA) and of the blood group B glycosyltransferase (GTB) are 99% homologous. With 8 different nucleotides between them, generating four residue substitutions at positions 176, 235, 266, and 268 in the protein sequence, GTA and GTB represent the two most homologous GTs known that use different naturally-occuring donor nucleotide substrates (Figure 5.2) (538-540). The four residues

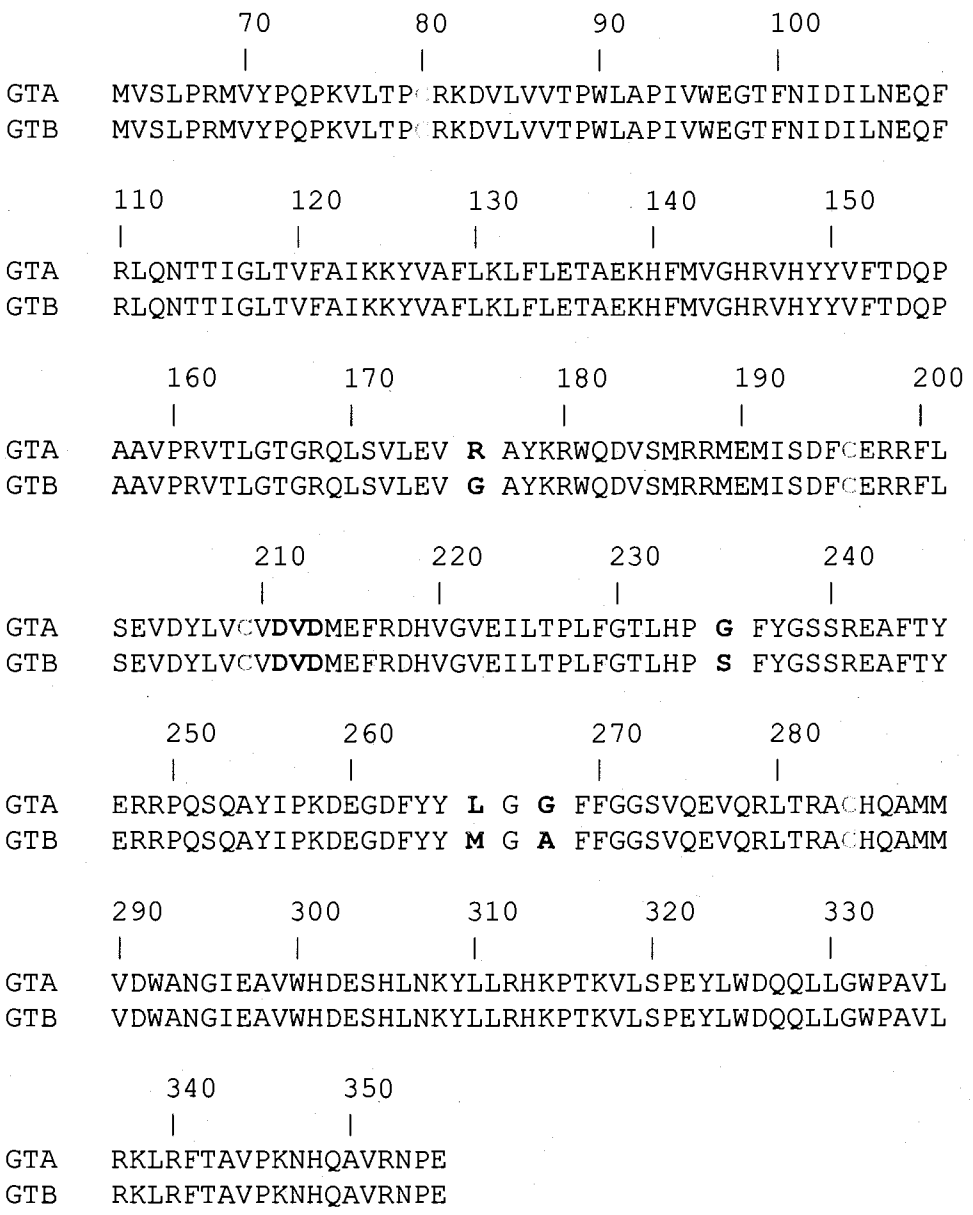


**Figure 5.2. GTA and GTB catalytic domain sequences.** Sequence alignment of the catalytic domain of native GTA and GTB. The four critical amino acids are highlighted in red, the four free cysteines are in orange and the DXD motif is in blue.

substituted between GTA and GTB were labeled as the 'critical residues', as they were considered most likely responsible for the difference in donor nucleotide specificity. Analysis of the ABO genes also revealed that blood group A has two major subgroups: $A_1$ and $A_2$ (541-545). The $A_2$ allele is characterized by a single nucleotide deletion in the C-terminal, which results in a change of reading frame and addition of 21 residues to the C-terminus of GTA (546). Thus, with an extended C-terminus, the $GTA_2$ enzyme displays diminished activity and restricted acceptor substrate usage compared to the $GTA_1$ enzyme (547). Furthermore, it has been shown that many instances of the O allele is a gene identical to the A allele except for a single nucleotide deletion at the N-terminus which results in a change of reading frame that alters the protein sequence after residue 88 and introduces a stop codon after residue 117 (539, 548). The transcribed mRNA from the O allele is rapidly degraded and the small quantity of protein that is translated is non-functional.

In addition to the major alleles of the ABO blood groups, there are many minor subtypes (549, 550). Other O alleles have been discovered which are A alleles comprising mutations that delete the activity of GTA, such as the mutation of critical residue 268 to arginine (551-555). Other minor alleles encode GTs with a weak A activity, such as the Ax (556, 557), the A3 (558), and the Ael alleles (559) or even GTs that display both A and B activities, such as the cis-AB (560-564) and B(A) alleles (556, 565). All of these different alleles correspond to mutant GTs and as such, offer clues about the structural basis of the activity of these enzymes.

*Glycosyltransferases*

GTs are localized to the Golgi apparatus and are classified as type II trans-membrane proteins: they have a short N-terminal cytoplasmic segment, one trans-membrane domain, a short stem region that contains a N-glycosylation site (566) and is sensitive to proteolysis, and a lumenal C-terminal catalytic domain (567, 568). GTs catalyze the transfer of a glycosyl moiety from a donor nucleotide-sugar to an acceptor substrate with a high degree of stereoselectivity and regioselectivity (569, 570). The transfer can be done with inversion or retention of the stereochemistry at the anomeric center relative to that of the donor sugar, and thus the enzymes are classified as either inverting or retaining GTs.

GTs have been grouped into many families according to sequence similarities (571, 572) and hydrophobic cluster analyses (573, 574), according to the type of sugar they transfer (575, 576), on the basis of the reaction catalyzed and the substrate specificity (577) and on other types of multiple sequence alignment scoring systems (578, 579). Currently, the Carbohydrate-Active Enzymes database (CAZy) contains more than 12,000 sequences that are divided into 78 families (580, 581).

Although GTs have very low sequence homology, they have similar catalytic domain structures (568, 582, 583) which suggests the possibility of a common ancestor (584, 585). See Table 5.1 for a compilation of all current GTs with available crystal structures. With all the GT structures that have been solve to date, two general folds have been mostly observed: the GT-A and GT-B folds (586-588). The GT-A fold is also referred to as the SpsA fold, to reflect the fact that SpsA was the first GT solved with this fold, while the GT-B fold is also referred to as the BGT fold, for the same reason (589). More recently, the GT-C fold has been described to refer to GTs with multiple membrane-spanning domains (578, 585).

**Table 5.1 Glycosyltransferases with available crystal structures**

| Family | Glycosyltransferase | Fold | Mechanism | # | Ref |
|---|---|---|---|---|---|
| GT-1 | TDP-epi-vancosaminylT GtfA (*Amycolatopsis orientalis*) | GT-B | Inverting | 2 | (Mulichak et al., 2003) |
| | UDP-glucosylT GtfB (*Amycolatopsis orientalis*) | GT-B | Inverting | 1 | (Mulichak et al., 2001) |
| | TDP-vancosaminylT GtfD (*Amycolatopsis orientalis*) | GT-B | Inverting | 1 | (Mulichak et al., 2004) |
| | UGlc:triterpene glucosylT (*Medicago truncatula*) | GT-B | Inverting | 2 | (Shao et al., 2005) |
| | UGlc:anthocyanidin 3-O-glucosylT (*Vitis vinifera*) | GT-B | Inverting | 2 | N.A. |
| GT-2 | Spore coat biosynthesis protein SpsA (*Bacillus subtilis*) | GT-A | Inverting | 5 | (Charnock et al., 1999) |
| GT-5 | Glycogen synthase GlgA (*Agrobacterium tumefaciens*) | GT-B | Retaining | 2 | (Buschiazzo et al., 2004) |
| | Glycogen synthase (*Pyrococcus abyssi*) | GT-B | Retaining | 2 | (Horcajada et al., 2005) |
| GT-6 | α1,3-galactosylT (*Bos taurus*) | GT-A | Retaining | 13 | (Gastinel et al., 2001) |
| | α-*N*-acetylgalactosaminylT GTA (*Homo sapiens*) | GT-A | Retaining | 19 | (Patenaude et al., 2002) |
| | α1,3-galactosylT GTB (*Homo sapiens*) | GT-A | Retaining | 13 | (Patenaude et al., 2002) |
| GT-7 | β1,4-galactosylT T1 (*Bos taurus*) | GT-A | Inverting | 25 | (Gastinel et al., 1999) |
| | β1,4-galactosylT T1 (*Homo sapiens*) | GT-A | Inverting | 5 | (Ramasamy et al., 2005) |
| GT-8 | α-galactosylT LgtC (*Neisseria meningitidis*) | GT-A | Retaining | 3 | (Persson et al., 2001) |
| | Glycogenin-1 (*Oryctolagus cuniculus*) | GT-A | Retaining | 3 | (Gibbons et al., 2002) |
| GT-9 | LPS HeptosylT II (*Escherichia coli*) | GT-B | Inverting | 1 | (Burling et al., 2003) |
| GT-13 | β1,2-*N*-acetylglucosaminylT GnTI (*Oryctolagus cuniculus*) | GT-A | Inverting | 3 | (Unligil et al., 2000) |
| GT-15 | α1,2-mannosylT Kre2p/Mnt1p (*Saccharomyces cerevisiae*) | GT-A | Retaining | 3 | (Lobsanov et al., 2004) |
| GT-20 | α,α-trehalose-phosphate synthase OtsA (*Escherichia coli*) | GT-B | Retaining | 3 | (Gibson et al., 2002) |

**Table 5.1 Glycosyltransferases with available crystal structures (continued)**

| Family | Glycosyltransferase | Fold | Mechanism | # | Ref |
|---|---|---|---|---|---|
| GT-27 | α-*N*-acetylgalactosaminylT ppGalNAcT1 (*Mus musculus*) | GT-A | Retaining | 1 | (Fritz et al., 2004) |
| GT-28 | β1,4-GlcNAcT MurG (*Escherichia coli*) | GT-B | Inverting | 2 | (Ha et al., 2000) |
| GT-35 | Maltodextrin phosphorylase MalP (*Escherichia coli*) | GT-B | Retaining | 11 | (O'Reilly et al., 1997) |
| | Liver glycogen phosphorylase (*Homo sapiens*) | GT-B | Retaining | 9 | (Rath et al., 2000) |
| | Muscle glycogen phosphorylase (*Homo sapiens*) | GT-B | Retaining | 1 | N.A. |
| | Muscle glycogen phosphorylase (*Oryctolagus cuniculus*) | GT-B | Retaining | 76 | (Gregoriou et al., 1998) |
| | Glycogen phosphorylase (*Saccharomyces cerevisiae*) | GT-B | Retaining | 1 | (Lin et al., 1996) |
| GT-42 | α2,3/2,8-sialylT CstII (*Campylobacter jejuni*) | ---- | Inverting | 2 | (Chiu et al., 2004) |
| GT-43 | β1,3-glucuronylT GlcAT-P (*Homo sapiens*) | GT-A | Inverting | 3 | (Kakuda et al., 2004) |
| | β1,3-glucuronylT GlcAT-I (*Homo sapiens*) | GT-A | Inverting | 2 | (Pedersen et al., 2000) |
| GT-44 | UGlc glucosylT Toxin B (*Clostridium difficile*) | GT-A | Retaining | 2 | (Reinert et al., 2005) |
| GT-63 | DNA β-glucosylT BGT (Bacteriophage T4) | GT-B | Inverting | 20 | (Vrielink et al., 1994) |
| GT-64 | α-N-acetylhexosaminylT Extl2 (*Mus musculus*) | GT-A | Retaining | 4 | (Pedersen et al., 2003) |
| GT-72 | DNA α-glucosylT AGT (Bacteriophage T4) | GT-B | Retaining | 5 | (Lariviere & Morera, 2004) |
| GT-78 | Mannosylglycerate synthase MgS (*Rhodothermus marinus*) | GT-A | Retaining | 4 | (Flint et al., 2005) |

All data were retrieved from the CAZy database (http://afmb.cnrs-mrs.fr/CAZY/GT.html), which had been last updated on January 3rd, 2006.

The sialyltransferase CstII structure, although similar to the GT-A fold, has been suggested to describe a new fourth fold (Figure 5.3) (580, 590).

A closer look at the two most common folds reveals that the GT-B fold consists of two Rossmann domains, with the active site located between the domains. The GTs with this structure do not appear to share any strictly conserved residues and there does not seem to be a bound divalent cation associated with catalysis (580, 591). On the other hand, the GT-A fold consists of one globular domain that separates into two subdomains: an N-terminal nucleotide-binding subdomain that resembles a Rossmann fold (592) and a C-terminal subdomain responsible for acceptor binding. The N-terminal subdomain has also been referred to as the 'SGC' domain, or SpsA GnTI Core domain (586) and as the 'UBD', or UDP-binding domain (593). The N-terminal subdomain contains a conserved motif termed 'DXD motif', which has been proposed to be involved in binding of a divalent cation (587, 594, 595), although one group has observed such motifs without bound metal ions (596). The DXD motif involved in metal ion binding is usually found in a type I β-turn that follows a stretch of hydrophobic residues (586) and the metal cation plays a role in binding of the donor nucleotide. Some studies have shown that mutation of aspartic residues of the DXD motif completely abolishes the activity of GTs (594, 595). Aside from the conserved folds and motifs, GTs also possess flexible loops that are thought to be important in preventing abortive hydrolysis of the diphospho-nucleotide donor (597) and/or in facilitating product release (586). It is known that such flexible loops play a critical role in enzyme function (598) and will thus be referred to as 'catalytic loops' in this chapter. The GTs can be found in one of two states: state I, or open form, is found when the GT is unliganded and the catalytic loops are disordered whereas state II, or closed form, is found when the GT is


**Figure 5.3. Glycosyltransferase folds.** Ribbon diagram of three glycosyltransferases representative of the different folds. **A.** *B. subtilis* pore coat polysaccharide biosynthesis protein (SpsA) represents the GT-A fold (PDB ID 1QGQ), **B.** Bacteriophage T4 DNA β-glucosyltransferase (BGT) represents the GT-B fold (PDB ID 1J39), **C.** *C. jejuni* sialyltransferase (CstII) represents a new fold (PDB ID 1RO7). Figures prepared with Setor (50).

bound by its substrates and the catalytic loops are ordered, closed over and interacting with the substrates (589).

There is no strict relationship that is observed between the fold of a GT and the nature of its mechanism. Both inverting and retaining GTs have been observed with the GT-A fold, and the same holds true for the GT-B fold. When it comes to understanding the mechanisms of GTs, both inverting and retaining mechanism have been thought to be analogous to the mechanisms of glycosylhydrolases (599). This has been shown to be true in the case of inverting GT structures, which like inverting glycosylhydrolases, support the $S_N2$ mechanism (Figure 5.4A). In inverting GTs displaying the GT-A fold, there is a sequential ordered mechanism whereby binding of donor is followed by loop closure and subsequent acceptor binding (600). Once substrates are bound, one acidic amino acid deprotonates the acceptor hydroxyl group which then attacks the anomeric carbon of the donor sugar in a direct displacement mechanism (572, 601, 602). This proceeds through an oxocarbenium-ion-like transition state (572, 601, 603, 604). There has been more debate about the mechanism of retaining GTs. Comparison with glycosylhydrolases would suggest a double displacement mechanism involving two residues with carboxyl groups acting as acid catalyst and nucleophile respectively, two inversions resulting in net retention of stereochemistry at the anomeric centre, two oxocarbenium-ion-like transition states (605) and a short-lived covalent glycosyl-enzyme intermediate (Figure 5.4B) (602, 606-611). Such a mechanism has been difficult to prove with available structures, and only one intermediate has been trapped involving a residue rather removed from the active site (599). Some quantum mechanical calculations have determined that GTs may proceed through a double-displacement reaction but that unlike glycosylhydrolases, may not need two catalytic

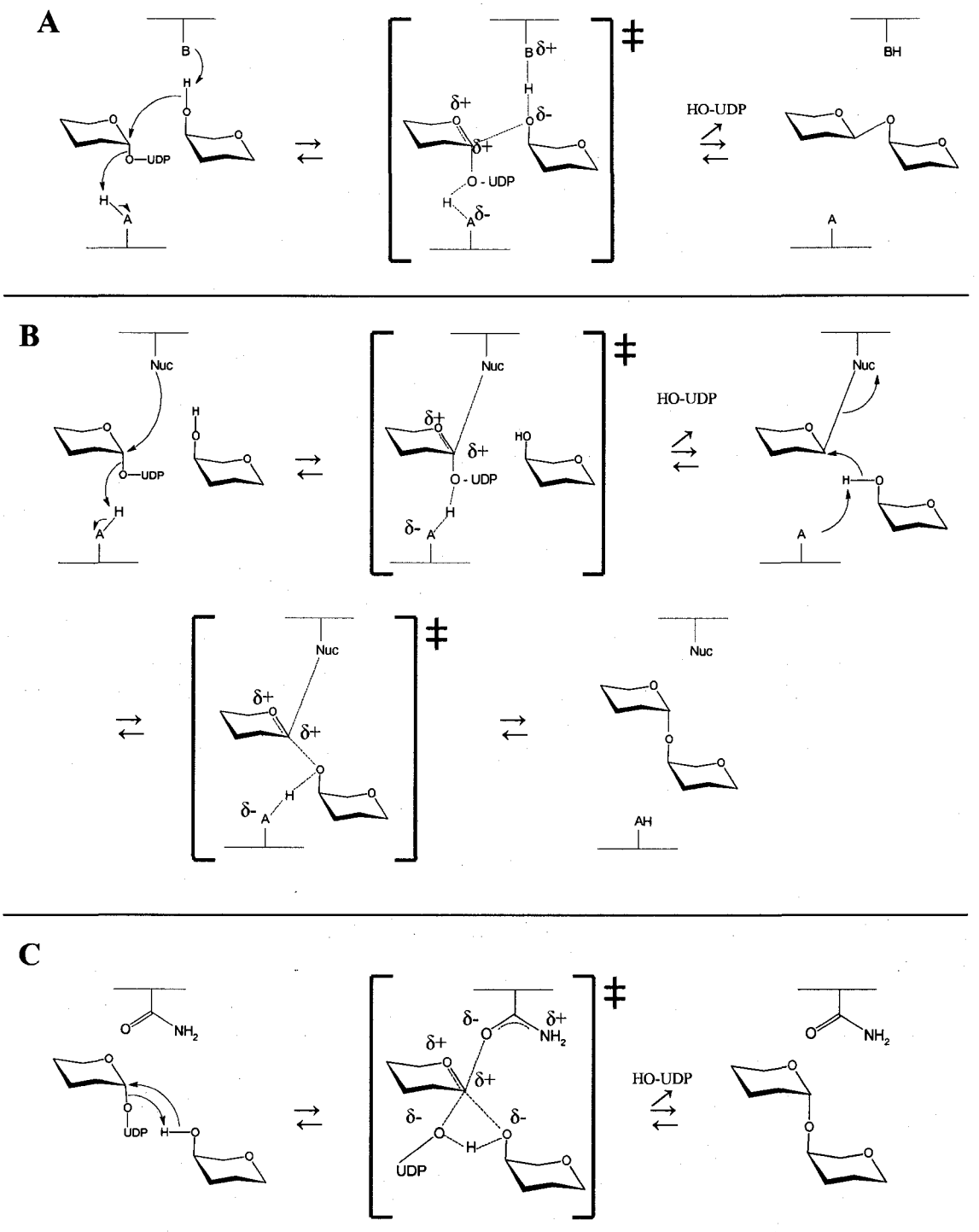


**Figure 5.4. Proposed mechanisms for glycosyltransferases. A.** Inverting GTs proceed through a direct displacement $S_N2$-like reaction via a single oxocarbenium ion-like transition state, **B.** Retaining GTs can proceed through a double-displacement reaction via two oxocarbenium ion-like transition states or, **C.** through a direct front-side displacement $S_Ni$-like reaction.

residues in the active site for the reaction to proceed (606). Despite this, many groups have proposed an alternative mechanism that involves a direct attack of the acceptor through a so-called $S_Ni$-like mechanism (Figure 5.4C). This mechanism was first proposed for LgtC (596) and was found to be energetically favorable through quantum mechanical calculations (612), although it has yet to be proven.

*Glycosyltransferases A and B*

GTA and GTB are type II membrane proteins of the Golgi that can be found in soluble form in serum, milk, and saliva (541, 613-615). The soluble form of both GTA and GTB has been partially purified from human plasma (616-619) while GTA has also been isolated from hog gastric mucosa (620), porcine submaxillary glands (621), human lung (536), human gastric mucosa (622) and human milk (623). Purification of the enzymes from their native environment, as well as the recent cloning and functional expression of the catalytic domains of both enzymes (624-626), has allowed for characterization of the activity and specificity of these enzymes.

GTA uses the nucleotide donor UDP-GalNAc to transform the H-antigen acceptor into the A-antigen (627, 628) while GTB uses the nucleotide donor UDP-Gal to transform the H-antigen acceptor into the B-antigen (Figure 5.5) (629, 630). Both enzymes have been shown to require a divalent cation for the transfer reaction (631, 632) and they both do this transfer with net retention of the stereochemistry of the donor sugar, and are therefore classified as retaining GTs (633). It has been shown with both native and recombinant purified enzyme that GTA and GTB have overlapping specificities *in vitro* (632, 634-637). Both A and B donors can act as competitive inhibitors of GTB and GTA, respectively (638, 639). These phenomena most likely occur because the donor sugars are very similar, with

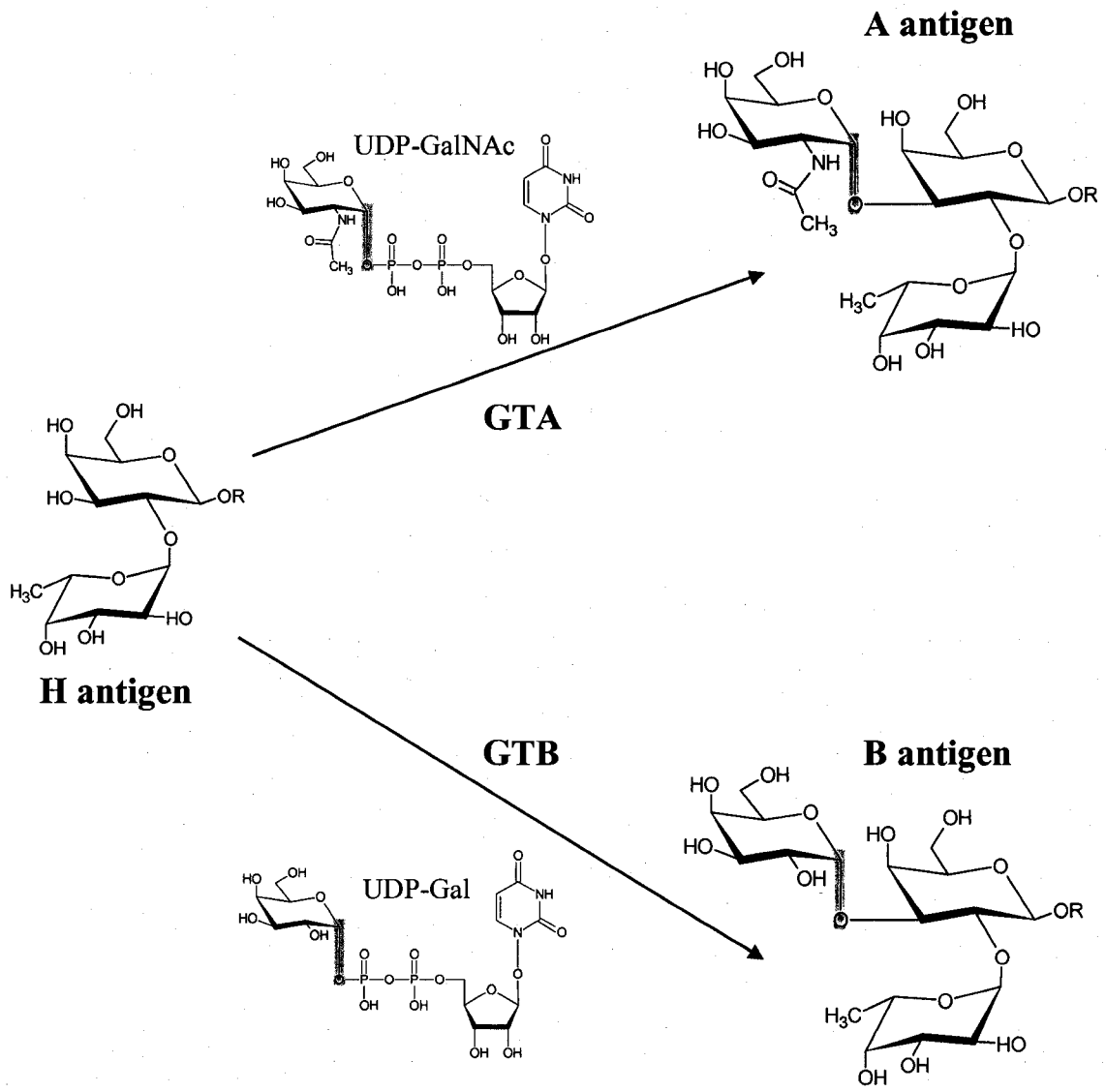


**Figure 5.5. Biosynthesis of the blood group A and B antigens.** The H antigen serves as acceptor substance and UDP-GalNAc and UDP-Gal serve as donors for the synthesis of the A antigen by GTA and of the B antigen by GTB, respectively. This reaction is done with retention of stereochemistry, as highlighted in blue. The chemical groups that differentiate the A and B antigens are highlighted in yellow.

the only difference between the A donor and the B donor being an N-acetyl group *vs* a hydroxyl group at position 2 on the donor sugar.

Further studies to understand the specificity of both enzymes focused on the four critical amino acid residues. Expression of chimeras of mixed GTA and GTB critical residues in HeLa cells revealed that residues 235, 266 and 268 played a role in specificity and that residues 266 and 268 particularly were crucial in donor sugar specificity (640). Similar experiments using purified recombinant chimeras of mixed GTA and GTB critical residues also demonstrated the residues 266 and 268 to be important in donor sugar specificity, with residue 266 most important in determining A *vs* B donor substrate specificity, residue 235 affecting acceptor binding and residue 176 possibly playing a role in enzyme turnover (624, 641). Another way of determining the specificity of GTA and GTB for their substrates was by modification of acceptor and donor hydroxyl groups and analyzing the effects on binding. These studies revealed that the position 4 on the galactose residue of the H-acceptor is critical for recognition (633, 642) while substitutions at position 3 on the galactose residue of the H-acceptor in some cases created competitive inhibitors of the enzymes (633, 642, 643). Studies on the fucose residue of the H-acceptor revealed that all substitutions were better tolerated by GTA than by GTB (644). Finally, all modifications of donor sugars were shown to affect binding to both enzymes (626, 645).

Studies focused on understanding the mechanism of GTA and GTB have suggested a pattern that is consistent with a Theorell-Chance mechanism, where donor binds before acceptor (646). This ordered addition of substrates would be consistent with the strict need for donor in affinity chromatography purification using immobilized acceptor matrices (621, 632, 639). Aside from the role of GTA and GTB in glycosyl transfer, it has also been

observed that both GTA and GTB appear to show constitutive donor hydrolase activity in the absence of acceptor (647).

To have a better understanding of the specificity, recognition and catalytic mechanism of GTA and GTB, the crystal structures of the two GTs were solved in native form as well as in complex with substrates (647). The crystals of GTA and GTB utilize mercury atoms to form. The structures of the catalytic domains of GTA and GTB adopted the GT-A fold (Figure 5.6A) (647, 648). The catalytic loop that has been shown to be important in the mechanism of the enzymes (649, 650) is not seen in the electron density, even when the enzymes are complexed with UDP. Critical residues 235, 266, and 268 are situated in the active pocket whereas critical residue 176 lies at the edge of the disordered catalytic loop (Figure 5.6B). The DXD motif in the N-terminal subdomain, D211-V212-D213, was shown to coordinate a manganese ion, with both aspartic acid residues of the motif interacting with the divalent cation and with the second aspartic acid residue showing a bidentate interaction (Figure 5.6C). Residue 235, which had been suggested to be important in acceptor binding (651), is found to affect the conformation of the aliphatic tail of the bound acceptor. This finding supports a role for residue 235 in differentiation between glycoconjugate structures carrying the H-antigen. Residues 266 and 268 are both found to occupy positions in the active site that are close to the modeled donor sugar. As such, both residues can provide a surface that is complementary to the bulk of the group defining the donor sugar. Beyond highlighting the role of the critical residues, the structures of GTA and GTB have allowed some speculation about the mechanism of the enzyme. With the modeled donor and the bound H-antigen, it is proposed that residue E303 could act as nucleophile for the reaction, based on the proximity to the anomeric center and the

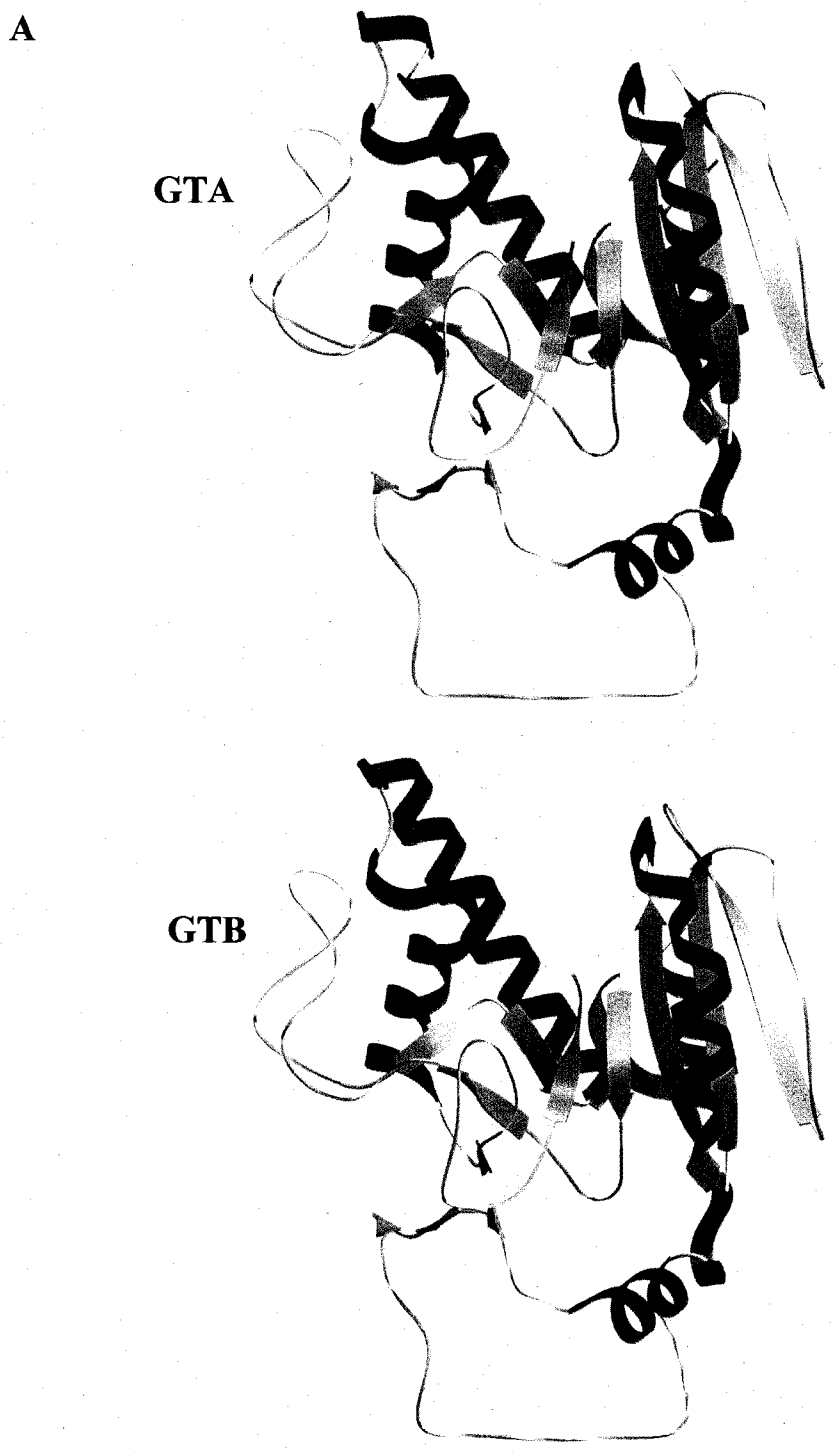


**Figure 5.6. Crystal structures of GTA and GTB. A.** Ribbon diagram of the catalytic domains of GTA and GTB showing the GT-A fold. (Continued on the next page)

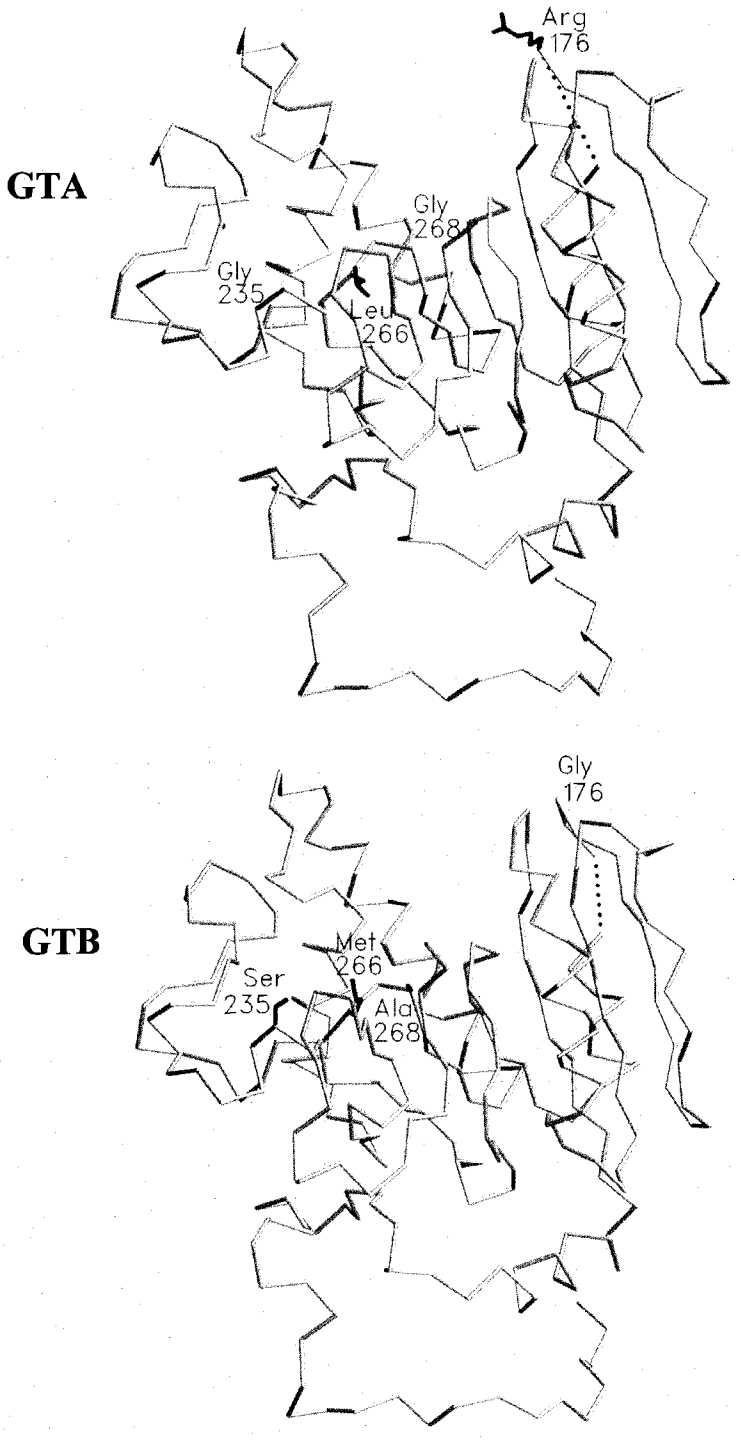


**Figure 5.6. Crystal structures of GTA and GTB (continued). B**. Backbone structures of GTA and GTB highlighting the position of the four critical residues (in red), with residues 235, 266, and 268 being in the binding pocket of the C-terminal domain and residue 176 being at the edge of the disordered catalytic loop in the N-terminal domain. (Continued on the next page)

C

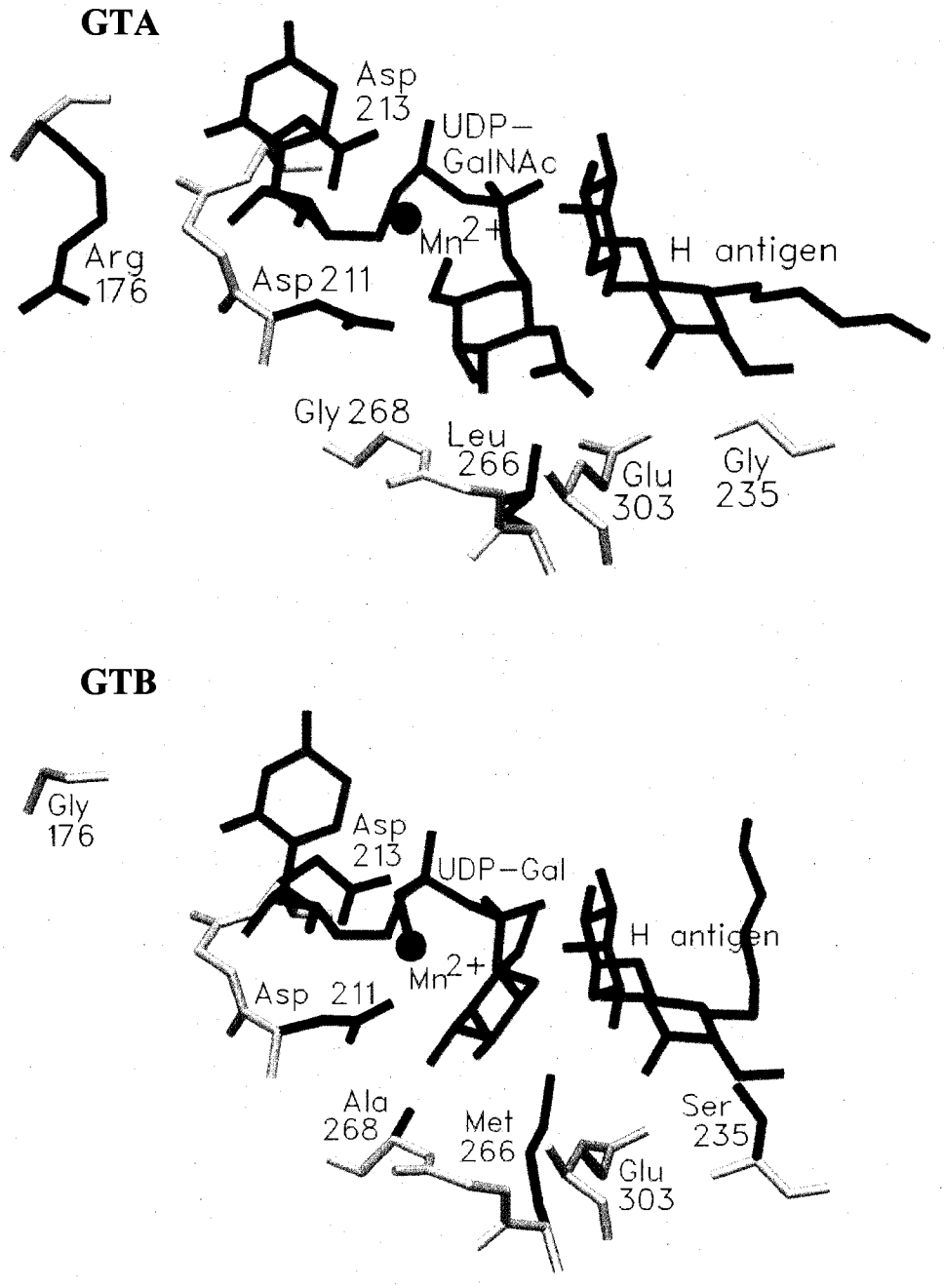


**Figure 5.6. Crystal structures of GTA and GTB (continued).** **C**. Active site cleft diagram showing bound UDP and H antigen molecules (green), modeled donor sugar (green), as well as the relative position of the four critical residues (red), the DXD motif (blue) with coordinated $Mn^{2+}$ ion (black), and the proposed nucleophile (yellow). Figures prepared with Setor (50).

acceptor molecule. Unfortunately, since the donor sugar was not fully observable in the electron density of any of the structures, it was impossible to unambiguously deduce more information about the mechanism of GTA and GTB.

Understanding the basis for specificity and recognition of GT is crucial. The enzymes in their purified form are used for the production of biologically active oligosaccharides (652, 653) and understanding how they work can help in the design of GTs that produce many types of oligosaccharides, with stereospecificity and regioselectivity that does not require blocking groups and separation of enantiomers. In the case of the blood group GTs, it is also important in the medical field as these enzymes are the cause of blood group mismatch and failure of tissue transplantation. Furthermore, the mechanism for the retaining GTs has yet to be unambiguously elucidated. This led our group to focus on the study of the structures of GTA and GTB. With the help of mutants and substrates inhibitors, our focus is directed at understanding how the blood group GTs recognize donors and acceptors, how major and minor alleles function, and how the transfer reaction occurs. In this respect, the structural basis for the cis-AB and B(A) phenotypes involving a mutation at residue 234 (564), the structural basis for the O2 phenotype involving mutations P74S, R176G, and G268R (555), as well as the structural basis for the Bel phenotype involving mutation M214R and the A-weak-B phenotype involving mutations M214V and M214T (654) were elucidated. Furthermore, the basis for inhibition by acceptor analogs as well as the contribution of critical residues 235 and 266 to acceptor binding and transfer was also elucidated (651, 655).

## RATIONALE

The ABO(H) blood groups are clinically relevant molecules in blood transfusion and organ transplantation. The study of the human ABO(H) blood group GTs is important to understand the specificity of these homologous enzymes for minimally different donor substrates as well as to resolve their mechanism of catalysis. The information gained through studies of the human ABO(H) blood group GTs will ultimately help in the engineering of the enzymes and in the design of inhibitors.

The objective of this research is to solve the x-ray crystal structures of two mutants of GTB: GTB M2 C80S, C196S and GTB M3 C80S, C196S, C209S, both in their native and complex forms. These mutants are designed to allow crystallization of GTB in the absence of mercury. It is hypothesized that they will show the entire structure of GTB, including stretches of residues that were missing in the heavy-atom derivative of wild-type GTB crystals.

## MATERIALS AND METHODS

*Protein Expression and Purification*

GTB M2 (GTB C80S/C196S mutant) and GTB M3 (GTB C80S/C196S/C209S mutant) were constructed by directed mutagenesis using PCR and the GTB-15 (residues 68-354) plasmid DNA as template by Dr. Nina O. Seto, IBS, NRCC. Fragments were amplified using SOE. The resulting gene was digested with EcoRI and HindIII, and inserted into the corresponding sites of pCWΔlac. Plasmids were transformed into *E. coli* BL21 (Novagen).

Mutant enzymes were expressed and purified from *E. coli* cultures as described previously (626). Briefly, cells transformed with the mutant enzymes were grown in TB medium containing M9 salts supplemented with 0.4% casamino acids, 5 μg/mL vitamin B-1 and 100 μg/mL ampicillin at 30 °C with vigorous shaking. Expression was induced at mid-log by adding IPTG to a final concentration of 1 mM. Cells were harvested 24 hrs after induction. Extraction of soluble material was done using a French Press, and cell debris were pelleted by centrifuging the lysate for 1 hour at 36,000 rpm. The supernatant was passed through a SP Sepharose Fast Flow column and washed with 50 mM MOPS pH 7.0, 0.5 M NaCl and 1 mM DTT. The fractions containing active material were subsequently applied to a UDP-hexanolamine Sepharose column in the presence of the divalent manganese cation. Mutant enzymes were eluted with 50 mM MOPS pH 7.0, 0.5 M NaCl, 1 mM DTT, 5 mM $MnCl_2$, ~4-10 mM UDP, and concentrated using a Centriplus 30 filtration unit (Amicon). Protein concentrations were estimated at 20 mg/mL using Bio-Rad's protein assay procedure, based on the method of Bradford using bovine gamma globulin as standard (656).

*Kinetic Analysis*

Kinetic analysis of GTB M2 and GTB M3 was carried out by Dr. Monica M. Palcic, Department of Chemistry, University of Alberta, Edmonton, AB, Canada as described previously (624).

*Crystallization*

GTB M2 and GTB M3 were crystallized using the hanging drop vapour diffusion method with conditions similar to the wild-type GTB enzyme (647) by Dr. S. Borisova,

University of Ottawa. Briefly, for the native GTB M2 and GTB M3, 10-15 μL drops containing 5.5-6 mg/mL protein in 35 mM sodium acetate pH 4.6, 45 mM ADA pH 7.5, 30 mM NaCl, 3-4 mM magnesium chloride, 3-3.5% PEG 4000 were suspended over a reservoir containing 50 mM sodium acetate, 50 mM ADA, 100 mM ammonium sulfate, 5 mM magnesium chloride, 10% PEG 4000 at 18 °C. Crystals for the complexes with H-acceptor, and UDP-2F-Gal and H-acceptor were obtained by soaking the crystals in reservoir solution containing 7 mM of H-antigen and/or 10-15 mM UDP-2F-Gal. All crystals were washed with cryoprotectant solution consisting of reservoir solution containing 30% MPD, mounted in cryo-loops (Hampton Research) and flash-frozen in liquid propane for storage and transportation to data collection facilities.

*Data Collection*

Data were collected at beamline X8C of the NSLS, BNL, using an ADSC Quantum 4R detector (Area Detector Systems Corporation, Poway, CA) and an Oxford Cryosystem model 600 (Oxford Cryosystems, Oxford, UK). Crystals were mounted into the stream of liquid nitrogen and collected at 100 °K using a wavelength of 1.15 Å. Data were reduced and scaled using the HKL2000 software (288).

*Structure Determination and Analysis*

For native GTB M2, native GTB (PDB ID 1LZ7) was used as the starting model for rigid body refinement in CNS (657). Three rounds of 25 cycles were performed using the whole molecule as a rigid body at low resolution for the first cycle, and then using three sub-domains defined by residues 68-113, 114-176, and 190-345 for the subsequent cycles at 3.5 and 3.0 Å respectively. This was followed by energy minimization using a range of

resolution of 6.0-3.5, 6.0-3.0 and 6.0-2.8 Å with fixed B-factors. A composite-omit map was calculated with data extending to maximum resolution and manual fitting was undertaken in Xtalview (658) and Setor (50). Electron density proved to be very clear for a portion of the catalytic loop corresponding to residues 184 to 198, and these residues were thus positioned manually. Furthermore, cysteines at position 80 and 196 were replaced by serines and N-terminal residues not part of the mutant (GTB-15 versus GTB-10 for the wild-type GTB structure) were deleted. Further energy minimization as well as simulated annealing was carried out with B-factors allowed to refine individually. Water molecules were added using the water_pick script from CNS. Rounds of manual fitting using 3Fo-2Fc and Fo-Fc electron density maps, followed by refinement and automated assignment of water molecules were done with increasing resolution until all data to maximum resolution were used. Finally, residues with alternate conformations were modeled. Quality of the structure was assessed throughout using Ramachandran plots and monitoring the values for the R-factor, Rfree, B-factors, and bond length and bond angle rmsd values.

GTB M2 in complex with UDP-2F-Gal was refined as described for the native GTB M2. Composite-omit electron density maps showed no electron density for the donor or UDP. GTB M2 in complex with UDP-2F-Gal and H-acceptor was refined as described. Composite-omit map showed clear density for the H-acceptor but none for the donor or UDP. The coordinates for H-acceptor were taken from the structure of the heavy-atom derivative of wild-type GTB in complex with UDP and H antigen (PBD ID 1LZJ). All further manipulations were done as described.

For native GTB M3, native GTB M2 was used as starting model for rigid body refinement. Manual fitting using a composite-omit map allowed the full catalytic loop to be

modeled in electron density. Cysteine 209 was changed to serine. Further refinement and analysis were done as described for native GTB M2. As was the case for GTB M2, the GTB M3 and UDP-2F-Gal complex showed no electron density for donor or UDP. GTB M3 in complex with UDP-2F-Gal and H-acceptor showed density for the H-acceptor only. Coordinates for the acceptor were taken from the structure of GTB M2 complex and all subsequent analyses were done as described.

## RESULTS AND DISCUSSION

There are four free cysteine residues in GTB: C80, C196, C209, and C284 (659). Wild-type GTB has been found to aggregate easily because of the presence of these free sulfhydryl groups and the mercury derivative has been shown to crystallize more easily (647). Conservative mutation of the first two cysteines to serine residues (GTB M2) and of the first three cysteines to serine residues (GTB M3) was accomplished in an effort to facilitate crystallization of GTB. Mutation of free cysteine residues was also employed with *Neisseria meningitidis* LgtC in order to resolve protein solubility issues (596). The first two cysteine-to-serine mutations do not affect the kinetics of GTB M2 as this mutant shows values for kcat, Km acceptor and Km donor comparable to the wild-type GTB, but the addition of the third mutation in GTB M3 renders an enzyme with a reduced kcat (about 2/3 of the wild-type value) and slightly higher Km for the acceptor.

*Crystallization*

Crystals of GTB M2 and GTB M3 in their native and H-antigen-complexed forms were obtained in 7 days and grew to dimensions of 0.4 x 0.4 mm on average in the absence of mercury. The data collected extends to high resolution and all crystals are found to be in space group $C222_1$ (see Table 5.2 for data collection and refinement statistics). In all data sets, there is one molecule per asymmetric unit. The packing of the GTB mutants reveals an interesting feature, similar to that observed in the crystals of heavy-atom derivatives of wild-type GTA and GTB (647): the N-termini of pairs of symmetry-related partners are found to be intertwined (Figure 5.7). As outlined in Table 5.3, there are many hydrogen bonds that stabilize this inter-molecular arrangement. Other GTs have been observed to crystallize in dimeric arrangements. Rabbit muscle glycogenin has been shown to form dimers in solution and to crystallize as a pentamer of dimers (660) while both human β1,3-glucuronyltransferase I (661) and *Rhodothermus marinus* mannosylglycerate synthase (662) have been shown to form oligomers that interact through neighbor's C-termini. It has been reported that GTs can form oligomers that are biologically relevant (663), and in the rabbit GnTI, this was shown to be dependent on a disulfide bridge created via cysteine 33 in the N-terminal part of the catalytic domain (664). In the case of wild-type GTB and GTB mutants, the N-termini interaction seen in crystals is unlikely to be of biological relevance: in the Golgi, the catalytic domains could not interact with each other in this fashion. Furthermore, whether or not GTB residue C80 can participate in dimer formation *in vivo*, it is not thought to be responsible for the observed packing since the intertwining of N-termini is observed even in GTB M2 and GTB M3, where C80 is mutated to serine.

**Table 5.2 Data collection and refinement statistics for GTB M2 and GTB M3, both in their unliganded and acceptor-bound states**

| | GTB M2 | GTB M2 + H acceptor | GTB M3 | GTB M3 + H acceptor |
|---|---|---|---|---|
| *Data collection* | | | | |
| Space group | $C222_1$ | $C222_1$ | $C222_1$ | $C222_1$ |
| Cell dimensions (Å) | a = 52.5 | a = 52.6 | a = 52.5 | a = 52.5 |
| | b = 149.3 | b = 149.4 | b = 148.9 | b = 149.7 |
| | c = 79.9 | c = 79.8 | c = 79.5 | c = 79.7 |
| No. observations | 116,309 | 165,696 | 136,771 | 264,267 |
| Unique reflections | 23,975 | 37,356 | 37,358 | 70,312 |
| Completeness (%)[a] | 93.6 (70.3) | 92.2 (68.1) | 98.1 (91.7) | 95.2 (67.5) |
| R symm (%)[a] | 8.2 (27.7) | 6.7 (19.8) | 4.3 (15.6) | 3.7 (16.7) |
| I/σI | 11.2 | 13.1 | 18.5 | 15.5 |
| *Refinement Statistics* | | | | |
| Resolution (Å) | 6.0 – 1.89 | 6.0 – 1.62 | 6.0 – 1.65 | 6.0 –1.32 |
| R cryst (%) | 19.02 | 19.47 | 17.50 | 19.36 |
| R free (%) | 22.17 | 21.28 | 19.89 | 20.80 |
| Rmsd | | | | |
| bond lengths (Å) | 0.005 | 0.005 | 0.004 | 0.004 |
| bond angles (°) | 1.268 | 1.303 | 1.267 | 1.252 |
| No. solvent atoms | 223 | 235 | 239 | 300 |
| B-factors (Å$^2$) | | | | |
| overall protein | 22.58 | 19.97 | 13.85 | 15.22 |
| H-antigen | - | 27.23 | - | 21.14 |

a Values in parentheses are for the highest resolution shell.

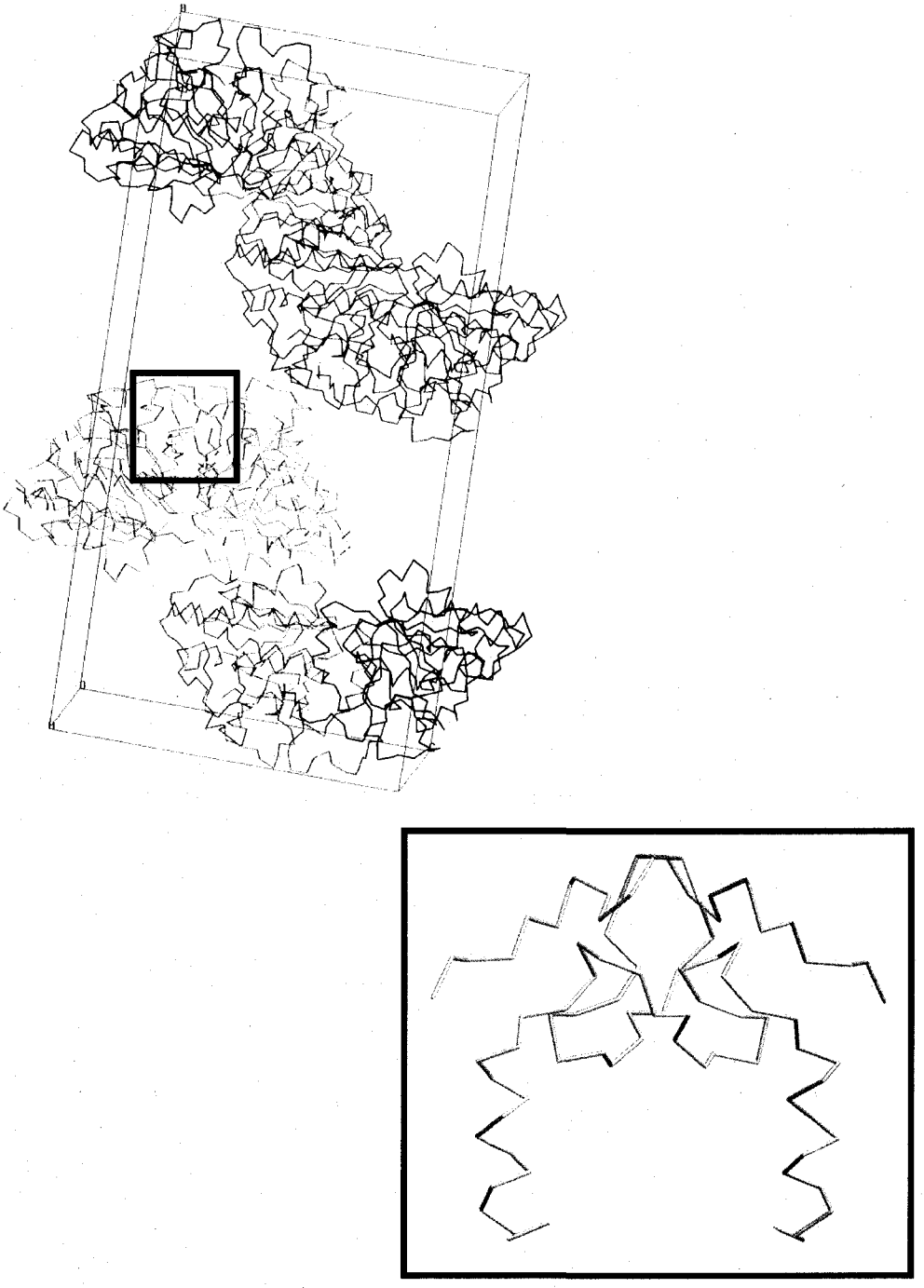

**Figure 5.7. Crystal packing and N-termini intertwinning**. GTB M2 and GTB M3 crystallize in space group $C222_1$. The molecule in the asymmetric unit (white) is shown in the unit cell with its symmetry-related partners. Highlighted in the close-up picture is the N-termini interaction that occurs in crystals of GTB M2 and GTB M3. This packing is also observed in crystals of wild-type GTA and GTB. Figures prepared with Setor (50).

**Table 5.3 Molecular interactions observed between the N-termini of symmetry-related partners**

| | | | Distance (Å) | | | |
|---|---|---|---|---|---|---|
| | | | GTB M2 | GTB M2 + H | GTB M3 | GTB M3 + H |
| OH Tyr 71 | --- | OD1 Asp 262 | 2.62 | 2.50 | 2.62 | 2.56 |
| OE1 Gln 73 | --- | O Ser 239 | 3.08 | - | 3.04 | 3.05 |
| OG1 Thr 78 | --- | O Asp 83 | 2.50 | 2.82 | 2.47 | 2.67 |
| NZ Lys 82 | --- | O Val 84 | - | - | 2.48 | 2.31 |
| N Leu 85 | --- | O Val 76 | 2.82 | 2.87 | 2.83 | 2.84 |
| N Asn 101 | --- | O Pro 89 | 2.80 | 2.88 | 2.85 | 2.84 |
| N Arg 241 | --- | NE2 Gln 73 | 2.68 | 2.65 | 2.66 | 2.71 |
| NH1 Arg 241 | --- | O Tyr 71 | 3.07 | 2.94 | 2.91 | 2.99 |
| NH2 Arg 241 | --- | O Tyr 71 | - | 2.99 | - | 3.02 |

*Overall Structure*

Both GTB M2 and GTB M3 consist of residues 68 to 354 inclusively, corresponding to the catalytic domain of the enzyme. In all structures, residues 68-70 and 346-354, corresponding to the N- and C-termini respectively, are disordered. In GTB M2, both native and in complex with H-acceptor, where residues C80 and C196 are replaced by serines, residues 177 to 183 are not observed in the electron density. These residues are part of the catalytic loop. This loop is disordered in heavy-atom derivatives of wild-type GTA and GTB structures as well as in other GT crystal structures. In GTB M3, both native and in complex with H-acceptor, where residues C80, C196, and C209 are replaced by serines, all residues of the catalytic loop are observed in the electron density (Figure 5.8).

The secondary structure elements and topology diagrams for both GTB M2 and GTB M3 are shown in Figure 5.9. The catalytic domain is organized into two sub-domains. The N-terminal subdomain, consisting of residues 71-224 and 338-345, provides the nucleotide-binding fold and consists of a mixed β-sheet flanked on either side by three α-helices, much like a Rossmann fold. The C-terminal subdomain, consisting of residues 225-337, provides the acceptor-binding site and is composed of a mixed β-sheet flanked by three helices on one side. Between the subdomains is the active site cleft where a total of nine β-strands, originating from both N- and C-terminal subdomains, form a central mixed β-sheet.

GTB M2 and M3 adopt the GT-A fold (587) as seen for the heavy-atom derivative of wild-type GTB (Figure 5.10A). Critical residues 235, 266 and 268 are all situated in the active site cleft whereas critical residue 176, which is part of the catalytic loop, is somewhat removed (Figure 5.10B). The active site cleft shows the conserved DXD motif, D211-V-D213, located in the N-terminal domain (Figure 5.10C). The DXD motif usually binds to

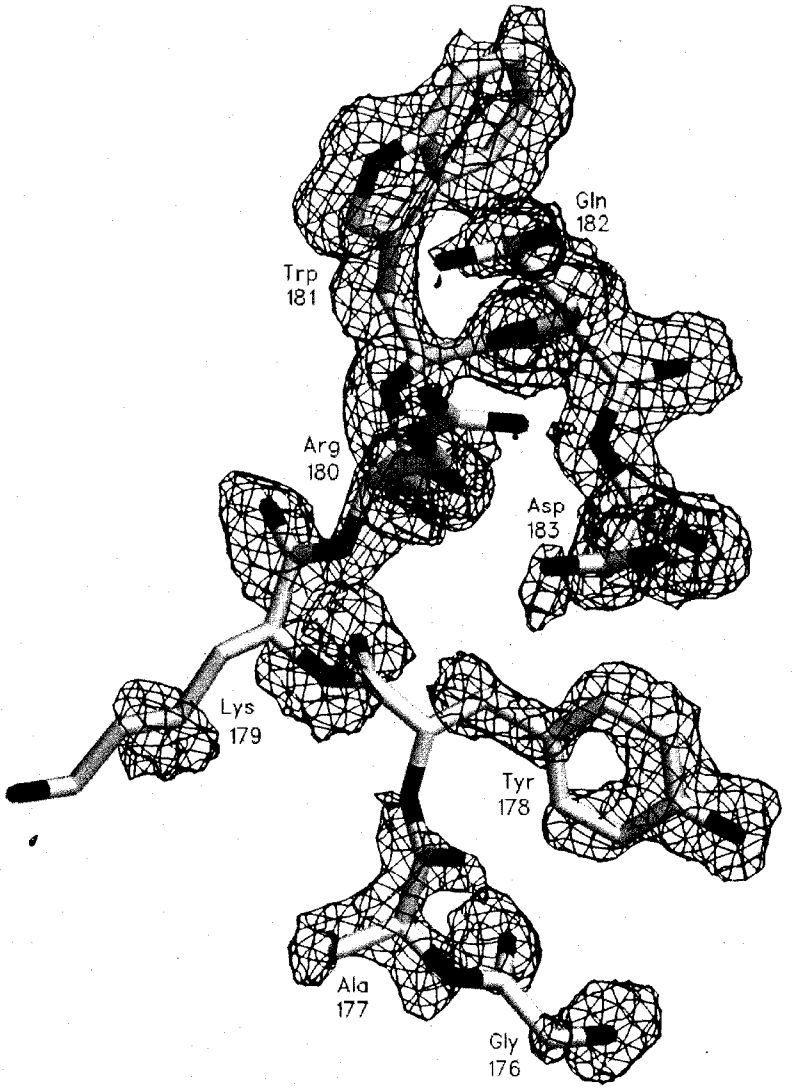


**Figure 5.8. Electron density for the GTB M3 catalytic loop**. Composite omit map electron density (red) is contoured at 0.5σ for the catalytic loop residues 176 to 183. These residues are not observed in the crystal structures of wild-type GTA and GTB, whether the enzymes are in their unliganded or substrate-bound state. GTB M3 provides the first GTB structure where the entire catalytic loop is observed. Figure prepared with Setor (50).

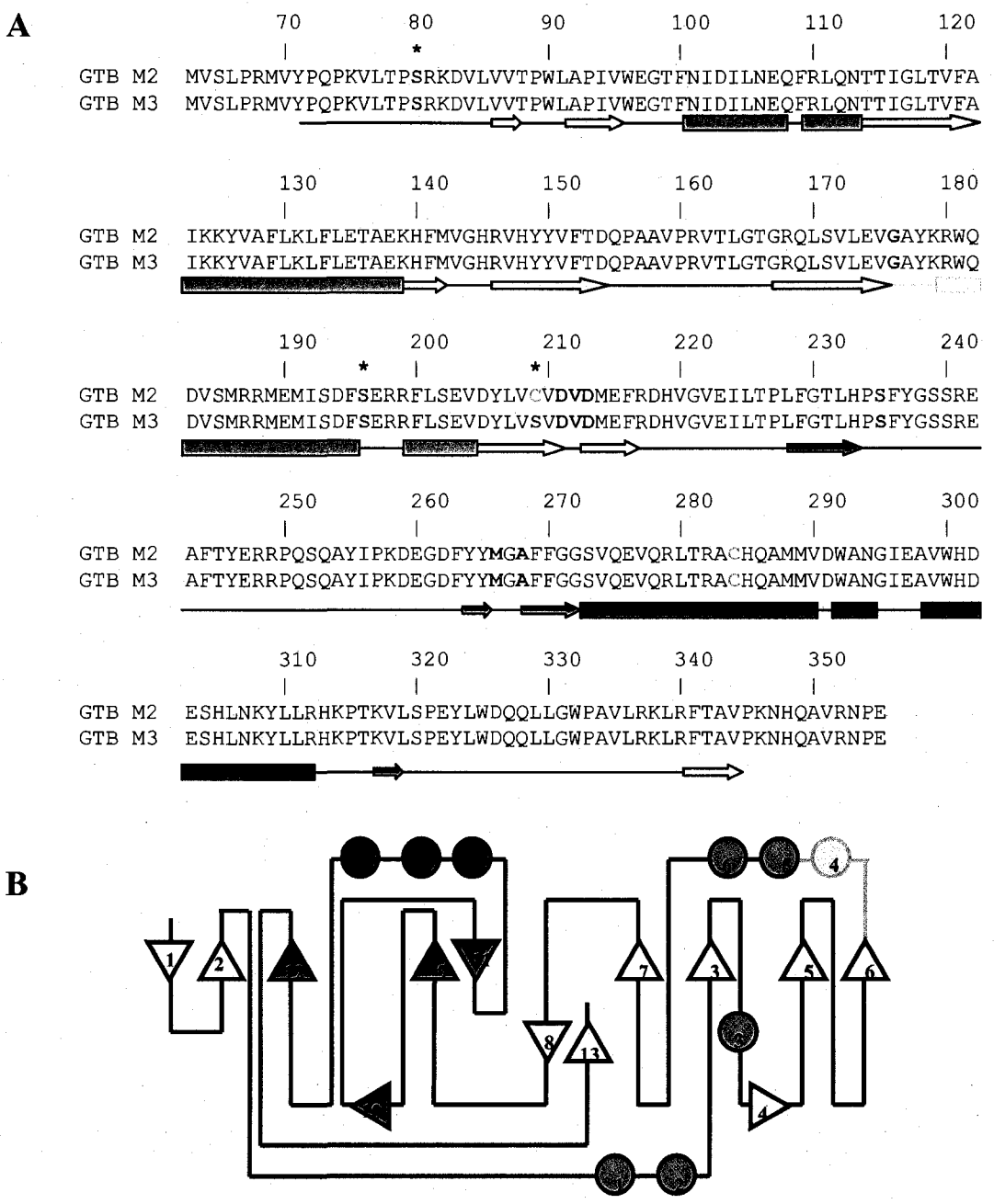


**Figure 5.9. Organization of GTB M2 and GTB M3. A.** Sequence alignment of GTB M2 and GTB M3. The mutation sites have been marked with stars: original cysteines are in orange while the serine mutation are in green. The critical residues are in red and the DXD motif, in blue. The secondary structure is imposed below the sequence. The β-sheets are depicted as arrows whereas the α-helices are depicted as rectangles, and are colored in shades of yellow in the N-terminal domain and in shades of blue in the C-terminal domain. The part of the loop that is not observed in GTB M2 as been shadowed. **B.** Topology diagram showing the arrangement of the secondary structure elements, with the same color code as in **A.**

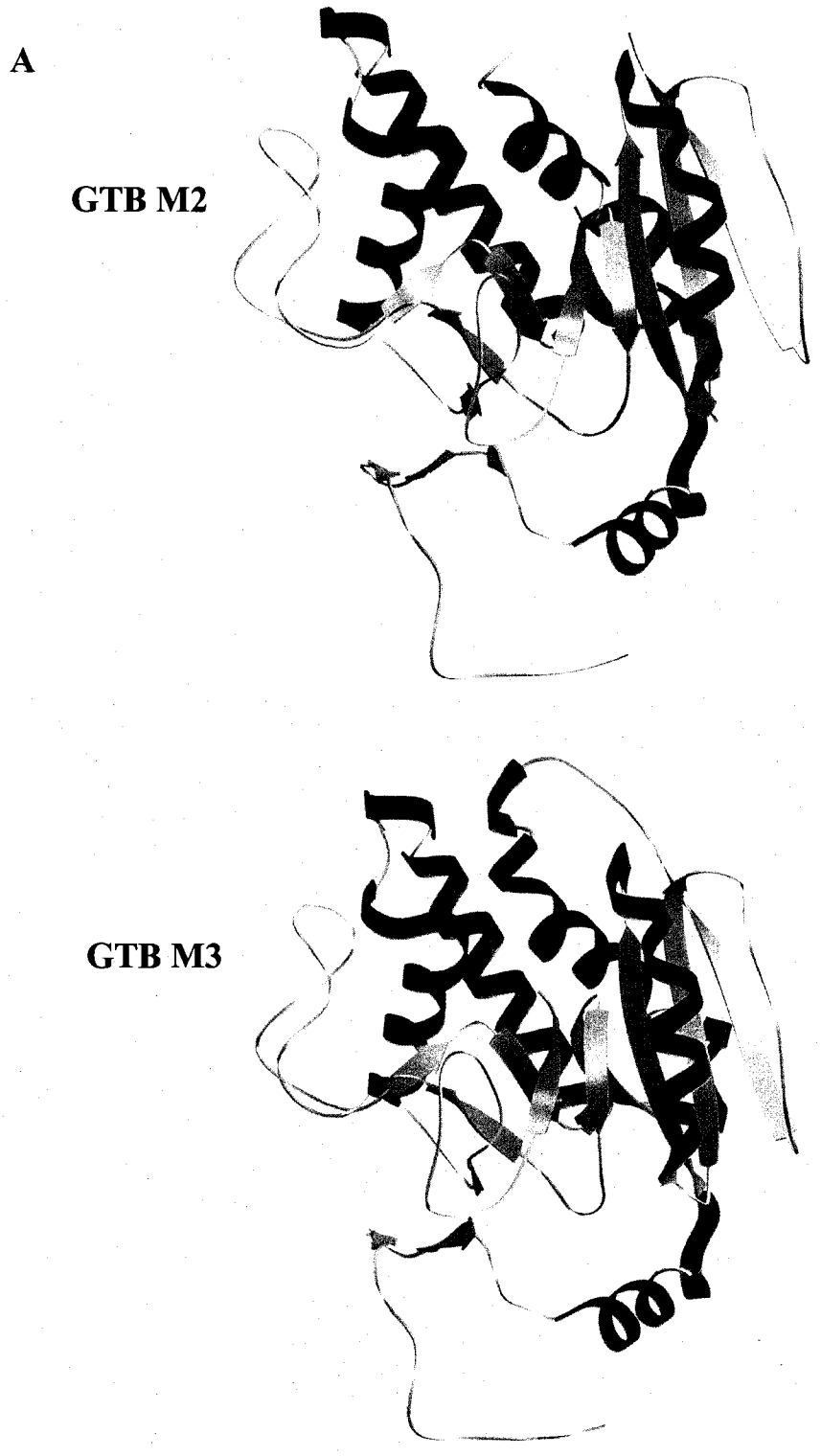


**Figure 5.10. Overall structure of GTB M2 and GTB M3. A.** Ribbon diagram of the catalytic domains of GTB M2 and GTB M3 showing the GT-A fold. (Continued on the next page.)

**B**

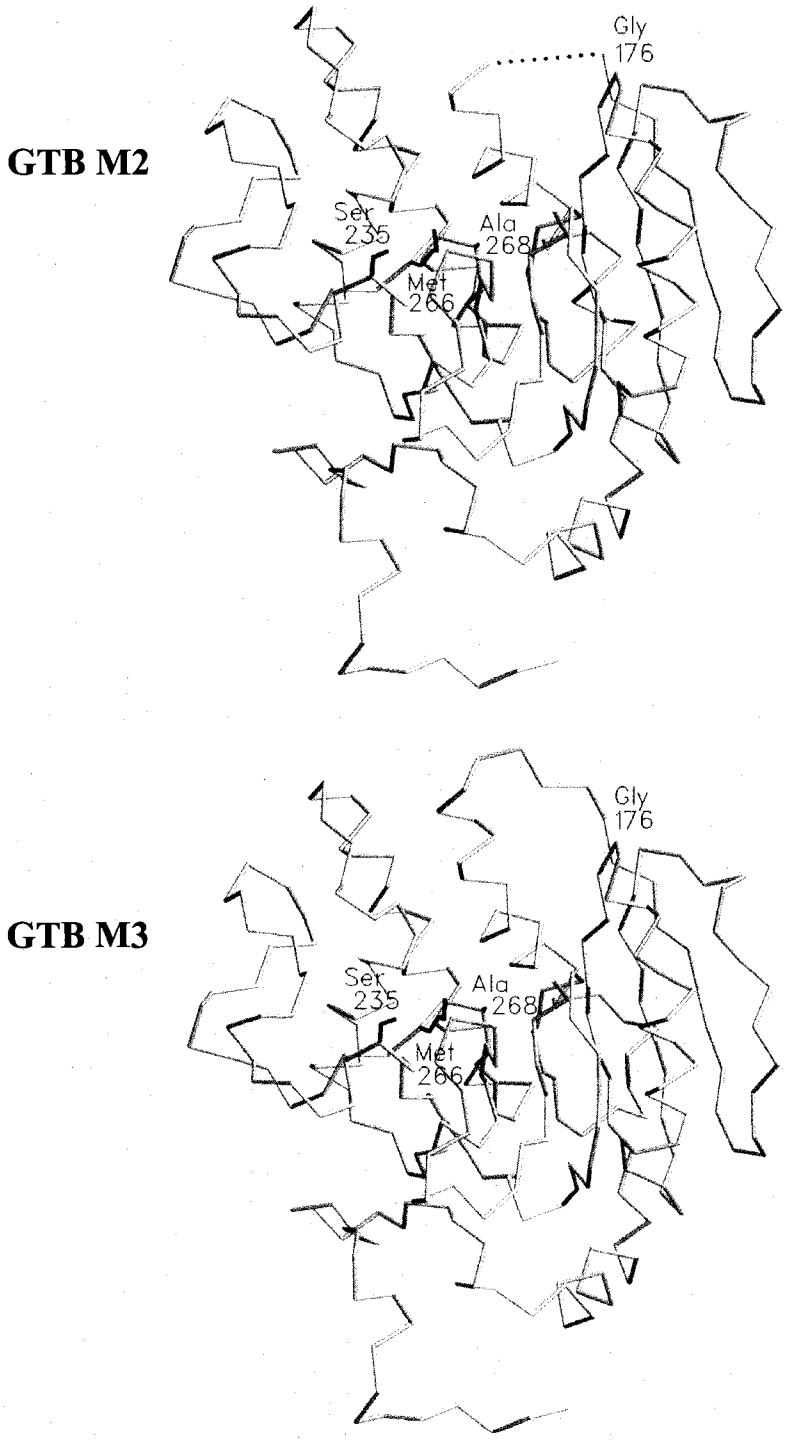


**Figure 5.10. Overall structure of GTB M2 and GTB M3 (continued). B.** Backbone structure of GTB M2 and GTB M3 highlighting the position of the four critical residues (in red) with residues 235, 266, and 268 being in the binding pocket of the C-terminal domain and residue 176 being at the hinge region in the catalytic loop in the N-terminal domain. (Continued on the next page.)

C

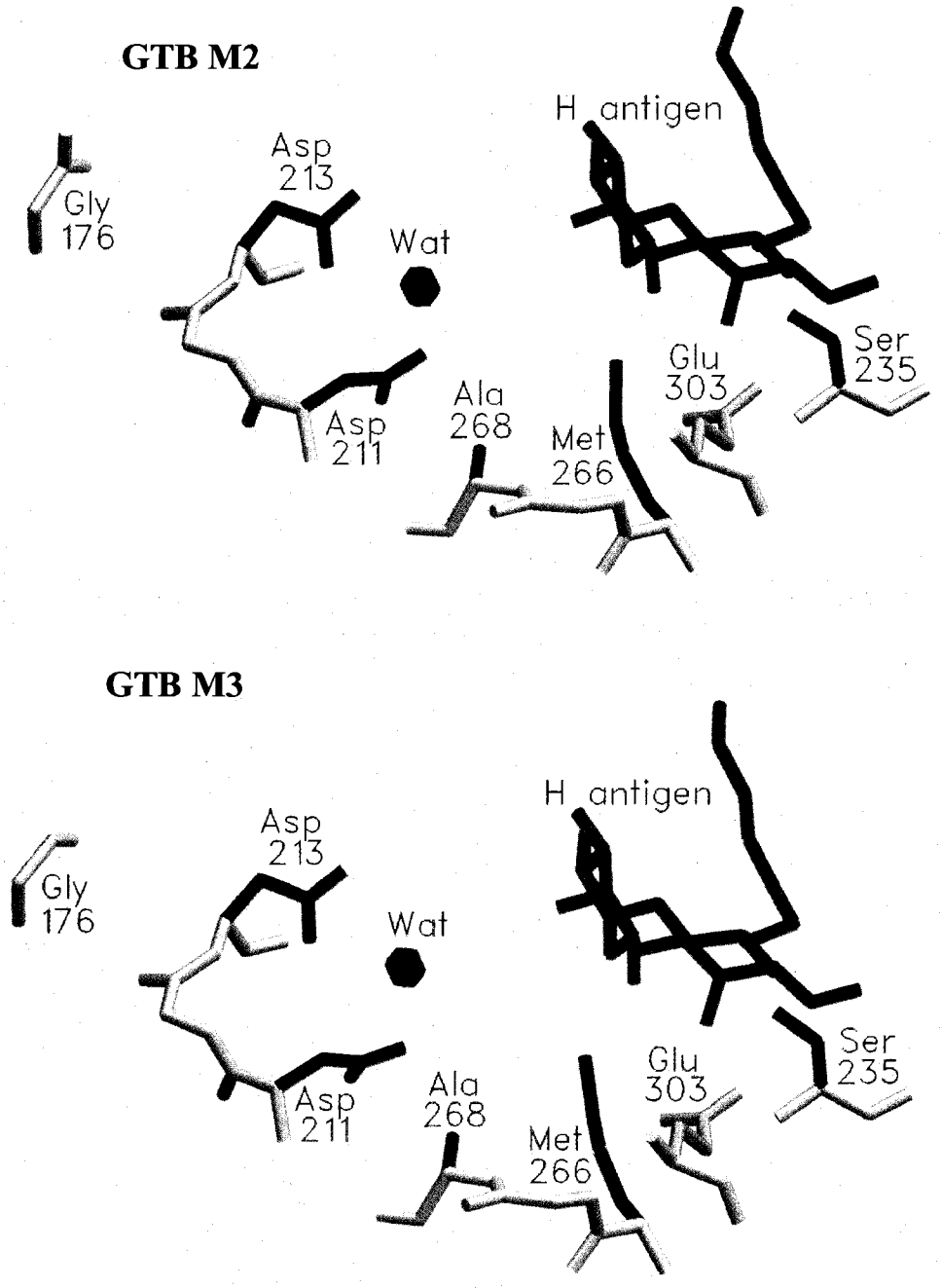


**Figure 5.10. Overall structure of GTB M2 and GTB M3 (continued). C.** Active site cleft diagram showing the bound H-antigen (green) as well as the relative position of the critical residues (red), the DXD motif (blue) and coordinated water molecule (black), and the proposed nucleophile (yellow). Figures prepared with Setor (50).

the pyrophosphate moiety of the UDP, but coordinates a water molecule in all structures except that of native GTB M2. The water molecules in these structures are shown to interact with both aspartic acid residues of the DXD motif; this includes a bidentate interaction with D213, as seen in the heavy-atom derivatives of wild-type GTB structures. Other structures, like those of Kre2p/Mnt1p, LgtC, and glycogenin have a catalytic loop histidine residue that interacts with the DXD-bound cation (596, 660, 665), but no such catalytic loop residue is found in the GTB M2 or GTB M3 structure. The structures of GTB M3, GTB M3 in complex with H-acceptor, and GTB M2 in complex with H-acceptor also reveal alternate conformations for several side chains. The slightly lower resolution for native GTB M2 did not allow observation of alternate side chain conformations. Overall, the structures of heavy-atom derivatives of wild-type GTB, GTB M2 and GTB M3 are quite similar, as seen from the rmsd between the different structures (Table 5.4).

*Acceptor Binding*

In the GTB M2 and GTB M3 structures in complex with H-acceptor, clear electron density is observed for the entire H-antigen (Figure 5.11A). A total of 544 $Å^2$ and 555 $Å^2$ is buried by the H-acceptor in the GTB M2 and GTB M3 structures, respectively. Although it is believed that donor binding must precede acceptor binding, we have previously shown that we are able to obtain structures of wild-type and mutant GTBs in complex with acceptor only (555, 651, 655).

As seen in the structure of heavy-atom derivative of wild-type GTB complexed with H-acceptor, the H-galactose 4-hydroxyl group makes hydrogen bonds to OD1 and OD2 of E303, while the H-galactose 6-hydroxyl group interacts with OG1 of T245 and NE1 of W300. The interaction of the H-galactose 4-hydroxyl group with NE2 of H233 is seen in

**Table 5.5 Molecular interactions observed between the H-acceptor and the mutant glycosyltransferases**

| | | | Distance (Å) | |
|---|---|---|---|---|
| | | | **GTB M2 + H** | **GTB M3 + H** |
| O4 Gal 452 | --- | NE2 His 233 | - | 2.87 |
| O4 Gal 452 | --- | OE1 Glu 303 | 3.20 | 3.22 |
| O4 Gal 452 | --- | OE2 Glu 303 | 2.67 | 2.75 |
| O6 Gal 452 | --- | OG1 Thr 245 | 2.83 | 2.82 |
| O6 Gal 452 | --- | NE1 Trp 300 | 3.28 | 3.32 |
| O4 Fuc 453 | --- | OD2 Asp 326 | 2.76 | 2.67 |

**A**

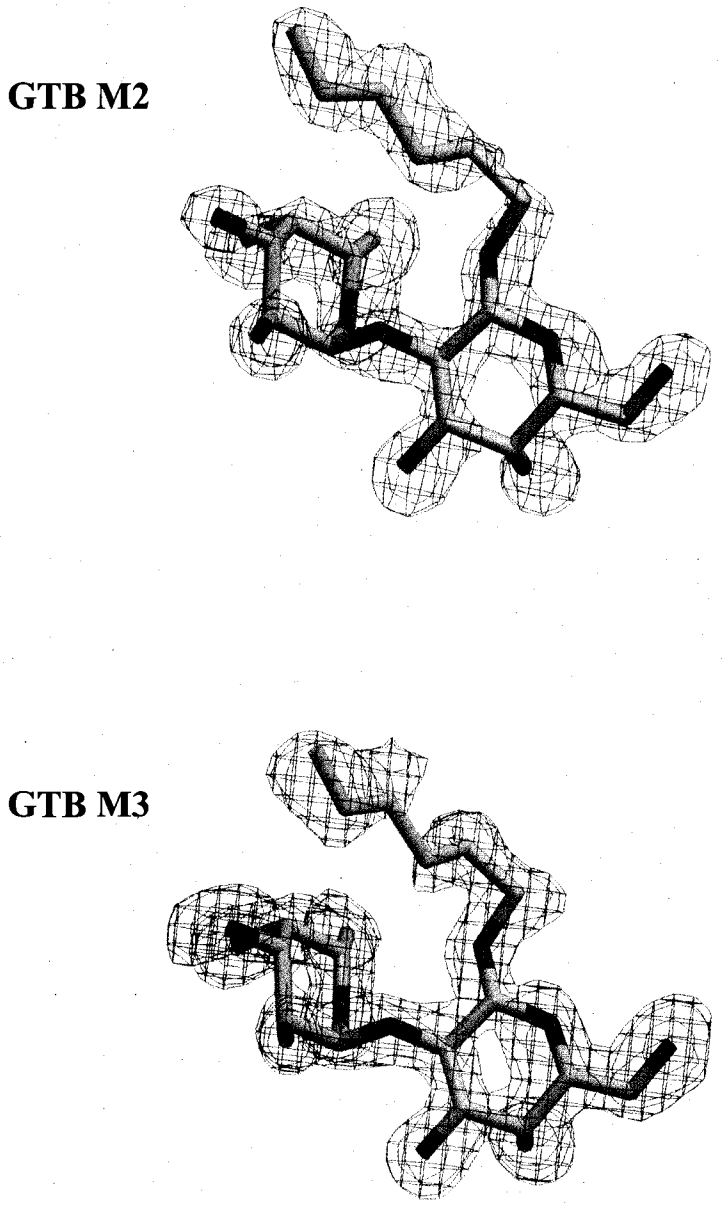


**Figure 5.11. H-antigen binding in GTB M2 and GTB M3. A.** Composite omit map electron density (blue) is contoured at 1.0 σ for the H antigen. (Continued on the next page.)

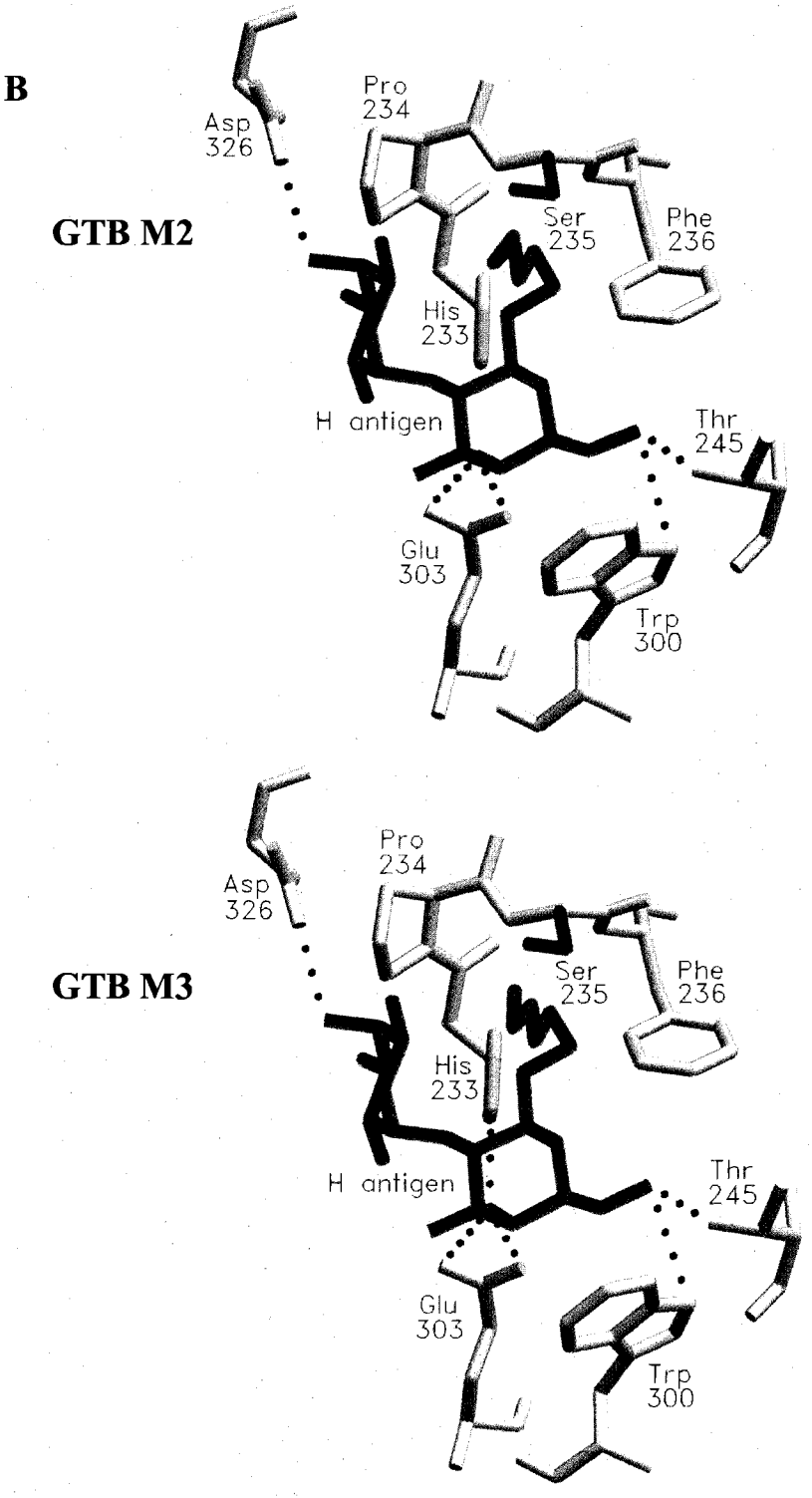


**Figure 5.11. H-antigen binding in GTB M2 and GTB M3 (continued). B.** Diagram showing the interactions of the H-antigen with residues of the C-terminal domain. Note that the interaction of H233 with the H antigen is only seen with the GTB M3 structures. (Continued on the next page.)

C

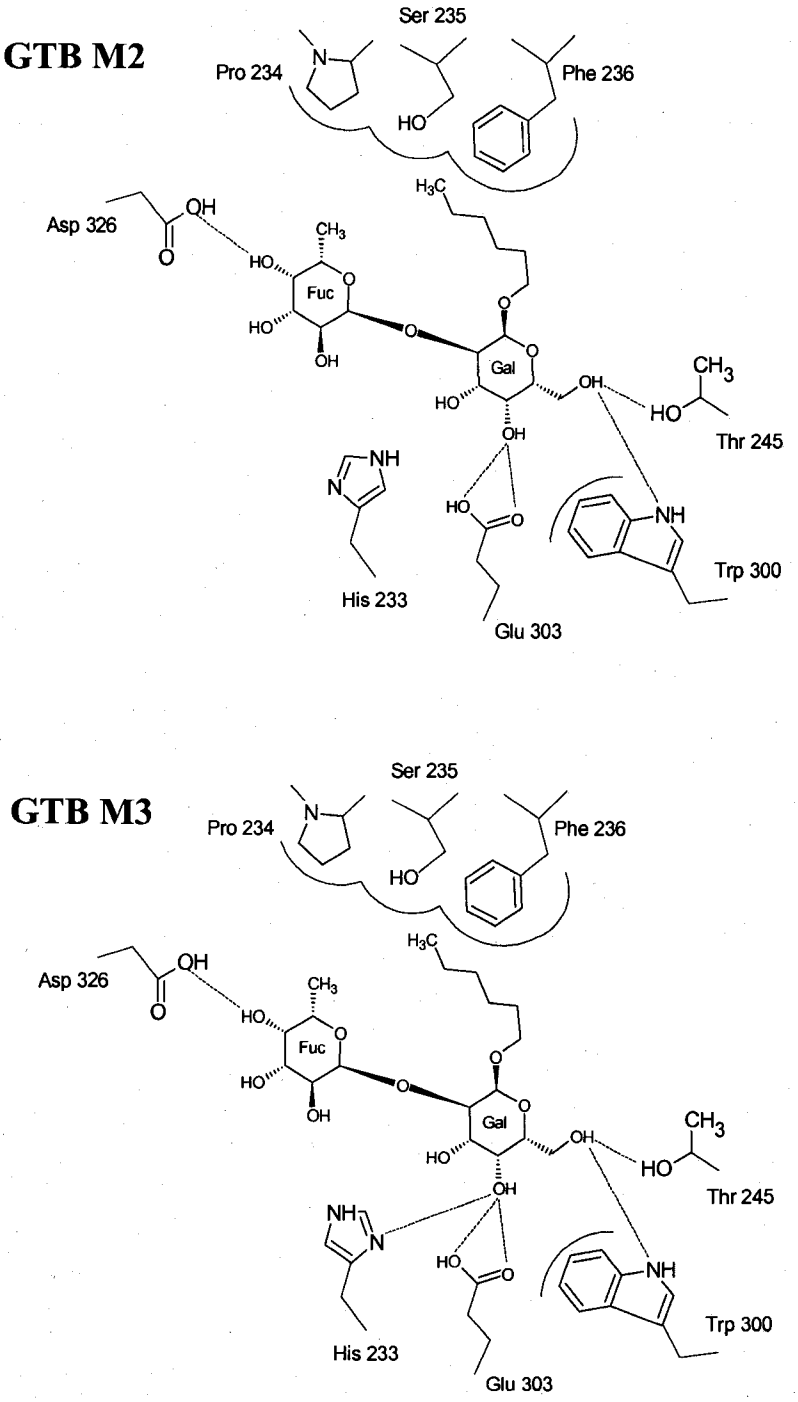


**Figure 5.11. H-antigen binding in GTB M2 and GTB M3 (continued). C.** Schematic diagram highlighting all interactions of the H-antigen with residues of the active-site cleft. Note that residue H233 is in a different conformation in the GTB M3 structures and can not interact with the H antigen. Figures A and B prepared with Setor (50).

the GTB M3 structures but not in the GTB M2 structures, as the histidine ring is found in different conformations in the two structures. The H-galactose also displays stacking interactions with the side chain of W300 and van der Waals contact with residues P234, F236 and critical residues S235 and M266. The H-fucose 4'-hydroxyl group makes a hydrogen bond to OD2 of D326. The interactions of the H-antigen with the protein are shown in Figure 5.11B, schematically depicted in Figure 5.11C and tabulated in Table 5.5.

*Cysteine-to-Serine Mutations*

The positions of the cysteine residues and cysteine-to-serine mutations in the GTB backbone are highlighted in Figure 5.12A. Wild-type residue C80 is located in the N-terminus of the catalytic domain. In the GTB M2 and GTB M3 structures, the hydroxyl group of residue S80 is oriented about 180° from the position of the sulfhydryl group of residue C80 in the wild-type GTB structure. This position is only adopted by C80 in the structure of the heavy-atom derivative of wild-type GTB in complex with UDP and H-acceptor. As seen in Figure 5.12B, there are no water molecules that bind to S80, nor are there any residues able to make hydrogen bonds with S80. Furthermore, it is seen that residues S80 from symmetry-related molecules are too far from each other to interact. Wild-type residue C196 is located in helix α5 (Figure 5.9A). Wild-type GTB could only be crystallized as the heavy-atom derivative and C196 binds a mercury atom, likely preventing packing and ordering of this helix segment. (Recent structures of wild-type GTB crystallized without mercury show the full helix α5 – Javier Alfaro, unpublished results). In GTB M2 and GTB M3, residue S196 makes hydrogen bonds to the backbone oxygen atoms of neighboring residues (Figure 5.12C). These interactions could help stabilize the secondary structure of α5. Wild-type residue C209 is located in strand β7, just before the

**Table 5.4 Residual mean square differences (Å) between all atoms and Cα of native GTB models and mutants GTB M2 and M3 models**
RMSD between Cα atoms are included in parentheses.

| | GTB M2 | GTB M2 + H | GTB M3 | GTB M3 + H |
|---|---|---|---|---|
| GTB | 1.10 (0.69) | 1.10 (0.71) | 1.80 (1.33) | 1.65 (1.23) |
| GTB + H | 1.25 (0.93) | 1.25 (0.94) | 1.59 (1.19) | 1.40 (1.00) |
| GTB M2 | | 0.33 (0.13) | 1.18 (0.64) | 1.07 (0.61) |
| GTB M2 + H | | | 1.15 (0.61) | 1.04 (0.58) |
| GTB M3 | | | | 0.49 (0.31) |
| GTB M3 + H | | | | |

**A**

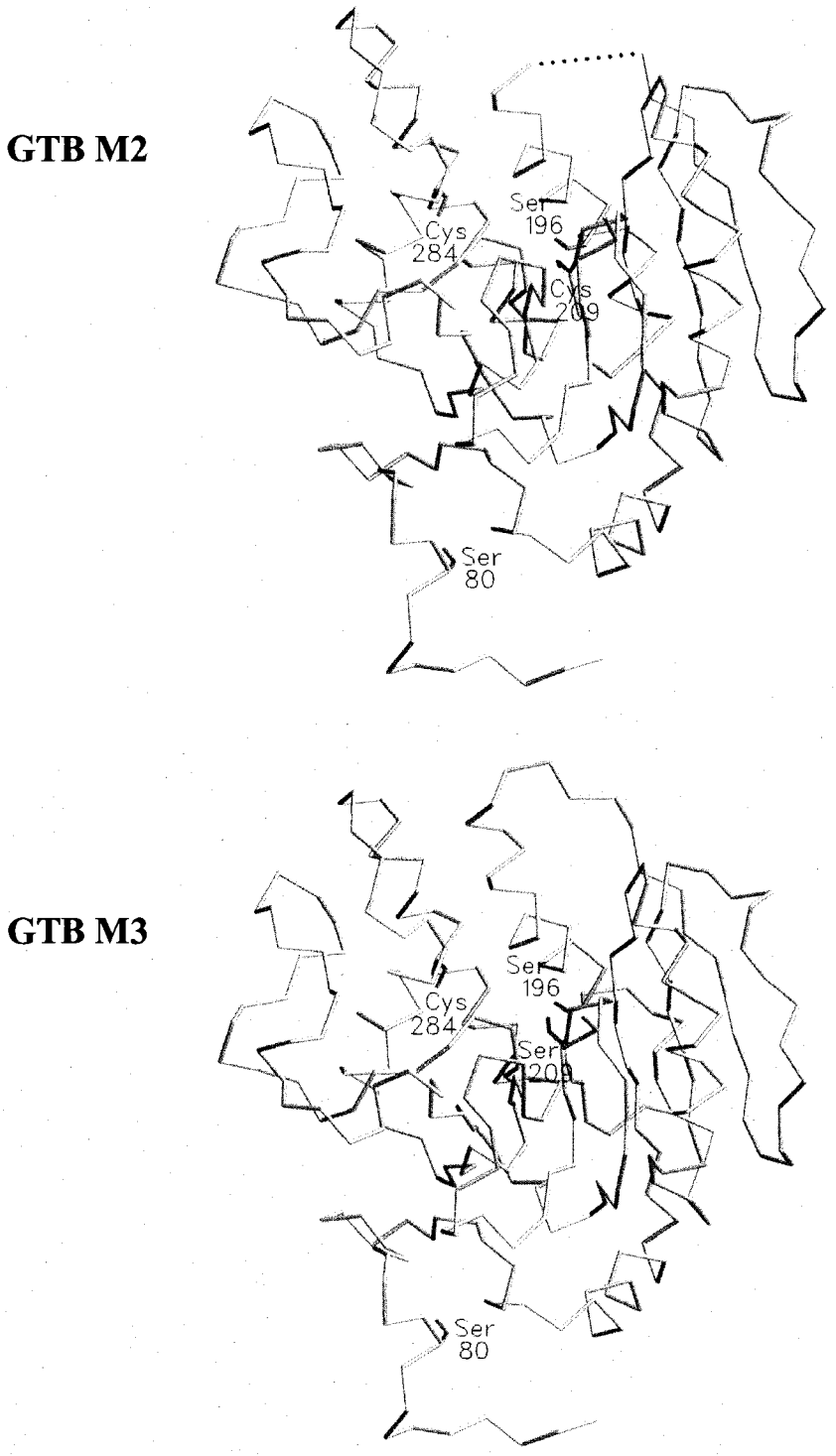


**Figure 5.12. Environment of the Cys-to-Ser mutations. A.** Backbone structure of GTB M2 and GTB M3 highlighting the position of the cysteines (orange) and the serine mutations (green). (Continued on the next page.)

**B**

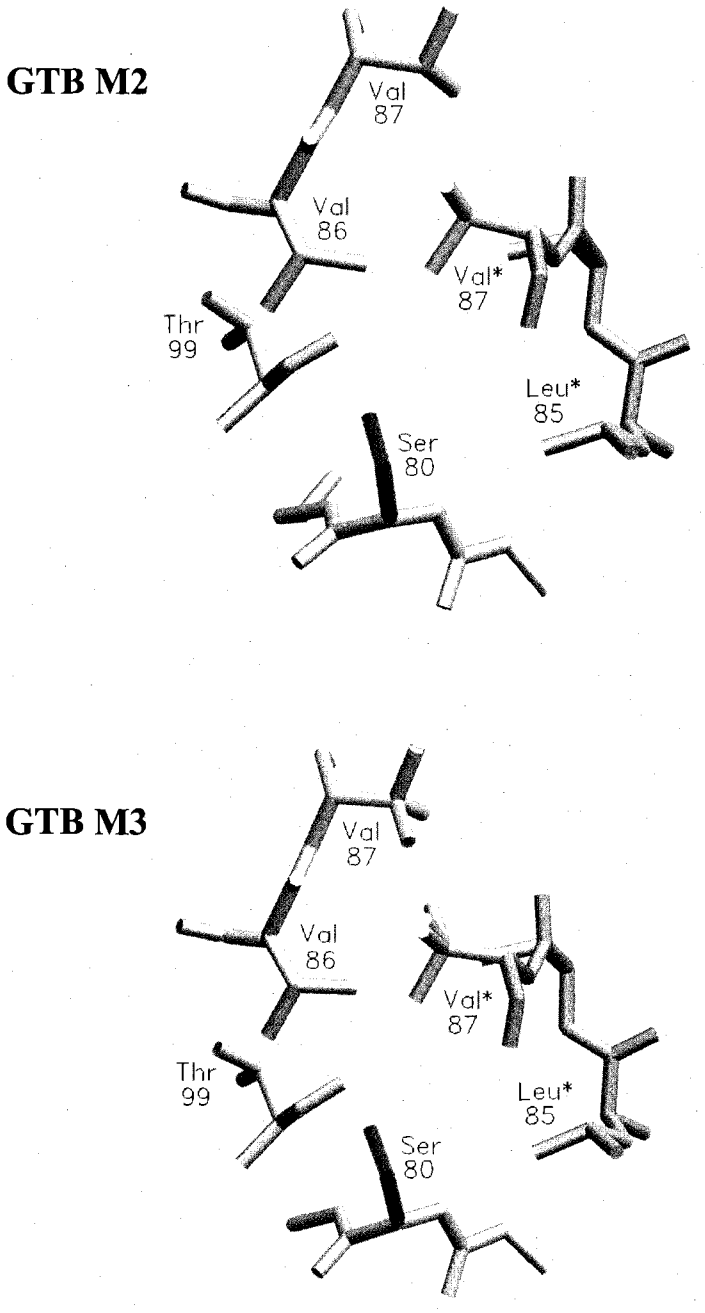


**Figure 5.12. Environment of the Cys-to-Ser mutations (continued). B.** Environment of mutation Ser 80. Neighboring residues contributed by a symmetry-related molecules are displayed on a yellow backbone and alternate conformations of Val 87 are seen in the GTB M3 structure. There are no hydrogen bonding partners for Ser 80 in neither of the structures. (Continued on the next page.)

C

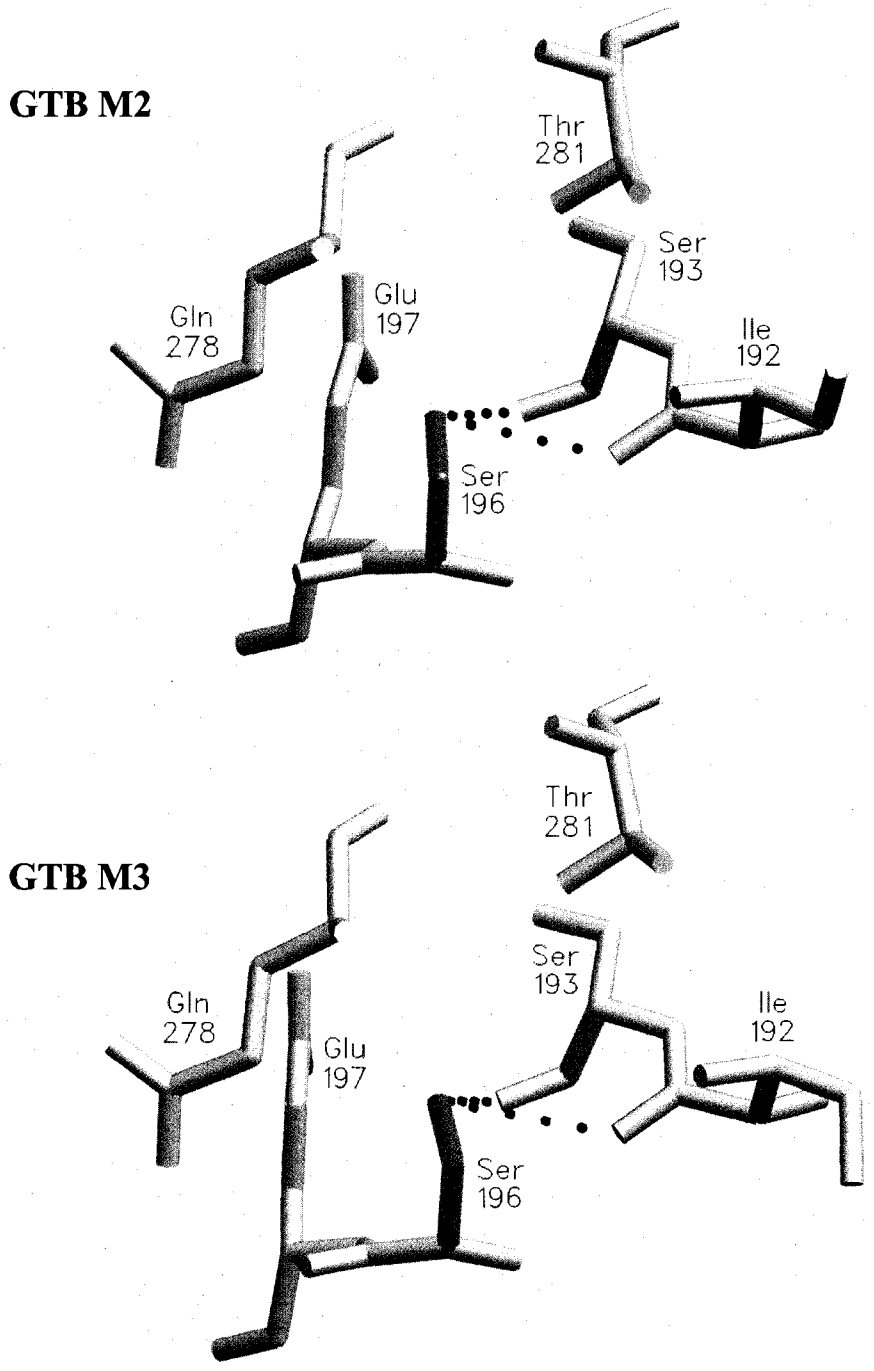


**Figure 5.12. Environment of the Cys-to-Ser mutations (continued). C.** Environment of mutation Ser 196. In both GTB M2 and GTB M3 structures, there are two hydrogen bonds provided by main chain carbonyl groups of Ile 192 and Ser 193. (Continued on the next page.)

**D**

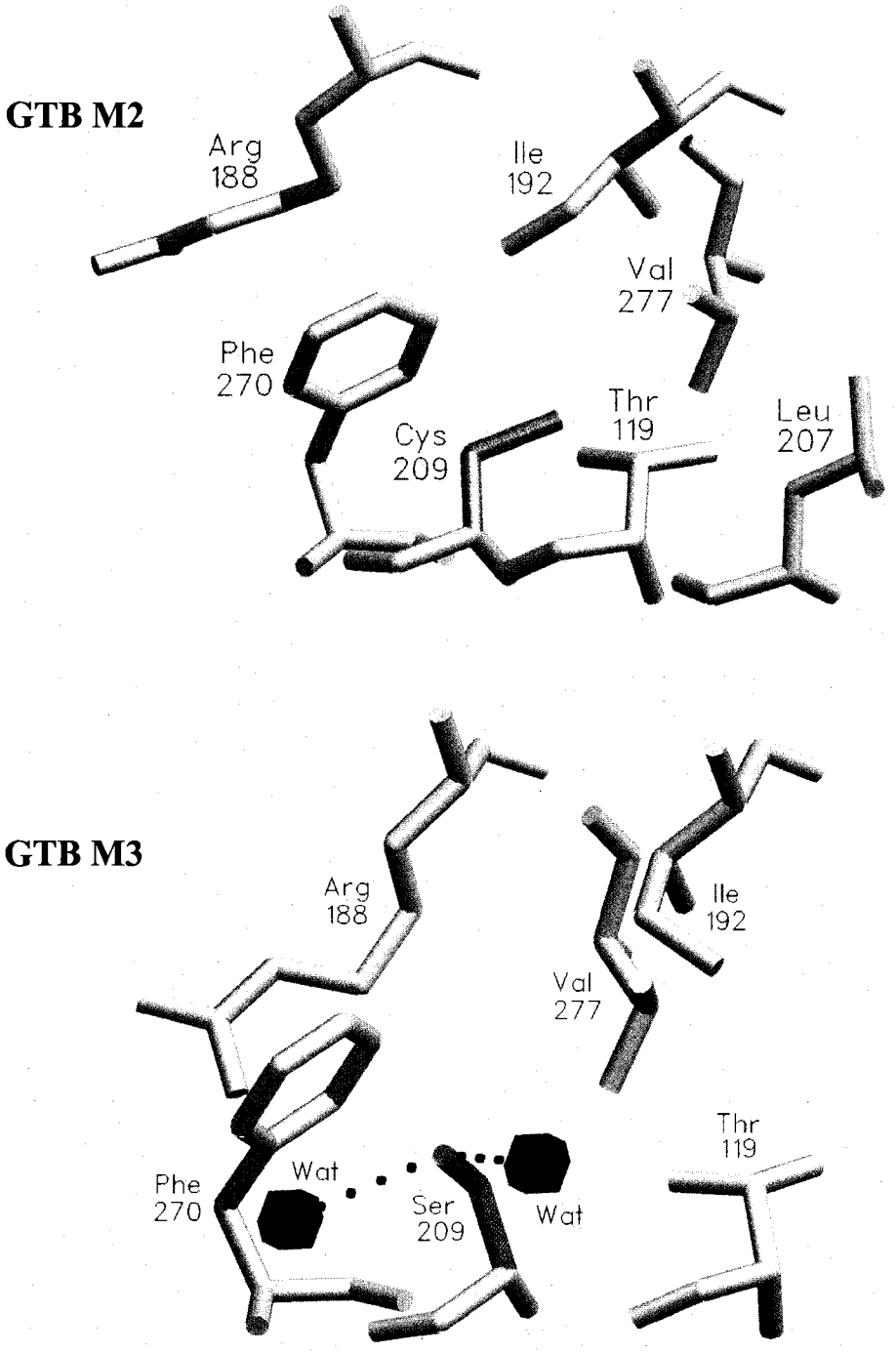


**Figure 5.12. Environment of the Cys-to-Ser mutations (continued). D.** Environment of native Cys 209 (GTB M2) and mutation Ser 209 (GTB M3). The native Cys residue is embedded in a hydrophobic pocket. The Ser mutation adopts a different conformation and is able to make hydrogen bonds to two neighboring water molecules. Figures prepared with Setor (50).

DXD motif. In GTB M2, C209 is tucked into a hydrophobic pocket lined by I192, L207, and V277 and may contribute to packing stability of the secondary structures and subdomain (Figure 5.12D). In GTB M3, residue 209 is mutated to serine. As a hydrophilic side chain, the serine is flipped out of the hydrophobic pocket and becomes part of the bottom of the active site. As a result of this change in conformation, there are now two water molecules that have moved into the active site and make hydrogen bonds to S209 (Figure 5.12D).

Concomitantly with the mutation of free cyteine residues to serines is the ordering of the catalytic loop. In GTB M2, mutations C80S and C196S result in ordering of residues 184 to 198 as compared with the heavy-atom derivative of wild-type GTB (Figure 5.13). These residues are part of helix α5 that follows the catalytic loop. The average B-factor for this region is around 28 $Å^2$ in the GTB M2 structures and 17 $Å^2$ in the GTB M3 structures. For GTB M3, the additional mutation of C209 to serine leads to the ordering of all residues of the catalytic loop. The average B-factor for residues 177 to 183, the tip of the catalytic loop, is around 32 $Å^2$ in the GTB M3 structures. Furthermore, in the GTB M3 structures, there is a change in the conformation of residues 198-205, although no clear structural reason for this change can be identified. Though the entire catalytic loop is ordered in GTB M3, the C-terminal residues 346-354 are not observed; this seems to differ from other structures, such as α1,3-GalT (666), β1,4-GalT (667, 668) and rabbit GnT1 (669), where ordering of the catalytic loop also leads to ordering of the C-terminus. Like GTB M3, other GT structures have been observed with a full catalytic loop in the absence of bound donor: Kre2p/Mnt1p, which is reported to have no flexible loop (665) and β1,4-GalT whose first structure was observed with full loop in the unliganded form (670).

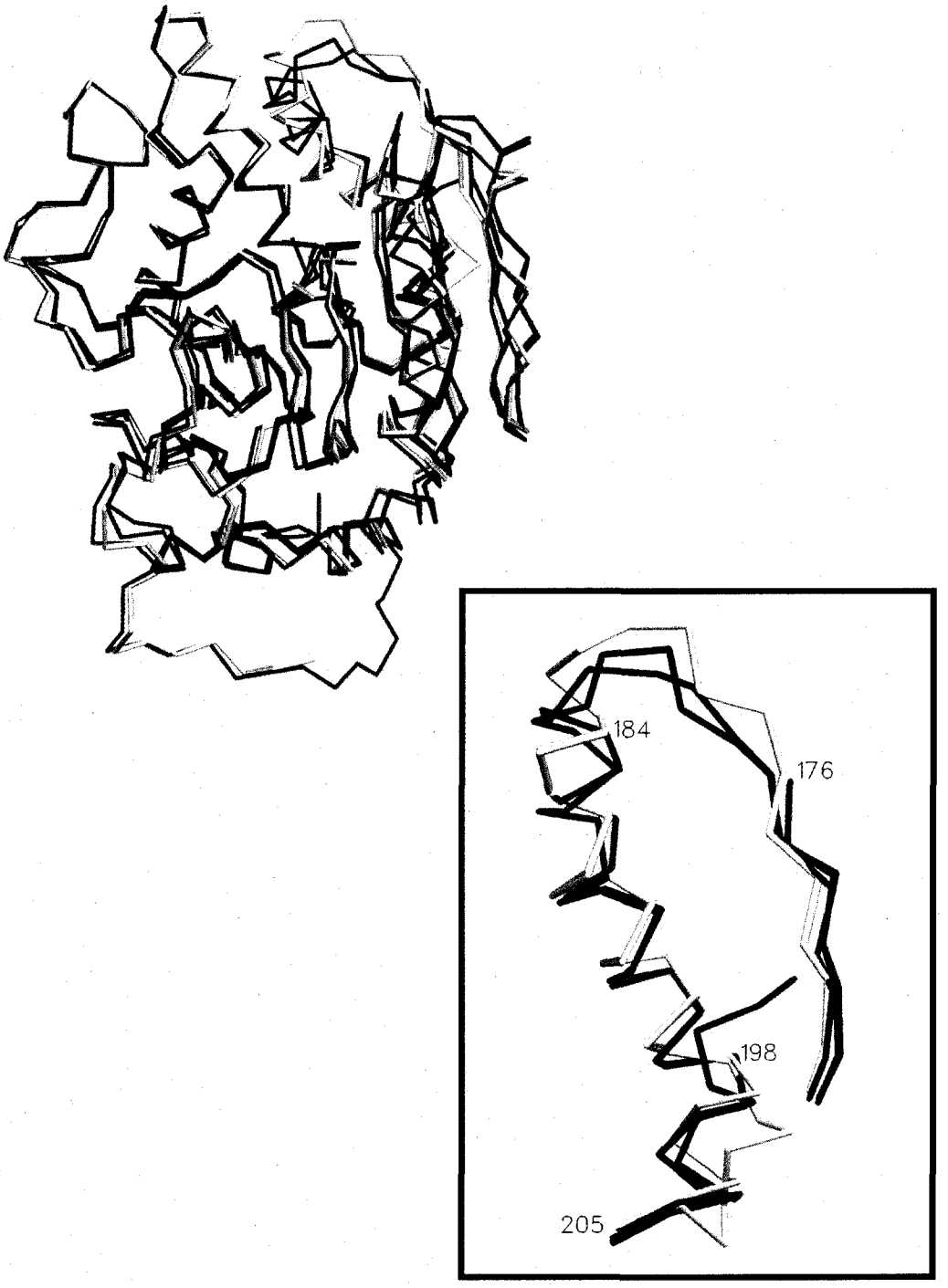


**Figure 5.13. Focus on the conformation of the catalytic loop.** Overlap of the backbone structures of native GTB (purple), GTB M2 (yellow), and GTB M3 (white) shows the conformation of the loop that is seen in part in GTB M2 and in full in GTB M3. Also overlapped are the backbone structures of bovine α1,3-GalT in its unliganded (green) and substrate-bound (dark gray) states to compare the overall conformation of the loops. Figures prepared with Setor (50).

Concomitantly to the ordering of the catalytic loop is the closing in of the active site cleft. When the C-terminal subdomain of GTB M3 is overlaped with the C-terminal subdomain of other GTs, it is seen that the N-terminal subdomain of GTB M3 is slightly rotated inwards compared with other N-terminal subdomains. With C-terminal subdomains overlapped, there is a maximal difference of about 1 Å between the N-terminal subdomain backbones of wild-type GTB and GTB M3. When GTB M3 is compared to other GT structures, it is also seen that the conformation of the catalytic loop in GTB M3 is not as closed-in over the binding site (Figure 5.13, comparison with bovine α1,3-GalT). This could be due to the absence of a nucleotide-donor, which would bind the top portion of the loop and anchor it down. Other GT structures in which the full catalytic loop is observed in the presence of bound donor reveal several interactions between residues of the catalytic loop and the UDP portion of the donor.

*Focus on the GTB M3 Structure*

GTB M2 and GTB M3 both possess the C80S and C196S mutations. It is seen that in both these structures, the helix α5 is ordered compared with the structures of heavy-atom derivatives of wild-type GTB. In heavy-atom derivatives of wild-type GTB structures, a mercury atom is seen interacting with C196 and most probably hinders packing of the helix. The structure of wild-type GTB in the absence of heavy atoms (Javier Alfaro, unpublished results) also shows the helix to be ordered. In GTB M3, the additional mutation of C209S occurs along with ordering of the full catalytic loop. The full loop is not observed in any of the other GTB structures including that of wild-type GTB. A comparison of the overall structure of GTB M2, GTB M3, and wild-type GTB reveals another difference: residues 198-205, which take part in a turn that follows the catalytic loop and helix α5, are found to

be in different conformations. The heavy-atom derivatives of wild-type GTB structures and the structures of GTB M2 show those residues to be in the same conformation, whereas they are different in the structure of wild-type GTB, and different still in the structure of GTB M3. The significance of these different conformations in this stretch of residues is not clear.

All of the differences in overall structure coincide with the mutation of a single residue: C209. It is seen that C209S in GTB M3 is placed to face the active site cleft. This side chain conformation of S209 allows for two water molecules to position themselves in the bottom of the active site cleft. One of these water molecules makes hydrogen bonds to both S209 and R188, a residue important in donor-sugar binding, seemingly locking R188 in one position.

In the GTB M2 structure, where residue 209 is a cysteine and there is no water molecule at the bottom of the pocket, R188 is found in a conformation that either makes a hydrogen bond to D211 of the DXD motif when GTB M2 is unliganded, or to D302, a proposed nucleophile for the GT retaining reaction mechanism, when GTB M2 is in complex with H-acceptor (Figure 5.14A). In heavy-atom derivatives of wild-type GTB structures, R188 is disordered and we see that residue D302 adopts different conformations (Figure 5.14B). In GTB M3, the side chain of R188 is found to make hydrogen bonds to D211 and D302 simultaneously, regardless of the bound state of the mutant (Figure 5.14C). The change observed in the conformation of the R188 side chain is the only obvious structural change that occurs in the GTB M3 structure when compared to GTB M2 and wild-type GTB structures.

In all GT structures solved to date, residues equivalent to D211-R188-D302 lie at the bottom of active site clefts and are found to interact with donor sugars. In EXTL2, these

A

GTB M2

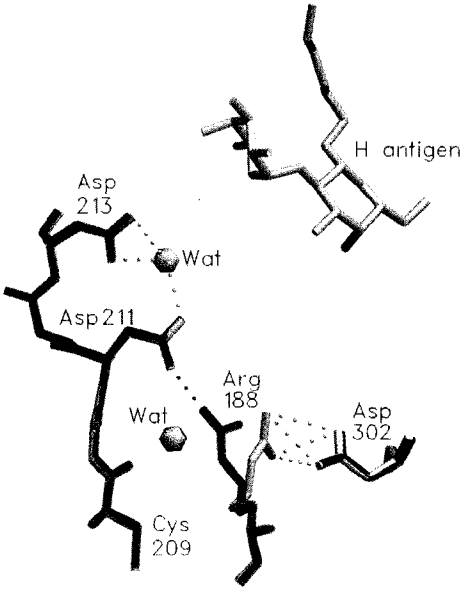


B

GTB

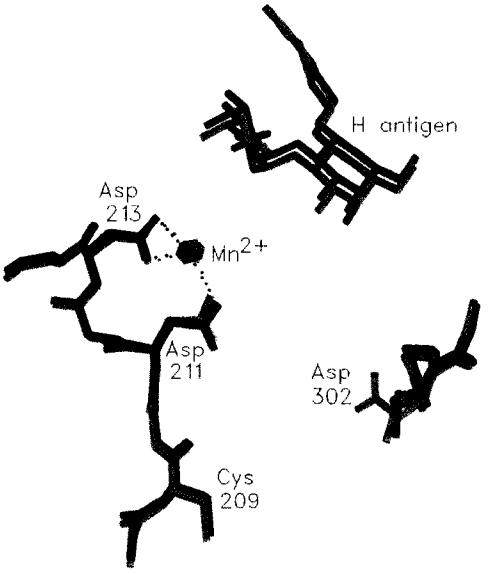


**Figure 5.14. Presence of triad.** **A.** Overlap of GTB M2 (green) and GTB M2 + H antigen (yellow) highlighting the DXD motif, and the residues involved in the triad: Asp 211, Arg 188, Asp 302. As seen, Arg 188 only interacts with Asp 211 of the DXD motif in the native structure and only interacts with the potential Asp 302 nucleophile in the acceptor-bound state. **B.** Overlap of GTB (dark blue), GTB + H antigen (purple), and GTB + H antigen + UDP (light blue) highlighting the DXD motif and the potential Asp 302 nucleophile. Residue Arg 188 is not observed in the structures of heavy-atom derivatives of wild-type GTB. (Continued on the next page.)

C

GTB M3

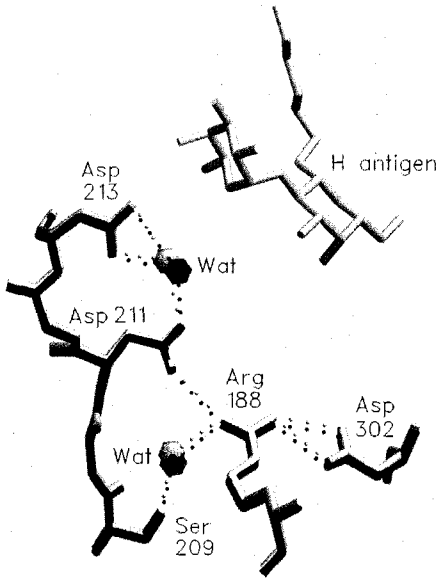


**Figure 5.14. Presence of triad (continued). C.** Overlap of GTB M3 (red) and GTB M3 + H antigen (white) highlighting the DXD motif, and the residues involved in the triad: Asp 211, Arg 188, Asp 302. As seen, Arg 188 interacts with both Asp 211 of the DXD motif and the potential Asp 302 nucleophile regardless of the state of the enzyme. This is due to the presence of a water molecule that is bound by Ser 209, the extra mutation of GTB M3, and Arg 188. Figures prepared with Setor (50).

residues have been postulated to serve to place the C1 carbon of the donor sugar in proper position for catalysis. In many GTs, mutation of one of these residues has yielded inactive enzyme (671, 672), pointing to a critical role in donor binding and possibly catalysis. In GTB, the mutation of the basic residue R188 to a serine generates an enzyme with extremely low kcat (Palcic, unpublished observation). The formation of a triad of D211-R188-D302 in GTB M3 occurs concomitantly with ordering of the full catalytic loop. Unfortunately, the connectivity between the formation of the D211-R188-D302 triad and ordering of the full catalytic loop is not clear and it is difficult to determine the significance of the observation. Additional structures, including that of wild-type GTB in complex with full donor displaying a fully ordered catalytic loop should shed light on the significance of the D211-R188-D302 triad.

## CONCLUSION

In this study, the structures of two mutants of the human ABO(H) blood group GTB were solved by x-ray crystallography: GTB M2 C80S, C196S and GTB M3 C80S, C196S, C209S. The results reveal that mutation of the first two free cysteine residues in GTB leads to ordering of helix α5, a helix that is disordered in crystals of heavy-metal derivatives of wild-type GTB. The third mutation of C209S, only present in GTB M3, leads to ordering of the full catalytic loop. Concomitantly with mutation C209S is the positioning of two water molecules in the active site cleft. One of these water molecules bridges S209 and R188, locking R188 in a conformation that allows simultaneous interaction with D211 of the DXD motif and potential nucleophile D302. The formation of this D211-R188-D302 triad is not

observed in other GTB structures with disordered catalytic loop, but the connectivity and significance of this observation remains to be elucidated.

# GENERAL CONCLUSION

The objective of this research was to use x-ray crystallography to resolve the structures of clinically relevant antibodies MR1 and BEC2 as well as that of mutants of the human blood GTB. These structural studies were geared towards obtaining protein complexes to gain insight into recognition mechanisms and ultimately achieve a greater understanding of the function of these proteins.

The structure of MR1 in complex with a peptide epitope of EGFRvIII brought to light the recognition mechanism of MR1 for the mutant receptor. MR1 can discriminate between the native EGFR and the mutant EGFRvIII by recognizing a strand-turn conformation present only in the mutant receptor. This conformation is allowed by the novel fusion junction glycine that appears at the N-terminus of the mutant receptor. The J-shaped groove on MR1 binds alternate residues of the peptide strand, confirming epitope-mapping results, and tightly hugs the peptide turn without interacting specifically with the fusion junction glycine. These findings reveal that peptides can be used as conformational epitopes to raise conformation-specific antibodies. The knowledge gained in this study will benefit the design of MR1-based therapeutics with greater affinity and specificity for use in the treatment of cancer. Further work should look at resolving the structure of MR1-1 to understand how mutations in the binding site of MR1 can affect both the affinity and specificity of the antibody for the mutant receptor and how this can translate into a better agent for cancer immunotherapy.

The structures of BEC2 in complex with both R24 and novel anti-$GD_3$ antibodies could not be obtained. Efforts to isolate an R24-like antibody by isolating antibodies from patients immunized with BEC2 as well as by biopanning of a llama naïve phage display library against both BEC2 and $GD_3$, were unsuccessful. Furthermore, despite all attempts,

BEC2 Fab could not be purified from the BEC2 digest. Lastly, efforts at producing antibody fragments of both R24 and BEC2 in bacterial and yeast expression systems for use in crystallization trials did not yield any soluble protein. Future work should center on the use of fresh BEC2 samples, should optimize expression of the antibody fragments and investigate new methods of isolating R24-like antibodies.

The structures of the GTB M2 and M3 mutants reveal the conformation of residues previously not modeled in the structures of both heavy-atom derivatives of wild-type and mutants human blood group ABO(H) GTs. In GTB M2, helix α5 is observed in the electron density, while GTB M3 shows both the helix and the full catalytic loop to be ordered. Concomitantly with ordering of the catalytic loop in GTB M3 is the formation of a triad of residues D211-R188-D302. This triad occurs through the bridging of R188 and S209 by a water molecule. Although the formation of the triad and the ordering of the catalytic loop occur simultaneously, it is difficult to assess the importance of this observation. Future work should focus on solving structures of human ABO(H) blood group GTs in complex with full donor to isolate structures with full catalytic loop, and relate the ordering of the loop to the conformation of residues D211, R188, and D302.

# REFERENCES


1. Blundell, T.L., and L.N. Johnson. 1976. Protein crystallography. Academic Press, New York. 565 pp.

2. Glusker, J.P., and K.N. Trueblood. 1985. Crystal structure analysis: a primer. Oxford University Press, Oxford.

3. McRee, D.E. 1993. Practical protein crystallography. Academic Press, San Diego.

4. Rhodes, G. 1993. Cystallography made crystal clear: a guide for users of macromolecular models. Academic Press, San Diego.

5. Sands, D. 1969. Introduction to crystallography. Dover Publications, Inc., New York. 165 pp.

6. Stout, G.H., and L.H. Jensen. 1989. X-ray structure determination: a practical guide. Wiley, New York. 453 pp.

7. 2001. International Tables for Crystallography. Kluwer Academic Publishers, London. 807 pp.

8. McPherson, A. 1999. Crystallization of biological macromolecules. Cold Spring Harbor Laboratory Press, Cold Spring Harbor, NY. 586 pp.

9. Bragg, W.L. 1913. The diffraction of short electromagnetic waves by a crystal. *Proc. Camb. Phil. Soc.* 17:43-57.

10. Janeway, C. 2001. Immunobiology: the immune system in health and disease. Garland, New York.

11. Hozumi, N., and S. Tonegawa. 1976. Evidence for somatic rearrangement of immunoglobulin genes coding for variable and constant regions. *Proc Natl Acad Sci U S A* 73:3628-3632.

12. Tonegawa, S., C. Brack, N. Hozumi, and V. Pirrotta. 1978. Organization of immunoglobulin genes. *Cold Spring Harb Symp Quant Biol* 42 Pt 2:921-931.

13. Weigert, M., L. Gatmaitan, E. Loh, J. Schilling, and L. Hood. 1978. Rearrangement of genetic information may produce immunoglobulin diversity. *Nature* 276:785-790.

14. Nemazee, D., D. Russell, B. Arnold, G. Haemmerling, J. Allison, J.F. Miller, G. Morahan, and K. Buerki. 1991. Clonal deletion of autospecific B lymphocytes. *Immunol Rev* 122:117-132.

15. Lanzavecchia, A. 1993. Identifying strategies for immune intervention. *Science* 260:937-944.

16. Behring, E., and S. Kitasato. 1890. *Deutsch. med. Wochenschr.* 16:1113-1114.

17. Neuberger, M.S., M.R. Ehrenstein, N. Klix, C.J. Jolly, J. Yelamos, C. Rada, and C. Milstein. 1998. Monitoring and interpreting the intrinsic features of somatic hypermutation. *Immunol Rev* 162:107-116.

18. Berek, C., and C. Milstein. 1987. Mutation drift and repertoire shift in the maturation of the immune response. *Immunol Rev* 96:23-41.

19. Janeway, C., F.S. Rosen, E. Merler, and C.A. Alper. 1967. The Gamma Globulins. Little Brown and Co., Boston.

20. Capra, J.D., and J.M. Kehoe. 1974. Structure of antibodies with shared idiotypy: the complete sequence of the heavy chain variable regions of two immunoglobulin M anti-gamma globulins. *Proc Natl Acad Sci U S A* 71:4032-4036.

21. Greenspan, N.S., and C.A. Bona. 1993. Idiotypes: structure and immunogenicity. *Faseb J* 7:437-444.

22. Jerne, N.K. 1974. Towards a network theory of the immune system. *Ann Immunol (Paris)* 125C:373-389.

23. Edelman, G.M. 1991. Antibody structure and molecular immunology. *Scand J Immunol* 34:1-22.

24. Davies, D.R., and H. Metzger. 1983. Structural basis of antibody function. *Annu Rev Immunol* 1:87-117.

25. Chothia, C., and A.M. Lesk. 1987. The evolution of protein structures. *Cold Spring Harb Symp Quant Biol* 52:399-405.

26. Kabat, E.A. 1968. Unique features of the variable regions of Bence Jones proteins and their possible relation to antibody complementarity. *Proc Natl Acad Sci U S A* 59:613-619.

27. Kabat, E.A., and T.T. Wu. 1971. Attempts to locate complementarity-determining residues in the variable positions of light and heavy chains. *Ann N Y Acad Sci* 190:382-393.

28. Wu, T.T., and E.A. Kabat. 1970. An analysis of the sequences of the variable regions of Bence Jones proteins and myeloma light chains and their implications for antibody complementarity. *J Exp Med* 132:211-250.

29. Chothia, C., and A.M. Lesk. 1987. Canonical structures for the hypervariable regions of immunoglobulins. *J Mol Biol* 196:901-917.

30. Chothia, C., A.M. Lesk, A. Tramontano, M. Levitt, S.J. Smith-Gill, G. Air, S. Sheriff, E.A. Padlan, D. Davies, W.R. Tulip, and et al. 1989. Conformations of immunoglobulin hypervariable regions. *Nature* 342:877-883.

31. Chothia, C., A.M. Lesk, E. Gherardi, I.M. Tomlinson, G. Walter, J.D. Marks, M.B. Llewelyn, and G. Winter. 1992. Structural repertoire of the human VH segments. *J Mol Biol* 227:799-817.

32. Shirai, H., A. Kidera, and H. Nakamura. 1996. Structural classification of CDR-H3 in antibodies. *FEBS Lett* 399:1-8.

33. Morea, V., A. Tramontano, M. Rustici, C. Chothia, and A.M. Lesk. 1998. Conformations of the third hypervariable region in the VH domain of immunoglobulins. *J Mol Biol* 275:269-294.

34. Oliva, B., P.A. Bates, E. Querol, F.X. Aviles, and M.J. Sternberg. 1998. Automated classification of antibody complementarity determining region 3 of the heavy chain (H3) loops into canonical forms and its application to protein structure prediction. *J Mol Biol* 279:1193-1210.

35. Foote, J., and G. Winter. 1992. Antibody framework residues affecting the conformation of the hypervariable loops. *J Mol Biol* 224:487-499.

36. Hamers-Casterman, C., T. Atarhouch, S. Muyldermans, G. Robinson, C. Hamers, E.B. Songa, N. Bendahman, and R. Hamers. 1993. Naturally occurring antibodies devoid of light chains. *Nature* 363:446-448.

37. Greenberg, A.S., D. Avila, M. Hughes, A. Hughes, E.C. McKinney, and M.F. Flajnik. 1995. A new antigen receptor gene family that undergoes rearrangement and extensive somatic diversification in sharks. *Nature* 374:168-173.

38. Nguyen, V.K., S. Muyldermans, and R. Hamers. 1998. The specific variable domain of camel heavy-chain antibodies is encoded in the germline. *J Mol Biol* 275:413-418.

39. Nguyen, V.K., R. Hamers, L. Wyns, and S. Muyldermans. 2000. Camel heavy-chain antibodies: diverse germline V(H)H and specific mechanisms enlarge the antigen-binding repertoire. *Embo J* 19:921-930.

40. Nguyen, V.K., C. Su, S. Muyldermans, and W. van der Loo. 2002. Heavy-chain antibodies in Camelidae; a case of evolutionary innovation. *Immunogenetics* 54:39-47.

41. Nguyen, V.K., R. Hamers, L. Wyns, and S. Muyldermans. 1999. Loss of splice consensus signal is responsible for the removal of the entire C(H)1 domain of the functional camel IGG2A heavy-chain antibodies. *Mol Immunol* 36:515-524.

42. Woolven, B.P., L.G. Frenken, P. van der Logt, and P.J. Nicholls. 1999. The structure of the llama heavy chain constant genes reveals a mechanism for heavy-chain antibody formation. *Immunogenetics* 50:98-101.

43. Muyldermans, S. 2001. Single domain camel antibodies: current status. *J Biotechnol* 74:277-302.

44. Muyldermans, S., T. Atarhouch, J. Saldanha, J.A. Barbosa, and R. Hamers. 1994. Sequence and structure of VH domain from naturally occurring camel heavy chain immunoglobulins lacking light chains. *Protein Eng* 7:1129-1135.

45. Desmyter, A., T.R. Transue, M.A. Ghahroudi, M.H. Thi, F. Poortmans, R. Hamers, S. Muyldermans, and L. Wyns. 1996. Crystal structure of a camel single-domain VH antibody fragment in complex with lysozyme. *Nat Struct Biol* 3:803-811.

46. Arbabi Ghahroudi, M., A. Desmyter, L. Wyns, R. Hamers, and S. Muyldermans. 1997. Selection and identification of single domain antibody fragments from camel heavy-chain antibodies. *FEBS Lett* 414:521-526.

47. Lauwereys, M., M. Arbabi Ghahroudi, A. Desmyter, J. Kinne, W. Holzer, E. De Genst, L. Wyns, and S. Muyldermans. 1998. Potent enzyme inhibitors derived from dromedary heavy-chain antibodies. *Embo J* 17:3512-3520.

48. Transue, T.R., E. De Genst, M.A. Ghahroudi, L. Wyns, and S. Muyldermans. 1998. Camel single-domain antibody inhibits enzyme by mimicking carbohydrate substrate. *Proteins* 32:515-522.

49. Conrath, K.E., M. Lauwereys, M. Galleni, A. Matagne, J.M. Frere, J. Kinne, L. Wyns, and S. Muyldermans. 2001. Beta-lactamase inhibitors derived from single-domain antibody fragments elicited in the camelidae. *Antimicrob Agents Chemother* 45:2807-2812.

50. Evans, S.V. 1993. SETOR: hardware-lighted three-dimensional solid model representations of macromolecules. *J Mol Graph* 11:134-138, 127-138.

51. Kohler, G., and C. Milstein. 1975. Continuous cultures of fused cells secreting antibody of predefined specificity. *Nature* 256:495-497.

52. Compton, B.J., M.A. Lewis, F. Whigham, J.S. Gerald, and G.E. Countryman. 1989. Analytical potential of protein A for affinity chromatography of polyclonal and monoclonal antibodies. *Anal Chem* 61:1314-1317.

53. Schuler, G., and M. Reinacher. 1991. Development and optimization of a single-step procedure using protein A affinity chromatography to isolate murine IgG1 monoclonal antibodies from hybridoma supernatants. *J Chromatogr* 587:61-70.

54. Pilcher, J.B., V.C. Tsang, W. Zhou, C.M. Black, and C. Sidman. 1991. Optimization of binding capacity and specificity of protein G on various solid matrices for immunoglobulins. *J Immunol Methods* 136:279-286.

55. Aybay, C., and T. Imir. 2000. Development of a rapid, single-step procedure using protein G affinity chromatography to deplete fetal calf serum of its IgG and to isolate murine IgG1 monoclonal antibodies from supernatants of hybridoma cells. *J Immunol Methods* 233:77-81.

56. Bjorck, L., and G. Kronvall. 1984. Purification and some properties of streptococcal protein G, a novel IgG-binding reagent. *J Immunol* 133:969-974.

57. Wikstrom, M., U. Sjobring, T. Drakenberg, S. Forsen, and L. Bjorck. 1995. Mapping of the immunoglobulin light chain-binding site of protein L. *J Mol Biol* 250:128-133.

58. Beckingham, J.A., S.P. Bottomley, R. Hinton, B.J. Sutton, and M.G. Gore. 1999. Interactions between a single immunoglobulin-binding domain of protein L from Peptostreptococcus magnus and a human kappa light chain. *Biochem J* 340 ( Pt 1):193-199.

59. Graille, M., E.A. Stura, N.G. Housden, J.A. Beckingham, S.P. Bottomley, D. Beale, M.J. Taussig, B.J. Sutton, M.G. Gore, and J.B. Charbonnier. 2001. Complex between Peptostreptococcus magnus protein L and a human antibody reveals structural convergence in the interaction modes of Fab binding proteins. *Structure* 9:679-687.

60. Porter, R.R. 1991. Lecture for the Nobel Prize for physiology or medicine 1972: Structural studies of immunoglobulins. 1972. *Scand J Immunol* 34:381-389.

61. Huse, W.D., L. Sastry, S.A. Iverson, A.S. Kang, M. Alting-Mees, D.R. Burton, S.J. Benkovic, and R.A. Lerner. 1989. Generation of a large combinatorial library of the immunoglobulin repertoire in phage lambda. *Science* 246:1275-1281.

62. Pluckthun, A. 1991. Antibody engineering: advances from the use of Escherichia coli expression systems. *Biotechnology (N Y)* 9:545-551.

63. Verma, R., E. Boleti, and A.J. George. 1998. Antibody engineering: comparison of bacterial, yeast, insect and mammalian expression systems. *J Immunol Methods* 216:165-181.

64. Maynard, J., and G. Georgiou. 2000. Antibody engineering. *Annu Rev Biomed Eng* 2:339-376.

65. Bird, R.E., K.D. Hardman, J.W. Jacobson, S. Johnson, B.M. Kaufman, S.-M. Lee, T. Lee, H.S. Pope, G.S. Riordan, and M. Whitlow. 1988. Single-chain antigen-binding proteins. *Science* 242:1038.

66. Holliger, P., T. Prospero, and G. Winter. 1993. "Diabodies": small bivalent and bispecific antibody fragments. *Proc Natl Acad Sci U S A* 90:6444-6448.

67. Essig, N.Z., J.F. Wood, A.J. Howard, R. Raag, and M. Whitlow. 1993. Crystallization of single-chain Fv proteins. *J Mol Biol* 234:897-901.

68. Whitlow, M., D. Filpula, M.L. Rollence, S.L. Feng, and J.F. Wood. 1994. Multivalent Fvs: characterization of single-chain Fv oligomers and preparation of a bispecific Fv. *Protein Eng* 7:1017-1026.

69. Desplancq, D., D.J. King, A.D. Lawson, and A. Mountain. 1994. Multimerization behaviour of single chain Fv variants for the tumour-binding antibody B72.3. *Protein Eng* 7:1027-1033.

70. Knappik, A., C. Krebber, and A. Pluckthun. 1993. The effect of folding catalysts on the in vivo folding process of different antibody fragments expressed in Escherichia coli. *Biotechnology (N Y)* 11:77-83.

71. Stanfield, R.L., M. Takimoto-Kamimura, J.M. Rini, A.T. Profy, and I.A. Wilson. 1993. Major antigen-induced domain rearrangements in an antibody. *Structure* 1:83-93.

72. Huston, J.S., D. Levinson, M. Mudgett-Hunter, M.S. Tai, J. Novotny, M.N. Margolies, R.J. Ridge, R.E. Bruccoleri, E. Haber, R. Crea, and et al. 1988. Protein engineering of antibody binding sites: recovery of specific activity in an anti-digoxin single-chain Fv analogue produced in Escherichia coli. *Proc Natl Acad Sci U S A* 85:5879-5883.

73. Raag, R., and M. Whitlow. 1995. Single-chain Fvs. *Faseb J* 9:73-80.

74. Alfthan, K., K. Takkinen, D. Sizmann, H. Soderlund, and T.T. Teeri. 1995. Properties of a single-chain antibody containing different linker peptides. *Protein Eng* 8:725-731.

75. Robinson, C.R., and R.T. Sauer. 1998. Optimizing the stability of single-chain proteins by linker length and composition mutagenesis. *Proc Natl Acad Sci U S A* 95:5929-5934.

76. Buchner, J., I. Pastan, and U. Brinkmann. 1992. A method for increasing the yield of properly folded recombinant fusion proteins: single-chain immunotoxins from renaturation of bacterial inclusion bodies. *Anal Biochem* 205:263-270.

77. Whitlow, M., and D. Filpula. 1993. Single-chain Fvs. In Tumour immunobiology - A practical approach. I. Press, editor Oxford. 279-291.

78. Griffiths, A.D., M. Malmqvist, J.D. Marks, J.M. Bye, M.J. Embleton, J. McCafferty, M. Baier, K.P. Holliger, B.D. Gorick, N.C. Hughes-Jones, and et al. 1993. Human anti-self antibodies with high specificity from phage display libraries. *Embo J* 12:725-734.

79. Kortt, A.A., R.L. Malby, J.B. Caldwell, L.C. Gruen, N. Ivancic, M.C. Lawrence, G.J. Howlett, R.G. Webster, P.J. Hudson, and P.M. Colman. 1994. Recombinant anti-sialidase single-chain variable fragment antibody. Characterization, formation of dimer and higher-molecular-mass multimers and the solution of the crystal structure of the single-chain variable fragment/sialidase complex. *Eur J Biochem* 221:151-157.

80. Nieba, L., A. Honegger, C. Krebber, and A. Pluckthun. 1997. Disrupting the hydrophobic patches at the antibody variable/constant domain interface: improved in vivo folding and physical characterization of an engineered scFv fragment. *Protein Eng* 10:435-444.

81. Brinkmann, U., Y. Reiter, S.H. Jung, B. Lee, and I. Pastan. 1993. A recombinant immunotoxin containing a disulfide-stabilized Fv fragment. *Proc Natl Acad Sci U S A* 90:7538-7542.

82. Glockshuber, R., M. Malia, I. Pfitzinger, and A. Pluckthun. 1990. A comparison of strategies to stabilize immunoglobulin Fv-fragments. *Biochemistry* 29:1362-1367.

83. Li, S.L., S.J. Liang, N. Guo, A.M. Wu, and Y. Fujita-Yamaguchi. 2000. Single-chain antibodies against human insulin-like growth factor I receptor: expression, purification, and effect on tumor growth. *Cancer Immunol Immunother* 49:243-252.

84. McGregor, D.P., P.E. Molloy, C. Cunningham, and W.J. Harris. 1994. Spontaneous assembly of bivalent single chain antibody fragments in Escherichia coli. *Mol Immunol* 31:219-226.

85. Young, N.M., C.R. MacKenzie, S.A. Narang, R.P. Oomen, and J.E. Baenziger. 1995. Thermal stabilization of a single-chain Fv antibody fragment by introduction of a disulphide bond. *FEBS Lett* 377:135-139.

86. Rajagopal, V., I. Pastan, and R.J. Kreitman. 1997. A form of anti-Tac(Fv) which is both single-chain and disulfide stabilized: comparison with its single-chain and disulfide-stabilized homologs. *Protein Eng* 10:1453-1459.

87. Hao, H.J., Y.Q. Jiang, Y.L. Zheng, R. Ma, and D.W. Yu. 2005. Improved stability and yield of Fv targeted superantigen by introducing both linker and disulfide bond into the targeting moiety. *Biochimie* 87:661-667.

88. Jespers, L., O. Schon, L.C. James, D. Veprintsev, and G. Winter. 2004. Crystal structure of HEL4, a soluble, refoldable human V(H) single domain with a germ-line scaffold. *J Mol Biol* 337:893-903.

89. Ward, E.S., D. Gussow, A.D. Griffiths, P.T. Jones, and G. Winter. 1989. Binding activities of a repertoire of single immunoglobulin variable domains secreted from Escherichia coli. *Nature* 341:544-546.

90. Davies, J., and L. Riechmann. 1994. 'Camelising' human antibody fragments: NMR studies on VH domains. *FEBS Lett* 339:285-290.

91. Zhang, J., J. Tanha, T. Hirama, N.H. Khieu, R. To, H. Tong-Sevinc, E. Stone, J.R. Brisson, and C.R. MacKenzie. 2004. Pentamerization of single-domain antibodies from phage libraries: a novel strategy for the rapid generation of high-avidity antibody reagents. *J Mol Biol* 335:49-56.

92. Jost, C.R., I. Kurucz, C.M. Jacobus, J.A. Titus, A.J. George, and D.M. Segal. 1994. Mammalian expression and secretion of functional single-chain Fv molecules. *J Biol Chem* 269:26267-26273.

93. Dorai, H., J.E. McCartney, R.M. Hudziak, M.S. Tai, A.A. Laminet, L.L. Houston, J.S. Huston, and H. Oppermann. 1994. Mammalian cell expression of single-chain Fv (sFv) antibody proteins and their C-terminal fusions with interleukin-2 and other effector domains. *Biotechnology (N Y)* 12:890-897.

94. Bei, R., J. Schlom, and S.V. Kashmiri. 1995. Baculovirus expression of a functional single-chain immunoglobulin and its IL-2 fusion protein. *J Immunol Methods* 186:245-255.

95. Whitelam, G.C., W. Cockburn, and M.R. Owen. 1994. Antibody production in transgenic plants. *Biochem Soc Trans* 22:940-944.

96. Nicholls, P.J., V.G. Johnson, M.D. Blanford, and S.M. Andrew. 1993. An improved method for generating single-chain antibodies from hybridomas. *J Immunol Methods* 165:81-91.

97. Ward, E.S. 1992. Antibody engineering: the use of Escherichia coli as an expression host. *Faseb J* 6:2422-2427.

98. Nygren, P.A., S. Stahl, and M. Uhlen. 1994. Engineering proteins to facilitate bioprocessing. *Trends Biotechnol* 12:184-188.

99. Porath, J., J. Carlsson, I. Olsson, and G. Belfrage. 1975. Metal chelate affinity chromatography, a new approach to protein fractionation. *Nature* 258:598-599.

100. Munro, S., and H.R. Pelham. 1986. An Hsp70-like protein in the ER: identity with the 78 kd glucose-regulated protein and immunoglobulin heavy chain binding protein. *Cell* 46:291-300.

101. Better, M., C.P. Chang, R.R. Robinson, and A.H. Horwitz. 1988. Escherichia coli secretion of an active chimeric antibody fragment. *Science* 240:1041-1043.

102. Skerra, A., and A. Pluckthun. 1988. Assembly of a functional immunoglobulin Fv fragment in Escherichia coli. *Science* 240:1038-1041.

103. Pugsley, A.P. 1993. The complete general secretory pathway in gram-negative bacteria. *Microbiol Rev* 57:50-108.

104. Tudyka, T., and A. Skerra. 1997. Glutathione S-transferase can be used as a C-terminal, enzymatically active dimerization module for a recombinant protease inhibitor, and functionally secreted into the periplasm of Escherichia coli. *Protein Sci* 6:2180-2187.

105. Pluckthun, A. 1994. Escherichia coli producing recombinant antibodies. *Bioprocess Technol* 19:233-252.

106. Huston, J.S., M. Mudgett-Hunter, M.S. Tai, J. McCartney, F. Warren, E. Haber, and H. Oppermann. 1991. Protein engineering of single-chain Fv analogs and fusion proteins. *Methods Enzymol* 203:46-88.

107. Skerra, A., and A. Pluckthun. 1991. Secretion and in vivo folding of the Fab fragment of the antibody McPC603 in Escherichia coli: influence of disulphides and cis-prolines. *Protein Eng* 4:971-979.

108. Field, H., G.T. Yarranton, and A.R. Rees. 1990. Expression of mouse immunoglobulin light and heavy chain variable regions in Escherichia coli and reconstitution of antigen-binding activity. *Protein Eng* 3:641-647.

109. Pluckthun, A. 1992. Mono- and bivalent antibody fragments produced in Escherichia coli: engineering, folding and antigen binding. *Immunol Rev* 130:151-188.

110. Knappik, A., and A. Pluckthun. 1995. Engineered turns of a recombinant antibody improve its in vivo folding. *Protein Eng* 8:81-89.

111. Duffaud, G.D., P.E. March, and M. Inouye. 1987. Expression and secretion of foreign proteins in Escherichia coli. *Methods Enzymol* 153:492-507.

112. Ayala, M., R.F. Balint, L. Fernandez-de-Cossio, J.W. Canaan-Haden, J.W. Larrick, and J.V. Gavilondo. 1995. Variable region sequence modulates periplasmic export of a single-chain Fv antibody fragment in Escherichia coli. *Biotechniques* 18:832, 835-838, 840-832.

113. Bowden, G.A., and G. Georgiou. 1990. Folding and aggregation of beta-lactamase in the periplasmic space of Escherichia coli. *J Biol Chem* 265:16760-16766.

114. Kiefhaber, T., R. Rudolph, H.H. Kohler, and J. Buchner. 1991. Protein aggregation in vitro and in vivo: a quantitative model of the kinetic competition between folding and aggregation. *Biotechnology (N Y)* 9:825-829.

115. Kipriyanov, S.M., G. Moldenhauer, and M. Little. 1997. High level production of soluble single chain antibodies in small-scale Escherichia coli cultures. *J Immunol Methods* 200:69-77.

116. Zettlmeissl, G., R. Rudolph, and R. Jaenicke. 1979. Reconstitution of lactic dehydrogenase. Noncovalent aggregation vs. reactivation. 1. Physical properties and kinetics of aggregation. *Biochemistry* 18:5567-5571.

117. Buchner, J., and R. Rudolph. 1991. Renaturation, purification and characterization of recombinant Fab-fragments produced in Escherichia coli. *Biotechnology (N Y)* 9:157-162.

118. White, C.E., N.M. Kempi, and E.A. Komives. 1994. Expression of highly disulfide-bonded proteins in Pichia pastoris. *Structure* 2:1003-1005.

119. Higgins, D.R., and J.M. Cregg. 1998. Introduction to Pichia pastoris. *Methods Mol Biol* 103:1-15.

120. Tschopp, J.F., P.F. Brust, J.M. Cregg, C.A. Stillman, and T.R. Gingeras. 1987. Expression of the lacZ gene from two methanol-regulated promoters in Pichia pastoris. *Nucleic Acids Res* 15:3859-3876.

121. Cregg, J.M., K.R. Madden, K.J. Barringer, G.P. Thill, and C.A. Stillman. 1989. Functional characterization of the two alcohol oxidase genes from the yeast Pichia pastoris. *Mol Cell Biol* 9:1316-1323.

122. Hellwig, S., F. Emde, N.P. Raven, M. Henke, P. van Der Logt, and R. Fischer. 2001. Analysis of single-chain antibody production in Pichia pastoris using on-line methanol control in fed-batch and mixed-feed fermentations. *Biotechnol Bioeng* 74:344-352.

123. Eldin, P., M.E. Pauza, Y. Hieda, G. Lin, M.P. Murtaugh, P.R. Pentel, and C.A. Pennell. 1997. High-level secretion of two antibody single chain Fv fragments by Pichia pastoris. *J Immunol Methods* 201:67-75.

124. Gurkan, C., S.N. Symeonides, and D.J. Ellar. 2004. High-level production in Pichia pastoris of an anti-p185HER-2 single-chain antibody fragment using an alternative secretion expression vector. *Biotechnol Appl Biochem* 39:115-122.

125. Marks, J.D., H.R. Hoogenboom, T.P. Bonnert, J. McCafferty, A.D. Griffiths, and G. Winter. 1991. By-passing immunization. Human antibodies from V-gene libraries displayed on phage. *J Mol Biol* 222:581-597.

126. Marks, J.D., H.R. Hoogenboom, A.D. Griffiths, and G. Winter. 1992. Molecular evolution of proteins on filamentous phage. Mimicking the strategy of the immune system. *J Biol Chem* 267:16007-16010.

127. Barbas, C.F., 3rd, J.D. Bain, D.M. Hoekstra, and R.A. Lerner. 1992. Semisynthetic combinatorial antibody libraries: a chemical solution to the diversity problem. *Proc Natl Acad Sci U S A* 89:4457-4461.

128. Proba, K., A. Worn, A. Honegger, and A. Pluckthun. 1998. Antibody scFv fragments without disulfide bonds made by molecular evolution. *J Mol Biol* 275:245-253.

129. Sieber, V., A. Pluckthun, and F.X. Schmid. 1998. Selecting proteins with improved stability by a phage-based method. *Nat Biotechnol* 16:955-960.

130. Jung, S., A. Honegger, and A. Pluckthun. 1999. Selection for improved protein stability by phage display. *J Mol Biol* 294:163-180.

131. Smith, G.P. 1985. Filamentous fusion phage: novel expression vectors that display cloned antigens on the virion surface. *Science* 228:1315-1317.

132. Mattheakis, L.C., R.R. Bhatt, and W.J. Dower. 1994. An in vitro polysome display system for identifying ligands from very large peptide libraries. *Proc Natl Acad Sci U S A* 91:9022-9026.

133. Boder, E.T., and K.D. Wittrup. 1997. Yeast surface display for screening combinatorial polypeptide libraries. *Nat Biotechnol* 15:553-557.

134. Georgiou, G., C. Stathopoulos, P.S. Daugherty, A.R. Nayak, B.L. Iverson, and R. Curtiss, 3rd. 1997. Display of heterologous proteins on the surface of microorganisms: from the screening of combinatorial libraries to live recombinant vaccines. *Nat Biotechnol* 15:29-34.

135. Tanha, J., G. Dubuc, T. Hirama, S.A. Narang, and C.R. MacKenzie. 2002. Selection by phage display of llama conventional V(H) fragments with heavy chain antibody V(H)H properties. *J Immunol Methods* 263:97-109.

136. Barbas, C.F., 3rd, J.E. Crowe, Jr., D. Cababa, T.M. Jones, S.L. Zebedee, B.R. Murphy, R.M. Chanock, and D.R. Burton. 1992. Human monoclonal Fab fragments derived from a combinatorial library bind to respiratory syncytial virus F glycoprotein and neutralize infectivity. *Proc Natl Acad Sci U S A* 89:10164-10168.

137. Fu, Y., L.N. Shearing, S. Haynes, P. Crewther, L. Tilley, R.F. Anders, and M. Foley. 1997. Isolation from phage display libraries of single chain variable fragment antibodies that recognize conformational epitopes in the malaria vaccine candidate, apical membrane antigen-1. *J Biol Chem* 272:25678-25684.

138. Griffiths, A.D., and A.R. Duncan. 1998. Strategies for selection of antibodies by phage display. *Curr Opin Biotechnol* 9:102-108.

139. Noronha, E.J., X. Wang, S.A. Desai, T. Kageshita, and S. Ferrone. 1998. Limited diversity of human scFv fragments isolated by panning a synthetic phage-display scFv library with cultured human melanoma cells. *J Immunol* 161:2968-2976.

140. Nissim, A., H.R. Hoogenboom, I.M. Tomlinson, G. Flynn, C. Midgley, D. Lane, and G. Winter. 1994. Antibody fragments from a 'single pot' phage display library as immunochemical reagents. *Embo J* 13:692-698.

141. McCafferty, J., A.D. Griffiths, G. Winter, and D.J. Chiswell. 1990. Phage antibodies: filamentous phage displaying antibody variable domains. *Nature* 348:552-554.

142. Parmley, S.F., and G.P. Smith. 1988. Antibody-selectable filamentous fd phage vectors: affinity purification of target genes. *Gene* 73:305-318.

143. Cai, X., and A. Garen. 1995. Anti-melanoma antibodies from melanoma patients immunized with genetically modified autologous tumor cells: selection of specific antibodies from single-chain Fv fusion phage libraries. *Proc Natl Acad Sci U S A* 92:6537-6541.

144. de Haard, H.J., N. van Neer, A. Reurs, S.E. Hufton, R.C. Roovers, P. Henderikx, A.P. de Bruine, J.W. Arends, and H.R. Hoogenboom. 1999. A large non-immunized human Fab fragment phage library that permits rapid isolation and kinetic analysis of high affinity antibodies. *J Biol Chem* 274:18218-18230.

145. Smith, G.P., S.U. Patel, J.D. Windass, J.M. Thornton, G. Winter, and A.D. Griffiths. 1998. Small binding proteins selected from a combinatorial repertoire of knottins displayed on phage. *J Mol Biol* 277:317-332.

146. Padlan, E.A. 1994. Anatomy of the antibody molecule. *Mol Immunol* 31:169-217.

147. Koshland, D.E. 1958. Application of a Theory of Enzyme Specificity to Protein Synthesis. *Proc Natl Acad Sci U S A* 44:98-104.

148. Wedemayer, G.J., P.A. Patten, L.H. Wang, P.G. Schultz, and R.C. Stevens. 1997. Structural insights into the evolution of an antibody combining site. *Science* 276:1665-1669.

149. Braden, B.C., and R.J. Poljak. 1995. Structural features of the reactions between antibodies and protein antigens. *Faseb J* 9:9-16.

150. Karlsson, R. 1994. Real-time competitive kinetic analysis of interactions between low-molecular-weight ligands in solution and surface-immobilized receptors. *Anal Biochem* 221:142-151.

151. Myszka, D.G. 1997. Kinetic analysis of macromolecular interactions using surface plasmon resonance biosensors. *Curr Opin Biotechnol* 8:50-57.

152. Liedberg, B., and e. al. 1983. Surface plasmon resonance for gas detection and biosensing. *Lab. Sensors Actuat.* 4:299-304.

153. Sjolander, S., and C. Urbaniczky. 1991. Integrated fluid handling system for biomolecular interaction analysis. *Anal Chem* 63:2338-2345.

154. Scatchard, G. 1949. *Ann. N. Y. Acad. Sci.* 51:660-672.

155. Salomon, D.S., R. Brandt, F. Ciardiello, and N. Normanno. 1995. Epidermal growth factor-related peptides and their receptors in human malignancies. *Crit Rev Oncol Hematol* 19:183-232.

156. Carpenter, G., and S. Cohen. 1979. Epidermal growth factor. *Annu Rev Biochem* 48:193-216.

157. Velu, T.J. 1990. Structure, function and transforming potential of the epidermal growth factor receptor. *Mol Cell Endocrinol* 70:205-216.

158. Schlessinger, J., Y. Shechter, M.C. Willingham, and I. Pastan. 1978. Direct visualization of binding, aggregation, and internalization of insulin and epidermal growth factor on living fibroblastic cells. *Proc Natl Acad Sci U S A* 75:2659-2663.

159. Haigler, H., J.F. Ash, S.J. Singer, and S. Cohen. 1978. Visualization by fluorescence of the binding and internalization of epidermal growth factor in human carcinoma cells A-431. *Proc Natl Acad Sci U S A* 75:3317-3321.

160. Haigler, H.T., J.A. McKanna, and S. Cohen. 1979. Direct visualization of the binding and internalization of a ferritin conjugate of epidermal growth factor in human carcinoma cells A-431. *J Cell Biol* 81:382-395.

161. Hillman, G.M., and J. Schlessinger. 1982. Lateral diffusion of epidermal growth factor complexed to its surface receptors does not account for the thermal sensitivity of patch formation and endocytosis. *Biochemistry* 21:1667-1672.

162. Zidovetzki, R., Y. Yarden, J. Schlessinger, and T.M. Jovin. 1981. Rotational diffusion of epidermal growth factor complexed to cell surface receptors reflects rapid microaggregation and endocytosis of occupied receptors. *Proc Natl Acad Sci U S A* 78:6981-6985.

163. Carpenter, G. 1987. Receptors for epidermal growth factor and other polypeptide mitogens. *Annu Rev Biochem* 56:881-914.

164. Carpenter, G., and S. Cohen. 1990. Epidermal growth factor. *J Biol Chem* 265:7709-7712.

165. Soderquist, A.M., and G. Carpenter. 1984. Glycosylation of the epidermal growth factor receptor in A-431 cells. The contribution of carbohydrate to receptor function. *J Biol Chem* 259:12586-12594.

166. Slieker, L.J., T.M. Martensen, and M.D. Lane. 1986. Synthesis of epidermal growth factor receptor in human A431 cells. Glycosylation-dependent acquisition of ligand binding activity occurs post-translationally in the endoplasmic reticulum. *J Biol Chem* 261:15233-15241.

167. Boonstra, J., P. Rijken, B. Humbel, F. Cremers, A. Verkleij, and P. van Bergen en Henegouwen. 1995. The epidermal growth factor. *Cell Biol Int* 19:413-430.

168. Bajaj, M., M.D. Waterfield, J. Schlessinger, W.R. Taylor, and T. Blundell. 1987. On the tertiary structure of the extracellular domains of the epidermal growth factor and insulin receptors. *Biochim Biophys Acta* 916:220-226.

169. Ward, C.W., and T.P. Garrett. 2001. The relationship between the L1 and L2 domains of the insulin and epidermal growth factor receptors and leucine-rich repeat modules. *BMC Bioinformatics* 2:4.

170. Kobe, B., and A.V. Kajava. 2001. The leucine-rich repeat as a protein recognition motif. *Curr Opin Struct Biol* 11:725-732.

171. Garrett, T.P., N.M. McKern, M. Lou, T.C. Elleman, T.E. Adams, G.O. Lovrecz, H.J. Zhu, F. Walker, M.J. Frenkel, P.A. Hoyne, R.N. Jorissen, E.C. Nice, A.W. Burgess, and C.W. Ward. 2002. Crystal structure of a truncated epidermal growth factor receptor extracellular domain bound to transforming growth factor alpha. *Cell* 110:763-773.

172. Lax, I., W.H. Burgess, F. Bellot, A. Ullrich, J. Schlessinger, and D. Givol. 1988. Localization of a major receptor-binding domain for epidermal growth factor by affinity labeling. *Mol Cell Biol* 8:1831-1834.

173. Lax, I., F. Bellot, R. Howk, A. Ullrich, D. Givol, and J. Schlessinger. 1989. Functional analysis of the ligand binding site of EGF-receptor utilizing chimeric chicken/human receptor molecules. *Embo J* 8:421-427.

174. Wu, D.G., L.H. Wang, G.H. Sato, K.A. West, W.R. Harris, J.W. Crabb, and J.D. Sato. 1989. Human epidermal growth factor (EGF) receptor sequence recognized by EGF competitive monoclonal antibodies. Evidence for the localization of the EGF-binding site. *J Biol Chem* 264:17469-17475.

175. Wu, D.G., L.H. Wang, Y. Chi, G.H. Sato, and J.D. Sato. 1990. Human epidermal growth factor receptor residue covalently cross-linked to epidermal growth factor. *Proc Natl Acad Sci U S A* 87:3151-3155.

176. Woltjer, R.L., T.J. Lukas, and J.V. Staros. 1992. Direct identification of residues of the epidermal growth factor receptor in close proximity to the amino terminus of bound epidermal growth factor. *Proc Natl Acad Sci U S A* 89:7801-7805.

177. Todd, R., and D.T. Wong. 1999. Epidermal growth factor receptor (EGFR) biology and human oral cancer. *Histol Histopathol* 14:491-500.

178. Hunter, T. 1984. The epidermal growth factor receptor gene and its product. *Nature* 311:414-416.

179. Cochet, C., G.N. Gill, J. Meisenhelder, J.A. Cooper, and T. Hunter. 1984. C-kinase phosphorylates the epidermal growth factor receptor and reduces its epidermal growth factor-stimulated tyrosine protein kinase activity. *J Biol Chem* 259:2553-2558.

180. Friedman, B., A.R. Frackelton, Jr., A.H. Ross, J.M. Connors, H. Fujiki, T. Sugimura, and M.R. Rosner. 1984. Tumor promoters block tyrosine-specific phosphorylation of the epidermal growth factor receptor. *Proc Natl Acad Sci U S A* 81:3034-3038.

181. Schlessinger, J. 1988. The epidermal growth factor receptor as a multifunctional allosteric protein. *Biochemistry* 27:3119-3123.

182. Weber, W., P.J. Bertics, and G.N. Gill. 1984. Immunoaffinity purification of the epidermal growth factor receptor. Stoichiometry of binding and kinetics of self-phosphorylation. *J Biol Chem* 259:14631-14636.

183. Yarden, Y., and J. Schlessinger. 1987. Self-phosphorylation of epidermal growth factor receptor: evidence for a model of intermolecular allosteric activation. *Biochemistry* 26:1434-1442.

184. Boni-Schnetzler, M., and P.F. Pilch. 1987. Mechanism of epidermal growth factor receptor autophosphorylation and high-affinity binding. *Proc Natl Acad Sci U S A* 84:7832-7836.

185. Cochet, C., O. Kashles, E.M. Chambaz, I. Borrello, C.R. King, and J. Schlessinger. 1988. Demonstration of epidermal growth factor-induced receptor dimerization in living cells using a chemical covalent cross-linking agent. *J Biol Chem* 263:3290-3295.

186. St-Pierre, P.R., and N.O. Petersen. 1992. Average density and size of microclusters of epidermal growth factor receptors on A431 cells. *Biochemistry* 31:2459-2463.

187. Brown, P.M., M.T. Debanne, S. Grothe, D. Bergsma, M. Caron, C. Kay, and M.D. O'Connor-McCourt. 1994. The extracellular domain of the epidermal growth factor receptor. Studies on the affinity and stoichiometry of binding, receptor dimerization and a binding-domain mutant. *Eur J Biochem* 225:223-233.

188. Odaka, M., D. Kohda, I. Lax, J. Schlessinger, and F. Inagaki. 1997. Ligand-binding enhances the affinity of dimerization of the extracellular domain of the epidermal growth factor receptor. *J Biochem (Tokyo)* 122:116-121.

189. Lemmon, M.A., Z. Bu, J.E. Ladbury, M. Zhou, D. Pinchasi, I. Lax, D.M. Engelman, and J. Schlessinger. 1997. Two EGF molecules contribute additively to stabilization of the EGFR dimer. *Embo J* 16:281-294.

190. Domagala, T., N. Konstantopoulos, F. Smyth, R.N. Jorissen, L. Fabri, D. Geleick, I. Lax, J. Schlessinger, W. Sawyer, G.J. Howlett, A.W. Burgess, and E.C. Nice. 2000. Stoichiometry, kinetic and binding analysis of the interaction between epidermal growth factor (EGF) and the extracellular domain of the EGF receptor. *Growth Factors* 18:11-29.

191. Lemmon, M.A., and J. Schlessinger. 1994. Regulation of signal transduction and signal diversity by receptor oligomerization. *Trends Biochem Sci* 19:459-463.

192. Moriki, T., H. Maruyama, and I.N. Maruyama. 2001. Activation of preformed EGF receptor dimers by ligand-induced rotation of the transmembrane domain. *J Mol Biol* 311:1011-1026.

193. Schlessinger, J., A.B. Schreiber, A. Levi, I. Lax, T. Libermann, and Y. Yarden. 1983. Regulation of cell proliferation by epidermal growth factor. *CRC Crit Rev Biochem* 14:93-111.

194. Schlessinger, J. 1986. Allosteric regulation of the epidermal growth factor receptor kinase. *J Cell Biol* 103:2067-2072.

195. Yarden, Y., and J. Schlessinger. 1987. Epidermal growth factor induces rapid, reversible aggregation of the purified epidermal growth factor receptor. *Biochemistry* 26:1443-1451.

196. Bertics, P.J., and G.N. Gill. 1985. Self-phosphorylation enhances the protein-tyrosine kinase activity of the epidermal growth factor receptor. *J Biol Chem* 260:14642-14647.

197. Decker, S.J. 1993. Transmembrane signaling by epidermal growth factor receptors lacking autophosphorylation sites. *J Biol Chem* 268:9176-9179.

198. Pike, L.J. 1992. Dimer formation and desensitization of the epidermal growth factor receptor. *J Lab Clin Med* 120:688-692.

199. Dunn, W.A., T.P. Connolly, and A.L. Hubbard. 1986. Receptor-mediated endocytosis of epidermal growth factor by rat hepatocytes: receptor pathway. *J Cell Biol* 102:24-36.

200. Murthy, U., M. Basu, A. Sen-Majumdar, and M. Das. 1986. Perinuclear location and recycling of epidermal growth factor receptor kinase: immunofluorescent visualization using antibodies directed to kinase and extracellular domains. *J Cell Biol* 103:333-342.

201. Carpenter, G., and S. Cohen. 1976. 125I-labeled human epidermal growth factor. Binding, internalization, and degradation in human fibroblasts. *J Cell Biol* 71:159-171.

202. Willingham, M.C., and I.H. Pastan. 1982. Transit of epidermal growth factor through coated pits of the Golgi system. *J Cell Biol* 94:207-212.

203. Willingham, M.C., A.V. Rutherford, M.G. Gallo, J. Wehland, R.B. Dickson, R. Schlegel, and I.H. Pastan. 1981. Receptor-mediated endocytosis in cultured fibroblasts: cryptic coated pits and the formation of receptosomes. *J Histochem Cytochem* 29:1003-1013.

204. Beguinot, L., R.M. Lyall, M.C. Willingham, and I. Pastan. 1984. Down-regulation of the epidermal growth factor receptor in KB cells is due to receptor internalization and subsequent degradation in lysosomes. *Proc Natl Acad Sci U S A* 81:2384-2388.

205. Xu, Y.H., S. Ishii, A.J. Clark, M. Sullivan, R.K. Wilson, D.P. Ma, B.A. Roe, G.T. Merlino, and I. Pastan. 1984. Human epidermal growth factor receptor cDNA is homologous to a variety of RNAs overproduced in A431 carcinoma cells. *Nature* 309:806-810.

206. Ullrich, A., L. Coussens, J.S. Hayflick, T.J. Dull, A. Gray, A.W. Tam, J. Lee, Y. Yarden, T.A. Libermann, J. Schlessinger, and et al. 1984. Human epidermal growth factor receptor cDNA sequence and aberrant expression of the amplified gene in A431 epidermoid carcinoma cells. *Nature* 309:418-425.

207. Fabricant, R.N., J.E. De Larco, and G.J. Todaro. 1977. Nerve growth factor receptors on human melanoma cells in culture. *Proc Natl Acad Sci U S A* 74:565-569.

208. Arteaga, C.L., S.D. Hurd, T.C. Dugger, A.R. Winnier, and J.B. Robertson. 1994. Epidermal growth factor receptors in human breast carcinoma cells: a potential selective target for transforming growth factor alpha-Pseudomonas exotoxin 40 fusion protein. *Cancer Res* 54:4703-4709.

209. Fontanini, G., S. Vignati, D. Bigini, A. Mussi, H. Lucchi, C.A. Angeletti, R. Pingitore, S. Pepe, F. Basolo, and G. Bevilacqua. 1995. Epidermal growth factor receptor (EGFr) expression in non-small cell lung carcinomas correlates with metastatic involvement of hilar and mediastinal lymph nodes in the squamous subtype. *Eur J Cancer* 31A:178-183.

210. Libermann, T.A., H.R. Nusbaum, N. Razon, R. Kris, I. Lax, H. Soreq, N. Whittle, M.D. Waterfield, A. Ullrich, and J. Schlessinger. 1985. Amplification, enhanced expression and possible rearrangement of EGF receptor gene in primary human brain tumours of glial origin. *Nature* 313:144-147.

211. Libermann, T.A., H.R. Nusbaum, N. Razon, R. Kris, I. Lax, H. Soreq, N. Whittle, M.D. Waterfield, A. Ullrich, and J. Schlessinger. 1985. Amplification and overexpression of the EGF receptor gene in primary human glioblastomas. *J Cell Sci Suppl* 3:161-172.

212. Turner, T., P. Chen, L.J. Goodly, and A. Wells. 1996. EGF receptor signaling enhances in vivo invasiveness of DU-145 human prostate carcinoma cells. *Clin Exp Metastasis* 14:409-418.

213. Hollstein, M.C., A.M. Smits, C. Galiana, H. Yamasaki, J.L. Bos, A. Mandard, C. Partensky, and R. Montesano. 1988. Amplification of epidermal growth factor receptor gene but no evidence of ras mutations in primary human esophageal cancers. *Cancer Res* 48:5119-5123.

214. Grandis, J.R., and D.J. Tweardy. 1993. TGF-alpha and EGFR in head and neck cancer. *J Cell Biochem Suppl* 17F:188-191.

215. Garcia de Palazzo, I., A. Klein-Szanto, and L.M. Weiner. 1993. Immunohistochemical detection of c-erbB-2 expression by neoplastic human tissue using monospecific and bispecific monoclonal antibodies. *Int J Biol Markers* 8:233-239.

216. Lemoine, N.R., C.M. Hughes, C.M. Barton, R. Poulsom, R.E. Jeffery, G. Kloppel, P.A. Hall, and W.J. Gullick. 1992. The epidermal growth factor receptor in human pancreatic cancer. *J Pathol* 166:7-12.

217. Petrides, P.E., S. Bock, J. Bovens, R. Hofmann, and G. Jakse. 1990. Modulation of pro-epidermal growth factor, pro-transforming growth factor alpha and epidermal growth factor receptor gene expression in human renal carcinomas. *Cancer Res* 50:3934-3939.

218. Yao, M., T. Shuin, H. Misaki, and Y. Kubota. 1988. Enhanced expression of c-myc and epidermal growth factor receptor (C-erbB-1) genes in primary human renal cancer. *Cancer Res* 48:6753-6757.

219. Gullick, W.J., J.J. Marsden, N. Whittle, B. Ward, L. Bobrow, and M.D. Waterfield. 1986. Expression of epidermal growth factor receptors on human cervical, ovarian, and vulval carcinomas. *Cancer Res* 46:285-292.

220. Ozanne, B., C.S. Richards, F. Hendler, D. Burns, and B. Gusterson. 1986. Over-expression of the EGF receptor is a hallmark of squamous cell carcinomas. *J Pathol* 149:9-14.

221. Berger, M.S., W.J. Gullick, C. Greenfield, S. Evans, B.J. Addis, and M.D. Waterfield. 1987. Epidermal growth factor receptors in lung tumours. *J Pathol* 152:297-307.

222. Gullick, W.J. 1991. Prevalence of aberrant expression of the epidermal growth factor receptor in human cancers. *Br Med Bull* 47:87-98.

223. Baselga, J., and J. Mendelsohn. 1994. The epidermal growth factor receptor as a target for therapy in breast carcinoma. *Breast Cancer Res Treat* 29:127-138.

224. Harris, A.L. 1994. What is the biological, prognostic, and therapeutic role of the EGF receptor in human breast cancer? *Breast Cancer Res Treat* 29:1-2.

225. LeMaistre, C.F., C. Meneghetti, L. Howes, and C.K. Osborne. 1994. Targeting the EGF receptor in breast cancer treatment. *Breast Cancer Res Treat* 32:97-103.

226. Chrysogelos, S.A., and R.B. Dickson. 1994. EGF receptor expression, regulation, and function in breast cancer. *Breast Cancer Res Treat* 29:29-40.

227. De Jong, K.P., R. Stellema, A. Karrenbeld, J. Koudstaal, A.S. Gouw, W.J. Sluiter, P.M. Peeters, M.J. Slooff, and E.G. De Vries. 1998. Clinical relevance of transforming growth factor alpha, epidermal growth factor receptor, p53, and Ki67 in colorectal liver metastases and corresponding primary tumors. *Hepatology* 28:971-979.

228. Mendelsohn, J., and J. Baselga. 2000. The EGF receptor family as targets for cancer therapy. *Oncogene* 19:6550-6565.

229. Ciardiello, F., and G. Tortora. 2001. A novel approach in the treatment of cancer: targeting the epidermal growth factor receptor. *Clin Cancer Res* 7:2958-2970.

230. Fletcher, L. 2001. PDL's mAb technology finds right timing. *Nat Biotechnol* 19:395-396.

231. Fan, Z., Y. Lu, X. Wu, and J. Mendelsohn. 1994. Antibody-induced epidermal growth factor receptor dimerization mediates inhibition of autocrine proliferation of A431 squamous carcinoma cells. *J Biol Chem* 269:27595-27602.

232. Goldstein, N.I., M. Prewett, K. Zuklys, P. Rockwell, and J. Mendelsohn. 1995. Biological efficacy of a chimeric antibody to the epidermal growth factor receptor in a human tumor xenograft model. *Clin Cancer Res* 1:1311-1318.

233. Fan, Z., J. Mendelsohn, H. Masui, and R. Kumar. 1993. Regulation of epidermal growth factor receptor in NIH3T3/HER14 cells by antireceptor monoclonal antibodies. *J Biol Chem* 268:21073-21079.

234. Fan, Z., J. Baselga, H. Masui, and J. Mendelsohn. 1993. Antitumor effect of anti-epidermal growth factor receptor monoclonal antibodies plus cis-diamminedichloroplatinum on well established A431 cell xenografts. *Cancer Res* 53:4637-4642.

235. Fan, Z., H. Masui, I. Altas, and J. Mendelsohn. 1993. Blockade of epidermal growth factor receptor function by bivalent and monovalent fragments of 225 anti-epidermal growth factor receptor monoclonal antibodies. *Cancer Res* 53:4322-4328.

236. Divgi, C.R., S. Welt, M. Kris, F.X. Real, S.D. Yeh, R. Gralla, B. Merchant, S. Schweighart, M. Unger, S.M. Larson, and et al. 1991. Phase I and imaging trial of indium 111-labeled anti-epidermal growth factor receptor monoclonal antibody 225 in patients with squamous cell lung carcinoma. *J Natl Cancer Inst* 83:97-104.

237. Flickinger, T.W., N.J. Maihle, and H.J. Kung. 1992. An alternatively processed mRNA from the avian c-erbB gene encodes a soluble, truncated form of the receptor that can block ligand-dependent transformation. *Mol Cell Biol* 12:883-893.

238. Petch, L.A., J. Harris, V.W. Raymond, A. Blasband, D.C. Lee, and H.S. Earp. 1990. A truncated, secreted form of the epidermal growth factor receptor is encoded by an alternatively spliced transcript in normal rat tissue. *Mol Cell Biol* 10:2973-2982.

239. Reiter, J.L., and N.J. Maihle. 1996. A 1.8 kb alternative transcript from the human epidermal growth factor receptor gene encodes a truncated form of the receptor. *Nucleic Acids Res* 24:4050-4056.

240. Reiter, J.L., D.W. Threadgill, G.D. Eley, K.E. Strunk, A.J. Danielsen, C.S. Sinclair, R.S. Pearsall, P.J. Green, D. Yee, A.L. Lampland, S. Balasubramaniam, T.D. Crossley, T.R. Magnuson, C.D. James, and N.J. Maihle. 2001. Comparative genomic sequence analysis and isolation of human and mouse alternative EGFR transcripts encoding truncated receptor isoforms. *Genomics* 71:1-20.

241. Sugawa, N., A.J. Ekstrand, C.D. James, and V.P. Collins. 1990. Identical splicing of aberrant epidermal growth factor receptor transcripts from amplified rearranged genes in human glioblastomas. *Proc Natl Acad Sci U S A* 87:8602-8606.

242. Haley, J.D., J.J. Hsuan, and M.D. Waterfield. 1989. Analysis of mammalian fibroblast transformation by normal and mutated human EGF receptors. *Oncogene* 4:273-283.

243. Huang, H.S., M. Nagane, C.K. Klingbeil, H. Lin, R. Nishikawa, X.D. Ji, C.M. Huang, G.N. Gill, H.S. Wiley, and W.K. Cavenee. 1997. The enhanced tumorigenic activity of a mutant epidermal growth factor receptor common in human cancers is mediated by threshold levels of constitutive tyrosine phosphorylation and unattenuated signaling. *J Biol Chem* 272:2927-2935.

244. Wikstrand, C.J., C.J. Reist, G.E. Archer, M.R. Zalutsky, and D.D. Bigner. 1998. The class III variant of the epidermal growth factor receptor (EGFRvIII): characterization and utilization as an immunotherapeutic target. *J Neurovirol* 4:148-158.

245. Moscatello, D.K., R.B. Montgomery, P. Sundareshan, H. McDanel, M.Y. Wong, and A.J. Wong. 1996. Transformational and altered signal transduction by a naturally occurring mutant EGF receptor. *Oncogene* 13:85-96.

246. Wong, A.J., J.M. Ruppert, S.H. Bigner, C.H. Grzeschik, P.A. Humphrey, D.S. Bigner, and B. Vogelstein. 1992. Structural alterations of the epidermal growth factor receptor gene in human gliomas. *Proc Natl Acad Sci U S A* 89:2965-2969.

247. Moscatello, D.K., M. Holgado-Madruga, A.K. Godwin, G. Ramirez, G. Gunn, P.W. Zoltick, J.A. Biegel, R.L. Hayes, and A.J. Wong. 1995. Frequent expression of a mutant epidermal growth factor receptor in multiple human tumors. *Cancer Res* 55:5536-5539.

248. Yamazaki, H., Y. Ohba, N. Tamaoki, and M. Shibuya. 1990. A deletion mutation within the ligand binding domain is responsible for activation of epidermal growth factor receptor gene in human brain tumors. *Jpn J Cancer Res* 81:773-779.

249. Jorissen, R.N., V.C. Epa, H.R. Treutlein, T.P. Garrett, C.W. Ward, and A.W. Burgess. 2000. Characterization of a comparative model of the extracellular domain of the epidermal growth factor receptor. *Protein Sci* 9:310-324.

250. Okamoto, S., K. Yoshikawa, Y. Obata, M. Shibuya, S. Aoki, J. Yoshida, and T. Takahashi. 1996. Monoclonal antibody against the fusion junction of a deletion-mutant epidermal growth factor receptor. *Br J Cancer* 73:1366-1372.

251. Reist, C.J., G.E. Archer, S.N. Kurpad, C.J. Wikstrand, G. Vaidyanathan, M.C. Willingham, D.K. Moscatello, A.J. Wong, D.D. Bigner, and M.R. Zalutsky. 1995. Tumor-specific anti-epidermal growth factor receptor variant III monoclonal antibodies: use of the tyramine-cellobiose radioiodination method enhances cellular retention and uptake in tumor xenografts. *Cancer Res* 55:4375-4382.

252. Nishikawa, R., X.D. Ji, R.C. Harmon, C.S. Lazar, G.N. Gill, W.K. Cavenee, and H.J. Huang. 1994. A mutant epidermal growth factor receptor common in human glioma confers enhanced tumorigenicity. *Proc Natl Acad Sci U S A* 91:7727-7731.

253. Ekstrand, A.J., N. Longo, M.L. Hamid, J.J. Olson, L. Liu, V.P. Collins, and C.D. James. 1994. Functional characterization of an EGF receptor with a truncated extracellular domain expressed in glioblastomas with EGFR gene amplification. *Oncogene* 9:2313-2320.

254. Batra, S.K., S. Castelino-Prabhu, C.J. Wikstrand, X. Zhu, P.A. Humphrey, H.S. Friedman, and D.D. Bigner. 1995. Epidermal growth factor ligand-independent, unregulated, cell-transforming potential of a naturally occurring human mutant EGFRvIII gene. *Cell Growth Differ* 6:1251-1259.

255. Fernandes, H., S. Cohen, and S. Bishayee. 2001. Glycosylation-induced conformational modification positively regulates receptor-receptor association: a study with an aberrant epidermal growth factor receptor (EGFRvIII/DeltaEGFR) expressed in cancer cells. *J Biol Chem* 276:5375-5383.

256. Chu, C.T., K.D. Everiss, C.J. Wikstrand, S.K. Batra, H.J. Kung, and D.D. Bigner. 1997. Receptor dimerization is not a factor in the signalling activity of a transforming variant epidermal growth factor receptor (EGFRvIII). *Biochem J* 324 ( Pt 3):855-861.

257. Hills, D., G. Rowlinson-Busza, and W.J. Gullick. 1995. Specific targeting of a mutant, activated FGF receptor found in glioblastoma using a monoclonal antibody. *Int J Cancer* 63:537-543.

258. Tang, C.K., X.Q. Gong, D.K. Moscatello, A.J. Wong, and M.E. Lippman. 2000. Epidermal growth factor receptor vIII enhances tumorigenicity in human breast cancer. *Cancer Res* 60:3081-3087.

259. Ding, H., P. Shannon, N. Lau, X. Wu, L. Roncari, R.L. Baldwin, H. Takebayashi, A. Nagy, D.H. Gutmann, and A. Guha. 2003. Oligodendrogliomas result from the expression of an activated mutant epidermal growth factor receptor in a RAS transgenic mouse astrocytoma model. *Cancer Res* 63:1106-1113.

260. Nagane, M., F. Coufal, H. Lin, O. Bogler, W.K. Cavenee, and H.J. Huang. 1996. A common mutant epidermal growth factor receptor confers enhanced tumorigenicity on human glioblastoma cells by increasing proliferation and reducing apoptosis. *Cancer Res* 56:5079-5086.

261. Pedersen, M.W., V. Tkach, N. Pedersen, V. Berezin, and H.S. Poulsen. 2004. Expression of a naturally occurring constitutively active variant of the epidermal growth factor receptor in mouse fibroblasts increases motility. *Int J Cancer* 108:643-653.

262. Lal, A., C.A. Glazer, H.M. Martinson, H.S. Friedman, G.E. Archer, J.H. Sampson, and G.J. Riggins. 2002. Mutant epidermal growth factor receptor up-regulates molecular effectors of tumor invasion. *Cancer Res* 62:3335-3339.

263. Ekstrand, A.J., N. Sugawa, C.D. James, and V.P. Collins. 1992. Amplified and rearranged epidermal growth factor receptor genes in human glioblastomas reveal deletions of sequences encoding portions of the N- and/or C-terminal tails. *Proc Natl Acad Sci U S A* 89:4309-4313.

264. Malden, L.T., U. Novak, A.H. Kaye, and A.W. Burgess. 1988. Selective amplification of the cytoplasmic domain of the epidermal growth factor receptor gene in glioblastoma multiforme. *Cancer Res* 48:2711-2714.

265. Wikstrand, C.J., L.P. Hale, S.K. Batra, M.L. Hill, P.A. Humphrey, S.N. Kurpad, R.E. McLendon, D. Moscatello, C.N. Pegram, C.J. Reist, and et al. 1995. Monoclonal antibodies against EGFRvIII are tumor specific and react with breast and lung carcinomas and malignant gliomas. *Cancer Res* 55:3140-3148.

266. Schlegel, J., A. Merdes, G. Stumm, F.K. Albert, M. Forsting, N. Hynes, and M. Kiessling. 1994. Amplification of the epidermal-growth-factor-receptor gene correlates with different growth behaviour in human glioblastoma. *Int J Cancer* 56:72-77.

267. Schwechheimer, K., S. Huang, and W.K. Cavenee. 1995. EGFR gene amplification--rearrangement in human glioblastomas. *Int J Cancer* 62:145-148.

268. Olapade-Olaopa, E.O., D.K. Moscatello, E.H. MacKay, T. Horsburgh, D.P. Sandhu, T.R. Terry, A.J. Wong, and F.K. Habib. 2000. Evidence for the differential expression of a variant EGF receptor protein in human prostate cancer. *Br J Cancer* 82:186-194.

269. Johns, T.G., E. Stockert, G. Ritter, A.A. Jungbluth, H.J. Huang, W.K. Cavenee, F.E. Smyth, C.M. Hall, N. Watson, E.C. Nice, W.J. Gullick, L.J. Old, A.W. Burgess, and A.M. Scott. 2002. Novel monoclonal antibody specific for the de2-7 epidermal growth factor receptor (EGFR) that also recognizes the EGFR expressed in cells containing amplification of the EGFR gene. *Int J Cancer* 98:398-408.

270. Humphrey, P.A., A.J. Wong, B. Vogelstein, M.R. Zalutsky, G.N. Fuller, G.E. Archer, H.S. Friedman, M.M. Kwatra, S.H. Bigner, and D.D. Bigner. 1990. Anti-synthetic peptide antibody reacting at the fusion junction of deletion-mutant epidermal growth factor receptors in human glioblastoma. *Proc Natl Acad Sci U S A* 87:4207-4211.

271. Moscatello, D.K., G. Ramirez, and A.J. Wong. 1997. A naturally occurring mutant human epidermal growth factor receptor as a target for peptide vaccine immunotherapy of tumors. *Cancer Res* 57:1419-1424.

272. Heimberger, A.B., L.E. Crotty, G.E. Archer, K.R. Hess, C.J. Wikstrand, A.H. Friedman, H.S. Friedman, D.D. Bigner, and J.H. Sampson. 2003. Epidermal growth factor receptor VIII peptide vaccination is efficacious against established intracerebral tumors. *Clin Cancer Res* 9:4247-4254.

273. Ciesielski, M.J., A.L. Kazim, R.F. Barth, and R.A. Fenstermaker. 2005. Cellular antitumor immune response to a branched lysine multiple antigenic peptide containing epitopes of a common tumor-specific antigen in a rat glioma model. *Cancer Immunol Immunother* 54:107-119.

274. Steplewski, Z., M.D. Lubeck, and H. Koprowski. 1983. Human macrophages armed with murine immunoglobulin G2a antibodies to tumors destroy human cancer cells. *Science* 221:865-867.

275. Lorimer, I.A., C.J. Wikstrand, S.K. Batra, D.D. Bigner, and I. Pastan. 1995. Immunotoxins that target an oncogenic mutant epidermal growth factor receptor expressed in human tumors. *Clin Cancer Res* 1:859-864.

276. Wikstrand, C.J., V.R. Cole, L.E. Crotty, J.H. Sampson, and D.D. Bigner. 2002. Generation of anti-idiotypic reagents in the EGFRvIII tumor-associated antigen system. *Cancer Immunol Immunother* 50:639-652.

277. Liu, Z., C. Panousis, F.E. Smyth, R. Murphy, V. Wirth, G. Cartwright, T.G. Johns, and A.M. Scott. 2003. Generation of anti-idiotype antibodies for application in clinical immunotherapy laboratory analyses. *Hybrid Hybridomics* 22:219-228.

278. Lorimer, I.A., A. Keppler-Hafkemeyer, R.A. Beers, C.N. Pegram, D.D. Bigner, and I. Pastan. 1996. Recombinant immunotoxins specific for a mutant epidermal growth factor receptor: targeting with a single chain antibody variable domain isolated by phage display. *Proc Natl Acad Sci U S A* 93:14815-14820.

279. Archer, G.E., J.H. Sampson, I.A. Lorimer, R.E. McLendon, C.T. Kuan, A.H. Friedman, H.S. Friedman, I.H. Pastan, and D.D. Bigner. 1999. Regional treatment of epidermal growth factor receptor vIII-expressing neoplastic meningitis with a single-chain immunotoxin, MR-1. *Clin Cancer Res* 5:2646-2652.

280. Kuan, C.T., C.J. Reist, C.F. Foulon, I.A. Lorimer, G. Archer, C.N. Pegram, I. Pastan, M.R. Zalutsky, and D.D. Bigner. 1999. 125I-labeled anti-epidermal growth factor

receptor-vIII single-chain Fv exhibits specific and high-level targeting of glioma xenografts. *Clin Cancer Res* 5:1539-1549.

281. Lorimer, I.A., and S.J. Lavictoire. 2000. Targeting retrovirus to cancer cells expressing a mutant EGF receptor by insertion of a single chain antibody variable domain in the envelope glycoprotein receptor binding lobe. *J Immunol Methods* 237:147-157.

282. Snitkovsky, S., T.M. Niederman, B.S. Carter, R.C. Mulligan, and J.A. Young. 2000. A TVA-single-chain antibody fusion protein mediates specific targeting of a subgroup A avian leukosis virus vector to cells expressing a tumor-specific form of epidermal growth factor receptor. *J Virol* 74:9540-9545.

283. Beers, R., P. Chowdhury, D. Bigner, and I. Pastan. 2000. Immunotoxins with increased activity against epidermal growth factor receptor vIII-expressing cells produced by antibody phage display. *Clin Cancer Res* 6:2835-2843.

284. Kuan, C.T., C.J. Wikstrand, G. Archer, R. Beers, I. Pastan, M.R. Zalutsky, and D.D. Bigner. 2000. Increased binding affinity enhances targeting of glioma xenografts by EGFRvIII-specific scFv. *Int J Cancer* 88:962-969.

285. Theuer, C.P., R.J. Kreitman, D.J. FitzGerald, and I. Pastan. 1993. Immunotoxins made with a recombinant form of Pseudomonas exotoxin A that do not require proteolysis for activity. *Cancer Res* 53:340-347.

286. Brinkmann, U., L.H. Pai, D.J. FitzGerald, M. Willingham, and I. Pastan. 1991. B3(Fv)-PE38KDEL, a single-chain immunotoxin that causes complete regression of a human carcinoma in mice. *Proc Natl Acad Sci U S A* 88:8616-8620.

287. Humphrey, P.A., L.M. Gangarosa, A.J. Wong, G.E. Archer, M. Lund-Johansen, R. Bjerkvig, O.D. Laerum, H.S. Friedman, and D.D. Bigner. 1991. Deletion-mutant epidermal growth factor receptor in human gliomas: effects of type II mutation on receptor function. *Biochem Biophys Res Commun* 178:1413-1420.

288. Otwinowski, Z., and W. Minor. 1997. Processing of X-ray diffraction data collected in oscillation mode. Academic Press, London. 307-326 pp.

289. Fitzgerald, P.M.D. 1988. MERLOT, an integrated package of computer programs for the determination of crystal structures by molecular replacement. *J. Appl. Crystallog.* 21:273-278.

290. Brunger, A.T. 1990. Extension of molecular replacement: a new search strategy based on Patterson correlation refinement. *Acta Crystallogr A* 46:46-57.

291. Brunger, A.T. 1992. X-PLOR version 3.1 a system for X-ray crystallography and NMR. In Yale University Press, New Haven.

292. Brunger, A.T. 1993. X-PLOR Manual, Version 3.1. In Yale University Press, New Haven.

293. Evans, S.V., D.R. Rose, R. To, N.M. Young, and D.R. Bundle. 1994. Exploring the mimicry of polysaccharide antigens by anti-idiotypic antibodies. The crystallization, molecular replacement, and refinement to 2.8 A resolution of an idiotope-anti-idiotope Fab complex and of the unliganded anti-idiotope Fab. *J Mol Biol* 241:691-705.

294. Brunger, A.T., J. Kuriyan, and M. Karplus. 1987. Crystallographic R factor refinement by molecular dynamics. *Science* 235:458-460.

295. Jones, T.A. 1978. A graphics model building and refinement system for macromolecules. *J. Appl. Crystallog.* 11:268-272.

296. Jones, T.A. 1982. FRODO: a graphics fitting program for macromolecules. Clarendon Press, Oxford. 303-317 pp.

297. Trakhanov, S., S. Parkin, R. Raffai, R. Milne, Y.M. Newhouse, K.H. Weisgraber, and B. Rupp. 1999. Structure of a monoclonal 2E8 Fab antibody fragment specific for the low-density lipoprotein-receptor binding region of apolipoprotein E refined at 1.9 A. *Acta Crystallogr D Biol Crystallogr* 55:122-128.

298. van den Elsen, J., L. Vandeputte-Rutten, J. Kroon, and P. Gros. 1999. Bactericidal antibody recognition of meningococcal PorA by induced fit. Comparison of liganded and unliganded Fab structures. *J Biol Chem* 274:1495-1501.

299. Vasudevan, S., T. Tsuruo, and D.R. Rose. 1998. Mode of binding of anti-P-glycoprotein antibody MRK-16 to its antigen. A crystallographic and molecular modeling study. *J Biol Chem* 273:25413-25419.

300. Larson, S.B., J.S. Day, S. Glaser, G. Braslawsky, and A. McPherson. 2005. The structure of an antitumor C(H)2-domain-deleted humanized antibody. *J Mol Biol* 348:1177-1190.

301. Yu, B., and D.L. Caspar. 1998. Structure of cubic insulin crystals in glucose solutions. *Biophys J* 74:616-622.

302. Reiter, Y., and I. Pastan. 1996. Antibody engineering of recombinant Fv immunotoxins for improved targeting of cancer: disulfide-stabilized Fv immunotoxins. *Clin Cancer Res* 2:245-252.

303. Almog, O., I. Benhar, G. Vasmatzis, M. Tordova, B. Lee, I. Pastan, and G.L. Gilliland. 1998. Crystal structure of the disulfide-stabilized Fv fragment of anticancer antibody B1: conformational influence of an engineered disulfide bond. *Proteins* 31:128-138.

304. Mol, C.D., A.K. Muir, M. Cygler, J.S. Lee, and W.F. Anderson. 1994. Structure of an immunoglobulin Fab fragment specific for triple-stranded DNA. *J Biol Chem* 269:3615-3622.

305. Tulip, W.R., J.N. Varghese, W.G. Laver, R.G. Webster, and P.M. Colman. 1992. Refined crystal structure of the influenza virus N9 neuraminidase-NC41 Fab complex. *J Mol Biol* 227:122-148.

306. Braden, B.C., H. Souchon, J.L. Eisele, G.A. Bentley, T.N. Bhat, J. Navaza, and R.J. Poljak. 1994. Three-dimensional structures of the free and the antigen-complexed Fab from monoclonal anti-lysozyme antibody D44.1. *J Mol Biol* 243:767-781.

307. Prasad, L., E.B. Waygood, J.S. Lee, and L.T. Delbaere. 1998. The 2.5 A resolution structure of the jel42 Fab fragment/HPr complex. *J Mol Biol* 280:829-845.

308. Schulze-Gahmen, U., J.M. Rini, and I.A. Wilson. 1993. Detailed analysis of the free and bound conformations of an antibody. X-ray structures of Fab 17/9 and three different Fab-peptide complexes. *J Mol Biol* 234:1098-1118.

309. Churchill, M.E., E.A. Stura, C. Pinilla, J.R. Appel, R.A. Houghten, D.H. Kono, R.S. Balderas, G.G. Fieser, U. Schulze-Gahmen, and I.A. Wilson. 1994. Crystal structure of a peptide complex of anti-influenza peptide antibody Fab 26/9. Comparison of two different antibodies bound to the same peptide antigen. *J Mol Biol* 241:534-556.

310. Rini, J.M., R.L. Stanfield, E.A. Stura, P.A. Salinas, A.T. Profy, and I.A. Wilson. 1993. Crystal structure of a human immunodeficiency virus type 1 neutralizing antibody, 50.1, in complex with its V3 loop peptide antigen. *Proc Natl Acad Sci U S A* 90:6325-6329.

311. Shoham, M. 1993. Crystal structure of an anticholera toxin peptide complex at 2.3 A. *J Mol Biol* 232:1169-1175.

312. Wien, M.W., D.J. Filman, E.A. Stura, S. Guillot, F. Delpeyroux, R. Crainic, and J.M. Hogle. 1995. Structure of the complex between the Fab fragment of a neutralizing antibody for type 1 poliovirus and its viral epitope. *Nat Struct Biol* 2:232-243.

313. Shenbagamurthi, P., B. Kundu, S. Raths, J.M. Becker, and F. Naider. 1985. Biological activity and conformational isomerism in position 9 analogues of the des-1-tryptophan,3-beta-cyclohexylalanine-alpha-factor from Saccharomyces cerevisiae. *Biochemistry* 24:7070-7076.

314. Craig, L., P.C. Sanschagrin, A. Rozek, S. Lackie, L.A. Kuhn, and J.K. Scott. 1998. The role of structure in antibody cross-reactivity between peptides and folded proteins. *J Mol Biol* 281:183-201.

315. Karlsson, K.A. 1991. Glycobiology: a growing field for drug design. *Trends Pharmacol Sci* 12:265-272.

316. Dwek, R.A. 1996. Glycobiology: toward understanding the function of sugars. *Chem. Rev.* 96:683.

317. Svennerholm, L. 1963. Chromatographic Separation of Human Brain Gangliosides. *J Neurochem* 10:613-623.

318. Stults, C.L., C.C. Sweeley, and B.A. Macher. 1989. Glycosphingolipids: structure, biological source, and properties. *Methods Enzymol* 179:167-214.

319. Hakomori, S. 1985. Aberrant glycosylation in cancer cell membranes as focused on glycolipids: overview and perspectives. *Cancer Res* 45:2405-2414.

320. Ritter, G., and P.O. Livingston. 1991. Ganglioside antigens expressed by human cancer cells. *Semin Cancer Biol* 2:401-409.

321. Kiarash, A., B. Boyd, and C.A. Lingwood. 1994. Glycosphingolipid receptor function is modified by fatty acid content. Verotoxin 1 and verotoxin 2c preferentially recognize different globotriaosyl ceramide fatty acid homologues. *J Biol Chem* 269:11138-11146.

322. Lingwood, C.A. 1996. Aglycone modulation of glycolipid receptor function. *Glycoconj J* 13:495-503.

323. Nudelman, E., S. Hakomori, R. Kannagi, S. Levery, M.Y. Yeh, K.E. Hellstrom, and I. Hellstrom. 1982. Characterization of a human melanoma-associated ganglioside antigen defined by a monoclonal antibody, 4.2. *J Biol Chem* 257:12752-12756.

324. Zeng, G., L. Gao, and R.K. Yu. 2000. Reduced cell migration, tumor growth and experimental metastasis of rat F-11 cells whose expression of GD3-synthase is suppressed. *Int J Cancer* 88:53-57.

325. Tai, T., L.D. Cahan, T. Tsuchida, R.E. Saxton, R.F. Irie, and D.L. Morton. 1985. Immunogenicity of melanoma-associated gangliosides in cancer patients. *Int J Cancer* 35:607-612.

326. Tsuchida, T., M.H. Ravindranath, R.E. Saxton, and R.F. Irie. 1987. Gangliosides of human melanoma: altered expression in vivo and in vitro. *Cancer Res* 47:1278-1281.

327. Portoukalian, J., G. Zwingelstein, N. Abdul-Malak, and J.F. Dore. 1978. Alteration of gangliosides in plasma and red cells of humans bearing melanoma tumors. *Biochem Biophys Res Commun* 85:916-920.

328. Ravindranath, M.H., and D.L. Morton. 1991. Role of gangliosides in active immunotherapy with melanoma vaccine. *Int Rev Immunol* 7:303-329.

329. Mond, J.J., Q. Vos, A. Lees, and C.M. Snapper. 1995. T cell independent antigens. *Curr Opin Immunol* 7:349-354.

330. Stein, K.E. 1992. Thymus-independent and thymus-dependent responses to polysaccharide antigens. *J Infect Dis* 165 Suppl 1:S49-52.

331. Hakomori, S. 1984. Tumor-associated carbohydrate antigens. *Annu Rev Immunol* 2:103-126.

332. Livingston, P.O., M.J. Calves, and E.J. Natoli, Jr. 1987. Approaches to augmenting the immunogenicity of the ganglioside GM2 in mice: purified GM2 is superior to whole cells. *J Immunol* 138:1524-1529.

333. Hirabayashi, Y., H. Higashi, S. Kato, M. Taniguchi, and M. Matsumoto. 1987. Occurrence of tumor-associated ganglioside antigens with Hanganutziu-Deicher antigenic activity on human melanomas. *Jpn J Cancer Res* 78:614-620.

334. Li, S.C., S. Serizawa, Y.T. Li, K. Nakamura, and S. Handa. 1984. Effect of modification of sialic acid on enzymic hydrolysis of gangliosides GM1 and GM2. *J Biol Chem* 259:5409-5410.

335. Bosslet, K., H.D. Mennel, F. Rodden, B.L. Bauer, F. Wagner, A. Altmannsberger, H.H. Sedlacek, and H. Wiegandt. 1989. Monoclonal antibodies against epitopes on ganglioside GD2 and its lactones. Markers for gliomas and neuroblastomas. *Cancer Immunol Immunother* 29:171-178.

336. Dohi, T., G. Nores, and S. Hakomori. 1988. An IgG3 monoclonal antibody established after immunization with GM3 lactone: immunochemical specificity and inhibition of melanoma cell growth in vitro and in vivo. *Cancer Res* 48:5680-5685.

337. Tai, T., I. Kawashima, N. Tada, and S. Ikegami. 1988. Different reactivities of monoclonal antibodies to ganglioside lactones. *Biochim Biophys Acta* 958:134-138.

338. Livingston, P.O., G. Ragupathi, and C. Musselli. 2000. Autoimmune and antitumor consequences of antibodies against antigens shared by normal and malignant tissues. *J Clin Immunol* 20:85-93.

339. Pestronk, A., V. Chaudhry, E.L. Feldman, J.W. Griffin, D.R. Cornblath, E.H. Denys, M. Glasberg, R.W. Kuncl, R.K. Olney, and W.C. Yee. 1990. Lower motor neuron syndromes defined by patterns of weakness, nerve conduction abnormalities, and high titers of antiglycolipid antibodies. *Ann Neurol* 27:316-326.

340. Nobile-Orazio, E., M. Carpo, G. Legname, N. Meucci, S. Sonnino, and G. Scarlato. 1990. Anti-GM1 IgM antibodies in motor neuron disease and neuropathy. *Neurology* 40:1747-1750.

341. Chiba, A., S. Kusunoki, T. Shimizu, and I. Kanazawa. 1992. Serum IgG antibody to ganglioside GQ1b is a possible marker of Miller Fisher syndrome. *Ann Neurol* 31:677-679.

342. Arnon, R., E. Crisp, R. Kelley, G.W. Ellison, L.W. Myers, and W.W. Tourtellotte. 1980. Anti-ganglioside antibodies in multiple sclerosis. *J Neurol Sci* 46:179-186.

343. Hirano, T., H. Hashimoto, Y. Shiokawa, M. Iwamori, Y. Nagai, M. Kasai, Y. Ochiai, and K. Okumura. 1980. Antiglycolipid autoantibody detected in the sera from systemic lupus erythematosus patients. *J Clin Invest* 66:1437-1440.

344. Endo, T., D.D. Scott, S.S. Stewart, S.K. Kundu, and D.M. Marcus. 1984. Antibodies to glycosphingolipids in patients with multiple sclerosis and SLE. *J Immunol* 132:1793-1797.

345. Latov, N. 1990. Neuropathy and anti-GM1 antibodies. *Ann Neurol* 27 Suppl:S41-43.

346. Steck, A.J., and D. Adams. 1991. Motor neuron syndromes and monoclonal IgM antibodies to gangliosides. *Adv Neurol* 56:421-425.

347. Graus, F., C. Cordon-Cardo, A.N. Houghton, M.R. Melamed, and L.J. Old. 1984. Distribution of the ganglioside GD3 in the human nervous system detected by R24 mouse monoclonal antibody. *Brain Res* 324:190-194.

348. Bernhard, H., S. Roth, J. Bauerschmitz, K.H. Meyer zum Buschenfelde, and W. Dippold. 1992. Immunorecognition of different ganglioside epitopes on human normal and melanoma tissues. *Int J Cancer* 51:568-572.

349. Zhang, S., C. Cordon-Cardo, H.S. Zhang, V.E. Reuter, S. Adluri, W.B. Hamilton, K.O. Lloyd, and P.O. Livingston. 1997. Selection of tumor antigens as targets for immune attack using immunohistochemistry: I. Focus on gangliosides. *Int J Cancer* 73:42-49.

350. Dippold, W.G., H.P. Dienes, A. Knuth, and K.H. Meyer zum Buschenfelde. 1985. Immunohistochemical localization of ganglioside GD3 in human malignant melanoma, epithelial tumors, and normal tissues. *Cancer Res* 45:3699-3705.

351. Urmacher, C., C. Cordon-Cardo, and A.N. Houghton. 1989. Tissue distribution of GD3 ganglioside detected by mouse monoclonal antibody R24. *Am J Dermatopathol* 11:577-581.

352. Real, F.X., A.N. Houghton, A.P. Albino, C. Cordon-Cardo, M.R. Melamed, H.F. Oettgen, and L.J. Old. 1985. Surface antigens of melanomas and melanocytes defined by mouse monoclonal antibodies: specificity analysis and comparison of antigen expression in cultured cells and tissues. *Cancer Res* 45:4401-4411.

353. Carubia, J.M., R.K. Yu, L.J. Macala, J.M. Kirkwood, and J.M. Varga. 1984. Gangliosides of normal and neoplastic human melanocytes. *Biochem Biophys Res Commun* 120:500-504.

354. Hakomori, S. 1996. Tumor malignancy defined by aberrant glycosylation and sphingo(glyco)lipid metabolism. *Cancer Res* 56:5309-5318.

355. Hersey, P., S.D. Schibeci, P. Townsend, C. Burns, and D.A. Cheresh. 1986. Potentiation of lymphocyte responses by monoclonal antibodies to the ganglioside GD3. *Cancer Res* 46:6083-6090.

356. Hersey, P., O. Jamal, C. Henderson, I. Zardawi, and G. D'Alessandro. 1988. Expression of the gangliosides GM3, GD3 and GD2 in tissue sections of normal skin, naevi, primary and metastatic melanoma. *Int J Cancer* 41:336-343.

357. Hakomori, S., and R. Kannagi. 1983. Glycosphingolipids as tumor-associated and differentiation markers. *J Natl Cancer Inst* 71:231-251.

358. Skipski, V.P., C.O. Gitterman, J.S. Prendergast, K. Betit-Yen, G. Lee, S. Luell, and C.C. Stock. 1980. Possible relationship between glycosphingolipids and the formation of metastasis in certain human experimental tumors. *J Natl Cancer Inst* 65:249-256.

359. Ravindranath, M.H., D.L. Morton, and R.F. Irie. 1989. An epitope common to gangliosides O-acetyl-GD3 and GD3 recognized by antibodies in melanoma patients after active specific immunotherapy. *Cancer Res* 49:3891-3897.

360. Kageshita, T., T. Ono, S. Hirai, A. Yoshii, T. Kimura, H. Nakakuma, K. Horikawa, K. Takatsuki, and S. Ferrone. 1992. Ganglioside, adhesion molecule, and HLA antigen expression in basal cell carcinoma lesions. *Cancer Res* 52:3201-3207.

361. Zeng, G., L. Gao, S. Birkle, and R.K. Yu. 2000. Suppression of ganglioside GD3 expression in a rat F-11 tumor cell line reduces tumor growth, angiogenesis, and vascular endothelial growth factor production. *Cancer Res* 60:6670-6676.

362. Ravindranath, M.H., T. Tsuchida, D.L. Morton, and R.F. Irie. 1991. Ganglioside GM3:GD3 ratio as an index for the management of melanoma. *Cancer* 67:3029-3035.

363. Esselman, W.J., and H.C. Miller. 1977. Modulation of B cell responses by glycolipid released from antigen-stimulated T cells. *J Immunol* 119:1994-2000.

364. Krishnaraj, R., E.E. Lengle, and R.G. Kemp. 1982. Murine leukemia. Proposed role for gangliosides in immune suppression. *Eur J Cancer Clin Oncol* 18:89-98.

365. Merritt, W.D., J.M. Bailey, and D.H. Pluznik. 1984. Inhibition of interleukin-2-dependent cytotoxic T-lymphocyte growth by gangliosides. *Cell Immunol* 89:1-10.

366. Portoukalian, J., G. Zwingelstein, and J.F. Dore. 1979. Lipid composition of human malignant melanoma tumors at various levels of malignant growth. *Eur J Biochem* 94:19-23.

367. Dippold, W.G., K.O. Lloyd, L.T. Li, H. Ikeda, H.F. Oettgen, and L.J. Old. 1980. Cell surface antigens of human malignant melanoma: definition of six antigenic systems with mouse monoclonal antibodies. *Proc Natl Acad Sci U S A* 77:6114-6118.

368. Fuentes, R., R. Allman, and M.D. Mason. 1997. Ganglioside expression in lung cancer cell lines. *Lung Cancer* 18:21-33.

369. Merritt, W.D., M.B. Sztein, and G.H. Reaman. 1988. Detection of GD3 ganglioside in childhood acute lymphoblastic leukemia with monoclonal antibody to GD3: restriction to immunophenotypically defined T-cell disease. *J Cell Biochem* 37:11-19.

370. Merritt, W.D., J.T. Casper, S.J. Lauer, and G.H. Reaman. 1987. Expression of GD3 ganglioside in childhood T-cell lymphoblastic malignancies. *Cancer Res* 47:1724-1730.

371. Westrick, M.A., W.M. Lee, B. Goff, and B.A. Macher. 1983. Gangliosides of human acute leukemia cells. *Biochim Biophys Acta* 750:141-148.

372. Siddiqui, B., J. Buehler, M.W. DeGregorio, and B.A. Macher. 1984. Differential expression of ganglioside GD3 by human leukocytes and leukemia cells. *Cancer Res* 44:5262-5265.

373. Ritter, G., E. Boosfeld, R. Adluri, M. Calves, H.F. Oettgen, L.J. Old, and P. Livingston. 1991. Antibody response to immunization with ganglioside GD3 and GD3 congeners (lactones, amide and gangliosidol) in patients with malignant melanoma. *Int J Cancer* 48:379-385.

374. Pukel, C.S., K.O. Lloyd, L.R. Travassos, W.G. Dippold, H.F. Oettgen, and L.J. Old. 1982. GD3, a prominent ganglioside of human melanoma. Detection and characterisation by mouse monoclonal antibody. *J Exp Med* 155:1133-1147.

375. Ritter, G., E. Boosfeld, M.J. Calves, H.F. Oettgen, L.J. Old, and P.O. Livingston. 1990. Antibody response to immunization with purified GD3 ganglioside and GD3 derivatives (lactones, amide and gangliosidol) in the mouse. *Immunobiology* 182:32-43.

376. Yan, X., S.V. Evans, M.J. Kaminki, S.D. Gillies, R.A. Reisfeld, A.N. Houghton, and P.B. Chapman. 1996. Characterization of an Ig VH idiotope that results in specific homophilic binding and increased avidity for antigen. *J Immunol* 157:1582-1588.

377. Livingston, P.O., G. Ritter, and M.J. Calves. 1989. Antibody response after immunization with the gangliosides GM1, GM2, GM3, GD2 and GD3 in the mouse. *Cancer Immunol Immunother* 29:179-184.

378. Helling, F., A. Shang, M. Calves, S. Zhang, S. Ren, R.K. Yu, H.F. Oettgen, and P.O. Livingston. 1994. GD3 vaccines for melanoma: superior immunogenicity of keyhole limpet hemocyanin conjugate vaccines. *Cancer Res* 54:197-203.

379. Livingston, P.O. 1995. Approaches to augmenting the immunogenicity of melanoma gangliosides: from whole melanoma cells to ganglioside-KLH conjugate vaccines. *Immunol Rev* 145:147-166.

380. Thurin, J., M. Herlyn, O. Hindsgaul, N. Stromberg, K.A. Karlsson, D. Elder, Z. Steplewski, and H. Koprowski. 1985. Proton NMR and fast-atom bombardment mass spectrometry analysis of the melanoma-associated ganglioside 9-O-acetyl-GD3. *J Biol Chem* 260:14556-14563.

381. Heidenheim, M., E.R. Hansen, and O. Baadsgaard. 1995. CDW60, which identifies the acetylated form of GD3 gangliosides, is strongly expressed in human basal cell carcinoma. *Br J Dermatol* 133:392-397.

382. Haverkamp, J., R.W. Veh, M. Sander, R. Schauer, J.P. Kamerling, and J.G. Vliegenthart. 1977. Demonstration of 9-O-acetyl-N-acetylneuraminic acid in brain gangliosides from various vertebrates including man. *Hoppe Seylers Z Physiol Chem* 358:1609-1612.

383. Cheresh, D.A., R.A. Reisfeld, and A.P. Varki. 1984. O-acetylation of disialoganglioside GD3 by human melanoma cells creates a unique antigenic determinant. *Science* 225:844-846.

384. Ritter, G., E. Ritter-Boosfeld, R. Adluri, M. Calves, S. Ren, R.K. Yu, H.F. Oettgen, L.J. Old, and P.O. Livingston. 1995. Analysis of the antibody response to immunization with purified O-acetyl GD3 gangliosides in patients with malignant melanoma. *Int J Cancer* 62:668-672.

385. Chapman, P.B., M. Lonberg, and A.N. Houghton. 1990. Light chain variants of an IgG3 anti-GD3 monoclonal antibody and the relationship among avidity, effector functions, tumor targeting, and antitumor activity. *Cancer Res* 50:1503-1509.

386. Hedberg, K.M., B. Dellheden, C.J. Wikstrand, and P. Fredman. 2000. Monoclonal anti-GD3 antibodies selectively inhibit the proliferation of human malignant glioma cells in vitro. *Glycoconj J* 17:717-726.

387. Welte, K., G. Miller, P.B. Chapman, H. Yuasa, E. Natoli, J.E. Kunicka, C. Cordon-Cardo, C. Buhrer, L.J. Old, and A.N. Houghton. 1987. Stimulation of T lymphocyte proliferation by monoclonal antibodies against GD3 ganglioside. *J Immunol* 139:1763-1771.

388. Tai, T., I. Kawashima, K. Furukawa, and K.O. Lloyd. 1988. Monoclonal antibody R24 distinguishes between different N-acetyl- and N-glycolylneuraminic acid derivatives of ganglioside GD3. *Arch Biochem Biophys* 260:51-55.

389. Dippold, W.G., A. Knuth, and K.H. Meyer zum Buschenfelde. 1984. Inhibition of human melanoma cell growth in vitro by monoclonal anti-GD3-ganglioside antibody. *Cancer Res* 44:806-810.

390. Nasi, M.L., M. Meyers, P.O. Livingston, A.N. Houghton, and P.B. Chapman. 1997. Anti-melanoma effects of R24, a monoclonal antibody against GD3 ganglioside. *Melanoma Res* 7 Suppl 2:S155-162.

391. Houghton, A.N., D. Mintzer, C. Cordon-Cardo, S. Welt, B. Fliegel, S. Vadhan, E. Carswell, M.R. Melamed, H.F. Oettgen, and L.J. Old. 1985. Mouse monoclonal IgG3 antibody detecting GD3 ganglioside: a phase I trial in patients with malignant melanoma. *Proc Natl Acad Sci U S A* 82:1242-1246.

392. Bajorin, D.F., P.B. Chapman, G. Wong, D.G. Coit, J. Kunicka, J. Dimaggio, C. Cordon-Cardo, C. Urmacher, L. Dantes, M.A. Templeton, and et al. 1990. Phase I evaluation of a combination of monoclonal antibody R24 and interleukin 2 in patients with metastatic melanoma. *Cancer Res* 50:7490-7495.

393. Bajorin, D.F., P.B. Chapman, G.Y. Wong, B.V. Cody, C. Cordon-Cardo, L. Dantes, M.A. Templeton, D. Scheinberg, H.F. Oettgen, and A.N. Houghton. 1992. Treatment with high dose mouse monoclonal (anti-GD3) antibody R24 in patients with metastatic melanoma. *Melanoma Res* 2:355-362.

394. Caulfield, M.J., B. Barna, S. Murthy, R. Tubbs, J. Sergi, S. Medendorp, and R.M. Bukowski. 1990. Phase Ia-Ib trial of an anti-GD3 monoclonal antibody in combination with interferon-alpha in patients with malignant melanoma. *J Biol Response Mod* 9:319-328.

395. Bukowski, R.M., S.A. Murthy, J. Finke, M.J. Caulfield, R. Tubbs, P. Herzog, J. Stanley, M. Edinger, L. Tuason, D. McLain, and et al. 1994. Phase I trial of cisplatin, WR-2721, and the murine monoclonal antibody R24 in patients with metastatic melanoma: clinical and biologic effects. *J Immunother Emphasis Tumor Immunol* 15:273-282.

396. Chachoua, A., R. Oratz, L. Liebes, R.S. Alter, A. Felice, D. Peace, J. Vilcek, and R.H. Blum. 1994. Phase Ib trial of granulocyte-macrophage colony-stimulating factor combined with murine monoclonal antibody R24 in patients with metastatic melanoma. *J Immunother Emphasis Tumor Immunol* 16:132-141.

397. Minasian, L.M., T.P. Szatrowski, M. Rosenblum, T. Steffens, M.E. Morrison, P.B. Chapman, L. Williams, C.F. Nathan, and A.N. Houghton. 1994. Hemorrhagic tumor necrosis during a pilot trial of tumor necrosis factor-alpha and anti-GD3 ganglioside monoclonal antibody in patients with metastatic melanoma. *Blood* 83:56-64.

398. Minasian, L.M., T.J. Yao, T.A. Steffens, D.A. Scheinberg, L. Williams, E. Riedel, A.N. Houghton, and P.B. Chapman. 1995. A phase I study of anti-GD3 ganglioside monoclonal antibody R24 and recombinant human macrophage-colony stimulating factor in patients with metastatic melanoma. *Cancer* 75:2251-2257.

399. Soiffer, R.J., P.B. Chapman, C. Murray, L. Williams, P. Unger, H. Collins, A.N. Houghton, and J. Ritz. 1997. Administration of R24 monoclonal antibody and low-dose interleukin 2 for malignant melanoma. *Clin Cancer Res* 3:17-24.

400. Kirkwood, J.M., R.A. Mascari, H.D. Edington, M.S. Rabkin, R.S. Day, T.L. Whiteside, D.R. Vlock, and J.M. Shipe-Spotloe. 2000. Analysis of therapeutic and

immunologic effects of R(24) anti-GD3 monoclonal antibody in 37 patients with metastatic melanoma. *Cancer* 88:2693-2702.

401. Steffens, T.A., D.F. Bajorin, and A.N. Houghton. 1992. Immunotherapy with monoclonal antibodies in metastatic melanoma. *World J Surg* 16:261-269.

402. Raymond, J., J.M. Kirkwood, D.R. Vlock, M.S. Rabkin, R.S. Day, T.L. Whiteside, R. Herberman, R.A. Mascari, and B. Simon. 1991. *Proc. Am. Soc. Clin. Oncol.* 10:298.

403. Creekmore, S., W. Urba, W. Kopp, C. Ewel, T. Hecht, J. Smith, J. Janik, R. Steis, R. Fenton, W. Sharfman, K. Conlon, M. Sznol, J. Holmlund, B. Curti, B. Gause, M. Houck, J. Beveridge, M. Jones, and D. Longo. 1992. Phase IB/II trial of R24 antibody and interleukin-2 (IL-2) in melanoma. *Proc. Annu. Meet. Am. Soc. Clin. Oncol.* 11:A1186.

404. Jurcic, J.G., D.A. Scheinberg, and A.N. Houghton. 1997. Monoclonal antibody therapy of cancer. *Cancer Chemother Biol Response Modif* 17:195-216.

405. Vadhan-Raj, S., C. Cordon-Cardo, E. Carswell, D. Mintzer, L. Dantis, C. Duteau, M.A. Templeton, H.F. Oettgen, L.J. Old, and A.N. Houghton. 1988. Phase I trial of a mouse monoclonal antibody against GD3 ganglioside in patients with melanoma: induction of inflammatory responses at tumor sites. *J Clin Oncol* 6:1636-1648.

406. Chapman, P.B., S.D. Gillies, A.N. Houghton, and R.M. Reilly. 1994. Mapping effector functions of a monoclonal antibody to GD3 by characterization of a mouse-human chimeric antibody. *Cancer Immunol Immunother* 39:198-204.

407. Chapman, P.B., H. Yuasa, and A.N. Houghton. 1990. Homophilic binding of mouse monoclonal antibodies against GD3 ganglioside. *J Immunol* 145:891-898.

408. Kaminski, M.J., C.R. MacKenzie, M.J. Mooibroek, T.E. Dahms, T. Hirama, A.N. Houghton, P.B. Chapman, and S.V. Evans. 1999. The role of homophilic binding in anti-tumor antibody R24 recognition of molecular surfaces. Demonstration of an intermolecular beta-sheet interaction between vh domains. *J Biol Chem* 274:5597-5604.

409. Durrant, L.G., M. Doran, E.B. Austin, and R.A. Robins. 1995. Induction of cellular immune responses by a murine monoclonal anti-idiotypic antibody recognizing the 791Tgp72 antigen expressed on colorectal, gastric and ovarian human tumours. *Int J Cancer* 61:62-66.

410. Mittelman, A., Z.J. Chen, C.C. Liu, S. Hirai, and S. Ferrone. 1994. Kinetics of the immune response and regression of metastatic lesions following development of humoral anti-high molecular weight-melanoma associated antigen immunity in three patients with advanced malignant melanoma immunized with mouse antiidiotypic monoclonal antibody MK2-23. *Cancer Res* 54:415-421.

411. Chapman, P.B., and A.N. Houghton. 1991. Induction of IgG antibodies against GD3 ganglioside in rabbits by an anti-idiotypic monoclonal antibody. *J Clin Invest* 88:186-192.

412. Chapman, P.B., L. Williams, N. Salibi, W.J. Hwu, S.E. Krown, and P.O. Livingston. 2004. A phase II trial comparing five dose levels of BEC2 anti-idiotypic monoclonal antibody vaccine that mimics GD3 ganglioside. *Vaccine* 22:2904-2909.

413. Chapman, P.B., P. Livingston, M.E. Morrison, L. Williams, and A.N. Houghton. 1994. Immunization of melanoma patients with anti-idiotypic monoclonal antibody BEC2 which mimics GD3 ganglioside: pilot trials using no immunological adjuvant. *Vaccine Research* 3:59-69.

414. Chapman, P.B., M. McCaffery, K. Zuklys, N. Giorgio, and A.N. Houghton. 1995. Immunization with BEC2 anti-idiotypic monoclonal antibody that mimics GD3 ganglioside: superiority of the intravenous route. *Proc. Am. Assoc. Cancer Res.* 36:493.

415. McCaffery, M., T.J. Yao, L. Williams, P.O. Livingston, A.N. Houghton, and P.B. Chapman. 1996. Immunization of melanoma patients with BEC2 anti-idiotypic monoclonal antibody that mimics GD3 ganglioside: enhanced immunogenicity when combined with adjuvant. *Clin Cancer Res* 2:679-686.

416. Grant, S.C., M.G. Kris, A.N. Houghton, and P.B. Chapman. 1999. Long survival of patients with small cell lung cancer after adjuvant treatment with the anti-idiotypic antibody BEC2 plus Bacillus Calmette-Guerin. *Clin Cancer Res* 5:1319-1323.

417. Yao, T.J., M. Meyers, P.O. Livingston, A.N. Houghton, and P.B. Chapman. 1999. Immunization of melanoma patients with BEC2-keyhole limpet hemocyanin plus BCG intradermally followed by intravenous booster immunizations with BEC2 to induce anti-GD3 ganglioside antibodies. *Clin Cancer Res* 5:77-81.

418. Giaccone, G., C. Debruyne, E. Felip, P.B. Chapman, S.C. Grant, M. Millward, L. Thiberville, G. D'Addario, C. Coens, L.S. Rome, P. Zatloukal, O. Masso, and C. Legrand. 2005. Phase III study of adjuvant vaccination with Bec2/bacille Calmette-Guerin in responding patients with limited-disease small-cell lung cancer (European Organisation for Research and Treatment of Cancer 08971-08971B; Silva Study). *J Clin Oncol* 23:6854-6864.

419. Pellizzari, A., H. Pang, and C.A. Lingwood. 1992. Binding of verocytotoxin 1 to its receptor is influenced by differences in receptor fatty acid content. *Biochemistry* 31:1363-1370.

420. Tur, M.K., M. Huhn, S. Sasse, A. Engert, and S. Barth. 2001. Selection of scFv phages on intact cells under low pH conditions leads to a significant loss of insert-free phages. *Biotechniques* 30:404-408, 410, 412-403.

421. Narang, S.A., F.L. Yao, J.J. Michniewicz, G. Dubuc, J. Phipps, and R.L. Somorjai. 1987. Hierarchical strategy for protein folding and design: synthesis and expression of T4 lysozyme gene and two putative folding mutants. *Protein Eng* 1:481-485.

422. Anand, N.N., S. Mandal, C.R. MacKenzie, J. Sadowska, B. Sigurskjold, N.M. Young, D.R. Bundle, and S.A. Narang. 1991. Bacterial expression and secretion of various single-chain Fv genes encoding proteins specific for a Salmonella serotype B O-antigen. *J Biol Chem* 266:21874-21879.

423. Shan, L., and D.J. Anderson. 2001. Effect of buffer concentration on gradient chromatofocusing performance separating protiens on a high-performance DEAE column. *J Chromatogr A* 909:191-205.

424. Horton, R.M., H.D. Hunt, S.N. Ho, J.K. Pullen, and L.R. Pease. 1989. Engineering hybrid genes without the use of restriction enzymes: gene splicing by overlap extension. *Gene* 77:61-68.

425. Ho, S.N., H.D. Hunt, R.M. Horton, J.K. Pullen, and L.R. Pease. 1989. Site-directed mutagenesis by overlap extension using the polymerase chain reaction. *Gene* 77:51-59.

426. Cupit, P.M., J.A. Whyte, A.J. Porter, M.J. Browne, S.D. Holmes, W.J. Harris, and C. Cunningham. 1999. Cloning and expression of single chain antibody fragments in Escherichia coli and Pichia pastoris. *Lett Appl Microbiol* 29:273-277.

427. Somerville, J.E., Jr., S.C. Goshorn, H.P. Fell, and R.P. Darveau. 1994. Bacterial aspects associated with the expression of a single-chain antibody fragment in Escherichia coli. *Appl Microbiol Biotechnol* 42:595-603.

428. Weidner, K.M., L.K. Denzin, and E.W. Voss, Jr. 1992. Molecular stabilization effects of interactions between anti-metatype antibodies and liganded antibody. *J Biol Chem* 267:10281-10288.

429. Muyldermans, S., C. Cambillau, and L. Wyns. 2001. Recognition of antigens by single-domain antibody fragments: the superfluous luxury of paired domains. *Trends Biochem Sci* 26:230-235.

430. Adey, N.B., A.H. Mataragnon, J.E. Rider, J.M. Carter, and B.K. Kay. 1995. Characterization of phage that bind plastic from phage-displayed random peptide libraries. *Gene* 156:27-31.

431. Harmsen, M.M., R.C. Ruuls, I.J. Nijman, T.A. Niewold, L.G. Frenken, and B. de Geus. 2000. Llama heavy-chain V regions consist of at least four distinct subfamilies revealing novel sequence features. *Mol Immunol* 37:579-590.

432. Conrath, K.E., U. Wernery, S. Muyldermans, and V.K. Nguyen. 2003. Emergence and evolution of functional heavy-chain antibodies in Camelidae. *Dev Comp Immunol* 27:87-103.

433. Vu, K.B., M.A. Ghahroudi, L. Wyns, and S. Muyldermans. 1997. Comparison of llama VH sequences from conventional and heavy chain antibodies. *Mol Immunol* 34:1121-1131.

434. Sheets, M.D., P. Amersdorfer, R. Finnern, P. Sargent, E. Lindquist, R. Schier, G. Hemingsen, C. Wong, J.C. Gerhart, and J.D. Marks. 1998. Efficient construction of a large nonimmune phage antibody library: the production of high-affinity human single-chain antibodies to protein antigens. *Proc Natl Acad Sci U S A* 95:6157-6162.

435. Schier, R., A. McCall, G.P. Adams, K.W. Marshall, H. Merritt, M. Yim, R.S. Crawford, L.M. Weiner, C. Marks, and J.D. Marks. 1996. Isolation of picomolar affinity anti-c-erbB-2 single-chain Fv by molecular evolution of the complementarity determining regions in the center of the antibody binding site. *J Mol Biol* 263:551-567.

436. Pereira, S., P. Van Belle, D. Elder, H. Maruyama, L. Jacob, M. Sivanandham, M. Wallack, D. Siegel, and D. Herlyn. 1997. Combinatorial antibodies against human malignant melanoma. *Hybridoma* 16:11-16.

437. Watters, J.M., P. Telleman, and R.P. Junghans. 1997. An optimized method for cell-based phage display panning. *Immunotechnology* 3:21-29.

438. Griffiths, A.D., S.C. Williams, O. Hartley, I.M. Tomlinson, P. Waterhouse, W.L. Crosby, R.E. Kontermann, P.T. Jones, N.M. Low, T.J. Allison, and et al. 1994. Isolation of high affinity human antibodies directly from large synthetic repertoires. *Embo J* 13:3245-3260.

439. Vaughan, T.J., A.J. Williams, K. Pritchard, J.K. Osbourn, A.R. Pope, J.C. Earnshaw, J. McCafferty, R.A. Hodits, J. Wilton, and K.S. Johnson. 1996. Human antibodies with sub-nanomolar affinities isolated from a large non-immunized phage display library. *Nat Biotechnol* 14:309-314.

440. Mao, S., C. Gao, C.H. Lo, P. Wirsching, C.H. Wong, and K.D. Janda. 1999. Phage-display library selection of high-affinity human single-chain antibodies to tumor-associated carbohydrate antigens sialyl Lewisx and Lewisx. *Proc Natl Acad Sci U S A* 96:6953-6958.

441. Becerril, B., M.A. Poul, and J.D. Marks. 1999. Toward selection of internalizing antibodies from phage libraries. *Biochem Biophys Res Commun* 255:386-393.

442. Poul, M.A., B. Becerril, U.B. Nielsen, P. Morisson, and J.D. Marks. 2000. Selection of tumor-specific internalizing human antibodies from phage libraries. *J Mol Biol* 301:1149-1161.

443. Awdeh, Z.L., A.R. Williamson, and B.A. Askonas. 1970. One cell-one immunoglobulin. Origin of limited heterogeneity of myeloma proteins. *Biochem J* 116:241-248.

444. Wenisch, E., S. Reiter, S. Hinger, F. Steindl, C. Tauer, A. Jungbauer, H. Katinger, and P.G. Righetti. 1990. Shifts of isoelectric points between cellular and secreted antibodies as revealed by isoelectric focusing and immobilized pH gradients. *Electrophoresis* 11:966-969.

445. Tsai, P.K., M.W. Bruner, J.I. Irwin, C.C. Ip, C.N. Oliver, R.W. Nelson, D.B. Volkin, and C.R. Middaugh. 1993. Origin of the isoelectric heterogeneity of monoclonal immunoglobulin h1B4. *Pharm Res* 10:1580-1586.

446. Mimura, Y., E.A. Kabat, T. Tanaka, M. Fujimoto, K. Takeo, and K. Nakamura. 1995. Microheterogeneity of mouse antidextran monoclonal antibodies. *Electrophoresis* 16:116-123.

447. Harris, W.J. 1995. Production of humanized monoclonal antibodies for in vivo imaging and therapy. *Biochem Soc Trans* 23:1035-1038.

448. Moorhouse, K.G., W. Nashabeh, J. Deveney, N.S. Bjork, M.G. Mulkerrin, and T. Ryskamp. 1997. Validation of an HPLC method for the analysis of the charge heterogeneity of the recombinant monoclonal antibody IDEC-C2B8 after papain digestion. *J Pharm Biomed Anal* 16:593-603.

449. Kroon, D.J., A. Baldwin-Ferro, and P. Lalan. 1992. Identification of sites of degradation in a therapeutic monoclonal antibody by peptide mapping. *Pharm Res* 9:1386-1393.

450. Coleman, L., and S.M. Mahler. 2003. Purification of Fab fragments from a monoclonal antibody papain digest by Gradiflow electrophoresis. *Protein Expr Purif* 32:246-251.

451. Regnier, F.E. 1987. The role of protein structure in chromatographic behavior. *Science* 238:319-323.

452. Stone, G.C., U. Sjobring, L. Bjorck, J. Sjoquist, C.V. Barber, and F.A. Nardella. 1989. The Fc binding site for streptococcal protein G is in the C gamma 2-C gamma 3 interface region of IgG and is related to the sites that bind staphylococcal protein A and human rheumatoid factors. *J Immunol* 143:565-570.

453. Deisenhofer, J. 1981. Crystallographic refinement and atomic models of a human Fc fragment and its complex with fragment B of protein A from Staphylococcus aureus at 2.9- and 2.8-A resolution. *Biochemistry* 20:2361-2370.

454. Sauer-Eriksson, A.E., G.J. Kleywegt, M. Uhlen, and T.A. Jones. 1995. Crystal structure of the C2 fragment of streptococcal protein G in complex with the Fc domain of human IgG. *Structure* 3:265-278.

455. Bjorck, L. 1988. Protein L. A novel bacterial cell wall protein with affinity for Ig L chains. *J Immunol* 140:1194-1197.

456. Akerstrom, B., and L. Bjorck. 1989. Protein L: an immunoglobulin light chain-binding bacterial protein. Characterization of binding and physicochemical properties. *J Biol Chem* 264:19740-19746.

457. Nilson, B.H., A. Solomon, L. Bjorck, and B. Akerstrom. 1992. Protein L from Peptostreptococcus magnus binds to the kappa light chain variable domain. *J Biol Chem* 267:2234-2239.

458. Porath, J., and B. Olin. 1983. Immobilized metal ion affinity adsorption and immobilized metal ion affinity chromatography of biomaterials. Serum protein affinities for gel-immobilized iron and nickel ions. *Biochemistry* 22:1621-1630.

459. Hale, J.E., and D.E. Beidler. 1994. Purification of humanized murine and murine monoclonal antibodies using immobilized metal-affinity chromatography. *Anal Biochem* 222:29-33.

460. Abe, N., and K. Inouye. 1993. Purification of monoclonal antibodies with light-chain heterogeneity produced by mouse hybridomas raised with NS-1 myelomas: application of hydrophobic interaction high-performance liquid chromatography. *J Biochem Biophys Methods* 27:215-227.

461. Qiu, J.X., M. Kai, E.A. Padlan, and D.M. Marcus. 1999. Structure-function studies of an anti-asialo GM1 antibody obtained from a phage display library. *J Neuroimmunol* 97:172-181.

462. Davies, J., and L. Riechmann. 1996. Single antibody domains as small recognition units: design and in vitro antigen selection of camelized, human VH domains with improved protein stability. *Protein Eng* 9:531-537.

463. Davies, J., and L. Riechmann. 1995. Antibody VH domains as small recognition units. *Biotechnology (N Y)* 13:475-479.

464. Riechmann, L. 1996. Rearrangement of the former VL interface in the solution structure of a camelised, single antibody VH domain. *J Mol Biol* 259:957-969.

465. Kortt, A.A., R.E. Guthrie, M.G. Hinds, B.E. Power, N. Ivancic, J.B. Caldwell, L.C. Gruen, R.S. Norton, and P.J. Hudson. 1995. Solution properties of Escherichia coli-expressed VH domain of anti-neuraminidase antibody NC41. *J Protein Chem* 14:167-178.

466. Voordijk, S., T. Hansson, D. Hilvert, and W.F. van Gunsteren. 2000. Molecular dynamics simulations highlight mobile regions in proteins: A novel suggestion for converting a murine V(H) domain into a more tractable species. *J Mol Biol* 300:963-973.

467. Hashimoto, Y., T. Ikenaga, K. Tanigawa, T. Ueda, I. Ezak, and T. Imoto. 2000. Expression and characterization of human rheumatoid factor single-chain Fv. *Biol Pharm Bull* 23:941-945.

468. Zdanov, A., Y. Li, D.R. Bundle, S.J. Deng, C.R. MacKenzie, S.A. Narang, N.M. Young, and M. Cygler. 1994. Structure of a single-chain antibody variable domain (Fv) fragment complexed with a carbohydrate antigen at 1.7-A resolution. *Proc Natl Acad Sci U S A* 91:6423-6427.

469. Clare, J.J., F.B. Rayment, S.P. Ballantine, K. Sreekrishna, and M.A. Romanos. 1991. High-level expression of tetanus toxin fragment C in Pichia pastoris strains containing multiple tandem integrations of the gene. *Biotechnology (N Y)* 9:455-460.

470. Clare, J.J., M.A. Romanos, F.B. Rayment, J.E. Rowedder, M.A. Smith, M.M. Payne, K. Sreekrishna, and C.A. Henwood. 1991. Production of mouse epidermal growth factor in yeast: high-level secretion using Pichia pastoris strains containing multiple gene copies. *Gene* 105:205-212.

471. Luo, D., N. Mah, M. Krantz, K. Wilde, D. Wishart, Y. Zhang, F. Jacobs, and L. Martin. 1995. Vl-linker-Vh orientation-dependent expression of single chain Fv-containing an engineered disulfide-stabilized bond in the framework regions. *J Biochem (Tokyo)* 118:825-831.

472. Luo, D., N. Mah, D. Wishart, Y. Zhang, F. Jacobs, and L. Martin. 1996. Construction and expression of bi-functional proteins of single-chain Fv with effector domains. *J Biochem (Tokyo)* 120:229-232.

473. Gram, H., R. Schmitz, and R. Ridder. 1998. Secretion of scFv antibody fragments. *Methods Mol Biol* 103:179-192.

474. Shi, X., T. Karkut, M. Chamankhah, M. Alting-Mees, S.M. Hemmingsen, and D. Hegedus. 2003. Optimal conditions for the expression of a single-chain antibody (scFv) gene in Pichia pastoris. *Protein Expr Purif* 28:321-330.

475. Zhang, W., M.A. Bevins, B.A. Plantz, L.A. Smith, and M.M. Meagher. 2000. Modeling Pichia pastoris growth on methanol and optimizing the production of a recombinant protein, the heavy-chain fragment C of botulinum neurotoxin, serotype A. *Biotechnol Bioeng* 70:1-8.

476. Tsumoto, K., Y. Nakaoki, Y. Ueda, K. Ogasahara, K. Yutani, K. Watanabe, and I. Kumagai. 1994. Effect of the order of antibody variable regions on the expression of the single-chain HyHEL10 Fv fragment in E. coli and the thermodynamic analysis of its antigen-binding properties. *Biochem Biophys Res Commun* 201:546-551.

477. Kipriyanov, S.M., S. Dubel, F. Breitling, R.E. Kontermann, and M. Little. 1994. Recombinant single-chain Fv fragments carrying C-terminal cysteine residues: production of bivalent and biotinylated miniantibodies. *Mol Immunol* 31:1047-1058.

478. Kelley, R.F., M.P. O'Connell, P. Carter, L. Presta, C. Eigenbrot, M. Covarrubias, B. Snedecor, J.H. Bourell, and D. Vetterlein. 1992. Antigen binding thermodynamics and antiproliferative effects of chimeric and humanized anti-p185HER2 antibody Fab fragments. *Biochemistry* 31:5434-5441.

479. Worn, A., and A. Pluckthun. 1998. Mutual stabilization of VL and VH in single-chain antibody fragments, investigated with mutants engineered for stability. *Biochemistry* 37:13120-13127.

480. Pantoliano, M.W., R.E. Bird, S. Johnson, E.D. Asel, S.W. Dodd, J.F. Wood, and K.D. Hardman. 1991. Conformational stability, folding, and ligand-binding affinity of single-chain Fv immunoglobulin fragments expressed in Escherichia coli. *Biochemistry* 30:10117-10125.

481. Freund, C., A. Ross, B. Guth, A. Pluckthun, and T.A. Holak. 1993. Characterization of the linker peptide of the single-chain Fv fragment of an antibody by NMR spectroscopy. *FEBS Lett* 320:97-100.

482. Buchner, J., M. Renner, H. Lilie, H.J. Hinz, R. Jaenicke, T. Kiefhabel, and R. Rudolph. 1991. Alternatively folded states of an immunoglobulin. *Biochemistry* 30:6922-6929.

483. Skerra, A. 1993. Bacterial expression of immunoglobulin fragments. *Curr Opin Immunol* 5:256-262.

484. Jung, S., and A. Pluckthun. 1997. Improving in vivo folding and stability of a single-chain Fv antibody fragment by loop grafting. *Protein Eng* 10:959-966.

485. Martineau, P., P. Jones, and G. Winter. 1998. Expression of an antibody fragment at high levels in the bacterial cytoplasm. *J Mol Biol* 280:117-127.

486. Jermutus, L., A. Honegger, F. Schwesinger, J. Hanes, and A. Pluckthun. 2001. Tailoring in vitro evolution for protein affinity or stability. *Proc Natl Acad Sci U S A* 98:75-80.

487. Rojas, G., A. Talavera, Y. Munoz, E. Rengifo, U. Krengel, J. Angstrom, J. Gavilondo, and E. Moreno. 2004. Light-chain shuffling results in successful phage display selection of functional prokaryotic-expressed antibody fragments to N-glycolyl GM3 ganglioside. *J Immunol Methods* 293:71-83.

488. Eastlund, T. 1998. The histo-blood group ABO system and tissue transplantation. *Transfusion* 38:975-988.

489. Clausen, H., and S. Hakomori. 1989. ABH and related histo-blood group antigens; immunochemical differences in carrier isotypes and their distribution. *Vox Sang* 56:1-20.

490. Oriol, R., J. Le Pendu, and R. Mollicone. 1986. Genetics of ABO, H, Lewis, X and related antigens. *Vox Sang* 51:161-171.

491. Oriol, R., R. Mollicone, P. Coullin, A.M. Dalix, and J.J. Candelier. 1992. Genetic regulation of the expression of ABH and Lewis antigens in tissues. *APMIS Suppl* 27:28-38.

492. Davidsohn, I., and R. Stejskal. 1972. Tissue antigens A, B and H in health and disease. *Haematologia (Budap)* 6:177-184.

493. Feizi, T. 1985. Demonstration by monoclonal antibodies that carbohydrate structures of glycoproteins and glycolipids are onco-developmental antigens. *Nature* 314:53-57.

494. Singhal, A., and S. Hakomori. 1990. Molecular changes in carbohydrate antigens associated with cancer. *Bioessays* 12:223-230.

495. Landsteiner, K. 1900. Zur Kenntniss der antifermentativen, lytischen und agglutinierenden Wikungen des Blutserums und der Lymphe. *Zentbl. Bakt. Parasitkde* 27:357-366.

496. Landsteiner, K. 1901. Uber Agglunationserscheinungen normalen menschlichen Blutes. *Wein. Klin. Wschr* 14:1132-1134.

497. von Descatello, A., and A. Sturli. 1902. Uber die isoagglutinine im serum gesunder und kranker Menschen. *Munchen Medicine Wchnschr* 49:1090-1095.

498. Eisler, M. 1930. Uber ein gemeinsames, Antigen in den Zellen des Menschen und in Shigabazillen. *Zeitscrift fur Immunforsch* 6:38.

499. Schiff, F. 1927. Uber den serologischen Nachweis der Blutgruppeneigenschaft O. *Klin. Wschr* 6:303.

500. Schiff, F. 1934. *Zeitscrift fur Immunitatsforsch* 82:302.

501. Witebsy, E., and N.C. Klendsshoj. 1941. The isolation of an O specific substance from gastric juice of secretors and carbohydrate-like substances from gastric juice of non-secretors. *Journal of Experimental Medicine* 73:655-667.

502. Morgan, W.T., and W.M. Watkins. 1948. The detection of a product of the blood group O gene and the relationship of the so-called O-substance to the agglutinogens A and B. *British Journal of Experimental Pathology* 29:159-173.

503. Landsteiner, K., and J. van der Scheer. 1925. On the antigens of red blood corpuscles. II. Flocculation reactions with alcoholic extracts of erythrocytes. *Journal of Experimental Medicine* 42:123-142.

504. Morgan, W.T., and W.M. Watkins. 1953. The inhibition of the haemagglutinins in plant seeds by human blood group substances and simple sugars. *British Journal of Experimental Pathology* 34:94-103.

505. Watkins, W.M., and W.T. Morgan. 1955. Inhibition by simple sugars of enzymes which decompose blood-group substances. *Nature* 175:676-677.

506. Watkins, W.M., and W.T. Morgan. 1957. Specific inhibition studies relating to the Lewis blood group system. *Nature* 180:1038-1040.

507. Kabat, E.A. 1956. Blood Group Substances. Their Chemistry and Immunochemistry. Academic Press, New York.

508. Morgan, W.T., and W.M. Watkins. 1969. Genetic and biochemical aspects of human blood-group A-, B-, H-, Le-a- and Le-b-specificity. *Br Med Bull* 25:30-34.

509. Kabat, E.A. 1973. Immunochemical studies on the carbohydrate moiety of water-soluble blood group A, B, H, Lea, and Leb substances and their precursor I antigens. In Carbohydrates in solution. American Chemical Society, Washington. 334-361.

510. Ceppelllini, R. 1959. Physiological genetics of human blood group factors. In Ciba Foundation Symposium on Biochemistry of Human Genetics. Little Brown and Co, Boston. 242-263.

511. Tuppy, H., and W.L. Staudenbauer. 1966. Microsomal incorporation of N-acetyl-D-galactosamine into blood group substance. *Nature* 210:316-317.

512. Abdelfattah-Gad, M., and H. Denk. 1980. Epithelial blood group antigens in human carcinomas of the distal colon: further studies on their pathologic significance. *J Natl Cancer Inst* 64:1025-1028.

513. Eckhardt, A.E., and I.J. Goldstein. 1983. Isolation and characterization of a family of alpha-D-galactosyl-containing glycopeptides from Ehrlich ascites tumor cells. *Biochemistry* 22:5290-5297.

514. Orntoft, T.F., P. Meldgaard, B. Pedersen, and H. Wolf. 1996. The blood group ABO gene transcript is down-regulated in human bladder tumors and growth-stimulated urothelial cell lines. *Cancer Res* 56:1031-1036.

515. Hakkinen, I. 1970. A-like blood group antigen in gastric cancer cells of patients in blood groups Q or B. *J Natl Cancer Inst* 44:1183-1193.

516. Denk, H., G. Tappeiner, and J.H. Holzner. 1974. Independent behaviour of blood group A- and B-like activities in gastric carcinomata of blood group AB individuals. *Nature* 248:428-430.

517. Kapadia, A., T. Feizi, D. Jewell, J. Keeling, and G. Slavin. 1981. Immunocytochemical studies of blood group A, H, I, and i antigens in gastric mucosae of infants with normal gastric histology and of patients with gastric carcinoma and chronic benign peptic ulceration. *J Clin Pathol* 34:320-337.

518. Breimer, M.E. 1980. Adaptation of mass spectrometry for the analysis of tumor antigens as applied to blood group glycolipids of a human gastric carcinoma. *Cancer Res* 40:897-908.

519. Koster, T., A.D. Blann, E. Briet, J.P. Vandenbroucke, and F.R. Rosendaal. 1995. Role of clotting factor VIII in effect of von Willebrand factor on occurrence of deep-vein thrombosis. *Lancet* 345:152-155.

520. Medalie, J.H., C. Levene, C. Papier, U. Goldbourt, F. Dreyfuss, D. Oron, H. Neufeld, and E. Riss. 1971. Blood groups, myocardial infarction and angina pectoris among 10,000 adult males. *N Engl J Med* 285:1348-1353.

521. Meade, T.W., J.A. Cooper, Y. Stirling, D.J. Howarth, V. Ruddock, and G.J. Miller. 1994. Factor VIII, ABO blood group and the incidence of ischaemic heart disease. *Br J Haematol* 88:601-607.

522. Epstein, A., and R. Ottenberg. 1908. Simple method of performing serum reactions. *Proc NY Pathology Society* 8:117-123.

523. von Dungern, E., and L. Hirszfeld. 1910. Uber Vererbung gruppenspezifischer Strukturen des Blutes. *Zeitscrift fur Immunforsch* 6:284-292.

524. Furuhata, T. 1927. On the heredity of human blood groups. *Japan Med. World* 7:197-209.

525. Dupont, M. 1934. Contribution a l'etude des antigenes des globules rouges. *Arch of Int. Med. Exp.* 9:133-167.

526. Springer, G.F. 1958. Relation of blood group active plant substances to human blood groups. *Acta Haematologica* 20:147-155.

527. Springer, G.F., P. Williamson, and W.C. Brandes. 1961. Blood group activity of Gram-negative bacteria. *Journal of Experimental Medicine* 113:1077.

528. Watkins, W.M., and W.T. Morgan. 1959. Possible genetical pathways for the biosynthesis of blood group mucopolysaccharides. *Vox Sang* 4:97-119.

529. Watkins, W.M. 1966. Blood-group substances. *Science* 152:172-181.

530. Bernstein, F. 1924. Ergebnisse einer biostatischen zusammenfassenden Betrachtung uber die erblichen Blutstrukturen des Menschen. *Klin. Wschr* 3:1495-1497.

531. Larsen, R.D., L.K. Ernst, R.P. Nair, and J.B. Lowe. 1990. Molecular cloning, sequence, and expression of a human GDP-L-fucose:beta-D-galactoside 2-alpha-L-fucosyltransferase cDNA that can form the H blood group antigen. *Proc Natl Acad Sci U S A* 87:6674-6678.

532. Reguigne-Arnould, I., P. Couillin, R. Mollicone, S. Faure, A. Fletcher, R.J. Kelly, J.B. Lowe, and R. Oriol. 1995. Relative positions of two clusters of human alpha-L-fucosyltransferases in 19q (FUT1-FUT2) and 19p (FUT6-FUT3-FUT5) within the microsatellite genetic map of chromosome 19. *Cytogenet Cell Genet* 71:158-162.

533. Ferguson-Smith, M.A., D.A. Aitken, C. Turleau, and J. de Grouchy. 1976. Localisation of the human ABO: Np-1: AK-1 linkage group by regional assignment of AK-1 to 9q34. *Hum Genet* 34:35-43.

534. Bennett, E.P., R. Steffensen, H. Clausen, D.O. Weghuis, and A.G. van Kessel. 1995. Genomic cloning of the human histo-blood group ABO locus. *Biochem Biophys Res Commun* 206:318-325.

535. Yamamoto, F., P.D. McNeill, and S. Hakomori. 1995. Genomic organization of human histo-blood group ABO genes. *Glycobiology* 5:51-58.

536. Clausen, H., T. White, K. Takio, K. Titani, M. Stroud, E. Holmes, J. Karkov, L. Thim, and S. Hakomori. 1990. Isolation to homogeneity and partial characterization of a histo-blood group A defined Fuc alpha 1----2Gal alpha 1----3-N-acetylgalactosaminyltransferase from human lung tissue. *J Biol Chem* 265:1139-1145.

537. Yamamoto, F., J. Marken, T. Tsuji, T. White, H. Clausen, and S. Hakomori. 1990. Cloning and characterization of DNA complementary to human UDP-GalNAc: Fuc alpha 1----2Gal alpha 1----3GalNAc transferase (histo-blood group A transferase) mRNA. *J Biol Chem* 265:1146-1151.

538. Breton, C., and A. Imberty. 1999. Structure/function studies of glycosyltransferases. *Curr Opin Struct Biol* 9:563-571.

539. Yamamoto, F., H. Clausen, T. White, J. Marken, and S. Hakomori. 1990. Molecular genetic basis of the histo-blood group ABO system. *Nature* 345:229-233.

540. Olsson, M.L., and M.A. Chester. 1995. A rapid and simple ABO genotype screening method using a novel B/O2 versus A/O2 discriminating nucleotide substitution at the ABO locus. *Vox Sang* 69:242-247.

541. Schachter, H., and M.A. Michaels. 1971. A quantitative difference in the activity of blood group A-specific N-acetylgalactosaminyltransferase in serum from A 1 and A 2 human subjects. *Biochem Biophys Res Commun* 45:1011-1018.

542. Schachter, H., M.A. Michaels, C.A. Tilley, M.C. Crookston, and J.H. Crookston. 1973. Qualitative differences in the N-acetyl-D-galactosaminyltransferases produced by human A1 and A2 genes. *Proc Natl Acad Sci U S A* 70:220-224.

543. Topping, M.D., and W.M. Watkins. 1975. Isolectric points of the human blood group A-1, A-2 and B gene-associated glycosyltransferases in ovarian cyst fluids and serum. *Biochem Biophys Res Commun* 64:89-96.

544. von Dungern, E., and L. Hirszfeld. 1911. Uber gruppenspezifische Strukturen des Blutes III. *Zeitscrift fur Immunforsch* 8:526-562.

545. Race, R.R., and R. Sanger. 1975. Blood Groups in Man. Blackwell, Oxford.

546. Yamamoto, F., P.D. McNeill, and S. Hakomori. 1992. Human histo-blood group A2 transferase coded by A2 allele, one of the A subtypes, is characterized by a single base deletion in the coding sequence, which results in an additional domain at the carboxyl terminal. *Biochem Biophys Res Commun* 187:366-374.

547. Schenkel-Brunner, H. 1982. Studies on blood-groups A1 and A2. Further evidence for the predominant influence of quantitative differences in the number of A antigenic sites present on A1 and A2 erythrocytes. *Eur J Biochem* 122:511-514.

548. Olsson, M.L., and M.A. Chester. 2001. Polymorphism and recombination events at the ABO locus: a major challenge for genomic ABO blood grouping strategies. *Transfus Med* 11:295-313.

549. Daniels, G. 1995. Hot spots in the red cell membrane: molecular aspects of some red cell antigens. *Immunol Invest* 24:199-212.

550. Ogasawara, K., R. Yabe, M. Uchikawa, N. Saitou, M. Bannai, K. Nakata, M. Takenaka, K. Fujisawa, Y. Ishikawa, T. Juji, and K. Tokunaga. 1996. Molecular genetic analysis of variant phenotypes of the ABO blood group system. *Blood* 88:2732-2737.

551. Yamamoto, F., P.D. McNeill, M. Yamamoto, S. Hakomori, I.M. Bromilow, and J.K. Duguid. 1993. Molecular genetic analysis of the ABO blood group system: 4. Another type of O allele. *Vox Sang* 64:175-178.

552. Grunnet, N., R. Steffensen, E.P. Bennett, and H. Clausen. 1994. Evaluation of histo-blood group ABO genotyping in a Danish population: frequency of a novel O allele defined as O2. *Vox Sang* 67:210-215.

553. Yamamoto, F., and P.D. McNeill. 1996. Amino acid residue at codon 268 determines both activity and nucleotide-sugar donor substrate specificity of human histo-blood group A and B transferases. In vitro mutagenesis study. *J Biol Chem* 271:10515-10520.

554. Amado, M., E.P. Bennett, F. Carneiro, and H. Clausen. 2000. Characterization of the histo-blood group O(2) gene and its protein product. *Vox Sang* 79:219-226.

555. Lee, H.J., C.H. Barry, S.N. Borisova, N.O. Seto, R.B. Zheng, A. Blancher, S.V. Evans, and M.M. Palcic. 2005. Structural basis for the inactivity of human blood group O2 glycosyltransferase. *J Biol Chem* 280:525-529.

556. Yamamoto, F., P.D. McNeill, M. Yamamoto, S. Hakomori, and T. Harris. 1993. Molecular genetic analysis of the ABO blood group system: 3. A(X) and B(A) alleles. *Vox Sang* 64:171-174.

557. Olsson, M.L., and M.A. Chester. 1998. Heterogeneity of the blood group Ax allele: genetic recombination of common alleles can result in the Ax phenotype. *Transfus Med* 8:231-238.

558. Yamamoto, F., P.D. McNeill, M. Yamamoto, S. Hakomori, T. Harris, W.J. Judd, and R.D. Davenport. 1993. Molecular genetic analysis of the ABO blood group system: 1. Weak subgroups: A3 and B3 alleles. *Vox Sang* 64:116-119.

559. Olsson, M.L., B. Thuresson, and M.A. Chester. 1995. An Ael allele-specific nucleotide insertion at the blood group ABO locus and its detection using a sequence-specific polymerase chain reaction. *Biochem Biophys Res Commun* 216:642-647.

560. Yamamoto, F., P.D. McNeill, Y. Kominato, M. Yamamoto, S. Hakomori, S. Ishimoto, S. Nishida, M. Shima, and Y. Fujimura. 1993. Molecular genetic analysis of the ABO blood group system: 2. cis-AB alleles. *Vox Sang* 64:120-123.

561. Yamamoto, M., X.H. Lin, Y. Kominato, Y. Hata, R. Noda, N. Saitou, and F. Yamamoto. 2001. Murine equivalent of the human histo-blood group ABO gene is a cis-AB gene and encodes a glycosyltransferase with both A and B transferase activity. *J Biol Chem* 276:13701-13708.

562. Roubinet, F., D. Janvier, and A. Blancher. 2002. A novel cis AB allele derived from a B allele through a single point mutation. *Transfusion* 42:239-246.

563. Seyfried, H., I. Walewska, and B. Werblinska. 1964. Unusual Inheritance of Abo Group in a Family with Weak B Antigens. *Vox Sang* 9:268-277.

564. Marcus, S.L., R. Polakowski, N.O. Seto, E. Leinala, S. Borisova, A. Blancher, F. Roubinet, S.V. Evans, and M.M. Palcic. 2003. A single point mutation reverses the donor specificity of human blood group B-synthesizing galactosyltransferase. *J Biol Chem* 278:12403-12405.

565. Yu, L.C., H.L. Lee, Y.S. Chan, and M. Lin. 1999. The molecular basis for the B(A) allele: an amino acid alteration in the human histoblood group B alpha-(1,3)-galactosyltransferase increases its intrinsic alpha-(1,3)-N-acetylgalactosaminyltransferase activity. *Biochem Biophys Res Commun* 262:487-493.

566. Kornfeld, R., and S. Kornfeld. 1985. Assembly of asparagine-linked oligosaccharides. *Annual Reviews in Biochemistry* 54:631-664.

567. Roth, J., P. Greenwell, and W.M. Watkins. 1988. Immunolocalization of blood group A gene specified alpha 1,3N-acetylgalactosaminyltransferase and blood group A substance in the trans-tubular network of the Golgi apparatus and mucus of intestinal goblet cells. *Eur J Cell Biol* 46:105-112.

568. Paulson, J.C., and K.J. Colley. 1989. Glycosyltransferases. Structure, localization, and control of cell type-specific glycosylation. *J Biol Chem* 264:17615-17618.

569. Watkins, W.M. 1986. Glycosyltransferases. Early history, development and future prospects. *Carbohydr Res* 149:1-12.

570. Leloir, L.F. 1974. The Fifth Feodor Lynen lecture 'I hate to bore people with my recollections'. In Biology and Chemistry of Eucaryotic Cell Surfaces. E.Y.C.S. Lee, E. E. eds, editor Academic Press, New York. 1-20.

571. Breton, C., E. Bettler, D.H. Joziasse, R.A. Geremia, and A. Imberty. 1998. Sequence-function relationships of prokaryotic and eukaryotic galactosyltransferases. *J Biochem (Tokyo)* 123:1000-1009.

572. Sinnott, M.L. 1990. Catalytic mechanisms of enzymatic glycosyl transfer. *Chemical Reviews* 90:1171-1202.

573. Campbell, J.A., G.J. Davies, V. Bulone, and B. Henrissat. 1997. A classification of nucleotide-diphospho-sugar glycosyltransferases based on amino acid sequence similarities. *Biochem J* 326 ( Pt 3):929-939.

574. Campbell, J.A., G.J. Davies, V.V. Bulone, and B. Henrissat. 1998. A classification of nucleotide-diphospho-sugar glycosyltransferases based on amino acid sequence similarities. *Biochem J* 329 (Pt 3):719.

575. Kleene, R., and E.G. Berger. 1993. The molecular and cell biology of glycosyltransferases. *Biochim Biophys Acta* 1154:283-325.

576. Fukuda, M.N., and O. Hindsgaul. 1992. Molecular Glycobiology. IRL Press, Oxford.

577. Biology, I.U.o.B.a.M. 1992. Enzyme nomenclature: recommendations of the nomenclature committee of the International Union of Biochemistry and Molecular Biology. In Academic Press, San Diego.

578. Kikuchi, N., Y.D. Kwon, M. Gotoh, and H. Narimatsu. 2003. Comparison of glycosyltransferase families using the profile hidden Markov model. *Biochem Biophys Res Commun* 310:574-579.

579. Oriol, R., I. Martinez-Duncker, I. Chantret, R. Mollicone, and P. Codogno. 2002. Common origin and evolution of glycosyltransferases using Dol-P-monosaccharides as donor substrate. *Mol Biol Evol* 19:1451-1463.

580. Breton, C., L. Snajdrova, C. Jeanneau, J. Koca, and A. Imberty. 2006. Structures and mechanisms of glycosyltransferases. *Glycobiology* 16:29R-37R.

581. Davies, G.J., T.M. Gloster, and B. Henrissat. 2005. Recent structural insights into the expanding world of carbohydrate-active enzymes. *Curr Opin Struct Biol* 15:637-645.

582. Colley, K.J. 1997. Golgi localization of glycosyltransferases: more questions than answers. *Glycobiology* 7:1-13.

583. Qasba, P.K., B. Ramakrishnan, and E. Boeggeman. 2005. Substrate-induced conformational changes in glycosyltransferases. *Trends Biochem Sci* 30:53-62.

584. Franco, O.L., and D.J. Rigden. 2003. Fold recognition analysis of glycosyltransferase families: further members of structural superfamilies. *Glycobiology* 13:707-712.

585. Liu, J., and A. Mushegian. 2003. Three monophyletic superfamilies account for the majority of the known glycosyltransferases. *Protein Sci* 12:1418-1431.

586. Unligil, U.M., and J.M. Rini. 2000. Glycosyltransferase structure and mechanism. *Curr Opin Struct Biol* 10:510-517.

587. Bourne, Y., and B. Henrissat. 2001. Glycoside hydrolases and glycosyltransferases: families and functional modules. *Curr Opin Struct Biol* 11:593-600.

588. Coutinho, P.M., E. Deleury, G.J. Davies, and B. Henrissat. 2003. An evolving hierarchical family classification for glycosyltransferases. *J Mol Biol* 328:307-317.

589. Heissigerova, H., C. Breton, J. Moravcova, and A. Imberty. 2003. Molecular modeling of glycosyltransferases involved in the biosynthesis of blood group A, blood group B, Forssman, and iGb3 antigens and their interaction with substrates. *Glycobiology* 13:377-386.

590. Chiu, C.P., A.G. Watts, L.L. Lairson, M. Gilbert, D. Lim, W.W. Wakarchuk, S.G. Withers, and N.C. Strynadka. 2004. Structural analysis of the sialyltransferase CstII from Campylobacter jejuni in complex with a substrate analog. *Nat Struct Mol Biol* 11:163-170.

591. Hu, Y., and S. Walker. 2002. Remarkable structural similarities between diverse glycosyltransferases. *Chem Biol* 9:1287-1296.

592. Lesk, A.M. 1995. NAD-binding domains of dehydrogenases. *Curr Opin Struct Biol* 5:775-783.

593. Gastinel, L.N., C. Bignon, A.K. Misra, O. Hindsgaul, J.H. Shaper, and D.H. Joziasse. 2001. Bovine alpha1,3-galactosyltransferase catalytic domain structure and its relationship with ABO histo-blood group and glycosphingolipid glycosyltransferases. *Embo J* 20:638-649.

594. Wiggins, C.A., and S. Munro. 1998. Activity of the yeast MNN1 alpha-1,3-mannosyltransferase requires a motif conserved in many other families of glycosyltransferases. *Proc Natl Acad Sci U S A* 95:7945-7950.

595. Busch, C., F. Hofmann, J. Selzer, S. Munro, D. Jeckel, and K. Aktories. 1998. A common motif of eukaryotic glycosyltransferases is essential for the enzyme activity of large clostridial cytotoxins. *J Biol Chem* 273:19566-19572.

596. Persson, K., H.D. Ly, M. Dieckelmann, W.W. Wakarchuk, S.G. Withers, and N.C. Strynadka. 2001. Crystal structure of the retaining galactosyltransferase LgtC from

Neisseria meningitidis in complex with donor and acceptor sugar analogs. *Nat Struct Biol* 8:166-175.

597. Charnock, S.J., and G.J. Davies. 1999. Structure of the nucleotide-diphospho-sugar transferase, SpsA from Bacillus subtilis, in native and nucleotide-complexed forms. *Biochemistry* 38:6380-6385.

598. Joseph, D., G.A. Petsko, and M. Karplus. 1990. Anatomy of a conformational change: hinged "lid" motion of the triosephosphate isomerase loop. *Science* 249:1425-1428.

599. Lairson, L.L., and S.G. Withers. 2004. Mechanistic analogies amongst carbohydrate modifying enzymes. *Chem Commun (Camb)* 2243-2248.

600. Ramakrishnan, B., E. Boeggeman, V. Ramasamy, and P.K. Qasba. 2004. Structure and catalytic cycle of beta-1,4-galactosyltransferase. *Curr Opin Struct Biol* 14:593-600.

601. Davies, G.J., L. Mackenzie, A. Varrot, M. Dauter, A.M. Brzozowski, M. Schulein, and S.G. Withers. 1998. Snapshots along an enzymatic reaction coordinate: analysis of a retaining beta-glycoside hydrolase. *Biochemistry* 37:11707-11713.

602. Davies, G.J., and B. Henrissat. 1995. Structures and mechanisms of glycosyl hydrolases. *Structure* 3:853-859.

603. Kim, S.C., A.N. Singh, and F.M. Raushel. 1988. Analysis of the galactosyltransferase reaction by positional isotope exchange and secondary deuterium isotope effects. *Arch Biochem Biophys* 267:54-59.

604. Murray, B.W., V. Wittmann, M.D. Burkart, S.C. Hung, and C.H. Wong. 1997. Mechanism of human alpha-1,3-fucosyltransferase V: glycosidic cleavage occurs prior to nucleophilic attack. *Biochemistry* 36:823-831.

605. Williams, S.J., and G.J. Davies. 2001. Protein--carbohydrate interactions: learning lessons from nature. *Trends Biotechnol* 19:356-362.

606. Andre, I., I. Tvaroska, and J.P. Carver. 2003. On the reaction pathways and determination of transition-state structures for retaining alpha-galactosyltransferases. *Carbohydr Res* 338:865-877.

607. Zechel, D.L., and S.G. Withers. 2000. Glycosidase mechanisms: anatomy of a finely tuned catalyst. *Acc Chem Res* 33:11-18.

608. McCarter, J.D., and S.G. Withers. 1994. Mechanisms of enzymatic glycoside hydrolysis. *Curr Opin Struct Biol* 4:885-892.

609. Walsh, C. 1979. Enzymic Reaction Mechanisms. Freeman, New York.

610. Sinnott, M.L. 1987. Enzyme Mechanisms. M.I.W. Page, A., editor The Royal Society of London, London. 259.

611. Wang, Y., S.S. Wong, M.N. Fukuda, H. Zu, Z. Liu, Q. Tang, and H.E. Appert. 1994. Identification of funtional cysteine residues in human galactosyltransferase. *Biochem Biophys Res Commun* 204:701-709.

612. Tvaroska, I. 2004. Molecular modeling insights into the catalytic mechanism of the retaining galactosyltransferase LgtC. *Carbohydr Res* 339:1007-1014.

613. Race, C., and W.M. Watkins. 1972. The enzymic products of the human A and B blood group genes in the serum of "Bombay" O(h) donors. *FEBS Lett* 27:125-130.

614. Sawicka, T. 1971. Glycosyltransferases of human plasma. *FEBS Lett* 16:346-348.

615. Kim, Y.S., J. Perdomo, A. Bella, Jr., and J. Nordberg. 1971. N-acetyl-D-galactosaminyltransferase in human serum and erythrocyte membranes. *Proc Natl Acad Sci U S A* 68:1753-1756.

616. Whitehead, J.S., A. Bella, Jr., and Y.S. Kim. 1974. An N-acetylgalactosaminyltransferase from human blood group A plasma. I. Purification and agarose binding properties. *J Biol Chem* 249:442-447.

617. Nagai, M., V. Dave, H. Muensch, and A. Yoshida. 1978. Human blood group glycosyltransferase. II. Purification of galactosyltransferase. *J Biol Chem* 253:380-381.

618. Nagai, M., V. Dave, B.E. Kaplan, and A. Yoshida. 1978. Human blood group glycosyltransferases. I. Purification of n-acetylgalactosaminyltransferase. *J Biol Chem* 253:377-379.

619. Takeya, A., O. Hosomi, and M. Ishiura. 1990. Complete purification and characterization of alpha-3-N-acetylgalactosaminyltransferase encoded by the human blood group A gene. *J Biochem (Tokyo)* 107:360-368.

620. Tuppy, H., and H. Schenkel-Brunner. 1969. Formation of blood-group A substance from H substance by an alpha-N-acetylgalactosaminyl transferase. Partial purification of the enzyme from hog gastric mucosa. *Eur J Biochem* 10:152-157.

621. Schwyzer, M., and R.L. Hill. 1977. Porcine A blood group-specific N-acetylgalactosaminyltransferase. I. Purification from porcine submaxillary glands. *J Biol Chem* 252:2338-2345.

622. Navaratnam, N., J.B. Findlay, J.N. Keen, and W.M. Watkins. 1990. Purification, properties and partial amino acid sequence of the blood-group-A-gene-associated alpha-3-N-acetylgalactosaminyltransferase from human gut mucosal tissue. *Biochem J* 271:93-98.

623. Kobata, A., and V. Ginsburg. 1970. Uridine diphosphate-N-acetyl-D-galactosamine: D-galactose alpha-3-N-acetyl-D-galactosaminyltransferase, a product of the gene that determines blood type A in man. *J Biol Chem* 245:1484-1490.

624. Seto, N.O., M.M. Palcic, C.A. Compston, H. Li, D.R. Bundle, and S.A. Narang. 1997. Sequential interchange of four amino acids from blood group B to blood group A glycosyltransferase boosts catalytic activity and progressively modifies substrate recognition in human recombinant enzymes. *J Biol Chem* 272:14133-14138.

625. Seto, N.O., M.M. Palcic, O. Hindsgaul, D.R. Bundle, and S.A. Narang. 1995. Expression of a recombinant human glycosyltransferase from a synthetic gene and its utilization for synthesis of the human blood group B trisaccharide. *Eur J Biochem* 234:323-328.

626. Seto, N.O., C.A. Compston, A. Szpacenko, and M.M. Palcic. 2000. Enzymatic synthesis of blood group A and B trisaccharide analogues. *Carbohydr Res* 324:161-169.

627. Hearn, V.M., Z.G. Smith, and W.M. Watkins. 1968. An a-N-acetyl-D-galactosaminyltransferase associated with the human blood-group A character. *Biochem J* 109:315-317.

628. Kobata, A., E.F. Grollman, and V. Ginsburg. 1968. An enzymic basis for blood type A in humans. *Arch Biochem Biophys* 124:609-612.

629. Kobata, A., E.F. Grollman, and V. Ginsburg. 1968. An enzymatic basis for blood type B in humans. *Biochem Biophys Res Commun* 32:272-277.

630. Race, C., D. Ziderman, and W.M. Watkins. 1968. An alpha-d-galactosyltransferase associated with the blood-group B character. *Biochem J* 107:733-735.

631. Schwyzer, M., and R.L. Hill. 1977. Porcine A blood group-specific N-acetylgalactosaminyltransferase. *J Biol Chem* 252:2346-2355.

632. Greenwell, P., A.D. Yates, and W.M. Watkins. 1986. UDP-N-acetyl-D-galactosamine as a donor substrate for the glycosyltransferase encoded by the B gene at the human blood group ABO locus. *Carbohydr Res* 149:149-170.

633. Lowary, T.L., and O. Hindsgaul. 1993. Recognition of synthetic deoxy and deoxyfluoro analogs of the acceptor alpha-L-Fuc p-(1-->2)-beta-D-Gal p-OR by the blood-group A and B gene-specified glycosyltransferases. *Carbohydr Res* 249:163-195.

634. Yates, A.D., J. Feeney, A.S. Donald, and W.M. Watkins. 1984. Characterisation of a blood-group A-active tetrasaccharide synthesised by a blood-group B gene-specified glycosyltransferase. *Carbohydr Res* 130:251-260.

635. Yates, A.D., and W.M. Watkins. 1982. The biosynthesis of blood group B determinants by the blood group A gene-specified alpha-3-N-acetyl-D-galactosaminyltransferase. *Biochem Biophys Res Commun* 109:958-965.

636. Goldstein, J., L. Lenny, D. Davies, and D. Voak. 1989. Further evidence for the presence of A antigen on group B erythrocytes through the use of specific exoglycosidases. *Vox Sang* 57:142-146.

637. Greenwell, P., A.D. Yates, and W.M. Watkins. 1979. Blood group A synthesizing activity of the blood group B gene specified alpha-D-galactosyltransferase. In Glycoconjugates. R. Schauer, Boer, P., Buddecke, E. et al., editor Stuttgart:Thieme, 268-269.

638. Race, C., and W.M. Watkins. 1974. Inhibition of the blood group A1 and A2 gene-specified N-acetyl-alpha-D-galactosaminyltransferases by uridine diphosphate D-galactose. *Carbohydr Res* 37:239-244.

639. Carne, L.R., and W.M. Watkins. 1977. Human blood group B gene-specified alpha-3-galactosyltransferase: purification of the enzyme in serum by biospecific adsorption onto blood group O erythrocyte membranes. *Biochem Biophys Res Commun* 77:700-707.

640. Yamamoto, F., and S. Hakomori. 1990. Sugar-nucleotide donor specificity of histo-blood group A and B transferases is based on amino acid substitutions. *J Biol Chem* 265:19257-19262.

641. Seto, N.O., C.A. Compston, S.V. Evans, D.R. Bundle, S.A. Narang, and M.M. Palcic. 1999. Donor substrate specificity of recombinant human blood group A, B and hybrid A/B glycosyltransferases expressed in Escherichia coli. *Eur J Biochem* 259:770-775.

642. Lowary, T.L., and O. Hindsgaul. 1994. Recognition of synthetic O-methyl, epimeric, and amino analogs of the acceptor alpha-L-Fuc p-(1-->2)-beta-D-Gal p-OR by the blood-group A and B gene-specified glycosyltransferases. *Carbohydr Res* 251:33-67.

643. Laferte, S., N.W. Chan, K. Sujino, T.L. Lowary, and M.M. Palcic. 2000. Intracellular inhibition of blood group A glycosyltransferase. *Eur J Biochem* 267:4840-4849.

644. Mukherjee, A., M.M. Palcic, and O. Hindsgaul. 2000. Synthesis and enzymatic evaluation of modified acceptors of recombinant blood group A and B glycosyltransferases. *Carbohydr Res* 326:1-21.

645. Sujino, K., T. Uchiyama, O. Hindsgaul, N.O. Seto, W.W. Wakarchuk, and M.M. Palcic. 2000. Enzymatic synthesis of oligosaccharide analogues: Evaluation of UDP-Gal analogues as donors for three retaining alpha-galactosyltransferases. *Journal of American Chemistry Society* 122:1261-1269.

646. Kamath, V.P., N.O. Seto, C.A. Compston, O. Hindsgaul, and M.M. Palcic. 1999. Synthesis of the acceptor analog alphaFuc(1-->2)alphaGal-O(CH2)7 CH3: a probe for the kinetic mechanism of recombinant human blood group B glycosyltransferase. *Glycoconj J* 16:599-606.

647. Patenaude, S.I., N.O. Seto, S.N. Borisova, A. Szpacenko, S.L. Marcus, M.M. Palcic, and S.V. Evans. 2002. The structural basis for specificity in human ABO(H) blood group biosynthesis. *Nat Struct Biol* 9:685-690.

648. Schachter, H. 1992. *Trends Glycosci. Glycotechnol.* 4:241-250.

649. Yazer, M.H., G.A. Denomme, N.L. Rose, and M.M. Palcic. 2005. Amino-acid substitution in the disordered loop of blood group B-glycosyltransferase enzyme causes weak B phenotype. *Transfusion* 45:1178-1182.

650. Yazer, M.H., and M.M. Palcic. 2005. The importance of disordered loops in ABO glycosyltransferases. *Transfus Med Rev* 19:210-216.

651. Letts, J.A., N.L. Rose, Y.R. Fang, C.H. Barry, S.N. Borisova, N.O. Seto, M.M. Palcic, and S.V. Evans. 2006. Differential recognition of the type I and II H antigen acceptors by the human ABO(H) blood group A and B glycosyltransferases. *J Biol Chem* 281:3625-3632.

652. Compston, C.A., C. Condon, H.R. Hanna, and M.A. Mazid. 1993. Rapid production of a panel of blood group A-active oligosaccharides using chemically synthesized di- and tri-saccharide primers and an easily prepared porcine (1-->3)-alpha-N-acetyl-D-galactosaminyltransferase. *Carbohydr Res* 239:167-176.

653. Warnock, D., X. Bai, K. Autote, J. Gonzales, K. Kinealy, B. Yan, J. Qian, T. Stevenson, D. Zopf, and R.J. Bayer. 2005. In vitro galactosylation of human IgG at 1 kg scale using recombinant galactosyltransferase. *Biotechnol Bioeng* 92:831-842.

654. Persson, M., J.A. Letts, B. Hosseini-Maaf, S.N. Borisova, M.M. Palcic, S.V. Evans, and M.L. Olsson. 2007. Structural effects of naturally-occurring human Blood group B galactosyltranferase mutations adjacent to the DXD motif. *J Biol Chem*

655. Nguyen, H.P., N.O. Seto, Y. Cai, E.K. Leinala, S.N. Borisova, M.M. Palcic, and S.V. Evans. 2003. The influence of an intramolecular hydrogen bond in differential recognition of inhibitory acceptor analogs by human ABO(H) blood group A and B glycosyltransferases. *J Biol Chem* 278:49191-49195.

656. Bradford, M.M. 1976. A rapid and sensitive method for the quantitation of microgram quantities of protein utilizing the principle of protein-dye binding. *Anal Biochem* 72:248-254.

657. Brunger, A.T., P.D. Adams, G.M. Clore, W.L. DeLano, P. Gros, R.W. Grosse-Kunstleve, J.S. Jiang, J. Kuszewski, M. Nilges, N.S. Pannu, R.J. Read, L.M. Rice, T. Simonson, and G.L. Warren. 1998. Crystallography and NMR system: A new

software suite for macromolecular structure determination. *Acta Crystallogr* D54:905-921.

658. McRee, D.E. 1999. XtalView/Xfit--A versatile program for manipulating atomic coordinates and electron density. *J Struct Biol* 125:156-165.

659. Yen, T.Y., R.K. Joshi, H. Yan, N.O. Seto, M.M. Palcic, and B.A. Macher. 2000. Characterization of cysteine residues and disulfide bonds in proteins by liquid chromatography/electrospray ionization tandem mass spectrometry. *J Mass Spectrom* 35:990-1002.

660. Gibbons, B.J., P.J. Roach, and T.D. Hurley. 2002. Crystal structure of the autocatalytic initiator of glycogen biosynthesis, glycogenin. *J Mol Biol* 319:463-477.

661. Pedersen, L.C., K. Tsuchida, H. Kitagawa, K. Sugahara, T.A. Darden, and M. Negishi. 2000. Heparan/chondroitin sulfate biosynthesis. Structure and mechanism of human glucuronyltransferase I. *J Biol Chem* 275:34580-34585.

662. Flint, J., E. Taylor, M. Yang, D.N. Bolam, L.E. Tailford, C. Martinez-Fleites, E.J. Dodson, B.G. Davis, H.J. Gilbert, and G.J. Davies. 2005. Structural dissection and high-throughput screening of mannosylglycerate synthase. *Nat Struct Mol Biol* 12:608-614.

663. Yamaguchi, N., and M.N. Fukuda. 1995. Golgi retention mechanism of beta-1,4-galactosyltransferase. Membrane-spanning domain-dependent homodimerization and association with alpha- and beta-tubulins. *J Biol Chem* 270:12170-12176.

664. Ouzzine, M., S. Gulberti, P. Netter, J. Magdalou, and S. Fournel-Gigleux. 2000. Structure/function of the human Galbeta1,3-glucuronosyltransferase. Dimerization and functional activity are mediated by two crucial cysteine residues. *J Biol Chem* 275:28254-28260.

665. Lobsanov, Y.D., P.A. Romero, B. Sleno, B. Yu, P. Yip, A. Herscovics, and P.L. Howell. 2004. Structure of Kre2p/Mnt1p: a yeast alpha1,2-mannosyltransferase involved in mannoprotein biosynthesis. *J Biol Chem* 279:17921-17931.

666. Boix, E., G.J. Swaminathan, Y. Zhang, R. Natesh, K. Brew, and K.R. Acharya. 2001. Structure of UDP complex of UDP-galactose:beta-galactoside-alpha -1,3-galactosyltransferase at 1.53-A resolution reveals a conformational change in the catalytically important C terminus. *J Biol Chem* 276:48608-48614.

667. Ramakrishnan, B., and P.K. Qasba. 2001. Crystal structure of lactose synthase reveals a large conformational change in its catalytic component, the beta1,4-galactosyltransferase-I. *J Mol Biol* 310:205-218.

668. Ramakrishnan, B., P.V. Balaji, and P.K. Qasba. 2002. Crystal structure of beta1,4-galactosyltransferase complex with UDP-Gal reveals an oligosaccharide acceptor binding site. *J Mol Biol* 318:491-502.

669. Unligil, U.M., S. Zhou, S. Yuwaraj, M. Sarkar, H. Schachter, and J.M. Rini. 2000. X-ray crystal structure of rabbit N-acetylglucosaminyltransferase I: catalytic mechanism and a new protein superfamily. *Embo J* 19:5269-5280.

670. Gastinel, L.N., C. Cambillau, and Y. Bourne. 1999. Crystal structures of the bovine beta4galactosyltransferase catalytic domain and its complex with uridine diphosphogalactose. *Embo J* 18:3546-3557.

671. Pedersen, L.C., J. Dong, F. Taniguchi, H. Kitagawa, J.M. Krahn, L.G. Pedersen, K. Sugahara, and M. Negishi. 2003. Crystal structure of an alpha 1,4-N-acetylhexosaminyltransferase (EXTL2), a member of the exostosin gene family involved in heparan sulfate biosynthesis. *J Biol Chem* 278:14420-14428.

672. Reinert, D.J., T. Jank, K. Aktories, and G.E. Schulz. 2005. Structural basis for the function of Clostridium difficile toxin B. *J Mol Biol* 351:973-981.

Bilingual

## EDUCATION

| | | |
|---|---|---|
| DOCTORATE | University of Ottawa – Faculty of Medicine –<br>Department of Biochemistry, Microbiology and Immunology<br>Thesis Supervisor: Stephen V. Evans<br>Thesis Co-Supervisor: John E. Baenziger | 1999-2007 |
| BACHELOR'S (HONOURS) | University of Ottawa – Faculty of Sciences -<br>Department of biochemistry<br>Honours Thesis Supervisor: Stephen V. Evans<br>Magna Cum Laude | 1996-1999 |

## EMPLOYMENT

| | | |
|---|---|---|
| TEACHING ASSISTANT | University of Ottawa – Sciences – Department of Bio-chemistry<br>Course: Laboratoire de biologie moléculaire<br>Supervisor: K. Dimock | Sept. 2001-<br>Dec. 2001 |
| TEACHING ASSISTANT | University of Ottawa – Sciences – Department of Bio-chemistry<br>Course: Laboratoire de biochimie II<br>Supervisor: M. Rodriguez | Jan. 2001-<br>Apr. 2001 |
| PEER HELPER | University of Ottawa<br>Supervisor: Dominique Leonard | Sept. 1999-<br>Apr. 2000 |

## SCHOLARSHIPS

| | | |
|---|---|---|
| University of Ottawa Excellence Scholarship | Amount equal to tuition fees | May 2000-<br>Dec. 2006 |
| Ontario Graduate Scholarship in Sciences and Technology (OGSST) | $15,000 | Sept. 2005-<br>Dec. 2006 |
| Ontario Graduate Scholarship (OGS) | $15,000 | Sept. 2004-<br>Aug. 2005 |
| National Research Council of Canada<br>Graduate Student Scholarship Supplement Program (GSSSP) | $7,500 | Sept. 2004-<br>Aug. 2005 |
| Fonds de la recherche en santé du Québec (FRSQ)<br>Doctoral Award | $21,800 | Sept. 2001-<br>Aug. 2004 |

| | | |
|---|---|---|
| Natural Sciences and Engineering Research Council of Canada (NSERC) PGS B | $38,200 | Sept. 2001-Aug. 2003 |
| Fonds formation chercheurs et aide recherche (FCAR) Master's Award | $20,000 | May 2000-Aug. 2001 |
| University of Ottawa Entrance Scholarship | $1,200 | Sept. 1996-Apr. 1997 |

## PUBLICATIONS

Refereed: **R.C. Landry**, A.C. Klimowicz, S.J. Lavictoire, S. Borisova, D.T. Kottachchi, I.A. Lorimer, and S.V. Evans (2001) Antibody Recognition of a Conformational Epitope in a Peptide Antigen: Fv-peptide Complex of an Antibody Fragment Specific for the Mutant EGF Receptor, EGFRvIII. *Journal of Molecular Biology*, vol.308, no.5, pp.883-893.

Non-refereed: **R.C. Landry**, S. Borisova, and S.V. Evans (2001) Antibody Recognition of a Conformational Epitope in a Peptide Antigen of the Tumor-Associated Variant of Epidermal Growth Factor Receptor, EGFRvIII. Brookhaven National Laboratory – National Synchrotron Light Source Activity Report, Beamline X8C, Abstract no. Land372

## POSTERS AND SEMINARS

**R.C. Landry**, T. Hirama, N.O.L. Seto, C.R. MacKenzie, and S.V. Evans (2004) Structural Studies of Ganglioside Mimicry by Monoclonal Antibody BEC2. University of Ottawa Graduate Poster Session.

**R.C. Landry**, and S.V. Evans (2003) Investigation Into the Mechanisms of Carbohydrate Mimicry by Antibodies. University of Ottawa Student Seminar Series.

**R.C. Landry**, and S.V. Evans (2002) Crystallization of *Neisseria meningitidis* PorB. University of Ottawa Graduate Poster Session. First place award - $120.

S. Borisova, **R.C. Landry**, I.A. Lorimer, and S.V. Evans (2001) Crystallization of dsFv-MR1 in Complex With a Peptide Antigen of a Variant of the Epidermal Growth Factor Receptor, EGFRvIII. Eight International Conference for the Crystallization of Biological Macromolecules, Florida.

**R.C. Landry**, and S.V. Evans (2001) Structure of MR1. University of Ottawa Seminar Series.

**R.C. Landry**, and S.V. Evans (2000) Solving the structure of MR1. University of Ottawa Graduate Poster Session.

**R.C. Landry**, and S.V. Evans (1999) Structure of 6B9. University of Ottawa Honours Poster Session. Second place award.

## OTHER SCHOLARLY ACTIVITIES

- Judge at the Ottawa Science Fair (April 2001 and 2002)
- Presentation of National Research Council of Canada's Antibody Engineering Laboratory to winners of the Regional Edition of Science Fair
- Two trips to Queens University, Kingston, Canada, and nine trips to the Brookhaven National Laboratory, New York, USA, for collection of x-ray diffraction data
- Training of one summer student and two undergraduate students
- Participation in a Structural Biology Journal Club